ISSN: 2153-1196 Volume 14, Number 5, April 2023

Scientific Research Publishing

Journal of Modern Physics

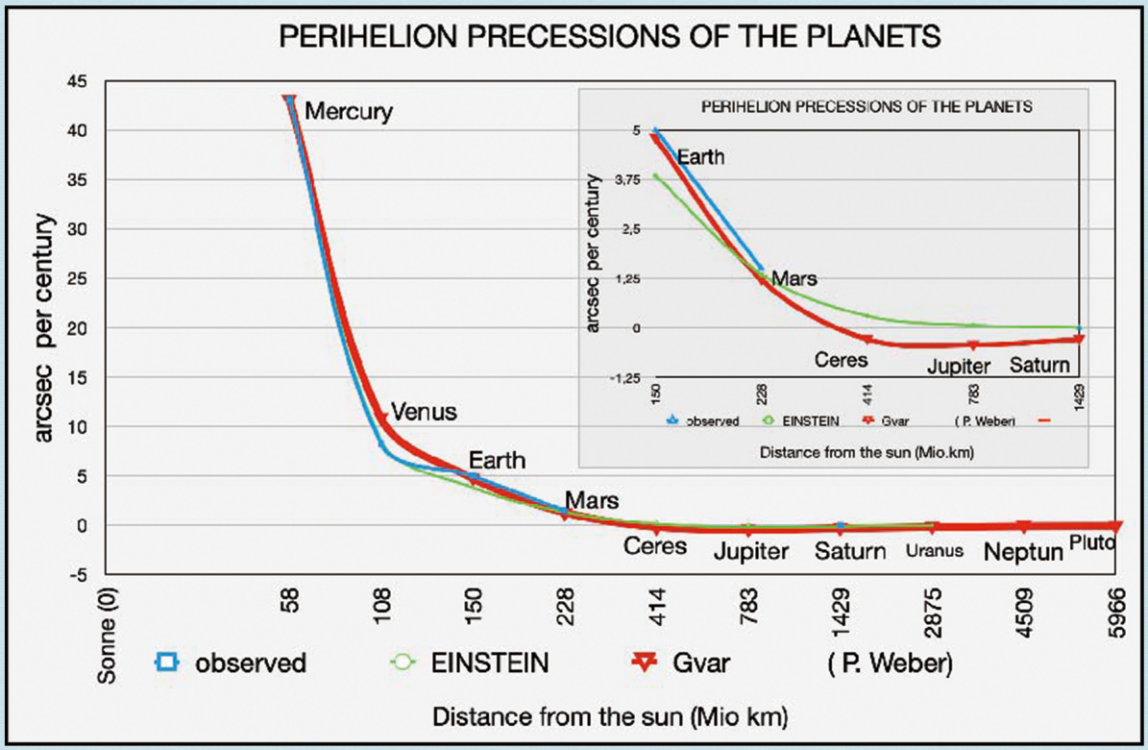

ISSN: 2153-1196

https://www.scirp.org/journal/jmp

Journal Editorial Board

ISSN: 2153-1196 (Print) ISSN: 2153-120X (Online)
https://www.scirp.org/journal/jmp

Editorial Board

Scientific Research Publishing

Journal of Modern Physics, 2023, 14, 553-776
https://www.scirp.org/journal/jmp
ISSN Online: 2153-120X
ISSN Print: 2153-1196

Table of Contents

Volume 14 Number 5 April 2023

Journal of Modern Physics, 2023, 14, 553-776
https://www.scirp.org/journal/jmp
ISSN Online: 2153-120X
ISSN Print: 2153-1196

The figure on the front cover is from the article published in Journal of Modern Physics, 2023, Vol. 14, No. 5, pp. 670-675 by Hans Peter Weber.

Journal of Modern Physics (JMP)
Journal Information

SUBSCRIPTIONS

The *Journal of Modern Physics* (Online at Scientific Research Publishing, https://www.scirp.org/) is published monthly by Scientific Research Publishing, Inc., USA.

Subscription rates:
Print: $89 per issue.
To subscribe, please contact Journals Subscriptions Department, E-mail: sub@scirp.org

SERVICES

Advertisements
Advertisement Sales Department, E-mail: service@scirp.org

Reprints (minimum quantity 100 copies)
Reprints Co-ordinator, Scientific Research Publishing, Inc., USA.
E-mail: sub@scirp.org

COPYRIGHT

PRODUCTION INFORMATION

For manuscripts that have been accepted for publication, please contact:
E-mail: jmp@scirp.org

Scientific Research Publishing

Journal of Modern Physics, 2023, 14, 553-561
https://www.scirp.org/journal/jmp
ISSN Online: 2153-120X
ISSN Print: 2153-1196

An Electron Model Based on the Fine Structure Constant

Arlen Young

Independent Researcher, Palo Alto, CA, USA
Email: arlen_young@yahoo.com

How to cite this paper: Young, A. (2023) An Electron Model Based on the Fine Structure Constant. *Journal of Modern Physics*, **14**, 553-561.
https://doi.org/10.4236/jmp.2023.145031

Received: March 6, 2023
Accepted: April 10, 2023
Published: April 13, 2023

Abstract

In previous publications, the author has proposed a model of the electron's internal structure, wherein a positively-charged negative mass outer shell and a negatively-charged positive mass central core are proposed to resolve the electron's charge and mass inconsistencies. That model is modified in this document by assuming the electron's radius is exactly equal to the classical electron radius. The attributes of the internal components of the electron's structure have been recalculated accordingly. The shape of the electron is also predicted, and found to be slightly aspherical on the order of an oblate ellipsoid. This shape is attributed to centrifugal force and compliant outer shell material. It is interesting to note that all of the electron's attributes, both external and internal, with the exception of mass and angular moment, are functions of the fine structure constant α, and can be calculated from just three additional constants: electron mass, Planck's constant, and speed of light. In particular, the ratios of the outer shell charge and mass to the electron charge and mass, respectively, are $\frac{3}{2\alpha}$. The ratios of the central core charge and mass to the electron charge and mass, respectively, are $1-\frac{3}{2\alpha}$. Attributes of the electron are compared with those of the muon. Charge and spin angular momentum are the same, while mass, magnetic moment, and radius appear to be related by the fine structure constant. The mass of the electron outer shell is nearly equal to the mass of the muon. The muon internal structure can be modeled exactly the same as for the electron, with exactly the same attribute relationships.

Keywords

Fine Structure Constant, Negative Mass, Electron Shape, Electron Structure, Electron Mass Inconsistency, Electron Charge Inconsistency, Muon

1. Introduction

The author has previously published a proposed model of the electron [1] which resolves large inconsistencies between the measured mass of the electron and the mass calculated from the spin angular momentum, and also between the measured charge of the electron and the charge derived from the magnetic dipole moment. The model introduces a positive charge and negative mass into the electron core and predicts the electron radius. This Dual-Charge Dual-Mass Model has been modified in this document by assuming that the radius exactly equals the classical electron radius. Interestingly, the consequence of this change is that the internal components of the electron become very simple functions of the fine structure constant. In fact, almost every attribute of the electron, both external and internal, is a function of the constant.

Many of the electron's attributes have been previously theoretically calculated, and are referenced herein to highlight their dependence on the fine structure constant. The intent of this document is to show that the components of the electron's internal structure also have very simple relations to the constant. The shape of the electron is also predicted as a function of the constant.

Values for the internal attributes of the electron can be calculated from the model using only four basic constants:

- Electron mass.
- Fine structure constant.
- Planck's constant.
- Speed of light.

The spin angular momentum S_Z is known from quantum theory. The theoretical expression for electron charge q is used to calculate the spin magnetic dipole moment M. The electron shape is then calculated from the ratio of the electron's electric and magnetic fields and the theoretical expression for the classical electron radius. Finally, the internal charges and masses are calculated for the electron and repeated for the muon.

It is interesting to compare the attributes of the electron with those of the muon. Charge and spin angular momentum are the same, while mass, magnetic moment, and radius appear to be related by the fine structure constant, as detailed below.

2. Derivations

Table 1 contains the base constants used in the model. They are the foundation

Table 1. Table of base constants.

constant	symbol	value [cgs]
fine structure constant	α	$7.2973525693 \times 10^{-3}$ [2]
Planck's constant	h	$6.62607015 \times 10^{-27}$ [3]
speed of light	c	$2.99792458 \times 10^{10}$ [4]
electron mass	m	$9.1093837015 \times 10^{-28}$ [5]

of the model. The only electron attribute that is a base constant is the measured value of the electron mass m. All other electron attributes are calculated as functions of these base constants. Their expressions and values derived from the calculations are listed in Table 2.

Unless otherwise specified, all units are CGS.

2.1. Magnetic Dipole Moment

The value of the electron spin angular momentum S is calculated from

$$S=\sqrt{s(s+1)}\frac{h}{2\pi}\quad [6],\ \text{where}\quad s=\frac{1}{2}. \tag{1}$$

When placed in a magnetic field, the electron spin axis precesses about the field vector at the Larmor precession frequency. The projection of the spin angular momentum vector of magnitude S on the Larmor precession axis is S_z.

The electron charge q is calculated from one of the expressions for the fine structure constant:

$$\alpha=\frac{q^2}{\left(\frac{h}{2\pi}\right)c}\quad [2],\quad q=-\sqrt{\alpha\left(\frac{h}{2\pi}\right)c} \tag{2}$$

Table 2. Table of derived electron attributes.

Constant	Expression	Value [cgs]
spin angular momentum	$S=\sqrt{s(s+1)}\frac{h}{2\pi},\ s=\frac{1}{2}$	$9.132859842\times10^{-28}$
projection of S on Larmor precession axis	$S_Z=s\frac{h}{2\pi}$ [6]	$5.272859088\times10^{-28}$
charge	$q=-\sqrt{\alpha\left(\frac{h}{2\pi}\right)c}$	$-4.803204713\times10^{-10}$
g-factor	$g_e=2\left(1+\sum_{i=1}^{\infty}C_i\left(\frac{\alpha}{\pi}\right)\right)$	2.002319304
magnetic dipole moment	$M=-\sqrt{\alpha\frac{h^3}{2^7\pi^3m^2c}}g_e$	$-9.284764698\times10^{-21}$ ($-9.2847647043\times10^{-21}$ [15])
classical electron radius	$R=\frac{q^2}{mc^2}$	$2.817940325\times10^{-13}$ ($2.8179403262\times10^{-13}$ [16])
shape eccentricity	$\frac{R}{r}=\sqrt{\frac{2M\alpha}{qR}}$	1.000579658
$\frac{\text{outer shell charge}}{\text{electron charge}}=\frac{\text{outer shell mass}}{\text{electron mass}}$	$\frac{q^-}{q}=\frac{m^+}{m}=\frac{3}{2\alpha}$	205.5539986
$\frac{\text{central core charge}}{\text{electron charge}}=\frac{\text{central core mass}}{\text{electron mass}}$	$\frac{q^+}{q}=\frac{m^-}{m}=1-\frac{3}{2\alpha}$	−204.5539986

For comparison with the NIST MKS value [7], the conversion to CGS is:

$$q = -1.602176634\times10^{-19}\,[\text{MKS}]\times(1/10)c = -4.803204713\times10^{-10}\ \text{emu}$$

The magnetic dipole moment of the electron M is derived from the gyromagnetic ratio of the electron γ_e, which is defined as

$$\gamma_e = \frac{M}{S_z} = \frac{q}{2mc}g_e \quad [8]. \tag{3}$$

The g-factor g_e has been calculated theoretically:

$$g_e = 2\left(1+a_e\right) \quad [9] \tag{4}$$

It can be expressed as an infinite number of fine structure constant terms:

$$a_e = \sum_{i=1}^{\infty} C_i\left(\frac{\alpha}{\pi}\right) \quad [10] \tag{5}$$

The condensed expression for M along with its value and the values of its factors are shown in **Table 2**.

2.2. Electron Shape

Insight into the shape of the electron can be gained by looking at the ratio of the electric field E at its surface to the magnetic field B at its center. For a spherical shape with classical electron radius R:

$$E = \frac{q}{r^2},\quad B = \frac{2M}{R^3} \quad [11],\quad R = \frac{q^2}{mc^2} \quad [12],\quad r = R \tag{6}$$

r = distance from center to a pole (intersection of the surface with the spin axis)

$$\frac{E}{B} = 0.998841691\alpha \tag{7}$$

The value of the $\frac{E}{B}$ ratio is remarkably close to the value of the fine structure constant, suggesting that the ratio is actually exactly equal to α and that the shape is actually slightly aspherical. R and r will have different values. While r is the distance from the center to a pole, R is assumed to be the radius at the equator. For $\frac{E}{B} = \alpha$,

$$\frac{R}{r} = \sqrt{\frac{2M\alpha}{qR}} = 1.000579658 \tag{8}$$

Therefore, the outer shell of the electron bulges slightly at the equator, probably caused by centrifugal force. A bulge as a function of centrifugal force indicates that the electron material is compliant, *i.e.*, not rigid.

The shape appears to be on the order of an oblate ellipsoid. The author calculated in [13] that the shape is a prolate spheroid. In the author's previous publications [1] [13] [14], a basic assumption was that the physical and electrical forces exactly balance out at the equator of the electron surface. The results were radii that were somewhat greater than the classical electron radius. The model

presented in this document assumes the radius to be exactly equal to the classical electron radius. As a result, the forces will not balance out to zero at the equator. There will be a net outward force causing a bulge and requiring tensile strength of the electron material to hold the electron together.

2.3. Internal Attribute Values

The author's previous publications [1] [13] [14] assume an internal electron structure consisting of an outer shell and a very small central core. These two components have opposite charges and masses. It was shown that such a structure could be used to resolve the electron's charge and mass inconsistencies. The same structure is assumed in this document. The following is a calculation of the charge q^- on the outer shell.

Consider a charged spherical shell of compliant material and radius *r*. Slice the shell into many rings, each parallel to the equatorial plane with a charge q' and radius r'. The outer shell is comprised of this stack of rings. Spin the shell at a rate ω. The magnetic moment for each ring is

$$\frac{1}{2}\frac{1}{c}q'\omega r'^2 \quad [14], \quad \sum q' = q^- \tag{9}$$

For very small ω, the shape of the stack of rings is spherical. As ω is increased, each ring will expand. When ω has increased to a value such that the ring at the equator has a radius of *R*, the model assumes that the radius r' of each ring has expanded by a factor of $\left(\frac{R}{r}\right)$. Therefore, the magnetic moment of each ring has increased by $\left(\frac{R}{r}\right)^2$. Consequently, the magnetic moment of the outer shell has changed by a factor of $\left(\frac{R}{r}\right)^2$ as a result of the shape change.

For the equator of the electron spinning at close to the speed of light, the magnetic moment *M* assuming a spherical shape is expressed by

$$M = \frac{1}{3}q^- R\,. \tag{10}$$

For the aspherical shape calculated above,

$$M = \frac{1}{3}\left(\frac{R}{r}\right)^2 q^- R = \frac{1}{3}\frac{2M\alpha}{qR}\frac{q^-}{q}qR\,. \tag{11}$$

This solution to this equation is

$$\frac{q^-}{q} = \frac{3}{2\alpha}. \tag{12}$$

In the author's previous publications [1] [13] [14], the outer shell was given a positive charge to enable all forces at the equator to be balanced. Balance cannot be achieved with a negative charge because the charge would be greater than the central core positive charge, and the repulsive force on the outer shell would be greater than its attractive force to the core. However, for the model in this doc-

ument, because the radius is the classical electron radius, the forces cannot be balanced. Consequently, the outer shell can have either a positive or negative charge. A negative charge was chosen so the corresponding mass of the outer shell is positive. There is some uncertainty as to how a negative mass shell would respond to a net inward force. The material would react opposite to the force, creating tensile stress to balance out the force. It seems like the material would react to its internal tensile stress by creating even more stress until it flies apart. By placing the negative mass at the center, any force on its material will be the outward electrical force from the outer shell charge, which will tend to compress the material.

For the negative mass central core to have a stable position at the center, the outer shell charge needs to be mobile. Normally, the central core will be positioned at exactly the center and the outer shell charge will be uniformly distributed across the shell surface. However, if the central core were to be perturbed off center, then there would be an attractive force on the core toward the nearest point on the outer shell. Since the core has negative mass, this force would actually move it back toward the center, counteracting the perturbation. Therefore, the position of the core will be stable.

The internal attributes are:

$q^+ \equiv$ charge of the central core.

$q^- \equiv$ charge of the outer shell.

$m^+ \equiv$ mass of the outer shell.

$m^- \equiv$ mass of the central core.

The relationships among the internal and external attributes are

$$\frac{q^-}{m^+} = \frac{q^+}{m^-} = \frac{q}{m} \quad [1] \tag{13}$$

The expressions and values for each are shown in Table 2.

3. Comparisons of Electron and Muon Attributes

The electron and muon are both leptons and share some common attributes. In particular, their charges and spin angular momentums are the same. Other muon attributes are quite different, but appear to be related to those of the electron via the fine structure constant α. In particular, those attributes are mass, magnetic moment and radius. The relationships are shown in Table 3. They are not exact functions of the fine structure constant, but they are quite close, and close enough to be of interest.

As can be seen in Table 3, the electron outer shell mass is very nearly equal to the muon mass, differing by less than 0.6%. When the muon decays, nearly all of its mass becomes the outer shell of the electron. The electron and muon magnetic moments and radii are related by the fine structure constant α, with a deviation of less than 0.6%. The muon radius was calculated using the same expression as for the classical electron radius. The electron mass was replaced with the muon mass.

Table 3. Muon constants and relations to electron attributes.

Constant	Expression	Value [cgs]
mass	m_μ	$1.883531627 \times 10^{-25}$ g [17]
$\frac{\text{muon mass}}{\text{electron mass}}$	$\frac{m_\mu}{m}$	206.768283
$\frac{\text{muon mass}}{\text{electron outer shell mass}}$	$\frac{m_\mu}{m^+} = \frac{2\alpha}{3}\frac{m_\mu}{m}$	1.005907374
magnetic moment	M_μ	$-4.49044830 \times 10^{-23}$ emu [18]
$\frac{\text{electron magnetic moment}}{\text{muon magnetic moment}}$	$\frac{M}{M_\mu}$	206.766988
$\text{moment ratio} \times \frac{\text{fine structure constant}}{3/2}$	$\frac{M}{M_\mu}\frac{2\alpha}{3}$	1.005901074
radius	$R_\mu = \frac{q^2}{m_\mu c^2}$	$1.36284941 \times 10^{-15}$ cm
$\frac{\text{electron radius}}{\text{muon radius}}$	$\frac{R}{R_\mu}$	206.768283
$\frac{\text{electron radius}}{\text{muon radius}} \times \frac{\text{fine structure constant}}{3/2}$	$\frac{R}{R_\mu}\frac{2\alpha}{3}$	1.005907374
shape eccentricity	$\frac{R_\mu}{r_\mu} = \sqrt{\frac{2M_\mu\alpha}{qR_\mu}}$	1.000582791
$\frac{\text{muon shape eccentricity}}{\text{electron shape eccentricity}}$	$\frac{R_\mu}{r_\mu} \div \frac{R}{r}$	1.000003131
$\frac{\text{outer shell charge}}{\text{muon charge}} = \frac{\text{outer shell mass}}{\text{muon mass}}$	$\frac{q_\mu^-}{q} = \frac{m_\mu^+}{m_\mu} = \frac{3}{2\alpha}$	205.5539986 (equal to the electron ratios)
$\frac{\text{central core charge}}{\text{muon charge}} = \frac{\text{central core mass}}{\text{muon mass}}$	$\frac{q_\mu^+}{q} = \frac{m_\mu^-}{m_\mu} = 1 - \frac{3}{2\alpha}$	−204.5539986 (equal to the electron ratios)

The muon internal structure can be modeled exactly the same as for the electron. The relationships between internal and external attributes are identical to those for the electron, as seen by comparing Table 2 and Table 3 entries.

If one were to assume that the muon and electron radii were the same, the above equations would show that all of the charge would reside on the outer surface, there would be no internal structure, and the shape would be a prolate ellipsoid.

4. Summary

The author has previously proposed the Dual Charge Dual Mass Model of the electron, which incorporates both positive and negative charges and masses to resolve the electron's charge and mass inconsistencies. That model has been

modified in this document by assuming the electron radius is exactly equal to the theoretically calculated value of the classical electron radius. The resulting model shows that every attribute of the electron, both external and internal and except for mass, can be theoretically calculated from just four constants: fine structure constant, total mass, Planck's Constant, speed of light. Every attribute, except for mass and angular momentum, is a function of the fine structure constant. In particular, the internal positive and negative charge and mass components of the electron are very simple functions of the constant. All of the attributes calculated from the model agree with theoretical and experimentally measured values to within at least nine significant figures.

The model also predicts the shape of the electron. The shape is predicted to be aspherical, with a slight bulge at the equator due to centrifugal force from its spin. The model requires that the electron material be compliant, *i.e.*, not rigid. The shape is on the order of an oblate ellipsoid. The ratio of the major and minor axes has been calculated.

Attributes of the electron are compared with those of the muon. Charge and spin angular momentum are the same, while mass, magnetic moment, and radius appear to be related by the fine structure constant. The muon internal structure can be modeled exactly the same as for the electron. The relationships between internal and external attributes are identical to those for the electron.

Conflicts of Interest

The author declares no conflicts of interest regarding the publication of this paper.

References

[1] Young, A. (2022) *Journal of Modern Physics*, **13**, 1287-1294. https://doi.org/10.4236/jmp.2022.139077

[2] NIST (2018) 2018 CODATA Value: Fine-Structure Constant. The NIST Reference on Constants, Units, and Uncertainty. https://physics.nist.gov/cgi-bin/cuu/Value?alph

[3] NIST (2018) 2018 CODATA Value: Planck Constant. The NIST Reference on Constants, Units, and Uncertainty. https://physics.nist.gov/cgi-bin/cuu/Value?h

[4] NIST (2018) 2018 CODATA Value: Speed of Light in Vacuum. The NIST Reference on Constants, Units, and Uncertainty. https://physics.nist.gov/cgi-bin/cuu/Value?c

[5] NIST (2018) 2018 CODATA Value: Electron Mass. The NIST Reference on Constants, Units, and Uncertainty. https://physics.nist.gov/cgi-bin/cuu/Value?me|search_for=electron+mass

[6] Nave, C.R. (2016) Electron Spin. HyperPhysics, Dept. of Physics and Astronomy, Georgia State University, Atlanta. http://hyperphysics.phy-astr.gsu.edu/hbase/spin.html

[7] NIST (2018) 2018 CODATA Value: Elementary Charge. The NIST Reference on Constants, Units, and Uncertainty. https://physics.nist.gov/cgi-bin/cuu/Value?e

[8] Yavorsky, B. and Detlaf, A. (1975) Handbook of Physics. Mir Publishers, Moscow, 477.

[9] NIST (2018) 2018 CODATA Value: Electron g-Factor. The NIST Reference on Constants, Units, and Uncertainty.
https://physics.nist.gov/cgi-bin/cuu/Value?eqgem

[10] Aoyama, T., Kinoshita, T. and Nio, M. (2019, February 22) *Atoms*, **7**, 28.
https://www.mdpi.com/2218-2004/7/1/28/htm
https://doi.org/10.3390/atoms7010028

[11] McDonald, K.T. (2008, August 10) Electromagnetic Fields of a Rotating Shell of Charge. Joseph Henry Laboratories, Princeton University, Princeton.
https://www.google.com/url?sa=t&rct=j&q=&esrc=s&source=web&cd=&ved=2ahUKEwii0fvEyLb9AhXJiO4BHReXBIEQFnoECCUQAQ&url=http%3A%2F%2Fkirkmcd.princeton.edu%2Fexamples%2Frotatingshell.pdf&usg=AOvVaw3nuuv3640EW2oztXV2nNdL

[12] Weisstein, E.W. (2007) Electron Radius. Wolfram Research, Champaign.
https://scienceworld.wolfram.com/physics/ElectronRadius.html

[13] Young, A. (2023) *Journal of Modern Physics*, **14**, 198-207.
https://doi.org/10.4236/jmp.2023.143014

[14] Young, A. (2022) *Journal of Modern Physics*, **13**, 1117-1127.
https://doi.org/10.4236/jmp.2022.137064

[15] NIST (2018) 2018 CODATA Value: Electron Magnetic Moment. The NIST Reference on Constants, Units, and Uncertainty.
https://physics.nist.gov/cgi-bin/cuu/Value?muem

[16] NIST (2018) 2018 CODATA Value: Classical Electron Radius. The NIST Reference on Constants, Units, and Uncertainty. https://physics.nist.gov/cgi-bin/cuu/Value?re

[17] NIST (2018) 2018 CODATA Value: Muon Mass. The NIST Reference on Constants, Units, and Uncertainty. https://physics.nist.gov/cgi-bin/cuu/Value?mmu

[18] NIST (2018) 2018 CODATA Value: Muon Magnetic Moment. The NIST Reference on Constants, Units, and Uncertainty.
https://physics.nist.gov/cgi-bin/cuu/Value?mumum

Journal of Modern Physics, 2023, 14, 562-572
https://www.scirp.org/journal/jmp
ISSN Online: 2153-120X
ISSN Print: 2153-1196

The Complex Field Theory and Mass Formation—An Alternative Model to Higgs Mechanism

Hossin Abdeldayem

NASA-Goddard Space Flight Center, Greenbelt, USA
Email: Hossin.abdeldayem@nasa.gov

How to cite this paper: Abdeldayem, H. (2023) The Complex Field Theory and Mass Formation—An Alternative Model to Higgs Mechanism. *Journal of Modern Physics*, **14**, 562-572.
https://doi.org/10.4236/jmp.2023.145032

Received: February 16, 2023
Accepted: April 14, 2023
Published: April 17, 2023

Abstract

The electromagnetic force, strong nuclear force, weak nuclear force, and gravitational force are the four fundamental forces of nature. The Standard Model (SM) succeeded in combining the first three forces to describe the most basic building blocks of matter and govern the universe. Despite the model's great success in resolving many issues in particle physics but still has several setbacks and limitations. The model failed to incorporate the fourth force of gravity. It infers that all fermions and bosons are massless contrary to experimental facts. In addition, the model addresses neither the 95% of the universe's energy of Dark Matter (DM) and Dark Energy (DE) nor the universe's expansion. The Complex Field Theory (CFT) identifies DM and DE as complex fields of complex masses and charges that encompasses the whole universe, and pervade all matter. This presumption resolves the issue of failing to detect DM and DE for the last five decades. The theory also presents a model for the universe's expansion and presumes that every material object carries a fraction of this complex field proportional to its mass. These premises clearly explain the physical nature of the gravitational force and its complex field and pave the way for gravity into the SM. On the other hand, to solve the issue of massless bosons and fermions in the SM, Higgs mechanism introduces a pure and abstractive theoretical model of unimaginable four potentials to generate fictitious bosons as mass donors to fermions and $W^{\pm}$ and Z bosons. The CFT in this paper introduces, for the first time, a physical explanation to the mystery of the mass formation of particles rather than Higgs' pure mathematical derivations. The analyses lead to uncovering the mystery of electron-positron production near heavy nuclei and never in a vacuum. In addition, it puts a constraint on Einstein's mass-energy equation that energy can never be converted to mass without the presence of dense dark matter and cannot be true in a vacuum. Furthermore, CFT provides different

perspectives and resolves real-world physics concepts such as the nuclear force, Casimir force, Lamb's shift, and the anomalous magnetic moment to be published elsewhere.

Keywords

Quantum Field Theory, Complex Field Theory, Standard Model, Higgs Mechanism, Bosons, Fermions

1. Introduction

The Standard Model (SM) [1] [2] [3] [4], was developed last century by several worldwide scientists and combined three of the four fundamental forces: electromagnetic force, strong nuclear force, and weak nuclear force. The model was a great success in developing the theory of particle physics, where the concepts of quarks [5] [6] [7] and Higgs bosons [8] [9], were introduced. The SM still has several limitations, where it failed to include the fourth fundamental force of gravity, covered neither the 95% of the universe's Dark Energy (DE) and Dark Matter (DM) [10] [11] [12] [13], nor mentioned the expansion of the universe [14] [15] [16]. The Complex Field Theory (CFT) 17 proposed that both DM and DE are complex fields of complex masses and complex charges, encompass the whole universe, and pervade all matter. This presumption explains the reason for failing to detect DM and DE for the last five decades, [18] [19], and presents a physical model for the universe's expansion. The CFT [17] also presumes that every material object carries a fraction of this complex field proportional to its mass, which led to understanding the physical nature of the gravitational force and its complex field. This important presumption paves the way for gravity into the SM. Higgs [8] in 1964 introduced a pure and abstractive theoretical mechanism. His mechanism went through several mathematical manipulations of gauge transformations and symmetry breaking to introduce three fictitious massless Goldston bosons that gave masses to Z and $W^{\pm}$ bosons and a massive fourth boson, which gave masses to fermions. The CFT in this paper provides a physical explanation for the mystery of the mass formation of particles. It shows how real mass can be generated from dark matter-energy interaction through the Mexican hat shape complex potential energy. The theory also offers new perspectives to several outstanding mysteries in physics such as the electron-positron pair production, which takes place only in the vicinity of heavy nuclei, where condensed dark matter is present and never in a vacuum and puts a constraint on Einstein's mass-energy relation ($E = mc^2$) that energy alone cannot generate mass without the presence of a dense dark matter and never in a vacuum. Furthermore, CFT resolves real-world physics concepts such as the nuclear force, Casimir force, Lamb's shift, and the anomalous magnetic moment to be published elsewhere.

2. Discussion

According to the complex field theory (CFT) [8], the whole universe is immersed in an ocean field of complex mass ($i\mu$) and complex charges ($\pm iq$). The field pervades the whole universe, and each material object carries a fraction of the complex mass and the complex charges in proportion to its mass and its velocity:

$$\begin{aligned} \left|i\mu(v,m)\right| &= \kappa(m) = \kappa\left[\Delta m(v) + m_o\right] \\ \left|iq(v,m)\right| &= \delta(m) = \delta\left[\Delta m(v) + m_o\right] \end{aligned} \tag{1}$$

where the absolute value of complex mass "$i\mu(v, m)$" and charge "$iq(v, m)$" on a material object are equal to $k(m_o)$ and $\delta(m_o)$, respectively when the object is at rest and each increases by "$\kappa\Delta m(v)$" and "$\kappa\Delta m(v)$" as the object's speed increases. "m_o" is the rest mass of the object. $\Delta m(v)$ is the relativistic mass increase, where $\Delta m(v) = m - m_o = (\gamma(v) - 1)m_o$, and $\gamma(v) = 1/\sqrt{1-(v/c)^2}$. All positively charged particles and neutral ones carry positive complex charges while negatively charged particles carry negative complex charges. The complex charges on the objects, "$iq(v, m)$" are the source for the gravitational field and the gravitational force between neutral masses. Note that the relativistic speed has a great effect on the mass, traveling with relativistic speed. The speed of a proton at the Large Hadron Collider (LHC) at the European Center for Nuclear Research (CERN) can reach up to ~99.9999991% of the speed of light [20]. Its relativistic mass can reach more than seven thousand times its rest mass and accordingly its complex (dark) mass and complex charge will dramatically increase. The complex field is nonuniformly [8] distributed in the universe. It is highly dense near heavy dynamic nuclei and large masses and lesser dense otherwise. The complex field ($\phi = \varphi_1 + i\varphi_2$) has zero spin and is expressed by the Klein-Gordan equation:

$$\left(\partial^\alpha \partial_\alpha + \mu^2\right)(\phi) = 0 \tag{2}$$

Equation (2) has the discrete plane wave solutions [21]:

$$\begin{aligned} \phi(x) &= \sum_k \left(i/\sqrt{2V\omega_k}\right)\left[a(k)e^{-ik\cdot x} + b^* e^{ik\cdot x}\right] = \phi^+ + \phi^- \\ \phi(x)^* &= \sum_k \left(-i/\sqrt{2V\omega_k}\right)\left[b(k)e^{-ik\cdot x} + a^* e^{ik\cdot x}\right] = \phi^{*+} + \phi^{*-} \end{aligned} \tag{3}$$

Note that ϕ^{*+} is not the complex conjugate of ϕ^+. The corresponding free Lagrangian for Equation (2) is:

$$\mathcal{L} = 1/2\left(\partial_\mu(\phi)\right)^2 - \left[1/2(i\mu)^2(\phi)^2 + (1/4)\lambda(\phi)^4\right] \tag{4}$$

The square bracket term is the intrinsic potential energy "V" due to the complex charges of dark matter:

$$V(\phi) = -1/2\,\mu^2\left(\phi^*\phi\right) + (1/4)\lambda\left(\phi^*\phi\right)^2 \tag{5}$$

The first term in Equation (5) is negative because of the imaginary nature of the complex mass ($\pm i\mu$). The second term is the field self-interaction, and λ is a positive scalar number. This potential energy function takes graphically the shape

of a Mexican hat, shown in Figure 1. The height at the peak is a measure of the potential energy and the complex mass density.

The interaction Lagrangian density is [21]:

$$\begin{aligned}\mathcal{L} = 1/2\left(\partial_\mu(\varphi)\right)^*\left(\partial_\mu(\varphi)\right) - \left[1/2(i\mu)^2(\varphi)^*(\varphi) + (1/4)\lambda\left(\varphi^*\varphi\right)^2\right] \\ + (iq)\left[-\left\{\left(\partial(\varphi)/\partial t\right)(\varphi)^* - \left(\partial(\varphi)^*/\partial t\right)(\varphi)\right\}\right]\end{aligned} \tag{6}$$

The corresponding intrinsic interaction Hamiltonian is:

$$\begin{aligned}H = \sum_k \omega_k\left[a^*(k)a(k) + 1/2 + b^*(k)b(k) + 1/2\right] \\ + q\sum_k \omega_k\left[b^*(k)b(k) - a^*(k)a(k)\right]\end{aligned} \tag{7}$$

Operating the Hamiltonian on a state of scalar particles "ϕ_n" and antiparticles "$\bar{\phi}_n$", then:

$$\begin{aligned}H\left|(\phi_n)(\bar{\phi}_n)\right\rangle = \left\{\sum_k \omega_k\left[a^*(k)a(k) + 1/2 + b^*(k)b(k) + 1/2\right]\left|(\phi_n)(\bar{\phi}_n)\right\rangle\right. \\ \left. - q\sum_k \omega_k\left[a^*(k)a(k) - b^*(k)b(k)\right]\left|(\phi_n)(\bar{\phi}_n)\right\rangle\right\}\end{aligned} \tag{8}$$

$$\begin{aligned}H\left|(\phi_n)(\bar{\phi}_n)\right\rangle = \omega_n(n+\bar{n})\left|(\phi_n)(\bar{\phi}_n)\right\rangle - q\omega_n(n-\bar{n})\left|(\phi_n)(\bar{\phi}_n)\right\rangle \\ + 1/2\sum_k \omega_k\left|(\phi_n)(\bar{\phi}_n)\right\rangle + 1/2\sum_k \omega_k\left|(\phi_n)(\bar{\phi}_n)\right\rangle\end{aligned} \tag{9}$$

The first term indicates that as the number of particles and antiparticles increases the energy increases. The second term indicates that the energy depends on the particle numbers of the positive particles and the negative antiparticles. This means that for a neutral system the term average to zero energy contribution. The third and fourth terms are the zero-point energies for particles and antiparticles. These terms either grow to infinite energies or it is a virtual and not real [21].

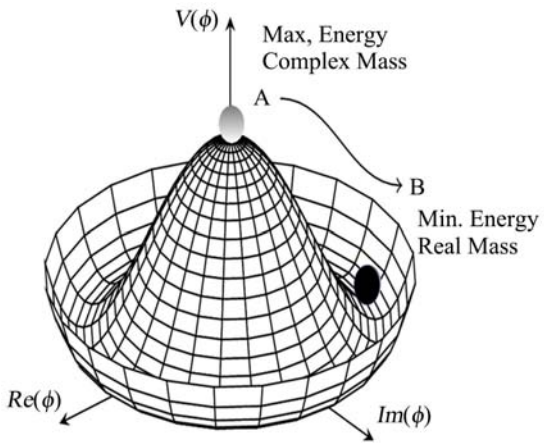

Figure 1. The Mexican hat representation of the potential energy of the complex field at every point in space.

3. Mass Formation

The Lagrangian in Equation (6) is a gauge invariant Lagrangian under global symmetry and at certain conditions, it has a local symmetry and gauge transformation as will be illustrated in special cases below. The height of the potential energy varies from one point to another depending on the potential energy level of the complex mass at the vertex. The force acting on the complex mass at any point in space is the gradient of the potential energy in Equation (5):

$$F_\alpha = -\partial_\alpha V(\varphi) = \mu^2 \varphi_\alpha - \lambda \varphi_\alpha^3 \tag{10}$$

The derivative of the potential energy $V(\varphi)$ at maximum = 0. This leads to:

$$\varphi = \pm \mu / \sqrt{\lambda} \tag{11}$$

Note that Higgs boson's mass of 125 GeV/c^2 was detected at a potential energy of 246 GeV to estimate $\lambda = 0.12$, where $\varphi = \pm \mu / \sqrt{2\lambda}$. In our case, to generate Z and W$^\pm$ of 90 GeV/c^2 and 80 GeV/c^2, respectively, the corresponding potential energy should be 177.1 GeV and 157.4 GeV and $\lambda = 3.87$, using Equation (11). This 157.4 GeV is the energy level for the conversion of up and down quarks to transform a proton to a neutron and vice versa.

The vertex of the Mexican hat potential energy "$V(\varphi)$" is always positive and the corresponding force is negative, which acts as a pulling attractive force for the complex mass ($i\mu$) towards the vertex, causing its buildup at the vertex. The buildup of the complex mass under the external force causes the instantaneous formation of massless particles starting from the tiniest elementary ones to the largest composite particles till the external force is fully exhausted. The complex massless particle at the vertex then rolls downhill as real mass to the bottom of the Mexican hat. In other words, the necessary conditions for real mass formation are the simultaneous presence of energy and complex mass.

This physical sequence of events is a must for the conversion of complex mass to real mass. This explains the outstanding mystery of why electron-positron production only takes place in the vicinity of massive nuclei, where dense complex mass exists, and the energy in Einstein's energy-mass Equation ($E = mc^2$) cannot generate mass in a vacuum without the presence of a dense complex mass, regardless of how high the energy might be.

In quantum electrodynamics, the energy density of the complex fields is:

$$u = (1/8\pi)\left[(iE)^* \cdot (iD) + (iB)^* \cdot (iH)\right] \tag{12}$$

Ignoring the magnetic effect for simplicity, the change in the energy density is:

$$\Delta u = \Delta\varepsilon\left(E^2/8\pi\right) \tag{13}$$

According to the first law of thermodynamics, this energy density should be balanced by work, which causes the complex mass to move toward the vertex.

The work per unit volume is:

$$w = p(\Delta V/V) = -p\left[\Delta(i\rho)/(i\rho)\right] \tag{14}$$

where "p" is the induced pressure and "$\Delta(i\rho)$" is the change in the complex mass

density. From (13) and (14),

$$p = -\rho\left(\Delta\varepsilon/\Delta\rho\right)\left(E^2/8\pi\right) = -\zeta\left(E^2/8\pi\right) \tag{15}$$

So, the pressure is also negative at the vertex in agreement with the pulling force in Equation (10) and "ζ" is the electrostrictive coefficient. The earlier claim that massive bosons (Z and $W^{\pm}$) are created from a vacuum does not fully explain the full story of the physics that is taking place at the vertex.

3.1. Bosons and the Complex Field Theory

As mentioned earlier, the SM presumes that all bosons are massless although nature tells otherwise. The conclusion is based on the use of Proca Lagrangian for the vector potential:

$$\mathcal{L} = -\left(1/16\right)F^{\alpha\beta}F_{\alpha\beta} + \left(m^2/8\pi\right)A^{\alpha}A_{\alpha} \tag{16}$$

where "A_{α}" is the vector potential field and α = 0, 1, 2, and 3. It is represented by the special orthogonal rotation group SO(3) and a spin = 1. For "A_{α}" to be a gauge invariant, the symmetry of the mass term in Equation (16) under the local transformation ($A_{\alpha} + \partial_{\alpha}\rho$) is examined, where $\rho = \rho\left(t, x, y, z\right)$:

$$m^2 A^{\alpha} A_{\alpha} \to m^2\left(A^{\alpha} + \partial\rho\right)\left(A_{\alpha} + \partial\rho\right) \tag{17}$$

Expanding the right side to the first order in $\partial\rho$:

$$m^2 A^{\alpha} A_{\alpha} \to m^2 A^{\alpha} A_{\alpha} + 2m^2 A^{\alpha}\partial\rho \neq m^2 A^{\alpha} A_{\alpha} \tag{18}$$

The transformation is not a gauge invariant unless

$$m^2 A^{\alpha}\partial\rho = 0 \tag{19}$$

Because both "$\partial\rho$" and "A" cannot be zeros, the mathematical convenience leads the standard model to let the mass m = 0 for all bosons although it is contrary to the experimental facts.

Instead of doubting the mathematical approach, the model denied the fundamental reality of nature. Higgs mechanism proposed mathematical gauge transformations and symmetry breaking to produce a set of fictitious massless bosons that give masses to the massive bosons, which are difficult to visualize physically. The different approach, taken by the CFT, reevaluates these mathematical models. It proves physically that the complex mass plays a major role in giving mass to massive bosons and explains that massless photons and gluons should be massless as follows:

$$m \to m + i\mu \tag{20}$$

$$A \to A + ia \tag{21}$$

Then

$$m^2 A^2 \to \left(m + i\mu\right)\left(m - i\mu\right)\left(A + ia\right)\left(A - ia\right) = \left(m^2 + \mu^2\right)\left(A^2 + a^2\right)$$

Applying again the same gauge transformation:

$$\begin{aligned} A &\to A + \partial R \\ a &\to a + \partial\rho \end{aligned} \tag{22}$$

Then

$$\begin{aligned} m^2A^2 &\to \left(m^2+\mu^2\right)\left(A^2+a^2\right) \\ &\to \left(m^2+\mu^2\right)\left[\left(A+\partial R\right)^2+\left(a+\partial\rho\right)^2\right] \\ &= \left(m^2+\mu^2\right)\left[\left(A^2+a^2\right)+2\left(A\partial R+a\partial\rho\right)+\left(\partial R\right)^2+\left(\partial\rho\right)^2\right] \end{aligned} \tag{23}$$

Keeping only the first order of (∂R) and ($\partial\rho$), then

$$\begin{aligned} m^2A^2 &\to \left(m^2+\mu^2\right)\left(A^2+a^2\right) \\ &\to \left(m^2+\mu^2\right)\left(A^2+a^2\right)+2\left(m^2+\mu^2\right)\left(A\partial R+a\partial\rho\right) \\ &\neq \left(m^2+\mu^2\right)\left(A^2+a^2\right) \end{aligned} \tag{24}$$

So, the transformation is a gauge invariant transformation only if

$$\left(m^2+\mu^2\right)\left(A\partial R+a\partial\rho\right)=0 \tag{25}$$

This means that either

$$m=\pm i\mu$$

or

$$A\partial R=-a\partial\rho$$

Nature tells us that massive bosons should have mass. The first option is unacceptable but the second one is the choice, which tells that the vector potential of the real charge times its variation should balance the equivalent potential of the complex charge times its variation and of negative magnitude.

The vector potential field for a massive boson is [21]:

$$A_\alpha = 1/\left(2\pi\right)^3\int \mathrm{d}^3k\left\{\left(1/\sqrt{2\omega_k}\right)\sum_{j=1}^{3}\left[\varepsilon_\alpha^j\left(k\right)a_j\mathrm{e}^{-ikx}+\varepsilon_\alpha^{j^*}\left(k\right)a_j^+\mathrm{e}^{ikx}\right]\right\} \tag{26}$$

where the basis for the polarization vectors "ε_α" can be aligned along the axes for simplicity and take the values (1, 0, 0, 0), (0, 1, 0, 0), (0, 0, 1, 0), and (1, 0, 0, 0). "a" and "a^+" are the annihilation and creation operators.

On the other hand, massless photons induce pure real vector potential "A" and massless gluons induce equivalent complex fields "iA" due to the complex charges on the subnuclear particles. Let us assume first that both photons and gluons have mass "m" and carry the complex mass "$i\mu$", then for the photons:

$$m^2A^2=\left(m^2+\mu^2\right)\left(A\right)^2 \tag{27}$$

And for the gluons, also:

$$m^2A^2=\left(m^2+\mu^2\right)\left(iA\right)\left(-iA\right)=\left(m^2+\mu^2\right)\left(A^2\right) \tag{28}$$

Both (27) and (28) are the same. Now, applying the gauge transformations on the photons and the gluons:

$$\begin{aligned} &A\to A+\partial R \\ &\text{or} \\ &A\to iA+i\partial R \end{aligned} \tag{29}$$

Applying the gauge transformation on photons and keeping only the first order of ∂R, then

$$\begin{aligned} m^2A^2 &\to \left(m^2+\mu^2\right)\left(A+\partial R\right)^2 \\ &= \left(m^2+\mu^2\right)\left(A^2+2A\partial R\right) \neq \left(m^2+\mu^2\right)A^2 \end{aligned} \tag{30}$$

Applying the gauge transformation on gluons and keeping only the first order of ∂R, then

$$\begin{aligned} m^2A^2 &\to \left(m^2+\mu^2\right)\left(iA+i\partial R\right)\left(-iA-i\partial R\right) \\ &= \left(m^2+\mu^2\right)\left(A^2+2A\partial R\right) \neq \left(m^2+\mu^2\right)A^2 \end{aligned} \tag{31}$$

This means that the transformation is a gauge invariant only if

$$\left(m^2+\mu^2\right)\left(2A\partial R\right)=0 \tag{32}$$

This means that either

$$\begin{aligned} &m=\pm i\mu \\ &\text{or} \\ &A=0 \\ &\text{or} \\ &\partial R=0 \end{aligned} \tag{33}$$

Since neither A nor ∂R cannot be zeros, the only option is that both photons and gluons are massless but carry pure complex mass "$\pm i\mu$". This agrees with the complex field theory assumption [17], which says that photons and gluons carry infinitesimal pure imaginary mass in proportion with their momenta.

The vector potential field for massless boson is [21]:

$$A_\alpha = 1/(2\pi)^3 \int \mathrm{d}^3k \left\{ \left(1/\sqrt{2\omega_k}\right) \sum_{j=1}^{2} \left[\varepsilon_\alpha^j(k) a_j \mathrm{e}^{-ikx} + \varepsilon_\alpha^{j*}(k) a_j^+ \mathrm{e}^{ikx} \right] \right\} \tag{34}$$

Note that it takes the same form as that for the massive boson except the sum is over 2 for the only two possible polarizations.

3.2. Fermions and the Complex Field Theory

Dirac equation

$$i\hbar\left(\partial\psi/\partial t\right)+i\hbar c\left(\alpha\cdot\nabla\psi\right)=\beta mc^2\psi \tag{35}$$

Using the natural units (c = $\hbar$ = 1), and considering only the time and the x-components then:

$$i\left(\partial\psi/\partial t\right)+i\alpha\left(\partial\psi/\partial x\right)=m\beta\psi \tag{36}$$

Which can also be expressed as [22]:

$$\begin{aligned} i\left(\partial\psi^L/\partial t\right)+i\alpha\left(\partial\psi^L/\partial x\right)&=m\beta\psi^L \\ i\left(\partial\psi^R/\partial t\right)+i\alpha\left(\partial\psi^R/\partial x\right)&=m\beta\psi^R \end{aligned} \tag{37}$$

where ψ^L and ψ^R are the left-handed and right-handed spinning relative to the particle's momentum.

Using the matrices representation of

$$\alpha^i = \begin{pmatrix} 0 & \sigma^i \\ \sigma^i & 0 \end{pmatrix}$$

and

$$\beta = \begin{pmatrix} I & 0 \\ 0 & -I \end{pmatrix} \tag{38}$$

β matrix acting on ψ switches its spinning orientation from left to right and vice versa. Equation (38) becomes:

$$\begin{aligned} i\left(\partial\psi^L/\partial t\right) + i\alpha\left(\partial\psi^L/\partial x\right) &= m\psi^R \\ i\left(\partial\psi^R/\partial t\right) + i\alpha\left(\partial\psi^R/\partial x\right) &= m\psi^L \end{aligned} \tag{39}$$

The mixing between the right-handedness and left-handedness in each of the equations above violates the weak charge conservation law, where the right-handed fermions (positive chirality) have weak isospin singlets ($I = I3 = 0$) while the left-handed fermions (negative chirality) have a weak isospin doublet ($I = 1/2$ and $I3 = \pm 1/2$). This mixing of left and right-handedness leads the standard model, again for mathematical convenience, to conclude that all fermions are massless. The CFT reevaluates the standard model presumption, by introducing a quartet mass matrix operator of the real mass and its complex mass along with the corresponding antimatters. The CFT considers antimatter as a substance of negative mass equal in magnitude and of opposite charge to the real matter. This consideration confirms the original definition of Dirac [23] [24], regarding electron-hole production, where the hole as an antimatter to the electron is of negative mass and has a positive charge. Note that the complex dark charges on matter and antimatter are opposite to each other and induce a real positive repelling force on each other. This repulsive gravitational force causes antimatter to behave as a substance with a negative mass to matter. The quartet mass matrix operator is:

$$M = \begin{pmatrix} m_1 & 0 & 0 & 0 \\ 0 & im_2 & 0 & 0 \\ 0 & 0 & -m_1 & 0 \\ 0 & 0 & 0 & -im_2 \end{pmatrix} = \begin{pmatrix} M_m & 0 \\ 0 & -M_m \end{pmatrix} \tag{40}$$

Dirac spinor:

$$\psi = \begin{pmatrix} \psi^1 = \text{particle} \\ \psi^2 = \text{Antiparticle} \\ \psi^3 = +\text{spin} \\ \psi^4 = -\text{spin} \end{pmatrix} \tag{41}$$

Using (39), (40), and (41), then,

$$\begin{aligned} i\left(\partial\psi^R/\partial t\right) + i\alpha\left(\partial\psi^R/\partial x\right) &= M_m\psi^R \\ i\left(\partial\psi^L/\partial t\right) + i\alpha\left(\partial\psi^L/\partial x\right) &= M_m\psi^L \end{aligned} \tag{42}$$

Equation (42) shows that the quartet concept of dark matter eliminated the mixing of right and left-handedness, preserved the mass for fermions, and conserved the law of weak charges unviolated.

4. Conclusion

The root origin for mass formation for particles has been discussed as due to the simultaneous presence of energy and complex mass. Energy alone is not enough to produce mass in the famous Einstein's Equation ($E = mc^2$) but a dense complex mass must be present. The outstanding mystery of why electron-positron pair production only takes place near heavy nuclei is now resolved where dense complex mass is present and never can take place in a vacuum. The current claim that Z and $W^{\pm}$ bosons are created from a vacuum is a wrong claim but a dense complex mass plus energy must be simultaneously present.

Conflicts of Interest

The author declares no conflicts of interest regarding the publication of this paper.

References

[1] Glashow, S. (1959) *Nuclear Physics*, **10**, 107. https://doi.org/10.1016/0029-5582(59)90196-8

[2] Salam, A. and Ward, J.C. (1959) *Nuovo Cimento*, **11**, 568-577. https://doi.org/10.1007/BF02726525

[3] Weinberg, S. (1967) *Physical Review Letters*, **19**, 1264-1266. https://doi.org/10.1103/PhysRevLett.19.1264

[4] Oerter, R. (2006) The Theory of Almost Everything. https://www.google.com/books/edition/The_Theory_of_Almost_Everything/KAMlsa8jjt4C?hl=en&gbpv=1&dq=r.+oerter+(2006).pdf&pg=PT2&printsec

[5] Kennedy, E. (2012) Particle Physics. InTech, Rijeka. http://www.issp.ac.ru/ebooks/books/open/Particle_Physics.pdf

[6] Hill, C.T. (2020) *Physics Today*, **73**, 63. https://doi.org/10.1063/PT.3.4480

[7] Leutwyler, H. (2008) Physics of the Light Quarks. https://arxiv.org/pdf/0808.2825v1.pdf

[8] Higgs, P.W. (1964) *Physical Review Letters*, **13**, 508-509. https://doi.org/10.1103/PhysRevLett.13.508

[9] Hill, C.T. (1977) Higgs Scalars and the Nonleptonic Weak Interactions. https://thesis.library.caltech.edu/4505/1/Hill_ct_1977.pdf

[10] NASA Science Universe—Dark Energy, Dark Matter. https://en.wikipedia.org/wiki/Dark_matter

[11] Biello, D. (2006, August 28). What Are Dark Matter and Dark Energy, and How Are They Affecting the Universe? *Scientific American*. https://www.scientificamerican.com/article/what-are-dark-matter-and

[12] Chu, M.-C. (2022, March) Dark Matter. Hong Kung Laureate Forum. https://hklaureateforum.org/en/dark-matter?gclid=Cj0KCQiAgOefBhDgARIsAMhqXA74TMWFQnO4E9ROJ7MvVyeJ64q_Oikd26L7GxXbjjrmH2AQt9AgQNkaAnq7EALw_wcB

[13] Trimble, V. (1987) *Annual Review of Astronomy and Astrophysics*, **25**, 425-472. https://doi.org/10.1146/annurev.aa.25.090187.002233

[14] Hubble's Exciting Universe: Measuring the Universe's Expansion Rae. https://hubblesite.org/hubble-30th-anniversary/hubbles-exciting-universe/measuring-the-universes-expansion-rate

[15] Irani, A. (2023) *Gravitation and Cosmology*, **9**, 210-215.

[16] Greshko, M. (2021, December) The Universe Is Expanding Faster than It Should Be. https://www.nationalgeographic.com/science/article/the-universe-is-expanding-faster-than-it-should-be

[17] Abdeldayem, H. (2022) *Current Trends in Physics*, **1**, 101. https://doi.org/10.29011/CTP-101.100001

[18] Perlmutter, S., Aldering, G., Goldhaber, G., Knop, R.A., Nugent, P., *et al.* (1999) *The Astrophysical Journal*, **517**, 565. https://doi.org/10.1086/307221

[19] Riess, A.G., Filippenko, A.V., Challis, P., Clocchiatti, A., Diercks, A., *et al.* (1998) *The Astronomical Journal*, **116**, 1009. https://doi.org/10.1086/300499

[20] CERN, the European Organization for Nuclear Research. https://public-archive.web.cern.ch/en/lhc/Facts-en.html

[21] Kalauber, R. (2013) Student Friendly Quantum Field Theory. Sandtrove Press, Fairfield.

[22] Eddie Boyes. https://www.youtube.com/watch?v=CNcTOSx2eMs

[23] Dirac, P. (1927) *Proceedings of the Royal Society of London. Series A*, **114**, 243-265.

[24] Kittel, C. (1986) Introduction to Solid State Physics. 6th Edition, John Wiley & Sons, Inc., Hoboken, 193.

Journal of Modern Physics, 2023, 14, 573-582
https://www.scirp.org/journal/jmp
ISSN Online: 2153-120X
ISSN Print: 2153-1196

How Dark Energy Might Be Produced by Black Holes

Eugene Terry Tatum

Independent Researcher, Bowling Green, KY, USA

Email: ett@twc.com

How to cite this paper: Tatum, E.T. (2023) How Dark Energy Might Be Produced by Black Holes. *Journal of Modern Physics*, **14**, 573-582.
https://doi.org/10.4236/jmp.2023.145033

Received: March 7, 2023
Accepted: April 15, 2023
Published: April 18, 2023

Abstract

If confirmed, the new galactic observations in support of rapidly growing supermassive black holes in association with their production of dark energy may provide for a quantum leap forward in our understanding of black holes, dark energy, and universal expansion. The primary implication of these observations is that growth of black holes may well be coupled with universal expansion ("cosmological coupling"). Study of the Flat Space Cosmology (FSC) model, in conjunction with these new observations, suggests a novel mechanism of "black hole dark energy radiation". This brief note gives a rationale for how the high gravitational energy density vacuum within or adjacent to a black hole horizon could be sufficiently energetic to pull entangled pairs of positive matter energy particles and negative dark energy "particles" of equal magnitude out of the horizon vacuum and send them off in opposite directions (*i.e.*, gravitationally-attractive matter inward and gravitationally-repelling dark energy outward). One effect would be that a black hole can rapidly grow in mass-energy without mergers or the usual accretion of pre-existing matter. A second effect would be continual production of dark energy within the cosmic vacuum, fueling a continuous and finely-tuned light-speed expansion of the universe.

Keywords

Astrophysics: Galaxies, Black Holes, Dark Energy, Vacuum Energy, Cosmological Coupling, Flat Space Cosmology, *ER = EPR*, Gravitized Vacuum, Dark Matter, Hawking Radiation

1. Introduction and Background

Physical theories are often based upon symmetries. In the theory of cosmic inflation, for instance, there is a symmetry between the vacuum and matter. A pre-

sumed primordial high energy vacuum reaches a critical point where elementary particles of matter and radiation are nearly instantaneously created within the vacuum. Whether or not inflation actually occurred as a remarkably sudden and explosive one-time process in the first 10^{-32} second of cosmic time, the theory at least entertains the possibility of a symmetry between the vacuum and matter.

The exact conditions of the earliest universe are shrouded in mystery for two important reasons. Firstly, we can only currently observe back to the cosmic microwave background (CMB) emission event (*i.e.*, the "recombination epoch"), which was some thousands of years after the Big Bang. Although it may be possible someday to detect gravitational waves of the earlier universe, that remains to be seen. Secondly, there are no Earth laboratories which can simulate the presumed high gravitational energy density environment of the early universe. In fact, there is only one place we can even look to for study of the highest gravitational energy densities in the universe we see today: the vicinity of black hole (BH) horizons. So, it goes without saying, what exactly occurs within the black hole horizon and its adjacent vacuum is currently poorly understood. The high energy density vacuum in such locations is likely to be full of surprises. As with current theories of inflation, we can only guess at what symmetries may exclusively reveal themselves in the vicinity of a BH horizon. Following the examples of inflationary theory and Hawking radiation, the symmetry theory presented herein contains something familiar: A likely intimate relationship, under high energy conditions, between vacuum energy and matter.

In the Flat Space Cosmology model (FSC) [1] [2] much is made of the "cosmological coincidence problem". This problem is due to the remarkable fact that the average cosmic densities of total matter energy and dark energy (*i.e.*, cosmic vacuum energy) are observed and calculated to be the same order of magnitude, with each representing slightly less than one nanojoule of energy per cubic meter of the cosmic vacuum. While current consensus is that the energy density partition of the universe is now approximately 32% total matter energy and 68% dark energy, it should be remembered that, in just the last decade, these numbers have already changed from a previous consensus of about 28% total matter energy and 72% dark energy. It remains entirely possible that the current numbers will converge even further. FSC predicts, largely from spatial flatness observations, that these two percentage numbers will ultimately continue to converge towards 50% total matter energy and 50% dark energy [3] [4].

Regardless of which cosmological model (inflationary cosmology or FSC) one favors at the present time, the "cosmological coincidence problem" is in need of an explanation. Frankly, one is sorely tempted to ask the following question:

"Are matter and dark energy possibly symmetry partners?"

The Preface to *Flat Space Cosmology—A New Model of the Universe* (the first listed reference) puts the relevant questions as follows:

"Are matter energy and dark energy within a scaling cosmic vacuum possibly two sides of the same cosmological coin? Could a continuous link between cosmic vacuum energy density and matter energy density have something to do

with quantum nonlocality through instantaneous (*i.e.*, faster than light!) conservation of cosmic energy? We suspect this may be the case in our matter-generating quintessence model. If so, it would not be the first time that matter and energy were found to be deeply interconnected."

New observations have just been reported from a study of the growth in mass of supermassive black holes in elliptical galaxies with redshifts ranging from $0 < z < 2.5$ [5]. Using criteria for coupling of BH mass growth with universal expansion over approximately 9 billion years of cosmic time, they found evidence for such cosmological coupling. There was the expected redshift dependence of the mass growth, and the BH cosmological contribution was interpreted as being in the form of vacuum energy. Furthermore, BH production gave the value of Ω_Λ measured by the 2020 Planck collaboration. Based upon their findings, they proposed that *stellar remnant black holes are the astrophysical origin of dark energy*.

In light of the above background of theory and observations, the purpose of this brief note is to present and discuss a novel theory of a possible symmetry occurring within and adjacent to high gravitational energy density BH horizons.

2. A Theory of Black Hole Dark Energy Radiation

The reader is referred to Figure 1 for a schematic illustration of how black hole dark energy radiation might work. Curve H represents a BH horizon. The paired arrows represent entangled particle pairs of an electrically-neutral matter particle NM (inwardly-attracted arrow) and a unit (*i.e.*, "particle") of dark energy DE (outwardly-repelled arrow) of equal and opposite-sign energy compared to its matter partner. FSC uses a convention wherein the gravitationally-attracting matter partner energy is "positive" and its gravitationally-repelling dark energy partner is "negative." Their combined virtual particle energy within the vacuum is presumed to add to zero.

Figure 1 illustrates two examples of the proposed particle interaction at or near every energetic black hole horizon. The weak theoretical Hawking radiation interaction is omitted for clarity. The ingested matter adds to the total matter energy and entanglement entropy of black hole BH, causing it to enlarge by an increment of mass and radius corresponding to the energy and entropy added to the BH. Meanwhile, the entangled dark energy partner "particle" is repelled from the BH horizon, owing to the negative sign of its energy. Thus, the negative

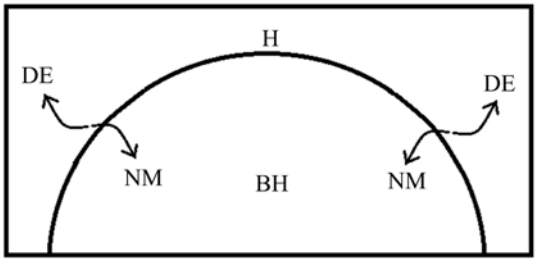

Figure 1. Black hole dark energy radiation (outward) and matter absorption (inward).

energy and the entropy added to the vacuum *balances* the vacuum's loss of potential matter energy among the virtual particles of the high gravitational energy vacuum in the vicinity of the BH horizon. By adding negative energy and entropy to the vacuum, the entangled dark energy partner to the ingested matter particle increases the total dark energy and entropy of the cosmic vacuum, as represented by increasing the surface area (*i.e.*, "gravitational" or "entanglement" entropy) of the cosmic BH horizon in proportion to the BH growth described above. In this manner, black holes embedded within their cosmic parent BH (*i.e.*, our universe) are *cosmologically coupled* to the universe expansion, without violating conservation of energy of the net zero energy FSC universe. At the same time as the FSC universe increases in total positive mass-energy, its total negative dark energy increases negatively by the same amount. The rationale for this type of net zero energy accounting within the cosmic vacuum was anticipated by the mathematical formalism of Dirac, and is more fully described in the third reference. The third figure of that reference is particularly illustrative.

Furthermore, in keeping with the theories known as *ER* = *EPR* and the Holographic Principle [6], what goes on in the bulk is presumably completely encoded within the cosmic BH horizon ("boundary") surface area, which represents the total entropy of the FSC universe (following the Bekenstein-Hawking BH entropy formula, $S = \pi r^2 / l_p^2$). Each square entropy microstate tile in the current FSC horizon is assumed to have sides of two Planck lengths, totalling to 10^{120} such tiles filling the surface area of the *current* FSC BH universe horizon.

3. Discussion

One can readily see from the above theoretical description that, despite the fact that the total matter energy and dark energy continually increase as the universe expands, their average *densities* within the increasing bulk volume *continually decrease*. In the FSC model, the average vacuum energy density following the Big Bang continually decreases, as the universe expands, by roughly 120 base ten logs (*i.e.*, 10^{120}) while the cosmic radius increases roughly 60 base ten logs (*i.e.*, 10^{60}) from the Planck scale epoch to the present. Thus, the FSC quintessence BH universe model's current vacuum energy density of about 10^{-9} joule per cubic meter is lower than the Planck scale epoch vacuum energy density calculated by quantum field theorists by a factor of approximately 10^{120}. One can readily see that there is no "cosmological constant problem", because Λ in the FSC model continually correlates with *inverse* cosmic entropy. This can only happen in a realistic quintessence model such as FSC. This has been shown in several prior FSC publications.

If the new observations of cosmologically-rapid BH growth hold up, the novel BH dark energy radiation theory presented herein would help to resolve a number of current cosmological conundrums. When applied to the FSC model, the nature of cosmic expansion dark energy becomes more understandable. Vacuum energy density, due to its inverse relationship with total cosmic entropy, appears

to continually drive a *finely-tuned* expansion of the universe in the forward time direction. This is the "entropic arrow of time." As described above, the "cosmological coincidence" and "cosmological constant" problems can be resolved. Furthermore, the BH holographic principle allows for information in the bulk of black holes of all sizes to be separately encoded in the horizon surface. Thus, as the universe grows, its black holes grow.

If the new observations can be confirmed and generalized, black holes should be continually coupled with universal expansion. They would *not* be expected to evaporate, as envisioned by Hawking! He envisioned BH ingestion of a *negative* energy partner, with corresponding evaporative decrease of BH mass and radius. What is presented herein is essentially a statistically more likely opposite radiative process, now that we have a better understanding of dark energy, which was unknown to Hawking at the time of his particular BH radiation proposal. Thus, astrophysicists would now have a new explanation for rapid BH growth in the early universe which does not entirely rely upon mergers and ongoing accretion of nearby matter. Instead, cosmologically rapid BH growth can, in effect, be *pulled* out of the cosmic vacuum, even if it *appears* to be empty of matter. Einstein's $E = mc^2$ insures this to be the case when the BH-adjacent vacuum is highly-energized, as it certainly must be. Furthermore, BH horizon-encoded information is not lost forever in BH interiors. Accordingly, there should be no "BH information paradox" to worry about. This BH holographic solution has been well-described by theorist Leonard Susskind [7].

It has long been theorized by Roger Penrose [8] that black holes are huge repositories of cosmic entropy, as defined by Bekenstein and Hawking. Hawking and Penrose's cosmological work [9] seemed to imply that our universe could behave in some fashion like a time-reversed BH. This concept inspired creation of the FSC model after Planck satellite observations appeared to support it. However, with the newly-reported observations of Farrah, *et al.*, in conjunction with the novel BH theory presented herein, a concept of BH time-reversal no longer appears to be absolutely necessary for FSC modelling. Somewhat like an infinite series of Russian (Matryoshka) dolls, our BH-like universe might simply be part of a temporally-infinite, fractal-like, hierarchy of BH-producing "parent" and "child" universes, as recently theorized [10] [11].

FSC has now been shown in numerous peer-reviewed physics and cosmology journal publications to be a viable cosmological model which follows general relativity with respect to what we know or suspect about black holes. A summary publication of comparisons made between FSC and the current inflationary standard model (ΛCDM) has identified eleven different categories where FSC appears to be superior [12].

With respect to the accumulated supernovae data (SNe), **Figure 2** is self-explanatory. It should be noted in this figure, first compiled and published by Ned Wright in 2015 with respect to the work of Betoule, *et al.* [13], that FSC, as a Flat Dark Energy Model, closely approximates the solid purple curve, upon which the *observational* blue dashed curve ("Evolving SNe") is *superimposed* (!). Given

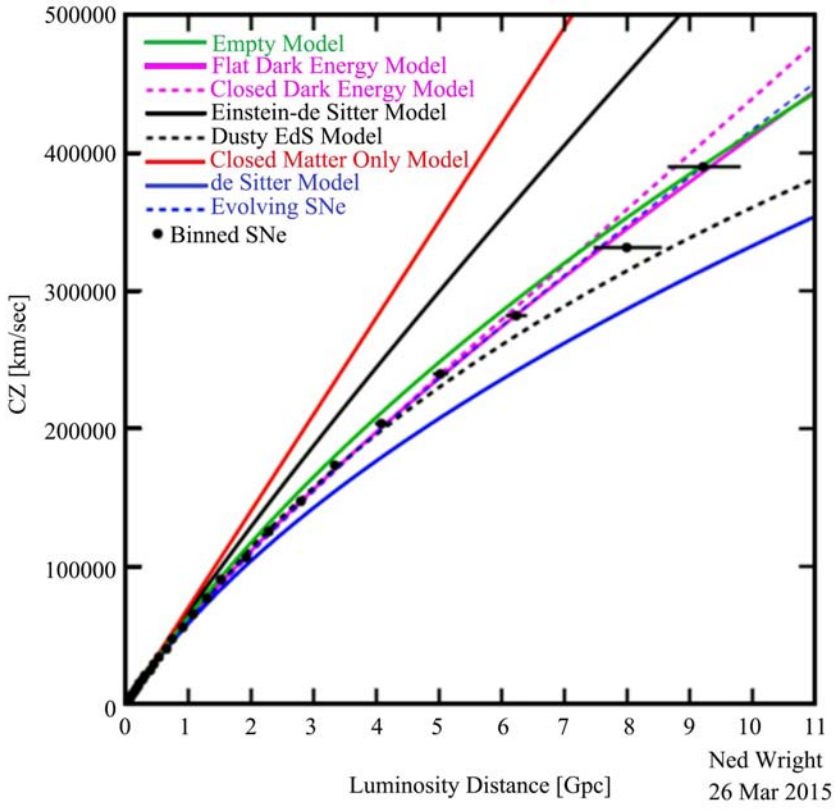

Figure 2. Universe models and SNe Data (FSC corresponds to the solid purple curve).

the accumulated type Ia supernovae data, even a realistic Milne-type finely-tuned "Empty Model" (the solid green curve of a perpetually-balanced net zero energy universe model, also like FSC) cannot yet be ruled out. Given the error bars shown, one does not need to be an expert in statistics to interpret the extremely close correlation between the accumulated SNe data and the Flat Dark Energy and Empty models. It would be foolish, at present, to rule out the possibility that we live in an FSC-like BH universe.

The 4-axis FSC log graph in Figure 3 [14] shows how total matter mass (baryonic plus dark matter) of the FSC BH cosmological model relates to cosmic time.

One can readily see that the FSC model matter mass-energy *grows steadily* with cosmological time moving in the forward direction. Given the fractal-like nature of such a model, it is not entirely surprising to see that individual black holes can copy this behavior in proportion to growth of the cosmological system as a whole. It is notable that, in the preceding roughly 13 billion years, the FSC model grows in total matter mass by a factor of ten (*i.e.*, one base ten log value). Similarly, over the last roughly 9 billion years, the oldest black holes in the new observational study were "observed" (actually predicted) to grow by about the same amount, assuming that the differently-aged galaxies chosen for study were representative of elliptical galaxy growth between the different time intervals chosen for study. At the time of the FSC book publication (June, 2021), it was

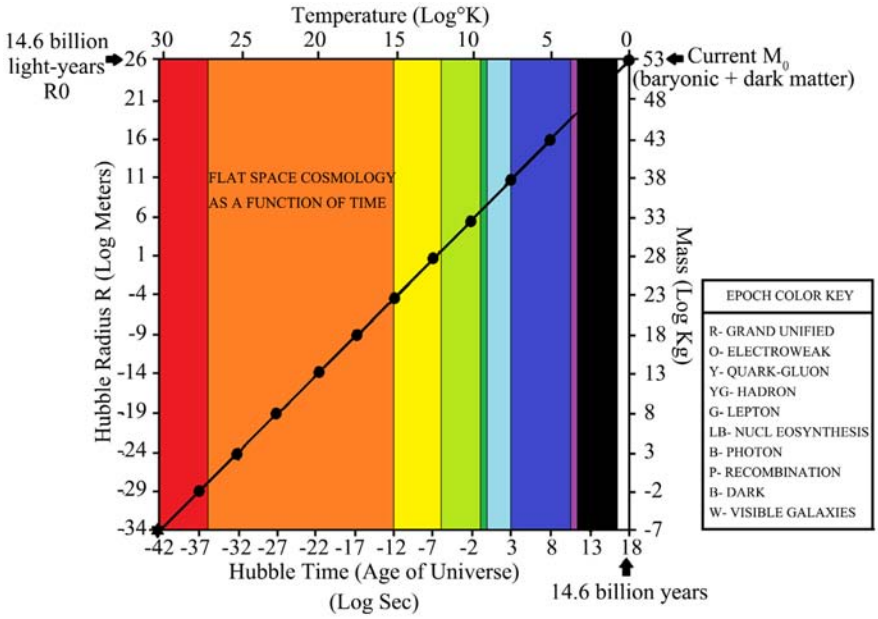

Figure 3. Flat space cosmology vs. time (Color-Coded Cosmic Epochs).

not known by what mechanism a BH model such as FSC could *simultaneously* grow in total matter mass-energy and total dark energy. Given the new observational study results, the present theory of BH dark energy production and BH mass-energy growth now seems entirely plausible as such a mechanism. Further observational studies along similar lines are eagerly anticipated.

A potential side benefit of considering the gravitational energy density of a high energy portion of the vacuum of space is what it may also suggest in regards to dark matter observations. A "gravitized vacuum" concept, as recently introduced [15], could lead to a viable alternative theory to the popular non-particulate MOND theory of dark matter. Thus, consideration of the possible effects of energized vacuum regions (proximal to black holes and to densely-packed galaxies) could open the way to understanding dark matter observations in addition to those pertaining to dark energy. These concepts pertaining to energized vacuum effects, as introduced recently and herein, suggest that the observational and theoretical landscape is now rich with opportunities! Treatment of cosmic vacuum energy density as a perpetual post-inflationary *constant* (as opposed to a spacetime-dependent *scalar* over cosmic time) may soon become a thing of the past. This comports with recent speculation by a number of theorists, including the current author, that many of the answers concerning cosmological conundrums may lie in a deeper physical understanding of the cosmic vacuum.

Not only does Penrose's concept of "gravitational entropy" and his "Weyl curvature hypothesis" seemingly apply to the Bekenstein-Hawking definition of BH entropy and the FSC model [16], but Verlinde's concept of "emergent gravity" (having to do with cosmic entropy and it's possible relationship to gravity) [17] [18] and Van Raamsdonk's concept of "entanglement entropy" from studies

of quantum entanglement [19] could conceivably apply as well. Without further discussion on these points, the reader is referred to the attached references exploring these concepts.

With all that has been presented and speculated above, a final word of caution is necessary. This author is in full agreement with Farrah, *et al.*, that the observational results they reported need to be taken in conjunction with numerous caveats and additional confirmatory observational studies.

4. Summary

Following the first observational evidence that rapid black hole (BH) growth is coupled with cosmological expansion ("cosmological coupling"), theorists have been scrambling to make sense of these findings. Although one possible interpretation of the data is that such black holes might be acquiring vacuum energy (*i.e.*, dark energy) interiors, this brief note offers a simpler explanation inspired by inflationary theory and the presumed mechanism of Hawking radiation.

Given the near-certainty that the vacuum very near a BH horizon has a high energy density, it is expected that such a vacuum has a rich sea of virtual particles popping into and out of existence. Largely based upon the FSC model, a theory is offered that entangled pairs of positive matter and negative dark energy particles may be pulled out of the horizon-adjacent vacuum. If such could happen, the likelihood is that the gravitationally-attractive matter particle would cross the horizon and enter the BH interior, while the gravitationally-repelling dark energy partner is repelled deeper into the outer vacuum as "black hole dark energy radiation". The result of this high energy interaction of entangled particles would be continuous BH growth, even in the absence of merger or ordinary accretion activity, while simultaneously stimulating universal expansion by the dark energy radiative process. The net effect of all of this would be *continuous finely-tuned cosmological coupling* between growing black holes and a growing universe while, at the same time, preserving cosmological conservation of energy.

If the proposed theoretical model is indeed correct, the following consequences appear likely: astrophysical black holes might *never* evaporate; the previously inexplicable early and rapid growth of black holes might now be adequately explained; more exotic theories of dark energy would become unnecessary; and the FSC model would, once again, be validated as a globally-accurate and useful cosmological model. Furthermore, as discussed, incorporation of the high energy vacuum concepts mentioned herein might help to resolve a number of current cosmological conundrums. To take but one example, a "gravitized" vacuum, as previously theorized, might also, by the $E = mc^2$ formula, provide an alternative to the non-particulate MOND theory of dark matter.

This author is in full agreement that further confirmatory observational studies are necessary.

Data Availability Statement

All data in this submission, including figures, has been either generated by the author himself or already made available to the author thru open-source materials freely available to the public. Appropriate credit and citations of original sources have been made where required. He is willing to make readily available all data and materials used in the production of this submission.

Acknowledgements

This paper is dedicated to the late Dr. Stephen Hawking and to Dr. Roger Penrose for their groundbreaking work on black holes and their possible application to cosmology. Dr. Tatum thanks Dr. Rudolph Schild of the Harvard-Smithsonian Center for Astrophysics for his past encouragement and support. Most importantly, he also thanks his friend and colleague, U.V.S. Seshavatharam, for his co-authorship on selected FSC publications.

Conflicts of Interest

The author declares no conflicts of interest regarding the publication of this paper.

References

[1] Tatum, E.T. and Seshavatharam, U.V.S. (2021) Flat Space Cosmology—A New Model of the Universe Incorporating Astronomical Observations of Black Holes, Dark Energy and Dark Matter. Universal Publishers, Irvine.

[2] Tatum, E.T. (2019) A Heuristic Model of the Evolving Universe Inspired by Hawking and Penrose. In: *New Ideas Concerning Black Holes and the Universe*, IntechOpen, London. https://doi.org/10.5772/intechopen.75238

[3] Tatum, E.T. (2019) *Journal of Modern Physics*, **10**, 974-979. https://doi.org/10.4236/jmp.2019.108064

[4] Tatum, E.T. (2019) *Journal of Modern Physics*, **10**, 1144-1148. https://doi.org/10.4236/jmp.2019.109074

[5] Farrah, D., *et al.* (2023) *The Astrophysical Journal Letters*, **944**, L31-L39. https://doi.org/10.3847/2041-8213/acb704

[6] Maldacena, J. and Susskind, L. (2013) *Fortschritte der Physik*, **61**, 781-811. https://doi.org/10.1002/prop.201300020

[7] Susskind, L. (2008) The Black Hole War. Little, Brown and Company, New York.

[8] Penrose, R. (2016) Fashion Faith and Fantasy in the New Physics of the Universe. Princeton University Press, Princeton. https://doi.org/10.1515/9781400880287

[9] Hawking, S. and Penrose, R. (1970) *Proceedings of the Royal Society of London. Series A*, **314**, 529-548. https://doi.org/10.1098/rspa.1970.0021

[10] Tatum, E.T. (2015) *Journal of Cosmology*, **25**, 13081-13111.

[11] Poplawski, N.J. (2016) *The Astrophysical Journal*, **832**, 96. https://doi.org/10.3847/0004-637X/832/2/96

[12] Tatum, E.T. (2018) *Journal of Modern Physics*, **9**, 1867-1882. https://doi.org/10.4236/jmp.2018.910118

[13] Betoule, M., *et al.* (2014) *Astronomy & Astrophysics*, **568**, Article No. A22.

https://doi.org/10.1051/0004-6361/201423413

[14] Tatum, E.T., Seshavatharam, U.V.S. and Lakshminarayana, S. (2015) *Frontiers of Astronomy, Astrophysics and Cosmology*, **1**, 98-104. http://pubs.sciepub.com/faac/1/2/3

[15] Tatum, E.T. (2018) *Journal of Modern Physics*, **9**, 2342-2345. https://doi.org/10.4236/jmp.2018.913148

[16] Tatum, E.T. (2018) *Journal of Modern Physics*, **9**, 1935-1940. https://doi.org/10.4236/jmp.2018.910121

[17] Verlinde, E. (2010) *Journal of High Energy Physics*, **2011**, Article No. 29. https://doi.org/10.1007/JHEP04(2011)029

[18] Verlinde, E. (2016) *SciPost Physics*, **2**, Article No. 016. https://doi.org/10.21468/SciPostPhys.2.3.016

[19] Van Raamsdonk, M. (2010) *International Journal of Modern Physics D*, **19**, 2429-2435. https://doi.org/10.1142/S0218271810018529

Journal of Modern Physics, 2023, 14, 583-603
https://www.scirp.org/journal/jmp
ISSN Online: 2153-120X
ISSN Print: 2153-1196

Explaining Pomeranchuk Effect by Parity of Magnetic Moments of Leptons and Hadrons for Superconductivity in ^{3}He and Graphene*

Reginald B. Little

Department of Natural Science, Stillman College, Tuscaloosa, USA
Email: redge_little@yahoo.com, rlittle@stillman.edu

How to cite this paper: Little, R.B. (2023) Explaining Pomeranchuk Effect by Parity of Magnetic Moments of Leptons and Hadrons for Superconductivity in ^{3}He and Graphene. *Journal of Modern Physics*, **14**, 583-603.
https://doi.org/10.4236/jmp.2023.145034

Received: July 27, 2022
Accepted: April 16, 2023
Published: April 19, 2023

Abstract

The mystery of superconductivity has intrigued scientists for 110 years now. The author in 2014 specifically predicted the superconductivity in carbon, sulfur and hydrogen compounds and generally predicted carbonaceous, hydrogeneous and sulfurous compounds in 2005 with reference to scattering to asymmetric orbital motions and associated spin and orbital exchanges between nuclei and electrons. The emphasis was in 2005 upon stronger electron and nuclear interactions and electron-phonon effects. But here the author develops more the un-gerade parity of the p and f orbitals and their contributions to the superconductivity at lower pressures and higher temperatures. On the bases of such, the role of parity from the origin and inflation of the Universe is noted and dark and bright energies and matters in the mature Universe are reasoned. Moreover, the superconductors are all reasoned by positive and negative nuclear magnetic moments (NMMs) with availability of un-gerade parities of p and f subshells and their orbitals. In addition to superconductivity, such positive and negative NMMs by Little Effect is presented for explaining Pomeranchuk Effect and thereby further explaining superconductivity and superfluidity of ^{3}He. On the bases of successes of Little Effect via positive and negative NMMs, in particular negative NMMs of ^{3}He, the superconductivity in twisted graphene is explained and also its recently discovered Pomeranchuk Effect.

Keywords

Superconductivity, Pomeranchuk Effect, Little Effect, Liquid State, Nuclear Magnetic Moments

*Freezing at higher temperatures can be explained by backward orbitals for nondissipative motions.

1. Nuclear Magnetic Moments for Explaining Various Phenomena

Above room temperature superconductivity was predicted in 2014 by the author in compounds containing carbon, sulfur and hydrogen at high pressures [1]. The roles of the p orbitals and their stronger electron-nuclear interactions relative to the d orbitals and wider gaps of frontier orbitals of 2p and 3p orbitals were proposed for inducing superconductivity at higher critical temperatures (T_c). The roles of nuclear motions as vibrations of nuclei transform to rotations of nuclei were also suggested by the author for inducing and mediating superconductivity at higher temperatures [2] [3] via proton orbitals and nuclear orbitals in general. In this work, the author develops more the transformations of nuclear motions from vibrations to rotations as facilitated by nuclear spins and nuclear magnetic moments (NMMs) for not only facilitating superconductivity, but also for better explaining some chemical reactions in general and, in particular, chemical reactions of nanostructures and biomolecules for better understanding biology.

2. Novel Theory of Liquid State and New Phenomena in Solids on Basis of Nuclear Magnetic Moments

Furthermore, the author introduced nuclear rotations as facilitated by nuclear spins and NMMs for facilitating and explaining various physical properties that are currently not well theorized such as the theory of the liquid state, the explanation of melting points of various substances, the properties of various liquids, and the vaporization of liquids. Such physical properties are here proposed to be better explained by differing nuclear motions in the different physical states as the gaseous state has nuclei translating and the plasma state has nuclei possibly rotating and revolving while translating. The author introduces that the liquid state is very mysterious as the transition from gaseous to liquid states involve nuclei transforming motions from translating/vibrating nuclei to rotating nuclei. The author further notes the solid state involves the nuclei vibrating; so, solidification can better be understood by including nuclear motions of rotating nuclei in liquids to vibrating nuclei in solids during freezing. The author notes various substances differ in gas to liquid transformations depending on their isotopic compositions of spins and NMMs for inducing translating nuclei to rotating nuclei in liquid states from gaseous states and vice versa. Also, such NMMs facilitate the transformations of rotating nuclei to vibrating nuclei during freezing and vice versa by the author's model [1] [2] [3] [6].

3. NMMs for Rotating Nuclei for Liquid to Vibrating Nuclei of Solids and Explaining Pomeranchuk Effect

Recently, scientists observed an unusual effect in such superconducting graphene of it freezing as it is heated (Pomeranchuk Effect) [4]. Such effect is unusual as most substances melt when heated as opposed to freezing during heating. This is unusual Pomeranchuk Effect and it is also observed in ^{3}He [5]. ^{3}He

also superconducts and superfluids at very low critical temperatures. The bi-layer and tri-layer graphene also have very low critical temperatures for superconductivity. But, moreover, ^{3}He has negative NMM and by the author's theory [6] [7], the negative NMMs cause both the Pomeranchuk Effect and the superconductivity and likewise in twisted bi-layer and tri-layer graphenes. So, again, the author's theory of magnetic moments of both positive and negative chiralties explain superconductivity [2] [6] [8]. The author discovers totally original effect of nuclear parity and sign (+/−) of NMMs for causing novel nuclear and electronic effects in chemistry and physics. But why would negative NMMs and lepton magnetic moments (LMMs) cause freezing with thermal energy?

3.1. Can the Pomeranchuk Effect Be Explained?

Yes, the author can explain the Pomeranchuk Effect [5] by Little's Effect [2]. So now Little's Effect involves phenomena of spin and spin and/or magnetic interactions so as to alter quantum state or orbital and/or quantum orbits of fermions like electrons, quarks, nucleons and nuclei [2]. The triple of e^- e^- e^- in graphene rings can have odd combinations for antiferromagnetism in combinations for net spin and net angular momenta of negative magnetic momental parity. So, the orbiting π electrons can have net negative magnetic moments and these electrons in graphene are relativistic. Relativism is uniqueness of electrons in graphene. Just as relativism manifests in nuclei and the protons and neutrons in ^{3}He have such relativistic nuclear orbitals for negative NMMs in ^{3}He. Helium has two stable isotopes: ^{3}He with −2.13 NMM with spin 1/2 at 0.000137% relative abundance and ^{4}He with 0 NMM with spin 0 at 99.999863% relative abundance. So, the resulting positive and negative NMMs in the graphene and in ^{3}He cause CW and CCW orbitals and revolutions to manifest quantum fields by the fractional, reversible fissing electrons and fractional, reversible fissing nuclei to transform the thermal energy to magnetic energy, electric energy, gravitational energy and even quantum fields [6] [7].

By Little's theory, the transformations of thermal, electric, gravity and magnetic spaces to quantum fields require both Br and Dk fields from larger C Frame and/or the transformations of Br spaces to Dk spaces and fields as the Br spaces are accumulated and transformed. By Little's theory such transforming irrational rarefied Dk and Br spaces to QF involves relativistic accumulations with compressions and bending to form complex fields with real (Re) and imaginary (Im) parts [6] [7]. By RB Little theory the real and imaginary parts of the wavefunctions are determined to be the Br and Dk gravities, respectively. RBL finds that the Dk field is difficult to detect in our sector of the Universe as the matter of our region transforms Dk fields to QFs by accumulating and combining Br and Dk fields into the real and imaginary parts of wavefunctions. But there is limited Dk spaces in our sector of Universe and this further gives basis for the limited amount of Dk spaces and fields as they are fused with Br to form quantum fields.

3.2. Novel Energetics by Nuclear Magnetic Moments for Relativistic Little Effect

By Little's theory [1] [2] [3], the resulting fusing of Br and Dk thermal spaces form electric, gravity and magnetic spaces and even quantum fields for manifesting complex phases of wavefunctions. The resulting rational complex fields bind more strongly to explain how heating and more thermal energy with the surrounding rare Dk (Im) fields can cause freezing as the thermal energy with the Br (Re) thermal are converted to E, B and QF for stronger binding for liquid to solid transformations at the higher temperatures. The fields cannot only come from bigger space of C frame, but also from smaller denser spaces of nuclei and nucleons so neutrons and protons can release dense Br and Dk (Re and Im) spaces to electronic lattices (due to thermal agitations) for forming quantum fields and stronger bindings and further explaining Pomeranchuk Effect. Bigger rotations in liquids compress and internalize to internal rotations with consequent vibrations between the rotating quanta as the liquids solidify; and vice versa, if solids melt the internal rotations transform to bigger rotations as the bigger vibrations are transformed to bigger rotations. All positive or all negative NMMs in a liquid when further heated reach an optimum denseness of positive or negative NMMs and fields about them individually; so excess thermal fields cause ultra-relativistic motions and dissipations so the rotating nuclei persist and excesses are dissipated to surroundings by Little Rules 1 and 3 [2] [3].

But unlike either all positive or all negative NMMs, if positive and negative NMMs exist together in the liquid then the interactions prevent ultra-relativistic rotations and the thermal fields and energies are accumulated and converted to opposing charges and poles about the nuclei with consequent stronger binding fields from the thermal field accumulations by Little Rules 1 and 2 [2] [3]. For example, recently experiments demonstrate novel magnetism in $TbMn_6Sn_6$. Such magnetism in $TbMn_6Sn_6$ can be reasoned by this substance having high relative abundances of stable nuclei having positive and negative NMMs. In $TbMn_6Sn_6$, Tb has one stable isotope with nonzero NMM: ^{159}Tb with +2.014 NMM with spin 3/2 at 100% relative abundance. Sn has three stable isotopes with nonzero NMMs: ^{115}Sn with −0.919 NMM with spin 1/2 at 0.34% relative abundance; ^{117}Sn with −1.001 NMM with spin 1/2 at 7.68% relative abundance; and ^{119}Sn with −1.047 NMM with spin 1/2 at 8.59% relative abundance. Mn has one stable isotopes with nonzero NMM: ^{55}Mn with +3.45 NMM with spin 5/2 at 100% relative abundance. The higher temperatures with transduction of thermal to E, B and QF then cause binding due to stronger interactions and freezing at the higher temperatures. So, the heat by Little's Effect is transduced to magnetic and quantum fields between the electrons in twisted graphene and ^{3}He so the extra quantum fields and/or magnetism cause freezing upon heating as the thermal energy is converted to magnetic fields and/or quantum fields for increased interactions for freezing. Null NMMs lack these internal nuclear pressures for such freezing at higher temperatures.

4. NMMs and LMMs Explaining Superconductivity in Bi-Layer and Tri-Layer Graphene

Scientists at MIT a couple of years ago observed very, very low temperature superconductivity in twisted bi-layer graphene and in last year twisted tri-layer graphene by twisting the layers by about 1 degree angle [9]. But how is this twisted graphene superconductivity accounted for by the author's suggested needed negative [with prevalent positive] nuclear magnetic moments (NMMs) theory of superconductivity [6] [7]? Here the author demonstrates that the electrons give the negative magnetic moments by negative leptonic magnetic moments (LMMs) for balancing the positive NMMs of rare ^{13}C of carbons for superconducting currents of resonating π electrons sandwiched between C nuclei in the bi-layer and tri-layer graphene layers. C has one stable isotopes with nonzero NMM: ^{13}C with +0.702 NMM with spin 1/2 at 1.07% relative abundance. Thereby it seems the prior magnetic moment theory of the author [6] [7] is capable of explaining graphene's low temperature superconductivity and the Pomeranchuk Effect [4] [5].

5. Electromagnetic Effects on Liquid State, Pomeranchuk Effect and Superconductivity

The author further notes the importance of external electromagnetic radiations of various types (radio waves, microwaves and infrared waves) and static magnetic fields and static electric fields for accelerating or decelerating such physical changes in addition to novel catalytic and chemical changes by affecting nuclear vibrations to rotations and vice versa. Electromagnetic fields that induce rotations can favor liquid state and hinder rotations like static fields can prevent liquid or induce freezing. This effect was previously predicted and archived by author [10] [11], but afterward experiments demonstrated the electric field preventing freezing. For electromagnetic fields that prevent rotations can induce freezing, favoring solids like static fields prevent vibrations for liquefaction. For instance, researchers recently observed electric field inducing freezing [12] [13]. The electromagnetic waves and fields are denser thermal spaces and gravity spaces, so they cause altered interactions of nonzero NMMs relative to null NMMs. In 2003, the author discovered the lowering of melting point by strong static magnetic field upon silicon in hydrogen atmosphere and such may be explained by the induced rotation of ^{29}Si nuclei in the silicon at lower temperatures in the magnetic field as the nuclei vibrations transform to nuclear rotations [14]. Si has one stable isotopes with nonzero NMM: ^{29}Si with −0.555 NMM with spin 1/2 at 4.68% relative abundance. Later researchers confirm RBL prior determination of strong magnetic field affecting freezing/melting [15] and also evaporation/condensation [16]. The author further notes important effects of this presented nuclear vibrations to nuclear rotations on various novel chemical and biochemical reaction dynamics, catalyses and enzymatics and novel ways of controlling such dynamics by long wavelength electromagnetic waves and magnetic

and electric fields. On such basis, the author has introduced novel effects of radiations on proteins, nucleic acids and other biochemical molecules for understanding life processes.

6. Why Nuclear and Nucleon Rotations Favor HTSC?

But here novel nuclear rotations and revolutions (relativistically); dynamics of nuclei rotating; and the interior rotations and revolutions (relativistically) of nuclei parts of nucleons are noted for explaining liquid state, liquid-solid phase transitions, sublimation, superconductivity and raising the temperature at which superconductivity occurs and finding substances that superconduct at both high temperatures and low pressures (toward atmospheric pressures). The similarity of liquid-solid phase transitions, liquid-crystal properties and superconductivity are related by this theory of RBL as these phenomena all depend on rotations or vibrations of nuclei and transitions of rotations to vibrations and vice versa. The clockwise (CW) and counterclockwise (CCW) rotations for symmetric and asymmetric rotations and revolutions are noted. Symmetric revolutions refer to the revolutions of electrons in most hydrogen and rotations of their nuclei and are arbitrarily given CW symmetry. Asymmetric orbits are given CCW symmetry. The theory [2] [3] [6] [7] here further develops the nuclear rotations and revolutions coupling to electronic orbitals and revolutions (revorbitals) for explaining superconductivity and other phenomena of physical properties, liquid crystalline properties, chemical properties, catalyses and enzymatics. But here the effects are related to the origin of the Universe and Inflation and a novel theory of bright and dark matter and interactions causing these novel phenomena of nuclear and electronic rotations and revolutions for novel properties of superconductivity, chemical transformations and nuclear reactions.

7. Parity in Mature Universe Related to Parity from Origin of Universe

The author here further develops his prior notion that bright (Br) and dark (Dk) matter with real and imaginary spaces and energies originated from the Origin of the Universe as before the Origin there was nothing (zero) and zero being infinity of zero (+1 − 1) and The Creator (−1) involved a Bang and the Bang manifested −1(s) and the Original Singularity. The Original Singularity accelerated (for time and – sensible change) in zero (1 − 1) and separates zero into 1(s) and −1(s) by Inflation of the Original Singularity as noted by the author's theory. The Inflation continues at the edge of the Universe as zero (1 − 1) at edge is perpetually separated into −1(s) and +1(s), but due to the original (−1) Singularity there is more −1. The acceleration stretches and rarefies the −1(s) in "sensible dynamics" across the bread of the universe and the acceleration is countered by the production (for "latent dynamics") of dense regions of −1(s) and +1(s) and the −1(s) are more abundant with tiny solute amounts of +1(s) in the mature Universe and manifest Dark Matter in its accumulations and in some regions +1

solvent and tinier amounts of −1 solutes (our sector of the Universe). The author proposes the stretched, fractional, irrational, superluminous −1 as dark (Im) energy and the clumps of −1 with tiny amounts of +1 as dark matter. Br matter in our sector of the universe is more clumps of +1 as Br (Re) with tinier amounts of −1 as fused to leptons and hadrons.

8. Dynamics of Clumped and Rarefied Br and Dk in Mature Universe

The author notes intrinsic time symmetry difference of Dk energy (Im) relative to Br energy (Re) as during Inflation the motion of Dk outward is simultaneous with Br and Dk clumps in latency. Such time symmetry differences of Br and Dk manifest as offset of real and imaginary components in wavefunctions for kinetic manifestations of wavefunctions. So as Br and Dk clumps experience sensible dynamics, the background (rarefied superluminous Dk) is perpetually stretching outward, but not rarefying to zero as the production of −1 (Im) at edge. But the denser clumps of +1 Br (Re) in our sector of Universe are confined and oscillate linearly, curvilinearly or spherically or composites of linear, curvaceous and spherically. But interacting with the rarefied Dk Background the Br moves against the Dk background to cause relative latent Dk background while Br is sensibly stretching or compressing. And in Dk sector the Dk clumps to move to stretch more in concert with Dk background and to compress to cancel the Dk background. So, in particles having similar clumped Dk and clumped Br, the background is cancelled as Br stretches and the Dk background cancels as the Dk clumped compresses. Thereby the rarefied Dk background causes temporal shift in the sensible and latent dynamics of clumped Br and clumped Dk. So that as clumped Br is sensible in compressing or stretching the clumped Dk at that moment is latent; and as the clumped Dk transforms from latent to sensibly dynamics of stretching or compressing then the clumped Br goes to latent. So, the imbalance of the perpetual rarefied superluminous Dk expansion in background creates imbalance between clumped Dk and clumped Br and time discontinuity to explain the clump Dk not interacting with clumped Br on some scales as in larger C Frame. On such larger scale, the rarefactions and irrationality cause Br and Dk (Re and Im) to manifest $v < c$ in complex space. But with compression and rational components of phase the linear combination causes curvature within the curving phase for C frame to collapse to L Frame of quantum fields. The clumped Dk and clumped Br exist in particles in our sector as nuclei with negative NMMs and nuclei with positive NMMs, respectively. Dark matter in other regions of the Universe has particles of negative NMMs, Dk gravity and Im spaces.

9. Such Rotations and Vibrations from Origin of Universe

The author here further develops his prior notion that bright (Br) and dark (Dk) matter and energy originated from the Origin of the Universe as before the Origin there was nothing (zero) and zero being infinity of zero (+1 − 1) and the

Creator (−1) involved a Bang and the Bang manifested −1(s) and the Original Singularity. The Original Singularity accelerated (for time and – sensible change) in zero (1 − 1) and separates zero into 1(s) and −1(s) by Inflation of the Original Singularity as noted by the author's theory. The Inflation continues at the edge of the Universe as zero (1 − 1) at edge is perpetually separated into −1(s) and +1(s) but due to the original −1 Singularity there is more −1. The acceleration stretches and rarefies the −1(s) in "sensible dynamics" across the bread of the universe and the acceleration is countered by the production (for "latent dynamics") of dense regions of −1(s) (Im) and +1(s) (Re) and the −1(s) are more abundant with tiny solute amounts of +1(s) in the mature Universe and manifest Dark Matter in its accumulations and in some regions +1 solvent and tinier amounts of −1 solutes (our sector of the Universe). The author proposes the stretched, fractional, irrationals, superluminous −1 as dark energy (Im) and the clumps of −1 with tiny amounts of +1 (Br, of Re amounts) as dark matter. Br matter in our sector of the universe is more clumps of +1 with tinier amounts of −1 as fused to leptons and hadrons.

The author notes intrinsic time symmetry difference of Dk energy relative to Br energy as during Inflation the motion of Dk outward is simultaneous with Br and Dk clumps in latency. So as Br and Dk clumps experience sensible dynamics the background (rarefied, superluminous Dk) is perpetually stretching outward but not rarefying to zero as the production of −1 at edge. But the denser clumps of +1 Br in our sector of Universe are confined and oscillate linearly, curvilinearly or spherically or composites of linear, curvaceous and spherically. But interacting with the rarefied Dk Background, the Br moves against the Dk Background to cause relative latent Dk Background while Br is sensibly stretching or compressing. And in Dk sector the Dk clumps move to stretch more in concert with Dk Background and to compress to cancel the Dk Background. So, in particles having similar clumped Dk and clumped Br the Background appears cancelled as Br stretches and the Dk Background cancels as the Dk clumped compresses. Thereby the rarefied Dk Background causes temporal shift in the sensible and latent dynamics of clumped Br and clumped Dk as clumped Br is sensible in compressing or stretching the clumped Dk at that moment is latent and as the clumped Dk transforms from latent to sensible dynamics of stretching or compressing then the clumped Br goes to latence. So, the imbalance of the perpetual, rarefied, superluminous, Dk expansion in Background creates imbalance between clumped Dk and clumped Br and time discontinuity to explain the clump Dk not interacting with clumped Br on some scales. The clumped Dk and clumped Br exist in particles in our sector as nuclei with negative NMMs and nuclei with positive NMMs. Dark matter in other regions of the Universe has particles of negative NMMs.

10. Distribution of Br and Dk in Mature Universe for Differing Transformations to QF

But in our region of the Universe these particles having tiny excess of Dk (Im)

are in nuclei having negative NMMs. Most of the matter in our sector of Universe has positive NMMs or null NMMs. The protons, neutrons and electrons in our region of Universe have bright matter characteristic with some tinier essence of Dk energy and Dk matter. The excess Br as by positive and null NMMs in most matter in our sector of Universe causes dissipative motions as the kinetic energy of moving Br particles readily transforms to thermal energy in the Dk Background as the motion cannot be rhythmically confined for long enough time against transforming in the rarefied Dk Background.

In such imbalance local space, the balance of Br and Dk motions of transport in the imbalanced Background cannot be sustained so the balanced motion dissipates to thermal space in the Dk Background rarefied space. Also balance and imbalance of electric and magnetic or vibrations and rotations for solid-liquid and liquid crystallinity for superconductivity and its relation to liquid crystallinity. So, system having balance of Br and Dk and electric and magnetic oscillations for liquid crystallinity as vibrations and rotations exchange for superconducting as the vibrations cannot dissipate as the rotations attract changing vibrations as changing electric create magnetic field and the induced magnetic field attracts then magnetic field of rotations for preventing dissipation for superconductivity and superfluidity. This is applied to proteins and nucleic acids and nanowater as part has positive and negative NMMs (for magnetic and rotations) and the other parts have null NMMs (for vibrations and electric). So, the liquid crystallinity and time crystal arises as the nonzero magnetic rotations prevent the null electric vibrations from dissipating. And the nonzero electric field prevents the magnetic rotations from exploding. Even in the atom the rotating nuclei and magnetism couple to surrounding electron pairs and electric. So the electric field prevents the nuclei from exploding and the magnetic prevent the electric from dissipating for perpetual motion of biomolecules for life. But in some systems with balance of clumped positive and negative NMMs, the Br and Dk motions locally may be balanced and in oppositions so the thermal space cannot escape the opposing motions of Br and Dk and the thermal energy is transduced to electric, gravitational, magnetic and/or quantum energies. So, the motion occurs without dissipation by the thermal as the thermal is transduced to organizing fields that sustain the superconductivity and superfluidity.

11. Internal Rotations of Electrons for QF and Internal Rotations of Nuclei for Quantum Fields

In addition to NMMs, the orbital motions of electrons can manifest different symmetries of Br and Dk in directionality as manifested by orbital parity. The nuclei cannot only flip electron spin as the electron cross the nuclei and interact with nuclei. But the electrons can change orbital directions as by interacting with nuclei. And orbitals of difference angular momenta have different symmetries of the nuclei altering parity as orbitals of even azimuthal quantum numbers manifest gerade symmetries as by interacting with nuclei and orbitals of odd azimuthal numbers manifest un-gerade symmetries as by interacting with nuclei. In

the model presented here, the author notes the elements having valence subshells occupied of un-gerade symmetry host superconductivity more readily as they impart more balance of odd and even parities and negative and positive momenta and Dk and Br fields (as computed by Im and Re numbers, respectively) as by interacting with nuclei with consequent transformations of thermal energies to magnetic energies and quanta. The occupancy in subshells of odd azimuthal quantum numbers (like p subshells and f subshells) contributes superconductivity at higher temperatures than electrons in orbitals of even azimuthal quantum numbers (like s and d subshells). The superconductivity occurs at even higher temperatures for the un-gerade subshells with nuclei having positive and negative NMMs. The superconductivity may be involving frontier orbitals where the ground state is gerade and there are low lying or accessible conduction states or impurities having un-gerade parity and/or positive and/or negative NMMs of the impurities.

12. Parity of Forward and Backward Motions and Superconductivity and Pomeranchuk Effect

Changes of linears to rotations require backward motions (Dk) (Im). Such backward motion can be accelerated at more energy densities or it can originate from Dk fields (Im). Parity therefore becomes important as C Frame transforms to L Frames. And Parity is necessary as L frames form NS and RS frames as forward (Re) and backward (Im) motions are produced or consumed. On the bases of such, further development of NMMs and lepton magnetic moments (LMMs), the subshell parity is further demonstrated here to explain patterns in superconductivities among elements and compounds of different elements with correlating the critical temperature and pressures required for the superconductivity. For instance, type I superconductivity was discovered in Hg at very low T_c in 1911 by Onnes [17] and such superconductivity is explained by this theory as Hg has electronic configuration with filled 6s and 5d orbitals and empty 6p orbitals. So, the superconductivity involves these frontier orbitals whereby the 6s or 5d electrons of gerade parity are excited in continuum betwixt 6p subshells of un-gerade parity. So, the 6p subshells impart mix of + and − orbital angular momenta of electrons in the orbitals for facilitating the transductions of thermal energies at higher temperatures to orbital magnetisms and the binding of scattered superconducting electrons at higher temperatures. The Hg also has isotopes of both positive and negative NMMs for facilitating such superconductivity. Hg has two stable isotopes with nonzero NMM: ^{199}Hg with +0.506 NMM with spin 1/2 at 16.87% relative abundance and ^{201}Hg with −0.560 NMM with spin 3/2 at 13.18% relative abundance. The positive and negative NMMs are like CW and CCW rotations and forward and reversal in time and they prevent vibrations from dissipating electron motions (electric vibrations) at lower temperatures. It is important that these aspects of the frontier orbitals of Hg of 6s and 5d valences and 6p conductions of gerade and un-gerade parities with isotopes of both posi-

tive and negative NMMs also explain the unusual lower melting temperature of Hg and it being the only liquid metal.

13. Different NMMs and Different Electron Configurations and Parities for Different T_c in Pure Metals

From Hg, then higher T_c(s) were observed in Pb and Nb. The NMMs and the electronic configurations contribute to HTSC as the NMMs can cause gerade and un-gerade and Br and Dk and the electronic configurations can have balanced or unbalanced spins orbitals of electrons are always unbalanced. But Br and Dk and + and − NMMs can cause balanced e^- e^- orbitals. On the bases of the orbital parity as developed more here and prior positive and negative NMMs already published, the increase in T_c from Hg to Pb follows from the valence of Pb involving unfilled 6p orbitals of un-gerade parity for the higher T_c of Pb. Pb has one stable isotope with nonzero NMM: ^{207}Pb with +0.582 NMM with spin 1/2 at 22.1% relative abundance. Comparing d electrons and p electrons can distinguish T_c (s) of Hg, Nd and Pb, as the d orbitals are like s orbitals as they are either gerade or un-gerade. But p orbitals and f orbitals are mix of gerade and un-gerade. The Nb is of a 4d has gerade orbitals in its subshell and should be less in T_c than 6p subshell of Pb and its un-gerade nature. But the NMMs of Nb counters the gerade nature of the 4d in Nb for increasing T_c. The Nb however may involve more of the unusually large +6.17 NMM with spin 9/2 with 100% of ^{93}Nb elements for affecting the gerade orbitals of 4d for explaining the superconductivity in ^{93}Nb. But the T_c of Nb is raised much higher by including Nb in compounds with some p block elements and the involvement of un-gerade p subshells and their orbitals as in NbN, NbSn and NbGe superconductors (in order of increasing T_c). It is important to note that all of the p block elements (^{15}N, ^{115}Sn, ^{117}Sn, ^{119}Sn, and ^{73}Ge) in these Nb superconducting compounds have isotopes of negative NMMs with further consistency to this theory of the author [2] [3] [6] [7]! N has one stable isotope with nonzero NMM: ^{15}N with −0.283 NMM with spin 1/2 at 0.368% relative abundance. Ge has one stable isotope with nonzero NMM: ^{73}Ge with −0.879 NMM with spin 9/2 at 7.73% relative abundance. Recently (after the original archivings of this manuscript [10] [11], experiments further substantiate this discovery of – NMMs raising T_c as Ti with its – NMMs has been observed to break record for T_c of elemental superconductors and it is transition metal of 3d series [18], Ti has two stable isotopes with nonzero NMM: ^{47}Ti with −0.788 NMM with spin 5/2 at 7.44% relative abundance and ^{49}Ti with −1.104 NMM with spin 7/2 at 5.41% relative abundance.

14. Electronic for Superconductivity in Carbon Compounds But Limits as by + and − NMMs

And then some carbon compounds as M-C_{60} (with M = K, Rb, and Cs at high pressures) and YbPdBC manifest even higher T_c than the Nb compounds and this can be reasoned by the model theory here by the p orbitals and lower prin-

ciple quantum numbers of B and C relative Sn and Ge in NbSn and NbGe. But B and C have positive NMMs but the un-gerade (positive and negative lobes) nature of the p orbitals and the positive and negative NMMs in Yb and Pd are explaining the superconductivity by this model [2] [3] [6] [7] in spite of only positive NMMs in the C and B. B has two stable isotopes with nonzero NMM: ^{10}B with +1.801 NMM with spin 3 at 19.9% relative abundance; and ^{11}B with +2.689 NMM with spin 3/2 at 80.1% relative abundance. Yb has two stable isotopes with nonzero NMM: ^{171}Yb with +0.491 NMM with spin 1/2 at 14.28% relative abundance and ^{173}Yb with −0.678 NMM with spin 5/2 at 16.13% relative abundance. Pd has one stable isotope with nonzero NMM: ^{105}Pd with −0.642 NMM with spin 5/2 at 22.33% relative abundance. The observed electric field induced refrigerating ability of Mn_3SnC with zirconium titanate [19] is further substantiating this theory of the author [6] described here as these materials have stable isotopes of large relative abundances with negative NMMs (Ti, Zr and Sn) and Mn has all positive NMMs for its stable isotope. Zr has one stable isotope with nonzero NMM: ^{91}Zr with −1.304 NMM with spin 5/2 at 11.22% relative abundance. Oxygen has one stable isotope with nonzero NMM: ^{17}O with −1.894 NMM with spin 5/2 at 0.038% relative abundance. The mix of positive and negative NMMs in this material proves author's theory of such mix NMMs trapping thermal energy and converting thermal energies to electric and magnetic energies and even quantum energies [6]. On the basis of this, the author has proposed in the past [2] [3] [6] [7] that higher and even room temperature superconductivity may be observed even at low pressures toward atmospheric pressure in thin films and single to few layer ^{10}B^{15}N and ^{11}B^{15}N and ^{13}C^{17}O graphene oxide on the basis of the author's theory as the ^{15}N and ^{17}O enriched in these structures to 100% would give 100% negative NMMs of ^{15}N and ^{17}O for supporting the superconductivity by the negative NMMs of the ^{15}N and ^{17}O in these compounds and the un-gerade natures the 2p orbitals of the ^{15}N and ^{17}O.

15. Backward and Forward Spatial Relativistic Frames of Copper Silicates for Superconductivity

And so the superconductors involving $CeCuSi_2$ can be reasoned on basis of the ^{29}Si and its negative NMM and the 3p subshell and orbitals for Si and its un-gerade parity by 3p and furthermore the Ce and its 4f orbital and contributions of un-gerade parity by 4f orbital in the unit cell. The Cu has 3d and it orbitals do not twist backward as the 3p orbitals of Si and 4f orbitals of Ce. Cu has two stable isotopes with nonzero NMM: ^{63}Cu with +2.22 NMM with spin 3/2 at 69.17% relative abundance; and ^{65}Cu with +2.38 NMM with spin 3/2 at 30.83% relative abundance. The ligands twist backward and the Cu center twist positively as it seeds and host the spatial directions with Ce and Si perturbing the spatial directions. And UBe_{13}, UPt and $UPdAl_3$ may be reasoned for their superconductivities by this model [2] [3] [6] [7] on basis of negative (−) 1.17 NMM of ^{9}Be and its s subshell and orbital of gerade symmetry with 100% relative abun-

dance and the 5f subshell and orbitals of U of un-gerade symmetry contributing un-gerade parity. U has one stable isotopes with nonzero NMM: ^{235}U with −0.35 NMM with spin 7/2 at 0.72% relative abundance. Be has one stable isotopes with nonzero NMM: ^{9}Be with −1.177 NMM with spin 3/2 at 100% relative abundance. Pt has one stable isotope with nonzero NMM: ^{195}Pt with +0.609 NMM with spin 1/2 at 33.82% relative abundance. And both U of 5f subshell contributing un-gerade parity to Pt of 6d and gerade and possible accessibility to 6p orbitals in Pt anions. The $UPdAl_3$ further manifest un-gerade orbital contributions of U to the superconductivity with negative NMMs of Pd and positive NMMs of the Al on the bases of this theory [2] [3] [6] [7] for providing forward and backward accelerated spaces for trapping thermal space, mechanical space, gravity space, electric space, magnetic space and quantum fields. Al has one stable isotopes with nonzero NMM: ^{27}Al with +3.64 NMM with spin 5/2 at 100% relative abundance.

16. Backward and Forward Spatial Relativistic Frames of Cuprates and Arsenides for Superconductivity

The cuprates may be reasoned for their superconductivity on basis of negative NMMs of few ^{17}O and the p subshells and orbitals seating the O with un-gerade parity for sustaining superconductivity with cations providing positive and negative NMMs. The arsenates of iron give strong evidence of this role of orbital magnetism and un-gerade nature of the orbital parity for the superconductivity as ^{75}As has all positive 1.43 NMMs with 3/2 spin with 100% and the ^{75}As lacks the negative NMMs as in cuprates as by ^{17}O for manifesting the superconductivity. But the positive NMMs in arsenates have central metals of iron with lone electrons spins for producing negative magnetic moments and such magnetism of the iron central atoms backwardly accelerate the superconducting 4p electrons about the As with their un-gerade parity to manifest the negative lepton moments in orbital motions by the electron spins of the iron for seating the superconductivity in arsenates by this model [2] [3] [6] [7]. Fe has one stable isotope with nonzero NMM: ^{57}Fe with +0.091 NMM with spin 1/2 at 2.12% relative abundance. The difference in magnetism of Cu and Fe in cuprates and arsenates leads to cuprates requiring negative NMMs of ^{17}O and orbital and subshells of p un-gerade for superconductivity, whereas iron arsenates do not need negative NMMs but positive NMMs of ^{75}As host superconductivity as the electron spin in Fe magnetically accelerate the un-gerade p subshells and orbitals for negative moments in the positive NMMs of the ^{75}As. Thereby, here it is reasoned the ferromagnetism with spin down aligning with negative orbital moments and Dk gravity may accelerate un-gerade orbital electrons to cause fields like emanating from nuclei having negative NMMs for countering motions of positive NMMs for preventing QF, magnetic, electric, gravitational spatial dissipations to thermal space and rarefaction of thermal space. The $v > c$ of the opposing motions prevents the thermal spatial rarefaction by this model and transduces thermal

space to electric and magnetic spaces and QF for explaining superconductivity, Pomeranchuk Effect, liquid state, liquid crystallinity, energy transduction and strange metallicity.

17. Backward and Forward Spatial Relativistic Frames of High Pressure Hydrogen Sulfides for Superconductivity

So now since 2005, the author [2] proposed higher temperature superconductivity in hydrogen and sulfur containing compounds and in hydrogen and carbon compounds and also in iron hydrogen compounds. Later in 2014 and 2015, the dramatic increase in T_c was computed and observed by Ma [20] and Eremet [21], respectively. But these great advancements toward room temperature superconductors of hydrogeneous sulfides also follow from the theory here [2] [3] [6] [7] as H and its p^+ and positive NMM and s orbitals act directly on the electrons. By such, the protons of positive NMMs act directly on valence electrons of S and S has 3p and its un-gerade symmetry manifest a negative type LMM (lepton magnetic moment) of the 3p electrons in S as in H the proton is its own nucleus unlike in other elements and likewise in He. The H acts directly on the electron of the central atoms for stronger effect without effects of other nucleons in the nuclei and without core electrons of the H. H is unique in its actions and the ^{3}He is unique in its nucleus' action on surrounding electrons of other elements as the H and ^{3}He lack other nucleons and their nuclei do not dilute by core electrons as the valence electrons are the core electrons for H and He. This uniqueness of H and He was reported 1st in the prior archives [10] [11] of this manuscript. It is important to point out recent experimental results of large team of scientists that substantiates the author's prior prediction [9] [10]. The mirror stable isotopes ^{3}T and ^{3}He have higher probabilities of p^+-p^+ and n^0-n^0 collisions relative to p^+-n^0 collisions when compared to collisions in heavier stable nuclei of heavier elements with more p^+-n^0 collisions [22].

18. Backward and Forward Spatial Relativistic Frames of High Pressure Hydrogen Lanthanides and Yttrium Hydrides for Superconductivity

So the power of the author's theory [2] [3] [6] [7] is manifested even more by developments after hydrogeneous sulfides as the LaH_{10} was found to superconduct at even higher T_c. The theory described here as reasoned by the author explains the higher T_c of LaH_{10} on basis of the contribution of the un-gerade orbital symmetry of 4f subshells of La relative to the lower speed orbital un-gerade symmetry of the 3p subshells of S in hydrogeneous sulfides. But the theory is further revealed in its power as it explains the lower T_c (higher T_c and lower pressure) of YH_{10} (La^3He) relative to LaH_{10} despite higher expected T_c predicted in YH_{10} by current electron-phonon models. La has two stable isotopes with nonzero NMM: ^{138}La with +3.71 NMM with spin 5 at 0.09% relative abundance; and ^{139}La with +2.78 NMM with spin 7/2 at 99.91% relative abundance. The YH has negative NMM which tends to raise the T_c, but the Y has s subshell orbitals

and s orbital is gerade symmetry, which diminishes the effect of backward motions of space with forward motions for trapping and accumulating thermal space and preventing rarefaction and dissipation of thermal space. Y has one stable isotope with nonzero NMM: ^{89}Y with −0.137 NMM with spin 1/2 at 100% relative abundance. But the La unlike the Y has 4f subshells of un-gerade symmetry for explaining the high T_c in LaH relative to YH. But the theory of the author [2] [3] [6] [7] as presented here reasons and explains the recent elevation of T_c in the YH_{10} by incorporating Pd as the Pd is more electronegative than Y and H and may fill its 5d subshells with availability of 5p subshell orbitals and the un-gerade parity of the 5p subshells for coupling with YH_{10} to raise the T_c as observed recently in such materials.

19. Backward and Forward Spatial Relativistic Frames of High Pressure Carbonaceous Hydrogen Sulfides for Superconductivity

So, in 2020 the superconductivity in carbonaceous hydrogen sulfides was observed. The theory presented [2] [3] [6] [7] here explains this superconductor as well as the carbon and sulfur are members of 2p and 3p subshells with the un-gerade parity of the p subshell orbitals for contributing negative moments by orbital Dk and – spaces for explaining the superconductivity from such orbital un-gerade parity balancing the positive NMMs of ^{1}H, ^{33}S and ^{13}C and gerade orbital symmetry for the balance hosting the superconductivity at high pressures. S has one stable isotopes with nonzero NMM: ^{33}S with +0.644 NMM with spin 3/2 at 0.76% relative abundance. But the theory [2] [3] [6] [7] presented here also explains the recent superconductivity in bi-layer and tri-layer graphene with slight twist between layers as the π orbitals and aromatic ring currents above and below the C nuclei host the superconductivity via pure p_z orbitals and their un-gerade parity. So some layers may have – parity of one graphene layer and + parity of an the nearby graphene layer for – parity aromatic rings of adjacent graphene sheets interacting to provide necessary balance of – and + magnetic moments for momentary rarefactions for Br and Dk gravities for manifesting the superconductivity as the opposing balanced motions of negative and positive NMMs and rarefactions to Br and Dk gravities for preventing thermal space to escape for transformations of the thermal energies to electric, gravitational and magnetic energies and even quantum energies for sustaining superconductivity.

There has been some controversy concerning the data on high pressure carbonaceous sulfur hydrides for near room temperature superconductivity as some noted that the electrical resistance change with temperature drops off more gradually in character in prior superconductors; but the carbonaceous sulfur hydride manifest a sharper dropoff in resistance over narrower temperature change with no broadening in applied magnetic field. In this theory of the RBL, the author (RBL) notes unlike with prior sulfur hydrides under pressure where there are core 2p ungerade orbitals to shield the sulfur 3p orbitals from nuclei of ^{33}S, with carbon doping and ^{13}C by the author's theory here there are 2p ungerard orbitals

with no core 1p to experience positive NMMs directly from ^{13}C nuclei for the observed effect as the higher energy nuclear magnetic moments (NMMs) more suddenly and dramatically below some temperature threshold alters resistance with very little effects of feeble external magnetic fields. The author here notes that the mechanism of high temperature superconductivity in high pressure hydrides involving nuclei of ^{1}H, ^{13}C, and La (with emerging 1s, 2p and 4f orbitals of ungerade symmetry) is much different from the mechanism of electronic shell effects in cuprates, arsenides, magnesium diborides and mercury of older superconductors. The electrical resistances verses temperature of the cuprates, arsenides, magnesium diboride and mercury are more gradual and altered by external magnetic fields as the electronic energies of these are much smaller than nuclear energies and NMMs reversibly seeped from high pressure carbonaceous hydrides for more gradual plots of the former older superconductors and less gradual sharper changes in resistance of the later recent super-hydrides.

The controversial magnetic susceptibility changes and plots of the carbonaceous sulfur hydrides may also be reasoned by similar effects of lack of core p orbitals inside 2p and lack of core f orbitals inside 4f. So the carbonaceous sulfur hydrides by ^{13}C feel the nuclei fields more directly without shielding by inner core subshell of similar azimuthal quantum symmetry. But here the author notes that the nuclei (with decrease in temperature) may be reversibly fissing and fusing fields of much higher energies (than the surrounding electronic energies) that more suddenly cause the drop off in electronic magnetic susceptibility as the fields from nuclei diminish but even in stretching and diminishing they are still much greater than electronic energies in surrounding shells about the nuclei and so the seeped fields order the electrons so the electrons cannot magnetize below the temperature. Above the critical temperature the nuclei fractionally reversibly fiss so violently that they over power the electronic organization of magnetism in the surrounding electronic shells according to the mechanism presented here. But below the temperature (T_c), the thermal agitations are more gentle and agitate nuclei to release energy that agitate more mildly to disrupt the magnetic order and to organize the superconductivity. By the mechanism of the author, above the critical temperature the nuclei agitate so violently that the superconductivity is not allowed and the magnetization is not allowed!

The observed spikes in the magnetic susceptibility data in carbonaceous sulfur hydrides may be quantum fluctuations of the nuclei according to the theory of the author of this current manuscript. The spikes in the magnetic susceptibility plots are same height as the agitating electronic and thermal fields cause the nuclei to fractionally reversibly fiss and fuse to release nuclear fields of huge energies. In older superconductors (of the cuprates, arsenides, magnesium diboride and mercury), the temperature agitates the electrons in surrounding shells (and also nuclei of zero NMMs for smaller nuclear effects) and the temperature change agitates different number of electrons for different noise (variation in spike heights) and broader magnetic susceptibility plots and the electrons are less sensitive to the noise agitating, according to the author of the current ma-

nuscript. The author notes that the agitations are released from H nuclei individually and are of similar magnitudes beyond some threshold of noise. But for the cuprates, arsenides, magnesium diboride and mercury superconductors, the thermal agitations involve nucleons and nuclei having many nucleons and more null NMMs and consequently broader range of fissing and fusing for more gradual magnetic susceptibility plots and electric resistivity plots. Hydrogen has only one nucleon and this is why the agitations have one height and also why the magnetic susceptibility plots and electrical resistivity plots are more sudden and less gradual!

20. Backward and Forward Spatial Relativistic Frames of Low Pressure Silver and Gold Nanocomposites for Superconductivity

From a purely theoretical perspective, the author is very intrigued by reports of superconductivity in silver nanostructures in gold nanofilms of Pandey and Thapa [23]. This controversial experimental study has not been replicated. But the author has for more than two years [6] reasoned the theoretical possibility of such by the theory here as the gold has 100% positive NMMs and the silver has 100% negative NMMs for balance of the NMMs and as further developed here the electronic configurations of both Ag and Au have filled 5s and 4d and 6s and 5d subshells for available empty 5p and 6p orbitals, respectively, of un-gerade parity for hosting the higher temperature superconductivity. Au has one stable isotope with nonzero NMM: ^{197}Au with +0.148 NMM with spin 3/2 at 100% relative abundance. Ag has two stable isotopes with nonzero NMM: ^{107}Ag with −0.114 NMM with spin 1/2 at 51.84% relative abundance; and ^{109}Ag with −0.131 NMM with spin 1/2 at 48.16% relative abundance. But the experimental verification has been missing. So NMMs are more powerful for lighter elements with fewer core electrons for stronger action of the NMM on valence. But the orbital gerade and un-gerade are more powerful for elements of larger atomic number as the electrons are accelerated more in these elements. Au is more accelerated and Ag is of 5s symmetry and can involve the superconducting electron with the nucleus of the Ag of negative NMM and the Au can involve the electron to the 6s of positive NMM of Au and the Au p orbitals are un-gerade and of stronger negative lepton magnetic moments!

Just as novel effects of nonzero NMMs in carbonaceous sulfur hydrides and associated greater nuclear fields and energies assisting room temperature superconductivity for prior controversial considerations of the experimental magnetic susceptibility and electrical resistance data, the prior data of silver nanostructure in nanothin gold can also be reasoned due to effects of NMMs on emerging subshells. The data of Thapa and Pandey was said to have repeating noise between plots. Such may be a result of nuclei of nonzero NMMs of Ag and Au as reasoned by the current author of this manuscript. But the repeating noise is due to the nuclei of the Ag and Au just as the repeating noise here is from H 1s and N 2p and carbonaceous sulfur hydrides feeling nuclear noise without inner buf-

fering core subshells of similar azimuthal symmetry. The random thermal energies agitate the denser nuclei and beyond some threshold the nuclei release the same pattern from lower energetic perspectives of atomic scales and macroscale. The disorder in the nuclei is faster than light as the dense disorders escaping the nuclei rarefy, such differences escape faster than lights and can by RBL theory be associated with gravity which is superluminous, what remains is the order, that confounds Hirsch and Skinner!

But in the case of the silver and gold the emerging subshells are conduction rather than valence and core as was considered for causing controversial data for carbonaceous sulfur hydrides. With Thapa and Pandey the Ag and Au have emerging 4f and 5g outer (empty) conduction bands that may be excited (such emerging outer conduction orbitals lack core electrons). Such excitations of these outer emerging conduction bands are possible as the density of states are greater for valence shells of larger quanta. Therefore, with increasing agitations, the nuclear magnetic moments (NMMs) may excite the electrons into these outer emerging subshell states during conduction and in these states the nuclei act more strongly on the conducting electrons without shielding from underlying subshells of similar azimuthal symmetry to cause this repeating noise. So in larger elements it is true that the core electrons of similar azimuthal symmetry more strongly muffle the nuclear fields. But also with bigger atoms the conduction subshells get closer in energy so nuclei can more affect electrons and excite electrons into these outer emerging orbital with novel effects such as superconductivity as seen in silver gold nanostructures. In such nano structures of Ag/Au the electron motions in the emerging conduction bands involve the frustration of classical mechanics by nuclei reversibly fissing and fusing fields for these nuclear disorders. Such nuclear disorders escape the nuclei and in surrounding electronic lattices stretch and order with release (superluminously of excess fields) and they transiently order to push the conducting electrons of emergent subshells without buffering from any inner core subshells of similar azimuthal symmetry. Such patterns from nuclei are quanta and if they do not match the core electrons then they transmit through not being absorbed by core subshell electrons of different azimuthal symmetries. Such nuclear pressures by the author's theory stretch out to gravity both bright and dark!

21. Conclusion

So what does Little's Effect explaining Pomeranchuk Effect have to do with superconductivity? Well as the theory [2] [3] [6] [7] was used as the negative and positive moments transform the thermal spaces to electric fields, gravitational fields, magnetic fields and quantum fields; then the heat and thermal fields cannot dissipate the superconductivity. The thermal energy is transduced to fields and potential energies that support the superconductivity (rather than the disorder thermal energy dissipating the superconductivity) thereby extending the author's theory of superconductivity already published for ^{3}He to twisted bi-

layer and tri-layer graphenes. The forward and backward motions of space as transmuting positive and negative NMMs and the Br and Dk gravities and thermal spaces from larger macroscopic spaces give Background spaces in superluminosity, which prevents the rarefaction of thermal spaces and accumulates thermal spaces to mechanical spaces, electric fields, gravity fields, magnetic fields and quantum fields for explaining how superconducting conditions may involve Pomeranchuk Effect of freezing as heating a liquid. And this theory also is consistent with the author new model of the liquid state as involving rotations of nuclei relative to surrounding electrons and relative to gaseous state involving random translocations of nuclei with their electrons and relative to the solid state as involving the vibrations of nuclei relative to surrounding electrons. So the gaseous, liquid and solid states not only involve differences in motions of whole atoms but differences in motions of nuclei relative to surrounding electrons inside atoms of substances. And this model further explains the strange metal state as it involves nuclei of high relative abundance of negative NMMs and these nuclei cannot accumulate the thermal energy and these dissipate the thermal energy at the highest rates. The Ohm conductor typically has nuclei of null NMMs and/or all positive NMMs and these Ohm conductors dissipate energy slower than strange metals. This prior comprehensive theory [1] [2] [3] [6] [7] explaining high temperature superconductivity, Pomeranchuk Effect, and liquid-solid phases and phase transitions by Little Effect as by nuclear spins of positive and negative NMMs fractionally fissing and fusing for nuclear spin liquids (as by nuclei as the nuclei in liquid state are explained by rotating nucleons and nuclei spins for nuclear spin liquid) interacting in hidden ways (superluminously) with surrounding quantum discontinuum of superconducting electronic lattices to sustain superconductivity at higher temperatures from electron-phonon scattering with nuclei releasing magnetic fields for causing magnetic vorticities induce in the superconductor by the nuclear spin liquid of positive and negative vorticities [6] is proven by researchers in 2022 [24] as they observed spin liquid having hidden magnetic fields that interact with a superconductor to cause vorticities in the superconductor.

Acknowledgements

RBL thanks Stillman College for having him as Associate Professor during last 5 years.

Conflicts of Interest

The author declares no conflicts of interest regarding the publication of this paper.

References

[1] Little, R.B. (2014) Communications with Emory University (The Office of Technology Transfer).

[2] Little, R.B. (2015) *International Journal of Physical Science*, **10**, 1-37. https://doi.org/10.5897/IJPS2014.4164

[3] Little, R.B. (2009) The Ferrochemistry of Carnon Nanotubes, Diamond, Nucleic Acids and Proteins: The Magnetic Synergism of Macromolecules and Life's Chemical Patterns. In: Ottenhouse, A.P., Ed., *Carbon Nanotubes*: *New Research*, Nova Science Publishers, Inc., Hauppauge, 223-279.

[4] Rozen, A., Park, J.M., Zondiner, U., Cai, Y., Rodan-Legrain, D., Taniguchi, T., Watanabe, K., Oreg, Y., Stern, A., Berg, E., Jarillo-Herroro, P. and Ilani, S. (2021) *Nature*, **592**, 214-219. https://doi.org/10.1038/s41586-021-03319-3

[5] Pomeranchuk, I. (1950) *Zhurnal Eksperimental' noi i Teoreticheskoi Fiziki*, **20**, 919.

[6] Little, R.B. (2020) *Journal of Superconductivity and Novel Magnetism*, **33**, 901-910. https://doi.org/10.1007/s10948-019-05293-4

[7] Little, R.B. (2014) On the Mechanism of above Room Temperature Superconductivity and Superfluidity by Relativistic Quantum Mechanics.

[8] Little, R.B. (2003) Neutron Activated and Laser Stimulated Chemical Luminescence and Condensation for the Mass Production of Diamond, Carbon Nanotube and Other Carbonaceous Articles. US Patent No. US10/874,411.

[9] Cao, Y., Fatemi, V., Fang, S., Watanabe, K., Taniguchi, T., Kaxiras, E. and Jarillo-Herrero, P. (2018) *Nature*, **556**, 43-50. https://doi.org/10.1038/nature26160

[10] Little, R.B. (2021) Explaining Pomeranchuk Effect by Parity of Magnetic Moments of Leptons and Hadrons for Superconductivity in ^{3}He and Graphene.

[11] Little, R.B. (2021) Ungerade Parity, Balanced Positive and Negative Nuclear Magnetic Moments for above Room Temperature, Lower Pressure Superconductivity.

[12] Lowe, J.M., Hinrichsen, V., Schremb, M. and Tropea, C. (2021) *Physical Review E*, **104**, Article ID: 064801. https://doi.org/10.1103/PhysRevE.104.064801

[13] Gaby, D.N., Fedoret, A.A. and Klemm, O. (2020) *Aerosal Science and Technology*, **54**, 1556. https://doi.org/10.1080/02786826.2020.1804522

[14] Little, R.B. (2005) *Journal of Cluster Science*, **16**, 53-63. https://doi.org/10.1007/s10876-005-2715-9

[15] Mohammad, B. and Tehrani, D.M. (2022) *Natural Gas Industry B*, **9**, 240. https://doi.org/10.1016/j.ngib.2022.01.002

[16] Verlhac, B., Niggli, L., Bergman, A., Kamber, U., Bagrov, A., Iusan, D., Nordstrom, L., Katsnelson, M.I., Wegner, D., Eriksson, O. and Khajetoorians, A.A. (2022) *Nature Physics*, **18**, 905. https://doi.org/10.1038/s41567-022-01633-9

[17] Onnes, H.K. (2011) The Superconductivity of Mercury. Communications from the Physical Laboratory of the University, Leiden, 122-124.

[18] Zhang, C., He, X., Change, L., Li, Z., Chen, C., Jin, C., *et al.* (2022) *Nature Communications*, **13**, 5411. https://doi.org/10.1038/s41467-022-33077-3

[19] Wu, P., Cai, J., Wang, Y., Liang, P., Wang, Y., Yan, J. and Wu, T. (2022) *Acta Materialia*, **237**, Article ID: 118154. https://doi.org/10.1016/j.actamat.2022.118154

[20] Li, Y., Hao, J., Liu, H., Li, Y. and Ma, Y. (2014) *The Journal of Chemical Physics*, **140**, Article ID: 174712. https://doi.org/10.1063/1.4874158

[21] Drozdov, A.P., Eremets, M.I. and Troyan, I.A. (2015) *Nature*, **525**, 73. https://doi.org/10.1038/nature14964

[22] Li, S., Cruz-Torres, R., Santiesteban, N., Ye, Z.H., Abrams, D., Alsalmi, S., Arrington, J., *et al.* (2022) *Nature*, **609**, 41-45. https://doi.org/10.1038/s41586-022-05007-2

[23] Thapa, D.K. and Pandey, A. (2018) Evidence for Superconductivity at Ambient

Temperatures and Pressure in Nanostructures.

[24] Persky, E., Bjorlig, A.V., Feldman, I., Almoalem, Altman, E., Berg, E., Kimchi, I., Ruhman, J., Kanigel, A. and Kalisky, B. (2022) *Nature*, **607**, 692-696. https://doi.org/10.1038/s41586-022-04855-2

Journal of Modern Physics, 2023, 14, 604-622
https://www.scirp.org/journal/jmp
ISSN Online: 2153-120X
ISSN Print: 2153-1196

The Significance of Generalized Gauge Transformation across Fundamental Interactions

Bi Qiao

Wuhan University of Technology, Wuhan, China
Email: biqiao@gmail.com

How to cite this paper: Qiao, B. (2023) The Significance of Generalized Gauge Transformation across Fundamental Interactions. *Journal of Modern Physics*, **14**, 604-622.
https://doi.org/10.4236/jmp.2023.145035

Received: March 10, 2023
Accepted: April 18, 2023
Published: April 21, 2023

Abstract

The author of this paper has put forward a unified program of gauge field from the mathematical and physical picture of the principal associated bundles: thinking that our universe may have more fundamental interactions than the four fundamental interactions, and these basic interaction gauge fields are only the projection components to the base manifold, that is our universe, from a unified gauge potential or connection of the principal associated bundle manifold on the base manifold. These components can satisfy the transformation of gauge potential, and can even be transformed from one basic interaction gauge potential to another basic interaction gauge potential, and can be summarized into a unified equation, that is, the generalized gauge Equation (GGE), but the gauge potential or connection on the principal bundle is invariant, corresponding to the invariance of gauge transformation [1]. In this paper, we will continue to discuss this aspect concretely, and specifically construct a spatiotemporal model with the frame bundle as the principal bundle, and the tensor bundle as the associated bundle, so that the four fundamental interactions, especially the electromagnetic interaction and the gravitational interaction, can be reflected in the bottom manifold, that is, the regional distributions in our universe. Furthermore, this paper studies the existence of gauge transformation across basic interactions by establishing a model of gauge transformation of basic interaction field; it is found that the unified expression formula is GGE and the expression relation on the curvature of space-time. Therefore, the author discusses the feasibility of the generalized gauge transformation across the basic electromagnetic interaction and the basic gravitational interaction, and on this basis, specifically determines a method or way to find the generalized gauge transformation, so as to try to realize the last step of the "unification" of the four fundamental interactions in physics, that is, the "unification" of electromagnetism and gravity.

Keywords

Generalized Gauge Transformation, Unification of Fundamental Interactions, Principal Bundle, Connection and Curvature

1. Introduction

Following the spirit of Einstein's unified field and Yang Mills' gauge field theory [2], many scholars tried to expand the gauge "quantum" field theory to the category of gravity, hoping to establish a grand unified theory of four fundamental interactions such as gravity and electromagnetic forces [3] [4] [5] [6], but until now, gravity has not been unified with the other three basic interactions; the quantization theory of gravitational field has always been inconsistent with the microscopic quantum field theory [7] [8] [9], which has also become an exciting point for the creation of various theoretical hypotheses such as superstring and loop quantum gravity [10] [11] [12]. These still inspire us to constantly think about a question today, that is, considering the experimental fact that gravity is so weak in the elemental particle region, can we say with certainty that gravity can be quantized?

The second question is whether there are more than four basic interactions in nature? There seems to be no principle that can limit the basic interactions of nature to four kinds, namely gravity, electromagnetic, weak and strong interactions. Dark matter and dark energy have put forward an interpretation of this question from the perspective of astrophysics or cosmic scale framework [13] [14] [15] [16]. Is dark matter and dark energy the real existence or the representation of some unknown basic interactions? Suppose that there are only four basic interactions in nature, so far, by constructing a very specific product form of structural group $U(1)\times SU(2)\times SU(3)$, electromagnetic, weak and strong interactions correspond to a standard model of gauge unified field theory, which has been basically completed [17] [18] [19] [20], so the difficulty of unified field theory of four interactions is the unification of gravitational interaction and electromagnetic interaction. Therefore, in this paper, the author uses the combination of the principal fiber bundle theory and the physical concept of gauge field [1] [21] [22] [23] to establish a model of gauge transformation of four fundamental interaction fields. Specifically reveal the physical meaning of gauge transformation and GGE across four basic interaction gauge fields, especially between electromagnetic field and gravitational field, as well as the significance of connection with space-time region, so as to try to realize the last step of the unification of the four fundamental interactions in physics, namely a "unity" of electromagnetism and gravity.

2. Basic Point of View

1) The four basic interactions of gravity, electromagnetic force and strong and

weak are forces related to the connection and curvature of space-time regions. Why is it so difficult to unify gravity and electromagnetic force? One possible reason is that gravity is very weak in the space-time region of quantum distribution, so its quantization is not worth and may not exist.

2) Similarly, the gravity of long-range interaction can reach a very strong vast area, and the short-range interaction such as strong and weak cannot reach these space-time areas. Although the electromagnetic force may be relative weak, it is still the long-range interaction, so it can intersect with gravity, which gives a foundation for the unification of electromagnetic force and gravitational force, namely the specification transformation across the basic interaction on the intersection of electromagnetic interaction and gravitational interaction. Therefore, the basis of unification can only be based on their space-time characteristics, which is represented by the invariance of gauge transformation, that is, from a mathematical and physical point of view, they are the projection components in the universal bottom manifold from the connection or curvature of the high-dimensional space-time manifold of the principal associated bundles of the universe.

3) The connection of the higher-dimensional space-time manifold of the principal bundle is the gauge potential, the curvature is the gauge field strength, and the connection of the associated bundle is the gauge field, which will not change with the gauge transformation. The gauge transformation is only the transformation between components where the base manifold (our universe) has an intersection domain of the interactions, and the meaning of the gauge transformation across the basic interactions is the transformation between the basic interaction components that are projected at the intersection domain, for example, the transformation of gauge potentials between electromagnetic interaction and gravitational interaction.

4) The four basic fields of the universe (gravity, electromagnetic force, weak force, strong force) are unified in one cosmic space-time gauge potential $\tilde{\boldsymbol{\omega}}$ (corresponding to a cosmic space-time gauge field). The corresponding gauge field and the mutual transformation between the four fundamental gauge fields can be expressed by a generalized gauge potential transformation Equation (GGE for short): its concise expression under certain conditions is the curvature similarity equation:

$$\boldsymbol{\Omega}_V = g_{UV}^{-1}\boldsymbol{\Omega}_U g_{UV}$$

here, $\boldsymbol{\Omega}_V$ and $\boldsymbol{\Omega}_U$ is the projected component of the curvature $\tilde{\boldsymbol{\Omega}}$ of the principal bundle on the bottom manifold region V and U respectively, g_{UV} is the conversion function of these region components, which is associated with a generalized gauge transformation. It shows that all different gauge potentials or curvatures are just the components of the unified connection or curvature of the spatiotemporal manifold of the principal associated bundle of the universe in different regions of the base manifold; based on this equation, we can determine a method or approach to find the generalized gauge transformation.

3. On the Construction of Principal Associated Bundles

3.1. Concept

The principal fiber bundle $P(M,G)$ is composed of a bundle manifold $P=G\times M$. The bottom manifold (which can represent our universe) M is composed of the structure group as a Lie group G; in order to meet the requirements of general relativity, M is matched with metric, G is a Lie group including 4 subgroups and their product $SO(1,3)\times U(1)\times SU(2)\times SU(3)$, and also contain the group element field that can include the conversion function between the four basic interactions (*i.e.* gravity, electromagnetic, weak and strong interactions). For the requirements of associated bundle, it is important to select the typical fiber F: F is required to include the basic interaction fields such as gravitational field and electromagnetic field.

3.2. The Relations between Projection Mapping of Principal Bundle and Associated Bundle

1) $\hat{\tau}: P\times F\to Q$, defined as $\hat{\tau}(p,f):=(p,f)=p\cdot f\in Q$. That is, $\forall p\in P$, $\hat{\tau}_p: F\to Q$; from this, one can define the topology of Q so that $\phi\subset Q$ is open if and only if $\hat{\tau}^{-1}[\phi]\subset P\times F$ is open, then Q is topological space, $\hat{\tau}$ is continuous mapping. Not only that, we can also prove that Q is a manifold.

2) $\hat{\pi}: Q\to M$, defined as: $\hat{\pi}(q):=\pi(p)\in M, \forall q=p\cdot f\in Q$. $\therefore$ more accurately, $\hat{\tau}_p: F\to\hat{\pi}^{-1}[x]$, $x\equiv\pi(p)$; $R_p: G\to\pi^{-1}[x]$, $x\equiv\pi(p)$, and $\hat{\tau}_p$, R_p are all differential homeomorphic maps. In other words, $\hat{\tau}_p$, R_p respectively brings the manifold structure of F or G into the fiber $\hat{\pi}^{-1}[x]$ of the associated bundle Q or the fiber $\pi^{-1}[x]$ of the principal bundle P.

3) $\tau: P\times F\to P, \tau(p,f):=p, \forall p\in P, f\in F$.

4) $\pi: P\to M$, and meet: $\pi^{-1}[\pi(p)]=\{pg\,|\,g\in G\}, \forall p\in P$.

Here, the relevant definitions in (3) and (4) have been given by [1] [23].

If every $x\in M$ has an open neighborhood $\mathcal{M}\subset M$, whose inverse image $\pi^{-1}[\mathcal{M}]$ and product manifold $\mathcal{M}\times G$ is differential homeomorphism, *i.e.* $\pi^{-1}[\mathcal{M}]=\mathcal{M}\times G$, then the corresponding $T_{\mathcal{M}}$ is local trivial, and the corresponding principal bundle is local trivial, where $\mathcal{M}$ may correspond to four regions, namely the gravitational interaction region V, electromagnetic interaction area U, strong interaction region W_1 and weak action area W_2. If $\mathcal{M}=M$, then $\pi^{-1}[\mathcal{M}]=P=M\times G$ is called as globe trivial. In general, it can be said that any principal bundle is local trivial, so one can extend the local trivialization to the principal associated bundle diagram of universe as see **Figure 1**.

Therefore, through the analysis of the requirements for the structure group G, manifold M and typical fiber F mentioned above, we can consider selecting the frame bundle as the principal bundle and the tensor bundle as its associated bundle to form a cosmic principal associated bundle structure.

3.3. The Frame Bundle as Principal Bundle

M is supposed as the n-dimensional manifold, $P\equiv\{x,\{e_\mu\}\,|\,x\in M\}$, $\{e_\mu\}$ is a

$$\begin{array}{ccccc} & & \pi^{-1}[\mathcal{M}]\times F & & \\ & & \tau\downarrow \quad \downarrow\hat{\tau} & & \\ \mathcal{M}\times G & \overset{T_{\mathcal{M}}}{\leftarrow} & \pi^{-1}[\mathcal{M}] \quad \hat{\pi}^{-1}[\mathcal{M}] & \overset{\hat{T}_{\mathcal{M}}}{\rightarrow} & \mathcal{M}\times F \\ & & \pi\downarrow \quad \downarrow\hat{\pi} & & \\ & & \mathcal{M} \quad = \quad \mathcal{M} & & \end{array}$$

Figure 1. A more specific structure of the principal associated bundle diagram of the universe, $\pi^{-1}[\mathcal{M}]$ and $\hat{\pi}^{-1}[\mathcal{M}]$ represent the principal fiber bundle and associated bundle on $\mathcal{M}$ respectively; here $\mathcal{M}$ represents the overall trivial or locally trivial region on *M*, which may correspond to four regions, namely, the region of gravitational interaction *V*; the region of electromagnetic interaction *U*; the region of strong interaction W_1 and the region of weak interaction W_2.

basis of T_xM, abbreviated as $e_\mu T_x$ represents the tangent space of $x\in M$. Then *P* can be proved to be $n+n^2$ dimensional manifold. Now choose $GL(n)$ as the structure group *G*, which is large enough to contain the subgroups $SO(1,3)$, $U(1)$, $SU(2)$, $SU(3)$, and $SO(1,3)\times U(1)\times SU(2)\times SU(3)$, then a frame bundle can be constructed by the following three steps:

1) Define the right action of the matrix group $GL(n)$ on *P*, $R: P\times GL(n)\to P$ as $R_g\left(x,e_\nu g_\mu^\nu\right)$, where g_μ^ν represents *g* matrix elements.

2) Define the projection map $\pi: P\to M$, that is, $\pi\left(x,e_\mu\right):=x,\forall\left(x,e_\mu\right)\in P$.

3) Define local trivial $T_U:\pi^{-1}[U]\to U\times G$, $T_U\left(x,e_\mu\right):=(x,h)$, where $h\equiv S_U\left(x,e_\mu\right)\in G$, $\left.\dfrac{\partial}{\partial x^\nu}\right|_x h_\mu^\nu=e_\mu$, and $S_U(pg)=S_U(p)g,\forall g\in G$. So T_U is differential homeomorphism.

The principal bundle $P\left(M,GL(n)\right)$ constructed by the above three steps is called the frame bundle and is recorded as *FM*.

3.4. Tensor Bundle as Associated Bundle

On the basis of *FM*, take manifold $F=\mathbb{R}^n$, then *F* is vector space, $f\in F$ can be expressed as a column matrix of *n* real numbers, namely $\left(f^1,\cdots,f^n\right)$; so we can define left action $\chi: G\times F\to F$ is $\left(\chi_g(f)\right)^\mu:=g_\nu^\mu f^\nu$, $\forall g\in GL(n)$, $f\in F$; by right and left actions one can determine $\xi:(P\times F)\times G\to P\times F$, $\xi_g: P\times F\to P\times F$. Specifically $\xi_g(p,f)=\left(pg,g^{-1}f\right)\Rightarrow$ $\xi_g\left(x,e_\mu;f^\rho\right)=\left(x,e_\nu g_\mu^\nu;\left(g^{-1}\right)_\sigma^\rho f^\sigma\right)$. Here $\left(x,e_\mu;f^\rho\right)\in P\times F$ can produce $v\equiv e_\mu f^\mu\in T_xM$, and on the same orbit $v=e_\mu f^\mu=v'=e'_\mu f'^\mu$; that is to say, every $q\in\hat{\pi}^{-1}[x]$ point (representing a orbit) 1-1 corresponds to vector *v* in T_xM, all different *v* in T_xM correspond to different *q* above to form a tangent bundle $\hat{\pi}^{-1}[x]$, namely $\hat{\pi}^{-1}[x]\overset{1\text{-}1}{\longleftrightarrow}T_xM$; so tangent bundle $Q=P\times F/\sim$ (here, ~representing equivalence relationship) is the associated bundle of *FM*. Further, *Q* can be regarded as the tangent bundle *TM* on *M*, $Q=TM$, so that the cross-section of any region $\hat{\sigma}[U]:U\to Q$ (because 1-1 corresponds to the vector of tangent space on *U*) is a tangent field on $U\subset M$. Since it is a vector field, at least preliminary description of the cross-section $\hat{\sigma}:U\to Q$ is related to the regional distribution. Different cross-sections correspond to different re-

gional distributions, and there is a transformation relationship of the transfer function between the cross-sections.

More than this, on the basis of *FM*, if the manifold $F=\left(\mathbb{R}^n\right)^*=\mathcal{T}_{\mathbb{R}^n}\left(0,1\right)$, $f=\left(f_1,\cdots,f_n\right)\in F$, $\left(\chi_g\left(f\right)\right)_\mu\coloneqq\left(g^{-1}\right)_\mu^\nu f_\nu$, then giving any point $\left(x,e_\mu;f_\rho\right)\in P\times F$, it can produce: $\beta\equiv e^\mu f_\mu\in T_x^*M$ (the dual space of T_xM), and there is $\beta=\beta'$ on the same orbital; all the different β in T_x^*M correspond to the different q above it to form a cotangent bundle $\hat{\pi}^{-1}\left[x\right]$, that is, $\hat{\pi}^{-1}\left[x\right]\xleftrightarrow{1\text{-}1}T_x^*M$; so the cotangent bundle $Q=P\times F/\sim$ is also an associated bundle of *FM*. Any of its section $\hat{\sigma}:U\to Q$ is a covector field (dual vector field) on $U\subset M$.

Further, if $P=FM$, $G=GL\left(n\right)$, $F=\mathcal{T}_{\mathbb{R}^n}\left(1,1\right)$, $f=\left(f_\nu^\mu\right)\in F$, then choose: 1) $\chi:G\times F\to F$; 2) $\hat{G}\equiv\left\{\chi_g:F\to F\middle|g\in G\right\}$ is a Lie transformation group, which is the homomorphic mapping or realization or representation of *G*, and *F* is the realization space; then the left action can be defined: $\left(\chi_g\left(f\right)\right)_\nu^\mu\coloneqq g_\alpha^\mu\left(g^{-1}\right)_\nu^\beta f_\beta^\alpha,\forall g\in GL\left(n\right),f\in F$. So any given point $\left(x,e_\mu;f_\sigma^\rho\right)\in P\times F\leftrightarrow T_b^a\coloneqq\left(e_\mu\right)^a\left(e^\nu\right)_b f_\nu^\mu$, that is, T_b^a is a tensor of type (1, 1) in point *x*. The necessary and sufficient condition of $T_b^a=T_b'^a$ is that the given points are on the same orbit. Then we get a tensor bundle of type (1, 1) on the bottom manifold *M*, which is also an associated bundle of *FM*. Any of its section $\hat{\sigma}:U\to Q$ is a (1, 1) type tensor field on $U\subset M$.

After consideration, the author boldly believes that one of the more universal possible structures of the principal associated bundles of the universe is the frame bundle plus $\left(k,l\right)$ tensor bundle as the associated vector bundle. According to the previous analysis and requirements, it can be considered that the principal associated bundle structure of the universe can accommodate the universal gauge fields and the corresponding four basic interactions. The main reasons are as follows:

1) Its structure group $GL\left(n\right)$ is a general linear transformation matrix group, which is sufficient to contain the subgroups $SO\left(1,3\right)$, $U\left(1\right)$, $SU\left(2\right)$, $SU\left(3\right)$ or subgroup product $G=SO\left(1,3\right)\times U\left(1\right)\times SU\left(2\right)\times SU\left(3\right)$ corresponding to the gauge transformation of the basic interactions required by the principal bundle sections transformation.

2) The (1, 3) tensor bundle, as the structure of the associated vector bundle, may be sufficient to contain all kinds of gravitation-related tensor fields, electromagnetic force gauge fields, etc. However, the relatively simple structure of the principal associated bundle of the universe may still be the frame bundle plus tangent bundle, *FM* + *TM*.

4. Principal Associated Bundles and Gauge Field

4.1. Gauge Selection and Section

Definition: Let $P\left(M,G\right)$ be the principal bundle, *U* be the open subset of *M*, C^∞ mapping $\sigma:U\to P$ is called a local section, if $\pi\left(\sigma\left(x\right)\right)=x,\forall x\in U$. Here

if $U=M$, then $\sigma:M\to P$, which is called the globe section. In the case of a local cross-section, we further explore the physical meaning of the cross-section: let U be the open subset of the bottom manifold M, and G be the structural group to construct a non-trivial principal bundle $P=U\times G$, where the free right-hand action of G on P is: $R:(U\times G)\times G\to U\times G$, that is, $\forall g_1\in G$, define $R_{g_1}:U\times G\to U\times G$ as: $R_{g_1}(x,g_2):=(x,g_2g_1)$, $\forall(x,g_1)\in U\times G$. Let $\sigma:U\to P$ and $\sigma':U\to P$ be the local section of P respectively, then $\forall x\in U$ has a unique group element field $g:U\to G$ such that: $\forall g(x)\in G, x\in U$, $\sigma'(x)=\sigma(x)g(x)^{-1}$. Therefore, there exists a representation group element such that $U(x)\equiv\rho(g(x))\in\hat{G}$, so that a local gauge transformation can be constructed to act on the local gauge field $\phi(x)$: $\phi'(x)=U(x)\phi(x)\equiv\rho(g(x))\phi(x),\forall\phi(x)\in\mathcal{V}$, where $\mathcal{V}$ is the representation space of $\hat{G}$, and $\hat{G}$ is a representation of G. At this time, $\phi(x)$ is actually a column matrix, and $\rho(g(x))$ is a square matrix, *i.e.* $\rho(g(x)):G\to\hat{G}$. In addition, if the tangent bundle TM is selected as the associated bundle of FM, then there is naturally: $F=\mathcal{V}$ (the representation space of ρ), through the left action $\chi:G\times F\to F$ as $\forall g_1\in G$, $\chi_{g_1}:F\to F$, $\chi_{g_1}(f_1):=\rho(g_1)(f_1),\forall f_1\in F$, then there is an associated bundle

$$\Phi(x)\equiv q=p\cdot f=\sigma(x)\cdot f(x)\in\hat{\pi}^{-1}[x]\subset Q,$$

where $f:U\to F=\mathcal{V},\forall f(x)\in F=\mathcal{V}$. So $\Phi(x)$ is determined by the cross-section σ and f. In addition, $g(x)$ can generate: 1) $\sigma'(x)=\sigma(x)g(x)^{-1}$, 2) $f'(x)=\chi_{g(x)}f(x)=\rho(g(x))f(x)=U(x)f(x)$ (*i.e.* gauge transformation), which is equivalent to

$$\begin{aligned}\Phi'(x)&=\sigma'(x)\cdot f'(x)=\sigma(x)g(x)^{-1}\cdot g(x)f(x)\\&=\sigma(x)\cdot g(x)^{-1}g(x)f(x)=\sigma(x)\cdot f(x)=\Phi(x)\in\hat{\pi}^{-1}[x]\end{aligned}.$$

It can be seen from the above that the so-called local (global) gauge transformation is actually the transformation section $\sigma(x)\to\sigma'(x)$, which is equivalent to the transformation of the frame and the transformation of the component of the physical field under the internal frame field, namely, $f(x)=\phi(x)\to f'(x)=\phi'(x)$, but the total physical field (internal vector $\Phi(x)$) is constant, *i.e.* $\Phi'(x)=\Phi(x)$. The so-called gauge selection is to select different cross-section while one cross-section on the associated bundle $\hat{\sigma}$ is exactly the invariant physical field $\Phi(x)$! In short, the change of cross-section on the principal bundle is the change of internal frame. If the internal frame change, it is equivalent to changing a gauge. Therefore, selecting a cross-section of the principal bundle is to select a gauge, as shown in **Figure 2**.

4.2. Construction of Generalized Gauge Transformation

The above discussion (including the generalization of the Yang-Mills potential [1] [2] [22] [23]) shows that in the very general principal associated bundle structure, that is, in $\phi'(x)=U(\vec{\theta}(x))\phi(x)$ equation, one can choose to define $U(\vec{\theta}(x))\equiv\rho(g(x))\in\hat{G}$, then one can construct a local gauge transformation:

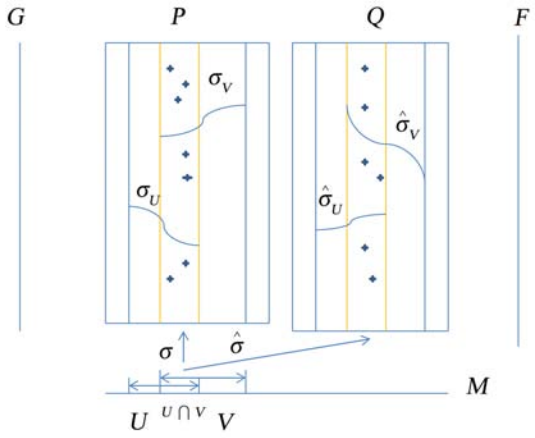

Figure 2. The cross-section of the principal bundle is the choice of gauge; the cross-section of the associated bundle is the gauge field $\Phi(x)$. $\forall x \in U \cap V$, then $\sigma_V(x) = \sigma_U(x) g_{UV}(x)$ represents the gauge transformation, where the conversion function $g_{UV}: U \cap V \to G$, $g_{UV}(x)$ is the group element field. Besides, W_1, W_2, $W_1 \cap W_2 \subset U$.

$$\phi'(x) = U(x)\phi(x) \equiv \rho\big(g(x)\big)\phi(x), \forall \phi(x) \in \mathcal{V},$$

where $\mathcal{V}$ is the representation space of $\hat{G}$. Then choose $F = \mathcal{V}$, $\forall f(x) \in F = \mathcal{V}$, define

$$\Phi(x) \equiv \sigma(x) \cdot f(x) \in \hat{\pi}^{-1}[x] \subset Q,$$

where $f(x) \in F$, F is a typical fiber, one can deduce $\Phi'(x) = \Phi(x)$. In addition, for the principal bundle *FM* and associated bundle *TM*, $q = \sigma(x) \cdot f^{\mu} = \big(x, e_{\mu}\big) f^{\mu} = e_{\mu} f^{\mu} = e'_{\mu} f'^{\mu} \equiv v \sim \Phi(x)$, v is called a space-time vector (representing a tangent vector of point *x*), and $\Phi(x)$ can be called an internal vector of point *x*; $\sigma(x)$ is called the internal frame of point *x*, and $f^{\mu}(x)$ is called the component of the internal vector expanded by the internal frame. But if $\sigma(x) g(x)^{-1} = \sigma'(x)$, there are also internal vectors that are invariant under the gauge transformation: $\Phi(x) = \Phi'(x)$, changing only its component $\phi(x) \to \phi'(x)$. In the discussion in [1] [22] [23] one also saw that in order to ensure the invariance of the total Lagrangian density $\mathcal{L}$ under local gauge transformation, that is, equivalent to cross-sectional transformation of the principal bundle *P*, the (electromagnetic) gauge potential $A_{\mu}(x)$ must be introduced, and make its across basic interaction gauge transformation (that is, cross section transformation $\sigma'(x) = \sigma(x) g(x)^{-1}$, where $g(x)$ is a group element field) to become (gravitational) gauge potential $A'_{\mu}(x)$, then $A_{\mu}(x) \to A'_{\mu}(x)$ (that is, the gauge potential transformation that satisfies GGE [1], and see Equation (2) below) also corresponds to an absolute invariance, that is, the connection $\tilde{\boldsymbol{\omega}}$ on the principal bundle, or the connection on the principal bundle is the gauge potential, which is invariant under the gauge potential transformation (it corresponds to the internal vector is invariant under gauge transformation), what change is only its component on the bottom manifold. A

connection on the principal bundle $P(M,G)$ is to the local triviality $T_U:\pi^{-1}[U]\to U\times G$ specifies a 1-form field $\boldsymbol{\omega}_U$ of C^∞ $\mathcal{G}$ value on U, that is, $\boldsymbol{\omega}_U$ is a connection on the bottom manifold region $U\subset M$. At this time, if $T_V:\pi^{-1}[V]\to V\times G$ is another local triviality, that is, $U\bigcap V\neq\varnothing$, and the transition function from T_U to T_V is g_{UV}, then the transformation between $\boldsymbol{\omega}_U$ and $\boldsymbol{\omega}_V$ is given by GGE description:

$$\boldsymbol{\omega}_V(Y)=\mathcal{A}d_{g_{UV}(x)^{-1}}\boldsymbol{\omega}_U(Y)+L^{-1}_{g_{UV}(x)*}g_{UV*}(Y),\ \forall x\in U\bigcap V,\ Y\in T_xM \tag{1}$$

where $L^{-1}_{g_{UV}(x)}$ is the inverse mapping of left translation $L_{g_{UV}(x)}$ generated by $g_{UV}(x)\in G$, $L^{-1}_{g_{UV}(x)*}\equiv\left(L^{-1}_{g_{UV}(x)}\right)_*$.

Or for general cases, define: $-iL_r\equiv\rho_*e_r\in\hat{\mathcal{G}}$, here $\hat{\mathcal{G}}$ is the representation of Lie algebra of G, or Lie algebra of $\hat{G}$, e_r is a basis vector of Lie algebra $\hat{\mathcal{G}}$, ρ_* is the push forward mapping of ρ, then one can define $\hat{A}_\mu(x)\equiv-i\vec{L}\cdot\vec{A}_\mu(x)=-iL_rA^r_\mu(x)\in\hat{\mathcal{G}}$, therefore, the Formula (1) becomes the Formula (2) below, and it can be proved that the right side of the Formula (2) also belongs to $\hat{\mathcal{G}}$, namely

$$\hat{A}'_\mu(x)=U\left(\vec{\theta}(x)\right)\hat{A}_\mu(x)U\left(\vec{\theta}(x)\right)^{-1}-k^{-1}\partial_\mu U\left(\vec{\theta}(x)\right)U\left(\vec{\theta}(x)\right)^{-1} \tag{2}$$

Here the transfer function $U\left(\vec{\theta}(x)\right)$ for the gauge potential transformation across the basic interactions can be determined by the chosen the cross-sections.

For example, if one take the general gauge potential on the bottom manifold (that is, it is not limited to the electromagnetic gauge potential, but also includes the gravitational gauge potential) as: $A^r_\mu(x)\to A'^r_\mu(x)$ (1 form field of real or complex value), then there are: $e_rA^r_a\in\Lambda_U(1,\mathcal{G})$, where e_r is the basis in Lie algebra $\mathcal{G}$. In addition,

$$\boldsymbol{\omega}=\sigma^*\tilde{\boldsymbol{\omega}}\to\boldsymbol{\omega}'=\sigma'^*\tilde{\boldsymbol{\omega}},\forall\boldsymbol{\omega},\boldsymbol{\omega}'\in\Lambda_M(1,\mathcal{G}),$$

where $\Lambda_M(1,\mathcal{G})$ is the set of 1-form fields of the valued Lie algebra $\mathcal{G}$ taken from M. So one can define: $\omega_a\equiv ke_rA^r_a\in\Lambda_M(1,\mathcal{G})$, or $\boldsymbol{\omega}\equiv ke_r\boldsymbol{A}^r\equiv k\boldsymbol{A}\in\Lambda_M(1,\mathcal{G})$, note that here $U\in M$, M is a general base manifold which is suitable to satisfy the local trivial condition, that is, the manifold of our "universe" which can be equipped with a suitable metric. The gauge potential of the so-called basic interaction respectively corresponds to the gauge potential of electromagnetism, gravitation, weak interaction, and strong interaction in the bottom manifold $U\bigcap V$, or W_1, W_2, $W_1\bigcap W_2\subset U$ as well as respectively corresponds to the relevant subgroups or subgroup product $SO(1,3)\times U(1)\times SU(2)\times SU(3)\in GL(n)$, etc.

Now we want to discuss that the $\boldsymbol{\omega}$ and $\boldsymbol{\omega}'$ defined in this way satisfy the transformation relation (1), $\boldsymbol{\omega}_V(Y)\to\boldsymbol{\omega}_U(Y)$, of course this is a cross basic interaction gauge potential, if it is the transformation between gravitational gauge potential and electromagnetic gauge potential, then its corresponding structure group may be the subgroup product $SO(1,3)\times U(1)\in GL(n)$.

For example, if $\omega_\mu\equiv ke_rA^r_\mu\in\Lambda_U(0,\mathcal{G})$, $\omega'_\mu\equiv ke_{r'}A^{r'}_\mu\in\Lambda_V(0,\mathcal{G})$, then it is uniformly written as $\omega_\mu(x)\equiv ke_rA^r_\mu(x)\in\mathcal{G}$, now let the gauge transformation

be

$$\sigma_V(x)=\sigma_U(x)g_{UV}(x)=\sigma'(x)=\sigma(x)g^{-1}(x) \tag{3}$$

Essentially it is possible to define the transition function as

$$g_{UV}(x)\equiv\sigma_U(x)^{-1}\sigma_V(x) \tag{4}$$

For the transformation between gravitational gauge potential and electromagnetic gauge potential, the establishment of Formula (1) seems to be no problem, but the most important thing to determine in Formula (1) is $g^{-1}(x)$ or the "choice" of $g_{UV}(x)$, *i.e.* what exactly does it equal? The "selection" of $g^{-1}(x)$ or $g_{UV}(x)$ is related to $\sigma_V(x)$ and $\sigma_U(x)$, that is, to the gauge transformation (3). In addition, $g_{UV}(x)$ is related to U and V area, and through σ_V, σ_U induce the cross sections of the associated bundle $\hat{\sigma}_V=\hat{\sigma}_U\Rightarrow\Phi'(x)=\Phi(x)$ and then determine the components of the gauge field $\Phi(x)$, *i.e.* ϕ_V, ϕ_U, in the base manifold *M*. This is just one of the mysteries of gauge transformation. Here the selection of the gauge with respect to ϕ_V gravitational field and ϕ_U electromagnetic field is determined by the V area corresponding to the gravitational area and U area corresponding to the electromagnetic force area in the "universal" base manifold, or it is determined by the "boundary conditions" and the intersection domain $U\bigcap V$ of the gravitational and electromagnetic effects respectively. The other two basic interactions, namely the strong interaction and the weak interaction, are basically considered to have no area intersection with the gravitational interaction, so Formulas (3) or (4) determines that $g_{UV}\equiv g^{-1}$ is the "group element" of gauge transformation, $g_{UV}:U\bigcap V\to G$, which can transform the electromagnetic field ϕ_U into the gravitational field ϕ_V. So this kind of gauge transformation across the basic interaction field can exist, and no "restriction" is found from the theoretical point of view of the principal associated bundles above.

Furthermore, if assume $\sigma_U:U\to P$ and $\sigma_V\to V$ are two local cross-sections of *P*, then there is a unique $g(x)\in G$, $\forall x\in U\bigcap V$ so that Equation (3) holds. It shows that a section transformation $\sigma_U\to\sigma_V$ of the principal bundle gives a group element field $g_{UV}\equiv g^{-1}$ on $x\in U\bigcap V$, and thus a local gauge transformation constructed with group element $g(x)$ can be determined, *i.e.*

$$U(x)\equiv\rho\left(g(x)\right)\in\hat{G} \tag{5}$$

Using $U(x)\equiv U\left(\boldsymbol{\theta}(x)\right)$ to act on the gauge field $\Phi(x)$ (column matrix) one can get the local gauge transformation (between electromagnetism and gravity),

$$\phi_V(x)=U(x)\phi_U(x)=\rho\left(g(x)\right)\phi_U(x) \tag{6}$$

That is, one can define:

$$U(x)\equiv\phi_V(x)\phi_U(x)^{-1} \tag{7}$$

Here, ρ is again defined as a homomorphic mapping: $G\to\hat{G}$, $\hat{G}$ is a representation of *G* or a Lie transformation group. Therefore $\rho\left(g(x)\right)$ is a re-

presentation of G (for example, it is possible $SO(1,3)\times U(1)$), that is, $U(x)$ is a group element field of Lie transformation G, and by the product of column matrix $\phi_V(x)$ and row matrix $\phi_U(x)^{-1}$ is defined as a matrix.

The question now is why it is said that $U(x)\equiv\phi_V(x)\phi_U(x)^{-1}$ represents the gauge transformation from the electromagnetic field to the gravitational field, rather than a gauge transformation between other gauge fields? That is, why is $\phi_U(x)$ an electromagnetic field, and $\phi_V(x)$ represents a gravitational field? The answer is: 1) the subgroup $SO(1,3)$ in the structural group G on our model (see Figure 2) corresponds to the gravitational field, and $U(1)$ corresponds to the electromagnetic field; 2) The area U in the region corresponds to the boundary condition of electromagnetic interaction, and V corresponds to the boundary condition of gravitational interaction in the bottom manifold of the principal and associated bundle of the universe, so the section of the principal bundle on the area U corresponds to electromagnetic interaction, and the section of principal bundle on the area V corresponds to gravitational interaction. Zone is a spacetime! Reflecting the introduced ($T_U\to T_V$) transition function $g_{UV}:U\bigcap V\to G$ is connected with the transformation of space-time "features", because in essence, both the gravitational gauge potential and the electromagnetic gauge potential are related to the regions. So they are also related to the connection properties of time and space, and are the projection of the "unchanged" principal bundle connection and the pull-back mapping of the related cross-sections in "our world", reflecting the different properties of time and space connection. Therefore, it is appropriate to introduce the definition of g_{UV} into Formula (4), so as to determine Formula (7). Hence there are also related to the determination of Formula (4) as following:

$$\boldsymbol{\omega}_U=\sigma_U^*\tilde{\boldsymbol{\omega}},\boldsymbol{\omega}_V=\sigma_V^*\tilde{\boldsymbol{\omega}},\forall\boldsymbol{\omega}_U\in\Lambda_U(1,\mathcal{G}),\boldsymbol{\omega}_V\in\Lambda_V(1,\mathcal{G}) \tag{8}$$

$\boldsymbol{\omega}_U$ under the pullback mapping of the section σ_U^* in the above formula corresponds to the electromagnetic gauge potential on the bottom manifold U, while $\boldsymbol{\omega}_V$ under the pullback mapping of the section σ_V^* corresponds to the gravitational gauge potential on the bottom manifold V, both are components of connection $\tilde{\boldsymbol{\omega}}$ of the principal bundle. This cross-basic interaction can be further explained by the cosmic principal associated bundles structure about the basic interactions that we constructed in Figure 2.

That is, on the bottom manifold, let the W_1 and W_2 areas represent the strong interaction area and the weak interaction area, and they have an intersecting area, that is, $W_1\bigcap W_2$; U represents the electromagnetic interaction area, and V represents the gravitational interaction area. Electromagnetic interaction is equivalent to "intermediary", it has intersections with W_1, W_2 and V, but considering that the strength of gravity is extremely small in the area of strong and weak interactions, it can be considered that V has no intersections with W_1, W_2! Therefore, from the point of view of physical experiment observation, at $x\in U\bigcap V$, based on the cross-sections σ_U^* and σ_V^*, only two basic interactions of electromagnetism and gravitation can be observed, which correspond to

two kinds of space-time connections $\boldsymbol{\omega}_U$ and $\boldsymbol{\omega}_V$ respectively, and these are the two components of the space-time connection $\tilde{\boldsymbol{\omega}}$ of the principal bundle, which is established on the basis of our universe. The unique group field $g_{UV}(x) \in G$ can be determined from the transformation relationship between $\boldsymbol{\omega}_U$ and $\boldsymbol{\omega}_V$ in Equation (4), where G is the structural group. Further, Formula (7) can be deduced to determine the gauge transformation $U(x)$ with more physical meaning, that is, $U(x)$ is a Lie transformation group element field of G, and it is composed of the product of column matrix $\phi_V(x)$ and row matrix $\phi_U(x)^{-1}$ as a matrix. These "requirements" are fed back to the structure group G. Fortunately, the structure group we choose for the principal associated bundle is the general linear matrix group $GL(n)$, which is large enough to meet the requirements of the matrix group for gauge transformations between basic interactions. Although the author is not yet able to say what the specific structure of those necessary subgroups is, $GL(n)$ certainly include $SO(1,3)\times U(1)\times SU(2)\times SU(3)$ as its subgroup. Here $\phi_V(x)$ or $\phi_U(x)$ belongs to the typical fiber F, namely $\phi: U \cap V \to F$.

For the case of the region $U \cap V$ where both the gravitational gauge potential and the electromagnetic gauge potential exist, it can be proved that both sides of the Equation (2) belong to the representation $\hat{\mathcal{G}}$ of Lie algebra, which is a kind of matrix expression equation. If Formula (7) is given, Formula (2) can be calculated in principle. Further, by introducing the generalized Yang-Mills field strength, that is, introducing R gauge potentials $A_\mu^r(x)$, then there should be R gauge field strengths $F_{\mu\nu}^r(r=1,\cdots,R)$ correspondingly, they can be expressed as:

$$F_{\mu\nu}^r(x) = \partial_\mu A_\nu^r - \partial_\nu A_\mu^r + k\sum_{s,t=1}^{R} C_{st}^r A_\mu^s(x) A_\nu^t(x), (r=1,\cdots,R) \tag{9}$$

Here C_{st}^r represents the structural constant of the Lie algebra $\hat{\mathcal{G}}$ of G under the basis $\{e_r\}$; the metric $g^{\mu\alpha}$, $g^{\nu\beta}$ can be used to improve the index of $F_{\alpha\beta}^r$: $F^{r\mu\nu} = g^{\mu\alpha} g^{\nu\beta} F_{\alpha\beta}^r$.

Then introduce the simplified notation: $\hat{F}_{\mu\nu}(x) \equiv -iL_r F_{\mu\nu}^r(x) \in \hat{\mathcal{G}}$, the similar Formula (9) can be changed to

$$\hat{F}_{\mu\nu}(x) = \partial_\mu \hat{A}_\nu(x) - \partial_\nu \hat{A}_\mu(x) + k\left[\hat{A}_\mu(x), \hat{A}_\nu(x)\right] \tag{10}$$

where $\left[\hat{A}_\mu(x), \hat{A}_\nu(x)\right]$ is the Lie bracket of the Lie algebra element $\hat{A}_\mu(x)$ and $\hat{A}_\nu(x)$. Among them, k is defined as the coupling constant, $k = e \leftrightarrow$ Electromagnetic gauge field; $k = -1 \leftrightarrow$ Gravitational gauge field; then consider Equation (10) and gauge transformation formula, an important mutual transformation matrix expression between electromagnetic intensity and gravitational intensity can be given by

$$\hat{F}'_{\mu\nu}(x) = U(\boldsymbol{\theta}(x)) \hat{F}_{\mu\nu}(x) U(\boldsymbol{\theta}(x))^{-1} \tag{11}$$

4.3. Existence of Generalized Gauge Transformation

The origin of the above Formula (11) can also be explained more clearly from

the curvature transformation relation ($\boldsymbol{\Omega} \to \boldsymbol{\Omega}'$). In fact, under the cross-section transformation σ, the transformation relationship of $\boldsymbol{\omega} \to \boldsymbol{\omega}'$ on the bottom manifold is Formula (1), but the transformation relationship of $\boldsymbol{\Omega} \to \boldsymbol{\Omega}'$ needs to prove the following theorems to get [1] [23]:

Theorem 1: $\boldsymbol{\Omega} \Leftrightarrow F_{\mu\nu}^{r}(x)$, *i.e.*

$$\begin{cases} \boldsymbol{\Omega} = d\boldsymbol{\omega} + \dfrac{1}{2}[\boldsymbol{\omega}, \boldsymbol{\omega}] \\ \Updownarrow \\ F_{\mu\nu}^{r}(x) = \partial_\mu A_\nu^r - \partial_\nu A_\mu^r + k\sum_{s,t=1}^{R} C_{st}^r A_\mu^s(x) A_\nu^t(x), (r = 1, \cdots, R) \end{cases} \tag{12}$$

Proof

Using Cartan's second structural equation, one can get

$$\begin{aligned} \boldsymbol{\Omega} &= d\boldsymbol{\omega} + \frac{1}{2}[\boldsymbol{\omega}, \boldsymbol{\omega}] = d\left(ke_r A_\mu^r \mathrm{d}x^\mu\right) + \frac{1}{2}\left[ke_s A_\mu^s \mathrm{d}x^\mu, ke_t A_\nu^t \mathrm{d}x^\nu\right] \\ &= ke_r \mathrm{d}A_\mu^r \wedge \mathrm{d}x^\mu + \frac{1}{2}k^2\left[e_s, e_t\right] A_\mu^s A_\nu^t \mathrm{d}x^\mu \wedge \mathrm{d}x^\nu \\ &= \frac{1}{2}ke_r\left(\partial_\mu A_\nu^r - \partial_\nu A_\mu^r\right)\mathrm{d}x^\mu \wedge \mathrm{d}x^\nu + \frac{1}{2}k^2 C_{st}^r e_r A_\mu^s A_\nu^t \mathrm{d}x^\mu \wedge \mathrm{d}x^\nu \\ &= \frac{1}{2}ke_r\left(\partial_\mu A_\nu^r - \partial_\nu A_\mu^r + kC_{st}^r A_\mu^s A_\nu^t\right)\mathrm{d}x^\mu \wedge \mathrm{d}x^\nu \\ &= \frac{1}{2}ke_r F_{\mu\nu}^r \mathrm{d}x^\mu \wedge \mathrm{d}x^\nu = k\boldsymbol{F} \end{aligned} \tag{13}$$

Here, note:

$$\left[e_s, e_t\right] = C_{st}^r e_r, \tag{14}$$

as well as

$$\begin{aligned} \mathrm{d}A_\mu^r \wedge \mathrm{d}x^\mu &= \frac{\partial A_\mu^r}{\partial x^\nu}\mathrm{d}x^\nu \wedge \mathrm{d}x^\mu = \left(\partial_\nu A_\mu^r\right)\mathrm{d}x^\nu \wedge \mathrm{d}x^\mu \\ &= \left(\partial_{[\mu} A_{\nu]}^r\right)\mathrm{d}x^\mu \wedge \mathrm{d}x^\nu = \frac{1}{2}\left(\partial_\mu A_\nu^r - \partial_\nu A_\mu^r\right)\mathrm{d}x^\mu \wedge \mathrm{d}x^\nu \end{aligned} \tag{15}$$

So from the Formula (13) one can have

$$\begin{cases} \boldsymbol{\Omega} = \dfrac{1}{2}ke_r\left(\partial_\mu A_\nu^r - \partial_\nu A_\mu^r + C_{st}^r e_r k^2 A_\mu^s A_\nu^t\right)\mathrm{d}x^\mu \wedge \mathrm{d}x^\nu = \dfrac{1}{2}ke_r F_{\mu\nu}^r \mathrm{d}x^\mu \wedge \mathrm{d}x^\nu \\ F_{\mu\nu}^r = \partial_\mu A_\nu^r - \partial_\nu A_\mu^r + C_{st}^r e_r k^2 A_\mu^s A_\nu^t \end{cases} \tag{16}$$

q.e.d.

Theorem 2: If the structural group is a matrix group, the GGE can be expressed by curvature transformation [1] [22] [23], $\boldsymbol{\Omega}_V = \mathcal{A}d_{g_{UV}^{-1}}\boldsymbol{\Omega}_U$, then it can also be expressed in a similar transformation form:

$$\boldsymbol{\Omega}_V = g_{UV}^{-1}\boldsymbol{\Omega}_U g_{UV} \tag{17}$$

Proof

1) According to Theorem 2, let $g_{UV}: U \cap V \to G$ be the local trivial transition function from T_U to T_V, then on $U \cap V$ of the bottom manifold, $\boldsymbol{\Omega}_V = \mathcal{A}d_{g_{UV}^{-1}}\boldsymbol{\Omega}_U$ can be established;

2) Suppose G is a matrix Lie group, because $\forall \boldsymbol{\Omega}_U \in \mathcal{G}$, $g_{UV}^{-1} \in G$, so one can obtain

$$\begin{aligned} \mathcal{A}d_{g_{UV}^{-1}} \boldsymbol{\Omega}_U &= I_{g_{UV}^{-1}*} \boldsymbol{\Omega}_U = I_{g_{UV}^{-1}*} \frac{\mathrm{d}}{\mathrm{d}t}\bigg|_{t=0} Exp\left(t\boldsymbol{\Omega}_U\right) \\ &= \frac{\mathrm{d}}{\mathrm{d}t}\bigg|_{t=0} I_{g_{UV}^{-1}}\left(Exp\left(t\boldsymbol{\Omega}_U\right)\right) = \frac{\mathrm{d}}{\mathrm{d}t}\bigg|_{t=0} g_{UV}^{-1}\left(Exp\left(tA\right)\right) g_{UV} \end{aligned} \tag{18}$$

Also because

$$\begin{aligned} & g_{UV}^{-1}\left(Exp\left(t\boldsymbol{\Omega}_U\right)\right) g_{UV} = g_{UV}^{-1}\left(I + t\boldsymbol{\Omega}_U + \frac{1}{2!}t^2\boldsymbol{\Omega}_U^2 + \frac{1}{3!}t^3\boldsymbol{\Omega}_U^3 + \cdots\right) g_{UV} \\ & = I + t g_{UV}^{-1}\boldsymbol{\Omega}_U g_{UV} + \frac{1}{2!}t^2 g_{UV}^{-1}\boldsymbol{\Omega}_U g_{UV} g_{UV}^{-1}\boldsymbol{\Omega}_U g_{UV} + \frac{1}{3!}t^3\left(g_{UV}^{-1}\boldsymbol{\Omega}_U g_{UV}\right)^3 + \cdots \\ & = Exp\left(t g_{UV}^{-1}\boldsymbol{\Omega}_U g_{UV}\right) \end{aligned} \tag{19}$$

hence Formula (18) becomes:

$$\begin{aligned} \mathcal{A}d_{g_{UV}^{-1}} \boldsymbol{\Omega}_U &= I_{g_{UV}^{-1}*} \boldsymbol{\Omega}_U = \frac{\mathrm{d}}{\mathrm{d}t}\bigg|_{t=0} \left(Exp\left(t g_{UV}^{-1}\boldsymbol{\Omega}_U g_{UV}\right)\right) \\ &= \frac{\mathrm{d}}{\mathrm{d}t}\bigg|_{t=0} \left(Exp\left(t I_{g_{UV}^{-1}}\left(\boldsymbol{\Omega}_U\right)\right)\right) = I_{g_{UV}^{-1}}\left(\boldsymbol{\Omega}_U\right) = g_{UV}^{-1}\boldsymbol{\Omega}_U g_{UV} \end{aligned} \tag{20}$$

So Formula (17) can be gotten by

$$\boldsymbol{\Omega}_V = \mathcal{A}d_{g_{UV}^{-1}} \boldsymbol{\Omega}_U = g_{UV}^{-1}\boldsymbol{\Omega}_U g_{UV}$$

Note that G is a matrix Lie group at this time. If $\forall \boldsymbol{\Omega}_U \in \mathcal{G}$, $g_{UV}^{-1} \in G$, then there is $\mathcal{A}d_{g_{UV}^{-1}} \boldsymbol{\Omega}_U = g_{UV}^{-1}\boldsymbol{\Omega}_U g_{UV}$, that is, $\mathcal{A}d_{g_{UV}^{-1}} \boldsymbol{\Omega}_U$ is equal to the product of three matrices, but if G is not a matrix Lie group, then $g_{UV}^{-1}\boldsymbol{\Omega}_U g_{UV}$ is meaningless, because at this time the product of the Lie group element g_{UV}^{-1} and its Lie algebra element $\boldsymbol{\Omega}_U$ is meaningless.

q.e.d.

Theorem 3: The following similar transformations are equivalent:

$$\boldsymbol{\Omega}_V = g_{UV}^{-1}\boldsymbol{\Omega}_U g_{UV} \Leftrightarrow \hat{F}'_{\mu\nu} = U\hat{F}_{\mu\nu}U^{-1} \tag{21}$$

In fact, from the above Formula (17), and then use the basis $\{e_r\}$ to expand the connection $\boldsymbol{\omega}$ and the curvature $\boldsymbol{\Omega}$ on the bottom manifold as $\boldsymbol{\omega} = e_r\boldsymbol{\omega}^r$ and $\boldsymbol{\Omega} = e_r\boldsymbol{\Omega}^r$ respectively, then $\boldsymbol{\omega}^r$ and $\boldsymbol{\Omega}^r$ are the (real-valued) 1-form and 2-form fields on the region U, respectively. Then ω_μ^r and $\Omega_{\mu\nu}^r$ represent the components of $\boldsymbol{\omega}^r$ and $\boldsymbol{\Omega}^r$ in the coordinate basis $\left\{\frac{\partial}{\partial x^\mu}\right\}$ in turn:

$$\omega_\mu^r = \boldsymbol{\omega}^r\left(\frac{\partial}{\partial x^\mu}\right) \tag{22}$$

$$\Omega_{\mu\nu}^r = \boldsymbol{\Omega}^r\left(\frac{\partial}{\partial x^\mu}, \frac{\partial}{\partial x^\nu}\right) \tag{23}$$

Then one can find:

$$\begin{cases} \omega_\mu^r = kA_\mu^r \\ \Omega_{\mu\nu}^r = kF_{\mu\nu}^r \end{cases} \tag{24}$$

That is, ω_{μ}^{r} and $\Omega_{\mu\nu}^{r}$ is k times of the gauge potential A_{μ}^{r} and the gauge field strength $F_{\mu\nu}^{r}$ respectively, so physically, the connection $\boldsymbol{\omega}$ and the curvature $\boldsymbol{\Omega}$ on the bottom manifold can represent the gauge potential and the gauge field strength respectively, so the Formula (24) can be deduced which proves that Formula (21) is correct, and vice versa.

q.e.d.

Now use Formula (21), $\hat{F}'_{\mu\nu} = U\hat{F}_{\mu\nu}U^{-1}$, one can determine the matrix representation of the transformation function as follows:

First of all, consider that there are many matrix expressions of gravitational intensity, which are diagonal matrix expressions of second-order covariant tensor [22] [23], namely

$$\left\{g_{jj}\right\} \equiv \begin{pmatrix} g_{00} & 0 & 0 & 0 \\ 0 & g_{11} & 0 & 0 \\ 0 & 0 & g_{22} & 0 \\ 0 & 0 & 0 & g_{33} \end{pmatrix} \tag{25}$$

and also consider the matrix expression of electromagnetic field strength is also a kind of matrix representation of second-order anti-symmetric covariant tensor $\hat{F}_{\mu\nu}(x)$, for example

$$\left\{\hat{F}_{\mu\nu}(x)\right\} \equiv \begin{pmatrix} 0 & -E_1 & -E_2 & -E_3 \\ E_1 & 0 & B_3 & -B_2 \\ E_2 & -B_3 & 0 & B_1 \\ E_3 & B_2 & -B_1 & 0 \end{pmatrix} \tag{26}$$

we find that the gravitational intensity can be a certain diagonal matrix expression of the second order metric tensor corresponding to $\left\{\hat{F}_{\mu\nu}(x)\right\}$. So we can always find such matrix similar transformation $\left\{U\left(\boldsymbol{\theta}(x)\right)\right\}$ to diagonalize $\left\{\hat{F}_{\mu\nu}(x)\right\}$ as the matrix representation of the electromagnetic tensor for obtaining a matrix expression of the gravitational strength, that is the expression of the diagonal matrix of the metric $\left\{g_{jj}\right\}$, such as the Schwarzschild vacuum solution, etc. [24] [25]. The similar diagonalization expression is presented as follows:

$$\begin{aligned} &\begin{pmatrix} u_{00} & u_{01} & u_{02} & u_{03} \\ u_{10} & u_{11} & u_{12} & u_{13} \\ u_{20} & u_{21} & u_{22} & u_{23} \\ u_{30} & u_{31} & u_{32} & u_{33} \end{pmatrix} \begin{pmatrix} 0 & -E_1 & -E_2 & -E_3 \\ E_1 & 0 & B_3 & -B_2 \\ E_2 & -B_3 & 0 & B_1 \\ E_3 & B_2 & -B_1 & 0 \end{pmatrix} \begin{pmatrix} u_{00} & u_{01} & u_{02} & u_{03} \\ u_{10} & u_{11} & u_{12} & u_{13} \\ u_{20} & u_{21} & u_{22} & u_{23} \\ u_{30} & u_{31} & u_{32} & u_{33} \end{pmatrix}^{-1} \\ &= \begin{pmatrix} g_{00} & 0 & 0 & 0 \\ 0 & g_{11} & 0 & 0 \\ 0 & 0 & g_{22} & 0 \\ 0 & 0 & 0 & g_{33} \end{pmatrix} \end{aligned} \tag{27}$$

Here, defining

$$\left\{U\left(\boldsymbol{\theta}(x)\right)\right\} \equiv \begin{pmatrix} u_{00} & u_{01} & u_{02} & u_{03} \\ u_{10} & u_{11} & u_{12} & u_{13} \\ u_{20} & u_{21} & u_{22} & u_{23} \\ u_{30} & u_{31} & u_{32} & u_{33} \end{pmatrix} = \begin{pmatrix} U_0 & U_1 & U_2 & U_3 \end{pmatrix} \tag{28}$$

Then one has

$$\left\{\hat{F}_{\mu\nu}(x)\right\}\left\{U\left(\boldsymbol{\theta}(x)\right)\right\}^{-1}=\left\{U\left(\boldsymbol{\theta}(x)\right)\right\}^{-1}\left\{g_{jj}\right\} \tag{29}$$

$$\left\{\hat{F}_{\mu\nu}(x)\right\}\left(U_0U_1U_2U_3\right)=\left(g_{00}U_0g_{11}U_1g_{22}U_2g_{33}U_3\right) \tag{29}$$

$$\left\{\hat{F}_{\mu\nu}(x)\right\}U_i=g_{ii}U_i, i=0,1,2,3 \tag{30}$$

which allows one to obtain

$$\begin{cases} g_{00}=-E_1u_{10}-E_2u_{20}-E_3u_{30} \\ g_{11}=E_1u_{01}+B_3u_{21}-B_2u_{31} \\ g_{22}=E_2u_{02}-B_3u_{12}+B_1u_{32} \\ g_{33}=E_3u_{03}+B_2u_{13}-B_1u_{23} \end{cases} \tag{31}$$

Now one can associate the eigenvalues and eigenvectors of the matrix, that is, g_{ii} is the ith eigenvalue of the matrix $\left\{\hat{F}_{\mu\nu}(x)\right\}$, and U_i is the eigenvector corresponding to g_{ii}. $\left\{U\left(\boldsymbol{\theta}(x)\right)\right\}^{-1}$ needs to be an invertible matrix, namely the eigenvectors of $\left\{\hat{F}_{\mu\nu}(x)\right\}$ need to be linearly independent, that is, the necessary and sufficient condition for the order n square matrix $\left\{\hat{F}_{\mu\nu}(x)\right\}$ similar to the diagonal matrix $\left\{g_{jj}\right\}$ is that $\left\{\hat{F}_{\mu\nu}(x)\right\}$ has n linearly independent eigenvectors $\left(U_0 \quad U_1 \quad U_2 \quad U_3\right)$. Certainly, these conditions for $\left\{\hat{F}_{\mu\nu}(x)\right\}$ can be satisfied. For example, from Equation (31), by taking $u_{20}=u_{30}=1$, $u_{01}=u_{31}=1$, $u_{02}=u_{12}=1=u_{23}=u_{13}$, one can get 4 linearly independent eigenvectors of $\left\{\hat{F}_{\mu\nu}(x)\right\}$ as

$$U_0=\begin{pmatrix} 1 \\ -\dfrac{g_{00}+E_2+-E_3}{E_1} \\ 1 \\ 1 \end{pmatrix} \tag{32}$$

$$U_1=\begin{pmatrix} 1 \\ 1 \\ \dfrac{g_{11}+B_2-E_1}{B_3} \\ 1 \end{pmatrix} \tag{33}$$

$$U_2=\begin{pmatrix} 1 \\ 1 \\ 1 \\ \dfrac{g_{22}-E_2+B_3}{B_1} \end{pmatrix} \tag{34}$$

$$U_3=\begin{pmatrix} \dfrac{g_{33}-B_1+B_3}{E_2} \\ 1 \\ 1 \\ 1 \end{pmatrix} \tag{35}$$

which proves that the most important conclusion in this paper: **it is existed that the (generalized) gauge transformation $U(\theta(x))$ across fundamental interactions**.

5. Conclusions and Prospects

1) On the basis of the program of the grand unification of physics proposed in [1], this paper concretely constructs a space-time model with the frame bundle as the principal bundle, and the tensor bundle as the associated bundle, so that the four basic interactions, especially the electromagnetic and gravitational interactions, can be reflected in the base manifold, that is, the regional distribution of our universe. Gravitation is basically zero in the region of strong and weak interaction, and can have an intersection domain with electromagnetic interaction. This shows that the basic interaction is related to the "characteristics" of regional space-time, or they are the connection or curvature of space-time, while in the path of unification of four basic functions, whether gravity needs "quantization" is not a key or necessary issue.

2) This paper studies the existence and feasibility of generalized gauge transformation across basic interactions; it is found that the unified expression formula is the generalized gauge equation GGE and its expression relationship on the space-time curvature. Therefore, the author discusses the existence and feasibility of the generalized gauge transformation across the electromagnetic interaction and the gravitational interaction throughout the paper, and on this basis, specifically determines a method or way to find the generalized gauge transformation, so as to try to realize the last step of the "unification" of the four basic interactions in physics, that is, the "unification" of electromagnetism and gravity.

3) This paper once again affirms this key point: all interactions in the world are unified in the gauge potential or curvature of the principal bundle in the universal picture, while the four basic interactions on the bottom manifold are only the components representation of the gauge potential or curvature of the principal bundle, and they can be transformed from one basic interaction to another basic interaction according to the GGE formulation.

4) Outlook: a) The basic interaction may transform with each other. The basic equation of transformation is GGE or the similar transformation expression of the curvature matrix. b) Finding the structure group which can express more gauge field components; simplifying and solving the GGE so that it can concretely express the transformation relationship between any two gauge field components, especially the transformation relationship between electromagnetic force and gravity, which is extremely important for solving human aerospace dynamics, will be an important task of the future physics research on the grand unification.

Conflicts of Interest

The author declares no conflicts of interest regarding the publication of this paper.

References

[1] Qiao, B. (2023) *Journal of Modern Physics*, **14**, 212-326. https://doi.org/10.4236/jmp.2023.143016

[2] Yang, C.N. and Mills, R.L. (1954) *Physical Review*, **96**, 191-195. https://doi.org/10.1103/PhysRev.96.191

[3] Georgi, H. and Glashow, S.L. (1974) *Physical Review Letters*, **32**, 438. https://doi.org/10.1103/PhysRevLett.32.438

[4] Georgi, H. (1975) Particles and Fields 1974. Amer. Inst. of Physics, New York.

[5] Lian, C., Ali, Z.A., Kwon, H. and Wong, B.M. (2019) *The Journal of Physical Chemistry Letters*, **10**, 3402-3407. https://doi.org/10.1021/acs.jpclett.9b01046

[6] Fritzsch, H. and Minkowski, P. (1975) *Annals of Physics*, **93**, 193. https://doi.org/10.1016/0003-4916(75)90211-0

[7] Hehl, F.W., von der Heyde, P., Kerlick, G.D. and Nester, J.M. (1976) *Reviews of Modern Physics*, **48**, 393. https://doi.org/10.1103/RevModPhys.48.393

[8] Ivanenko, D. and Sardanashvily, G. (1983) *Physics Reports*, **94**, 1. https://doi.org/10.1016/0370-1573(83)90046-7

[9] Hehl, F., McCrea, J., Mielke, E. and Neeman, Y. (1995) *Physics Reports*, **258**, 1. https://doi.org/10.1016/0370-1573(94)00111-F

[10] Polchinski, J. (2005) String Theory. Vol. 1, 2, Cambridge University Press, Cambridge.

[11] Kaku, M. (1999) Introduction to Superstrings and M-Theory. Springer, New York. https://doi.org/10.1007/978-1-4612-0543-2

[12] Carlo Rovelli, C. (1998) *Loop Quantum Gravity*, *Living Reviews in Relativity*, **1**, Article No. 1. https://doi.org/10.12942/lrr-1998-1

[13] Clifton, T. and Ferreira, P. (2009) *Scientific American*, **300**, 48-55. https://doi.org/10.1038/scientificamerican0409-48

[14] Joyce, A., Lombriser, L. and Schmidt, F. (2016) *Annual Review of Nuclear and Particle Science*, **66**, 95. https://doi.org/10.1146/annurev-nucl-102115-044553

[15] Carroll, S. (2012) Dark Matter vs. Modified Gravity: A Trialogue.

[16] Hossenfelder, S. and McGaugh, S.S. (2018) *Scientific American*, **319**, 36-43. https://doi.org/10.1038/scientificamerican0818-36

[17] Cao, T.Y. (2019) Conceptual Developments of 20th Century Field Theories. Cambridge University Press, Cambridge, 320. https://doi.org/10.1017/9781108566926

[18] Oerter, R. (2006) The Theory of Almost Everything: The Standard Model, the Unsung Triumph of Modern Physics (Kindle ed.). Penguin Group, London, 2.

[19] Langacker, P. (2009) The Standard Model and Beyond. CRC Press, Boca Raton, 670 p.

[20] Nesti, F. and Percacci, R. (2010) *Physical Review D*, **81**, Article ID: 025010. https://doi.org/10.1103/PhysRevD.81.025010

[21] Chen, X.S. and Chen, W.H. (1983) Handout on Differential Geometry. Peking University Press, Beijing.

[22] Duan, Y.S. (2020) General Relativity and Gravity Gauge Theory. Science Press, Beijing.

[23] Lian, C.B. and Zhou, B. (2019) Introduction to Differential Geometry and General Relativity. Second Edition, Vol. I, II, III, Science Press, Beijing.

[24] Misner, C.W., Throne, K.S. and Wheeler, J.A. (2020) Gravitation. Freeman W H

Company, San Francisco.

[25] Wald, R.M. (1984) General Relativity. The University of Chicago Press, Chicago and London. https://doi.org/10.7208/chicago/9780226870373.001.0001

Journal of Modern Physics, 2023, 14, 623-665
https://www.scirp.org/journal/jmp
ISSN Online: 2153-120X
ISSN Print: 2153-1196

Particles Composition and Interactions Using the Nuon Model

René Brun

CERN, Geneva, Switzerland
Email: rene.brun@cern.ch

How to cite this paper: Brun, R. (2023) Particles Composition and Interactions Using the Nuon Model. *Journal of Modern Physics*, **14**, 623-665.
https://doi.org/10.4236/jmp.2023.145036

Received: February 7, 2023
Accepted: April 18, 2023
Published: April 21, 2023

Abstract

The Standard Model in Particle Physics has been able to make many predictions confirmed later with a flow of experimental results. With the discovery of the Higgs boson at the LHC, one is full of admiration for the people contributing to this model fifty years ago and its predictions that have been confirmed gradually. The original particle quark constituent model has evolved with the deep inelastic experiments to a quark and gluons system, then to a more general system with virtual quarks. This work is the result of observations while working at CERN in Geneva with many different experiments at the ISR, SPS, LEP, LHC colliders. A new model based on nuons is introduced, that allows accurate evaluations of the particle masses (mesons and baryons) and magnetic moment, computes very accurately the kinematics distributions for particles and jets observed in the p-p collisions at the LHC (elastic and inelastic) and at lower energy machines. This new model looks at a first glance in contradiction with the quark model because it can build the elementary particles with nuons only, *i.e.* electrons and neutrinos. However, all the existing physics involved in electron, positron and neutrino interactions may be used to explain interactions between composite particles such as protons or heavy ions.

Keywords

Standard Model, Particle Masses, Particles Interactions, Elastic Scattering, Deep Inelastic, Jets, Charge Density

1. Introduction: Motivation and Ideas

The Standard Model (SM) [1]-[8] has been successful in describing particle interactions since its introduction in the late sixties. Many predictions have found their confirmations in the past 3 or 4 decades. The search for the Higgs boson

and its properties is the best proof of confidence of the vast majority of physicists for its predictions.

I have started my career as a nuclear physicist at a time where the Standard Model was shaping-up, then I spent all my professional career as an applied physicist developing general tools for the simulation of detectors, e.g. GEANT [9], or data analysis tools such as PAW [10] and ROOT [11]. Thanks to these tools I have been in contact with very many experiments in the world of High Energy or Nuclear Physics in the past four decades. During these developments, I have always been very interested by the research topics of these experiments and I had the unique opportunity to have a very good overview of the main challenges in Physics during these four decades. The beautiful results obtained in the past few years by the LHC experiments are a fantastic summary of the Physics observations predicted by the Standard Model.

However, there are several areas where the standard Model has problems, e.g. its lack of precise predictions for the particle masses and lifetimes. Theoretical approaches, such as Lattice QCD [12], compute at best the nucleon mass with one per mille accuracy. The description of the nucleon in terms of valence quarks, sea quarks and gluons is far from optimal. My small brain has always difficulties in imagining a brownian motion of the official nucleon components playing a ping-pong exercise in a mollases. The Parton Distribution Functions (PDF) coming from the deep inelastic experiments are complex when used in the analysis of LHC data. Far too many parameters are required to match the experimental results. Even a simple process such as proton-proton elastic scattering requires complex explanations. As an example no theoretical model was able to predict accurately the results from TOTEM [13]. These partons distribution functions were perfect at a time where computing was in the infancy and only a brownian motion proposed. The model with a few quarks was OK when only a few ten of particles was known. It is not appropriate anymore today with several hundred particles discovered.

Nature very often offers very interesting observations such as the mass difference between charged and neutral particles, the fact that the neutron has a small negative charge vanishing only after a few fermis in contrast with the sharp change for the proton or the fact that the neutron is stable when bound in a nucleus. I have always been puzzled by the fact that all particles decay into electrons, photons, neutrinos or the stable proton. Being constituted of other particles means being a bound state of these particles, at the exception of the photon. Quantum field theoretic processes have no problem turning one kind of particles into other kinds of particles. When looking at the Feynman diagram **Figure 1**, I see two conceptual problems: virtuality and Schrodinger cats. Mathematically speaking, it is simple to show the virtual W boson decaying into final products, here electron and neutrino can be dead or alive in the muon or W! This simple observation was a strong incentive to develop the nuon model described in the following chapters.

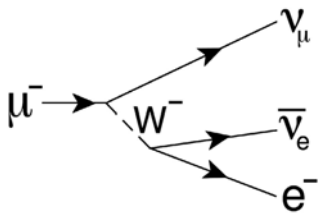

Figure 1. Muon decay diagram.

It is obvious that the proposal for a new model for particle constituents is going to meet very strong objections, to say the least. This work started with a simple idea to evaluate particle masses. Following the initial good results obtained, it was tempting to test the model with well-known physics processes such as elastic scattering. The even better results with this process were a new incentive for more ambitious tests, like the production of particles in proton-proton inelastic collisions at the LHC and jets physics. The next step has been the investigation of the deep inelastic processes and the comparisons with HERA [14] data. One of the last chapters of this paper considers the formation of nuclei and their collisions compared to results in Pb-Pb or Au-Au collisions at CERN or BNL.

The nuons model is not in contradiction with the standard model. It provides an alternative to the quarks/gluons constituents model. Of course, the model must (and it does) reproduce the experimental results traditionally explained by the partons collisions in deep-inelastic scattering and jets physics. The hadron-hadron collisions are interpreted as a convolution of collisions between the leptons of the nuons.

Degrees of freedom, such as introduced later with the nuons, may be understood as elementary ones, related to foundation of the description. But it is not the only possibility. They may be interpreted as an attempt to introduce optimized degrees of freedom, such as a kind used in an interactive picture of a Hamiltonian description. It is generally known, that symmetries and resulting relations may not be of elementary level, but may be the consequence of dynamic, often of stochastic nature. If indeed it is the case one may shed the light on difficult non-perturbative domains. Establishing possible interpretations of the system presented in the later sections is out of scope of this present work. Independently, if the presented results may lead to alternative and/or equivalent picture of Standard Model and its elementary fields, or to better control properties of dynamic processes, it is of importance to collect and present observations in a systematic way. Of course, a valid possibility is that this is just collection of puzzling but otherwise accidental features. This work is organized as follows.

2. The Nuon Model

As illustrated in **Figure 2**, if one considers only the final and stable states, all particles decay into $\nu_e, \overline{\nu_e}, \nu_\mu, \overline{\nu_\mu}, e^+, e^-, \gamma$ or protons. This looks like an incentive to imagine a model where particles are built out of these basic building

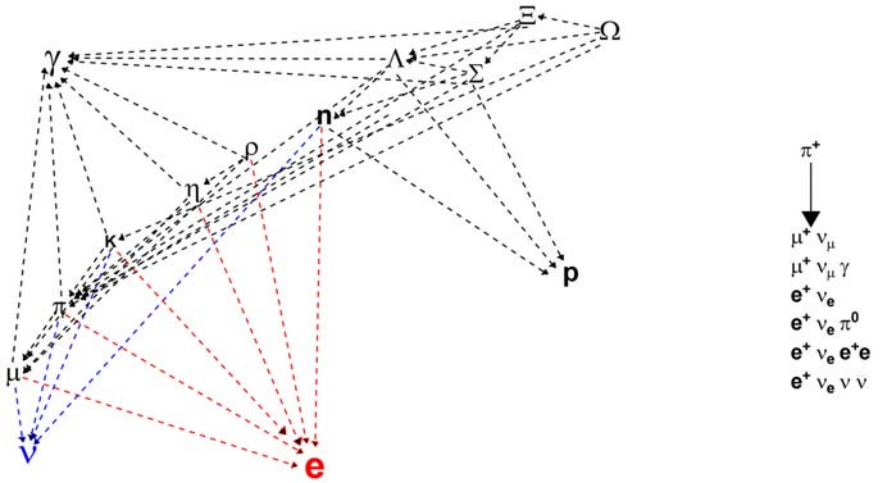

Figure 2. Particles decay examples (left) and π^+ decays (right).

blocks, except the photon that is the result of an intermediate process. When looking more precisely into all possible decay branching modes, it becomes intuitive to imagine an intermediate system, here called a nuon, with which all other particles can be built. We assume a nuon (contraction for neutrinos and electrons) to be a very stable bound state [$e^+\nu_e e^-\overline{\nu_e}$] behaving like a neutrino when it is free and not bound itself inside a particle because protected by the neutrinos acting as a possible shielding material. Each nuon inside a particle can be considered as a dipole rotating around the axial nuons of this particle and its positron and electron are subject to electromagnetic interactions with their counterparts in other nuons.

Nature is full of examples where structures are stable for a given scale and temperature, for example atoms, molecules, cells, animals, planets, solar systems, galaxies. Concerning the nucleon, one assumes that around one billionth of a second after the big bang, the temperature/pressure/energy combination was such that the quarks and the gluons were in a regime where they could stabilise. In this model, it is assumed that under these conditions, stable nuons could form structures such as muons, pions, kaons, protons, etc.

Giving this assumption, let's see now how these nuons can assemble into units of N nuons assuming only electromagnetic-type interactions between the dipoles electron/positron of the respective nuons . The units (*i.e.* particles) are assumed to have a spherical shape. In fact it could be any shape, an ellipsoid, but while testing different models, the sphere proved to be the simplest and most intuitive that still gives nice results. For each particle, we assume $N-2$ nuons rotating around an axis consisting of 2 nuons. In addition the nuons rotate around themselves and their own axis points to the centre of the particle. Just to give a simple example at this point, the proton is built with 64 nuons rotating around the 2 axis nuons and a pion has 4 nuons rotating around the 2 axial nuons. Particles can be seen as solenoids built with N rotating dipoles. In the section on p-p elastic scattering we will see that an estimation of the rotation speed of the non

axial nuons is about 0.06*c. This rotation speed is also in perfect agreement with the angular velocity when computing the magnetic moment of the proton, neutron or muon. Its low absolute value is also interesting because it does not require complex relativistic corrections. Positive particles are built with $N-2$ nuons, 2 axial nuons and a positron at the centre of the sphere. The radial nuons have their electrons near the centre and their positron near the outside radius, a neutrino is very close to the centre and an antineutrino between the electron and the positron. The axial line of a positive particle has a one central positron, 2 electrons, 2 positrons + N neutrinos. Negative particles have an electron at the centre and an opposite configuration for the radial nuons. During the original design, it was expected that the neutral particles will have nothing at their centre, but this case proved not to work. The minimisation system could not find any convergent point. Instead the only possible configuration found was to place a system $e^+\overline{\nu}_e e^-$ or $e^+\nu_e e^-$ (eg for a neutron and antineutron respectively). This configuration provides too an easy explanation for the neutron decay $n \to p + \overline{\nu}_e + e^-$. In this model, the electron, positron and neutrino components of the nuon are like the *partons* of the classical model.

2.1. Goals and Constraints

A new model for particles needs to be coherent with proven observables:

- It must be able to predict as accurately as possible particles mass, radius, magnetic moment (if any), binding energy, life time.
- It must be able to predict or be consistent with the results of various collision/interaction types, e.g. elastic scattering, hard collisions with precise generation of the collision products, particle types, kinematics and jets.
- It must be able to test the particles components geometry and density with results e.g. of the deep inelastic experiments.
- It must be predictive when tested at new collision energies or configurations.
- The number of parameters in the model must be as small as possible.

2.2. Making Particles

Assuming N nuons in a cube with a side of about 1 fermi, we generate nuons at random positions inside the cube, then using the MINUIT [15] system part of the ROOT library we minimise the function $F = F_C + \alpha F_G$ where F_C is the sum of the Coulomb forces at the centre of the particle and F_G is the deviation from a spherical shape and α is a normalisation factor. Each nuon is at position (x_i, y_i, z_i) with radius $r_i = \sqrt{x_i^2 + y_i^2}$ and $R_i = \sqrt{x_i^2 + y_i^2 + z_i^2}$. z is by definition the axis joining the 2 axial nuons (see **Figure 3**). $F_C = \sum q_i q_j / r_{ij}^2$ and $F_G = \sum \left(rmean^2 - r_i^2 \right)$ where $rmean$ is a free parameter representing the sphere radius. So, the input to MINUIT is a system with $3*N+2$ free parameters and the 2 conditions of F (3 parameters for each nuon, the $3N+1$th parameter is the sphere radius and the $3N+2$ is the distance between the electron and the positron expressed in percentage of the radius). In fact, the condition that F_C

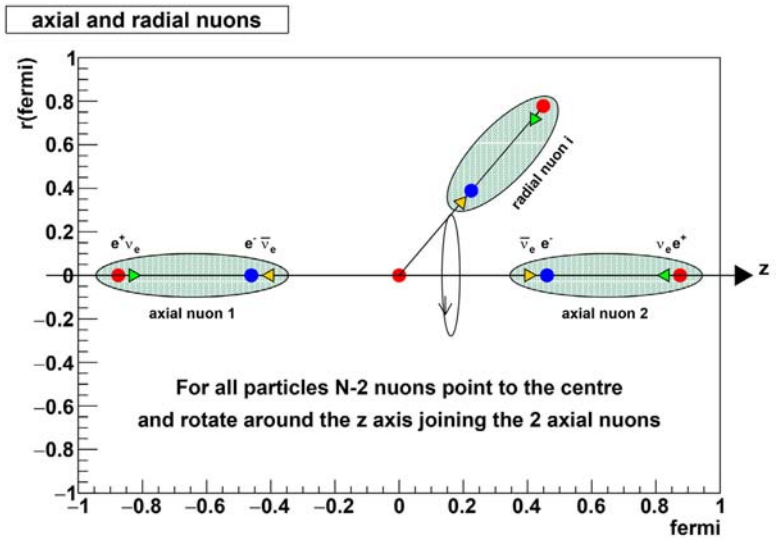

Figure 3. Axial and radial nuons schema.

must be minimal at the centre of the particle is only one among many other possibilities that have been tested. What we see in reality with the 2 conditions F_C and F_G is that the problem is somehow equivalent to finding a sphere where N objects are equidistant on its surface. Instead of this materialist point to point approach a more elegant probabilistic but difficult approach using quantum mechanics could have been developed.

A program *findall* has been initially written to compute all cases for $5 < N < 150$, then expended to compute the masses of all known mesons and baryons for $5 < N < 785$. MINUIT minimizes the function F and finds the best values for the $3N + 2$ parameters. What we observe is quite interesting. At the end of the minimisation process the nuons have moved to stable positions inside the particle, in most cases reproducing configurations with a lot of symmetry (see later), pentagons, hexagons, decagons, and/or combinations of all these basic figures. F has smaller values for particles with the highest symmetries. For a given value of N, several solutions are possible and all values of N give at least one solution.

2.3. Computing Particle Masses

Because the system is built with $N-2$ nuons rotating around the 2 axial nuons, we compute the inertia of the system $I = \sum m_i r_i^2$ and its total energy (mass) $M = I\Omega^2$ where Ω is the angular speed $\Omega = v/(2\pi R)$. Two parameters are used in this computation: the electron mass and a global normalisation coefficient.

When looking at the results we see that the obtained mass values lie nicely on a straight line (see Figure 4). This not surprising as it is easy to demonstrate that when n points are distributed on the surface of a sphere $\sum\left(x_i^2 + y_i^2\right)/R^2 = \frac{2n}{3}$.

From this figure we conclude that the best mass match for a proton corresponds to $N = 64 + 2$, *i.e.* the case where 64 radial nuons rotate around 2 axial nuons.

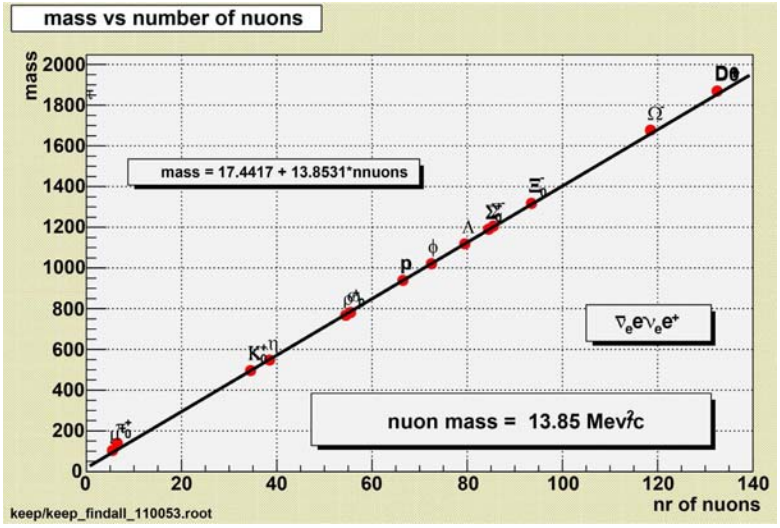

Figure 4. Particles Mass vs number of nuons + 2.

Then we can build the *Mendeleev*-like table shown in Figure 5 for the case of 20 particles ranging from the muon with 3 + 2 nuons, the pion with 4 + 2, the kaon with 32 + 2, up to the D_0 with 130 + 2. As one can see in the column (PDG − nuons)/PDG the relative error on the mass is at the per mile level or better when compared to the PDG tables [16]. Also note the very precise calculation of the neutral vs charged particle mass with the same number of nuons. This behaviour is in particular very striking for (π,π_0), (K^+,K_0), (p,n), (D^+,D_0). The muon and pion masses are predicted with a relative precision of 10^{-7}.

Using a simple line fit, we can say that the mass of a particle made of N nuons is proportional to N with $mass_N = 18 + 13.84 * N$, *i.e.* that the nuon mass is about 13.84 MeV/c^2. The nuon mass is likely due to a system rotating at high speed around the nuon axis.

The linearity shown later in Figure 4 has been observed in the past by several authors, see for example KOIDE [17] or GREULICH [18] or PAASCH [19]. The particle masses seem to be in a first approximation (with a precision of a few per cent) a function of a running number N. In a following section, we will see that the same program has been used to compute the masses for a much larger number of particles (135 mesons and 133 baryons). The linear fit for these 268 particles gives a very close result, around 14 MeV/c^2 per nuon.

The muon is considered as a composite object and a *neutral* muon μ_0 is emerging with a mass = 101.565 MeV/c^2. It could be that this neutral particle decays with similar channels than the π_0 with the missing energy attributed to a neutrino? An interesting debate!

In Figure 6, a proton is represented with indications of the size and the direction of the force for each external positron. In Figure 7(left) we show a zoom on a front view (radial view) of a proton exhibiting the positrons outside the *nuon-spoke*, the electrons inside and neutrinos, antineutrinos as double cone objects in yellow and blue respectively. On the picture (right) we show a neutron with the same perspective.

MBP-de-Rene findall_66020.root with 200586 events **Tue Feb 7 11:32:02 2023**

nuons	quarks	spin	rings	PDG mass (MeV/c^2)	nuons model mass (MeV/c^2)	PDG-nuons / PDG	mmexp/mmq (μn)	mm_nuons (μn)	epot_energy (MeV)	life time PDG (seconds)
μ^+ 3		1/2	1	105.658	105.658 [6e-06]	1.780e-07 (4875)	8.89/?? 0	8.892	0 ± 0	2.2e-06
π^+ 4	$u\bar{d}$	0	1	139.570 R = 0.657	139.570 [5e-06] R = 0.633855	9.060e-07 (4873)	?? 0	0.000	0 ± 0	2.6e-08
π_0 4	$(u\bar{u}-d\bar{d})/\sqrt{2}$	0	1	134.977	134.977 [0]	6.258e-07 (4869)	-?? 0	0.000	0 ± 0	8.4e-17
K^+ 32	$u\bar{s}$	0	2	493.677	493.586 [0.42]	1.852e-04 (29191)	?? 0	0.000	0 ± 0	1.24e-08
K_0 32	$d\bar{s}$	0	2	497.611	497.279 [0.53]	6.667e-04 (30462)	-?? 0	0.000	0 ± 0	5.11e-08
η 36	$(u\bar{u}+d\bar{d}-2s\bar{s})/\sqrt{6}$	0	2	547.862	547.894 [1.5]	-5.920e-05 (30775)	-?? 0	0.000	0 ± 0	3.5e-08
p 64	uud	1/2	3	938.272 R = 0.8768	938.272 [0.73] R = 0.875718	1.447e-08 (26941)	2.793/2.79 0	2.790	0 ± 0	1e+40
n 64	udd	1/2	3	939.565	939.536 [0.88] R = 0.831374	3.079e-05 (27469)	-1.913/1.86 0	-1.958	0 ± 0	885.7
ϕ 70	$s\bar{s}$	1	4	1019.461	1019.913 [0.3]	-4.431e-04 (4853)	-?? 0	-1.806	0 ± 0	1.55e-22
Λ 77	uds	1/2	4	1115.683	1117.473 [0.27]	-1.604e-03 (4807)	-0.613/0.61 0	-1.646	0 ± 0	2.63e-10
Σ^+ 82	uus	1/2	4	1189.370	1190.979 [1.2]	-1.353e-03 (1343)	2.458/2.69 0	2.587	0 ± 0	8.02e-11
Σ_0 82	uds	1/2	4	1192.640	1188.514 [0.97]	3.460e-03 (1334)	-0.61/0.82 0	-1.545	0 ± 0	7.4e-20
Ξ^- 91	dss	1/2	4	1321.710	1318.579 [0.62]	2.369e-03 (1248)	-0.651/0.51 0	-2.515	0 ± 0	1.64e-10
Ξ_0 91	uss	1/2	4	1314.860	1314.985 [0.73]	-9.521e-05 (1423)	-1.25/1.44 0	-1.393	0 ± 0	2.9e-10
Ω^- 116	sss	3/2	5	1672.450	1671.816 [0.53]	3.788e-04 (1258)	-2.02/1.83 0	-2.381	0 ± 0	8.21e-11
D^+ 130	$c\bar{d}$	0	5	1869.660	1871.083 [0.48]	-7.613e-04 (1191)	?? 0	0.000	0 ± 0	1.04e-12
D_0 130	$c\bar{u}$	0	5	1864.840	1864.080 [0.5]	4.075e-04 (1351)	-?? 0	0.000	0 ± 0	4.1e-13

kDz0 = 0.63026 kMass = 17.2878 kDrpm = 0.0062 kNdrp = 0.28503 kBeta = 0.05968 6.950e-04

Figure 5. Particles mass and magnetic moment.

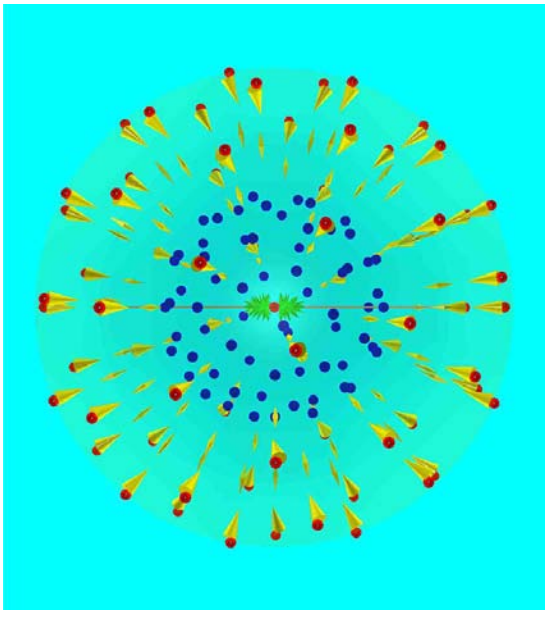

Figure 6. Coulomb forces at the position of the external positrons. The size of the cone is proportional to the force and the cone axis indicates the direction of the force.

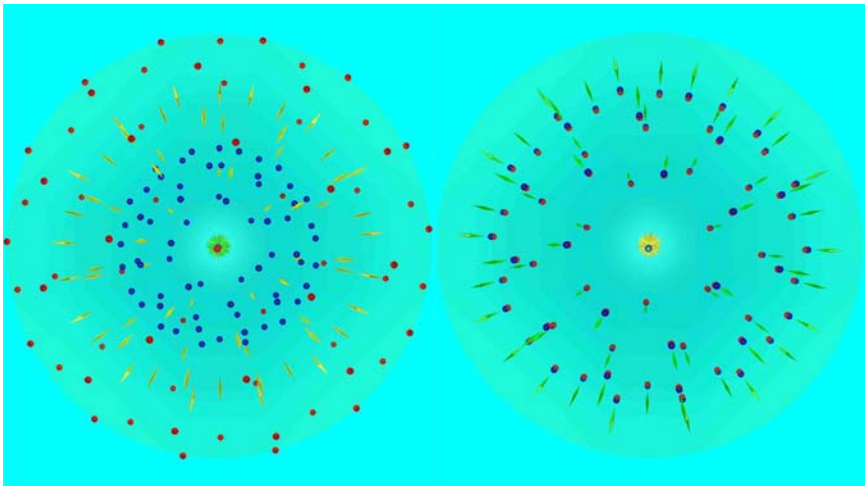

Figure 7. Proton (left) and Neutron (right) front view. Red circles are positrons, dark blue circles are electrons, yellow cones are antineutrinos and green cones are neutrinos.

2.4. Determination of the Proton Radius vs. Proton Energy

There are at at least two reasons to select the case $N = 64$ radial nuons + 2 axial nuons for the proton and neutron. It is the only combination that gives a precise mass at rest for the proton (0.938276 GeV) for a radius of 0.876 fermi. As we will see later, the orbital rotation speed has been found to be $0.05968 * c$, the best value explaining the shape of the *dip* for the proton-proton elastic scattering at 7 TeV. This value combined with the proton radius gives also a perfect match for the proton magnetic moment (see later). Since the first experiments at the *ISR* we know that the elastic and inelastic proton-proton cross-sections are rising with the collision energy. For example the elastic cross-section has been measured and parameterized by TOTEM [13] to be

$$fppel = 11.84 - 1.617 * \ln(s) + 0.1359 * \ln^2(s)$$

where s is the square of the collision energy. In the following chapters we will use this formula to estimate the proton radius as a function of the collision energy. We take $R = k\sqrt{fppel}$ and we compute the parameter k such that $R = 0.876$ fermi for $\sqrt{s} = 20$ GeV.

2.5. Computing Magnetic Moment

In Figure 5 two columns with labels "*mmexp*/*mmq*" and "$mm_n uons$" are shown with results expressed in nuclear magnetic moments (μn). The "*mmexp*" are the experimental values for particles with a magnetic moment. The "*mmq*" are the values from the quark model. The "$mm_n uons$" values are the results from the nuons model. The magnetic moment is simply $mm = \sum q_i r_i v_i$ where q_i, r_i, v_i are respectively the charge, the orbital radius and speed of the electron or positron of nuon *i*. A nuon has a positron with charge $q = 1$ at radius *rp* and velocity *vp* and an electron $q = -1$ at radius *re* and velocity *ve*. We set $vp = kBeta * rp/R$ where $kBeta$ and R are respectively the velocity of the most

external positron or electron of the particle and R its radius. In the same way for the electron, we set $ve = kBeta * re/R$. So the magnetic moment of one orbiting nuon is $mn = kBeta * \left(rp^2 - re^2\right)/R$. We find that $kBeta = 0.05968$ gives a perfect value for the muon, proton and neutron magnetic moment. This value is also in agreement with the value used for the proton-proton elastic scattering and also the value of a distance parameter used in inelastic proton-proton interactions as we will see later. The total magnetic moment for a charged particle is the sum of magnetic moments of its nuons plus (the magnetic moment of the central electron or positron)*particlemass/protonmass. For neutral particles we add the magnetic moments of the nuons and the magnetic moment of the bound electron-positron system at the center. This works well for the neutron, but it looks like for other neutral particles we have to assume that the contribution from the central system vanishes.

The top part of Figure 8 shows the radius of the positive (in black) and neutral particles (in red) as a function of N. The bottom part of the picture shows the density plot of the z positions of the nuons vs N for $5 < N < 120$ with an indication where the standard particles lie. In Figure 9 we show a few cases μ (N= 5), π (N= 6), K (N= 34), p (N= 66), Λ (N= 79), Ξ (N= 93), Ω (N= 118) from a data base of a few hundred particles for each value of N. On the left side we display the histogram of the z positions of the centre of the nuons with in green the z position of the 2 axial nuons, in red the z position of the centre of the nuons for neutral particles and in blue for charged particles. We see that the muons have 3 radial nuons orbiting at z = 0, the pions 4 orbital nuons also at z = 0, the kaons have 2 major z positions on each side of the z axis, the protons have 3, etc. The second column shows the radial views (y vs x), the third column a 3-D scatter-plot view x, y, z for many particles with the given N. Each peak along

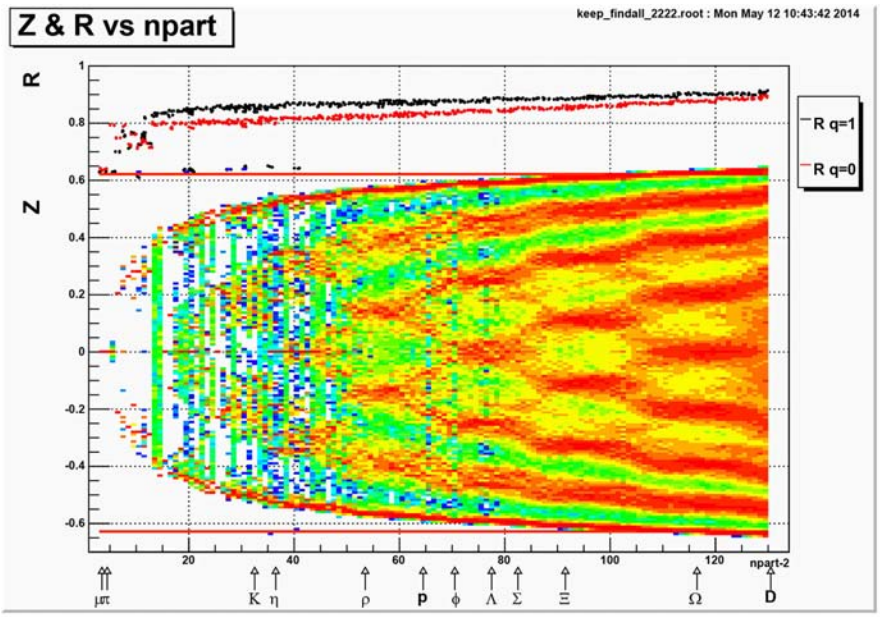

Figure 8. Particle radius vs N (top), z vs N (bottom).

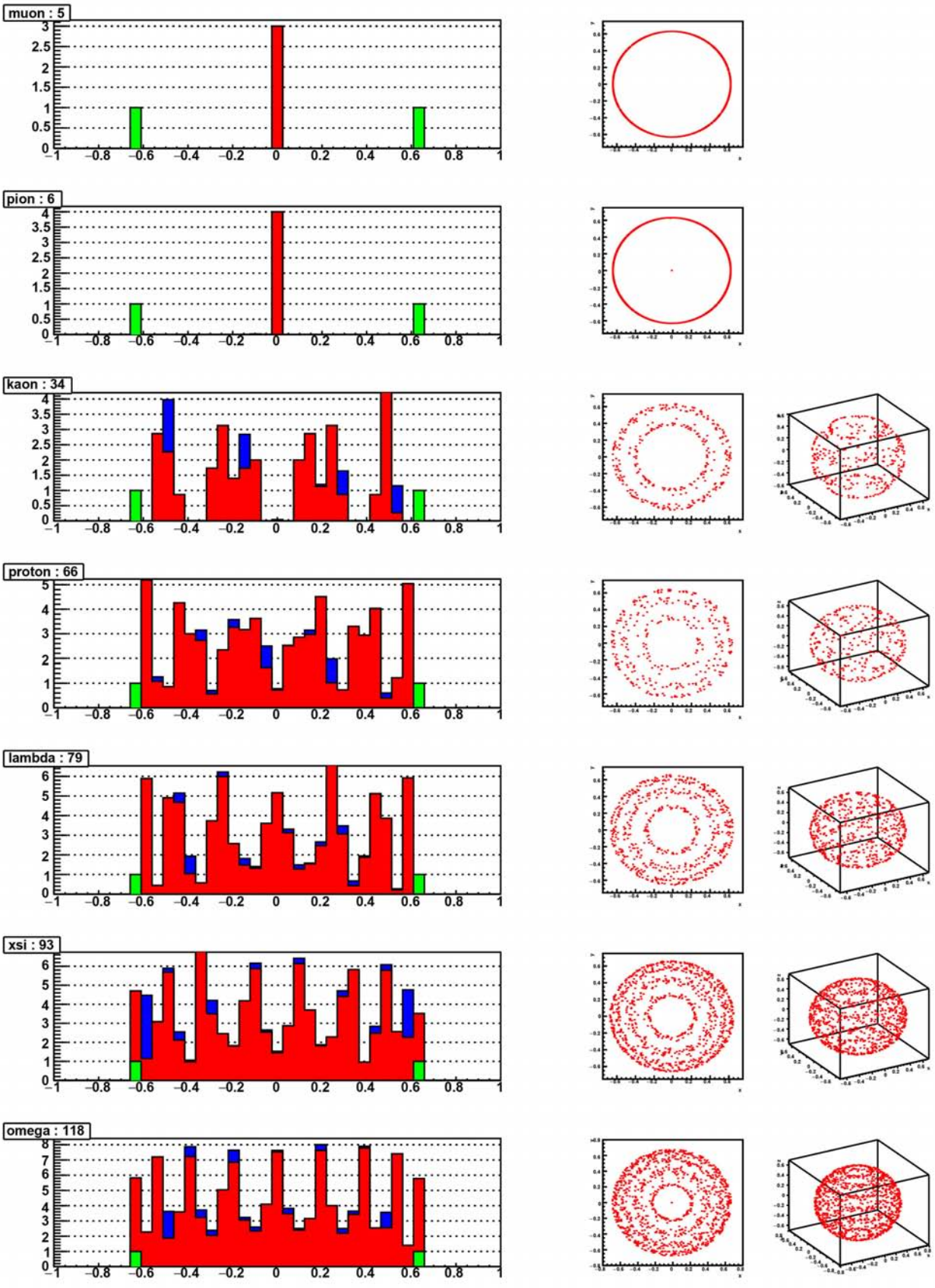

Figure 9. Some particles.

z has a Gaussian distribution and any z value in the same ring generates about the same value for the minimisation function F described above. At this point note that assuming an ellipsoidal shape instead of a spherical shape for N greater than 66 generates more symmetric and stable results. However because the computation time is already pretty high when using a simple sphere model, it is multiplied by a large factor when using an ellipsoid. The computation time becomes proportional to N^5 instead of N^2. For example the minimization time for a proton ($N = 66$) is about 10 seconds and it took several weeks to compute a data base of particles of a reasonable size for the work described in the following sections. It is indeed possible to improve the computation time in the future and test the expected benefits of an ellipsoid model instead of a sphere with far more statistics for the masses well above the proton mass.

2.6. Particles Stability and Life-Time

In the results shown in Figure 5 only 20 well known particles are shown. However the program converges for many more values. It is interesting to note that for all values of N from 7 to 33 the F value is bad. This is easy to understand. The muon ($N - 2 = 3$) and pion ($N - 2 = 4$) are systems with only one ring with all x, y nuon positions being at $z = 0$ for the radial nuons. Making 2 rings such as the kaon ($N - 2 = 32$) requires larger values of N. The investigation of the particles stability and life-time requires more work. During the minimisation process with MINUIT, local minima are observed. Understanding these local minima is a prerequisite to continue the work on particles life time.

Figure 10 shows the force vs radius in case of a proton.

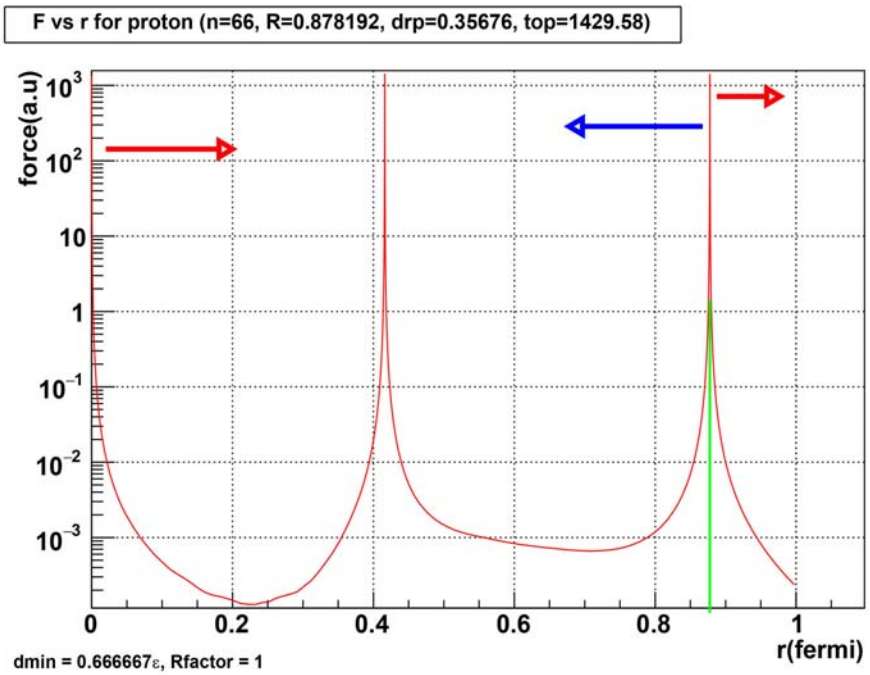

Figure 10. Attractive/repulsive forces in proton vs radius.

2.7. Nuons, Quarks/Gluons and the Strong Force

At a first glance, the nuon model appears to contradict the conventional quark/gluons model. However, as we will see in the section about charge density in the neutrons, quarks are seen in a nucleon from the nuon model perspective as objects having only a statistical behaviour and not a concrete object behaviour. In the same way the gluons properties and the strong force are just macroscopic properties of something described in more detail with the nuons. In particular, we will see in the section on p-p elastic scattering that the nuon model reproduces very precisely the experimental results for p-p and p-$\overline{\text{p}}$ elastic scattering for energies ranging from $\sqrt{s} = 27.43\,\text{GeV}$, as seen at the ISR, to $\sqrt{s} = 13\,\text{TeV}$, at the LHC/TOTEM.

When colliding protons against protons (see later), we see the interactions of the electrons/positrons inside the nuons of the respective protons. In a sense a proton is just a highly symmetric and beautiful assembly of electron/positron pairs (dipoles). In the current collisions model, neutrinos and antineutrinos are ignored, at the exception of the neutrinos on the rotation axis. Colliding protons is a bit like colliding quarks and gluons in p-p collisions or one or more electron/positron pair in an e^+e^- collider with 3 possible cases:

- Radial electron/positron of first proton against radial electron/positron of second proton.
- Radial electron/positron of first proton against the 2 axial nuons of the second proton, *i.e.* 2 electrons + 3 positrons + 66 neutrinos. Similar to the first case, but the collision involves more energy.
- 2 axial nuons of first proton against 2 axial nuons of second proton. This special case carries of course a lot more energy as it is the equivalent of 2($5e^+e^-$ + 66 neutrinos) collisions.

Jets appear as soon as the electrons get very close. To calculate at this point the amount of energy involved, one can make a very rough estimate that, for example at $\sqrt{s} = 7\,\text{TeV}$ each nuon is about 7000/(2 * 66) = 53 GeV if one assumes that the energy is distributed evenly across all nuons. When analyzing the dynamics of the proton-proton collisions, we see that the total energy of all radial nuons is about 73 per cent of the total energy and the remaining 27 percent is carried by the axial nuons. More precisely the fraction of the proton-proton energy in central collisions is

$$kAxial = (66+6+1)/(66*4+1) = 0.275472\,.$$

This gives a maximum energy maxPt = $kAxial\sqrt{s}$ for the axial-axial collisions of 540 GeV for a pp collider at 1.96 TeV, 1.93 TeV for a pp collider at 7 GeV and 3.58 TeV for a pp collider at 13 GeV, see **Figure 11**. Based on this simple construction parameter, a maximum Pt for jets is, by definition, equal to maxPt, and this prediction is confirmed by all experimental results, in particular by the latest results at the LHC over more than 10 orders of magnitude, as we will see later.

The electrons/positrons (Figure 12) are assumed to behave like a gaussian wave with a standard deviation kElecSigma = ϵ equal to about 0.0001 fermi.

Figure 13 illustrates how the elastic, deep and highly inelastic cases are taken into account during the simulations. Highly inelastic collisions are generated when two waves are very close (distance d < kElecSigma). Elastic interactions require d > 30 kElecSigma. Of course, all possible cases may be encountered, e.g. in a proton-proton collision at the LHC energies.

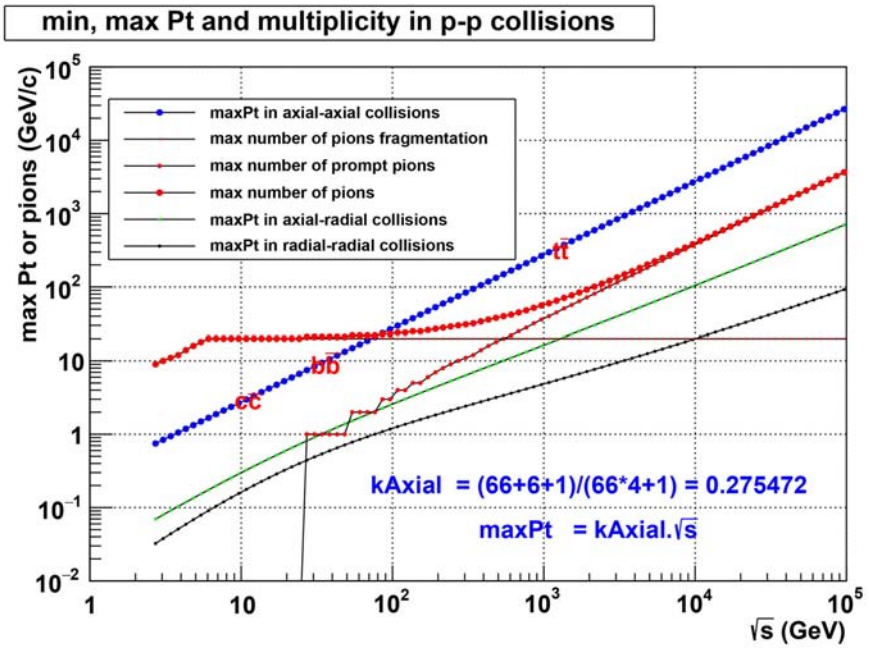

Figure 11. Maximum energy per type of collision and maximum number of pions.

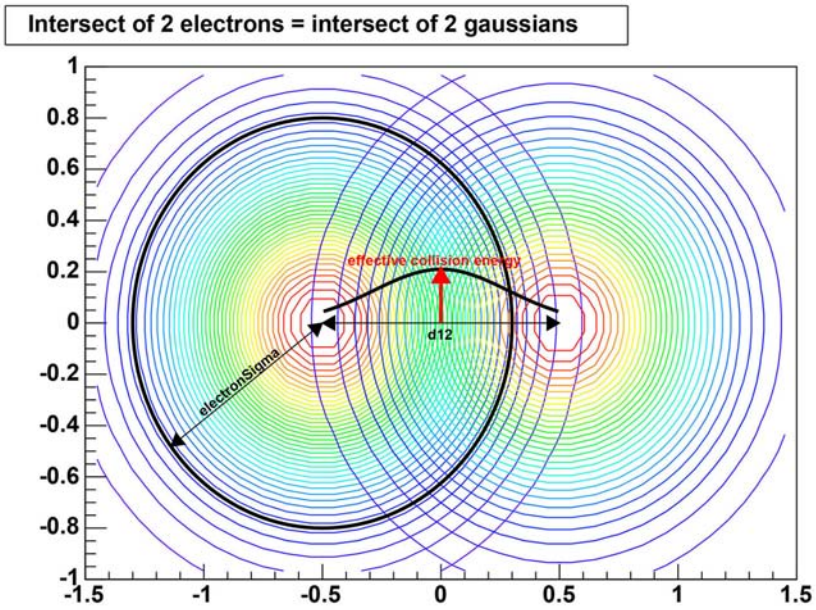

Figure 12. Colliding electrons. Each electron is taken as a gaussian with standard deviation *electronSigma*.

3. Computing Masses of All Know Mesons and Baryons

The Particle Data Group PDG [16] is reporting each year the status of the known mesons and baryons. The PDG tables in the 2022 version include 135 mesons and 133 baryons. The program findall has been extended to compute the masses of all particles reported in this last issue. The following Figure 14 shows the masses of all mesons and baryons versus the number of nuons per particle. The complete results are shown in Figure 15 and Figure 16.

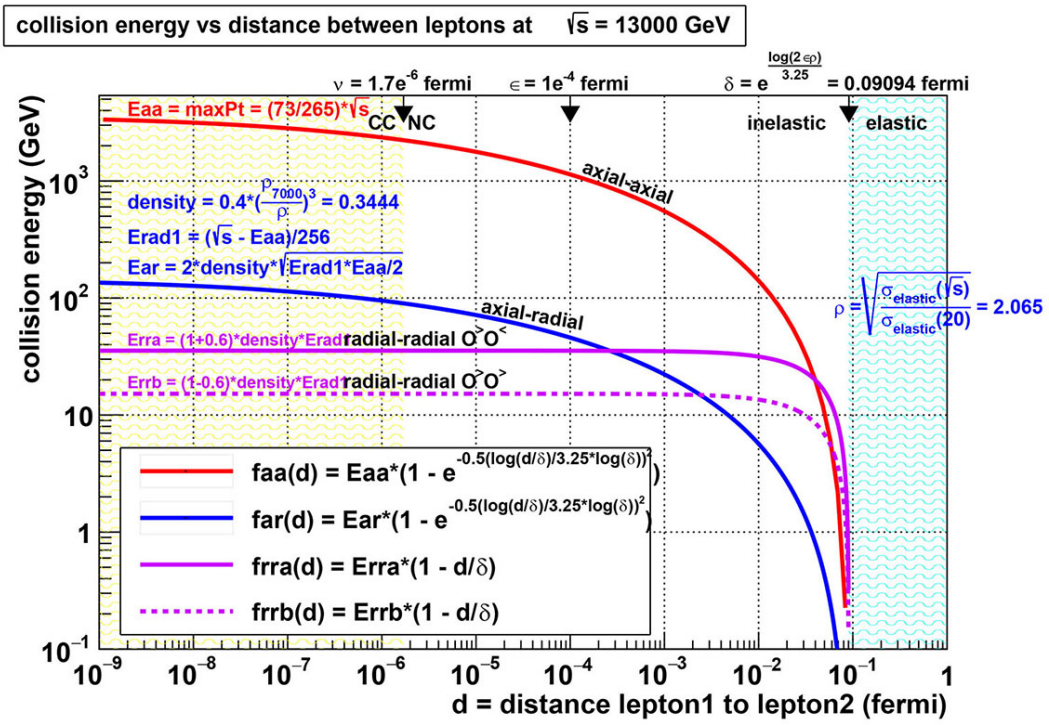

Figure 13. Energy generated by axial-axial, axial-radial or radial-radial electron/positron collisions as a function of the distance between the colliding objects.

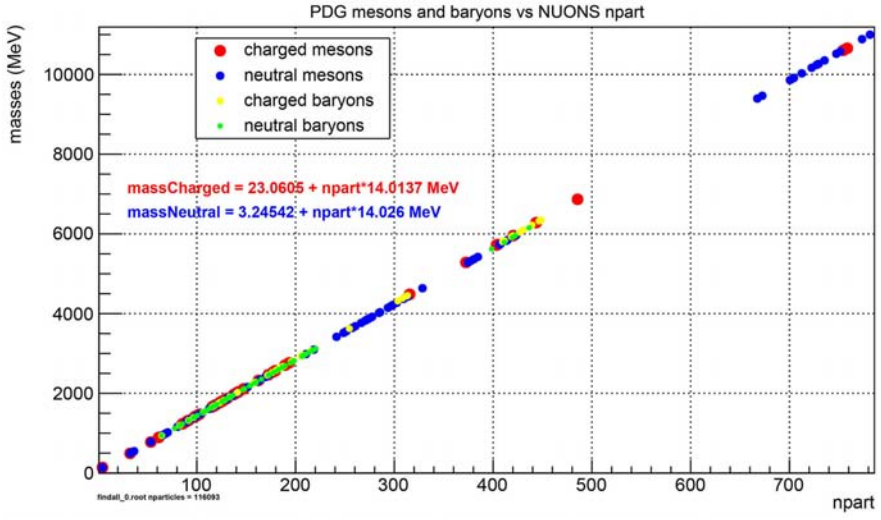

Figure 14. PDG mesons and baryons vs the number of nuons per particle.

name	PDG mass	N	nuons mass	rerr
--- Light Unflavored Mesons				
π^+	139.57	4 (2566)	139.57	2.4e-06
π_0	134.98	4 (2568)	134.98	2.1e-06
η	547.86	36 (15612)	547.94	-1.3e-04
$\rho(770)^+$	775.26	53 (17)	778.93	-4.7e-03
$\omega(782)$	782.65	53 (18)	781.23	1.8e-03
$\eta(958)$	957.78	65 (24)	950.03	8.1e-03
$f_0(980)$	990.00	68 (28)	991.01	-1.0e-03
$a_0(980)$	980.00	67 (14)	977.63	2.4e-03
$\phi(1020)$	1019.46	70 (2602)	1019.91	-4.4e-04
$h_1(1170)$	1166.00	80 (27)	1160.82	4.4e-03
$b_1(1235)$	1229.50	85 (19)	1232.64	-2.6e-03
$a_1(1260)$	1230.00	85 (19)	1232.64	-2.2e-03
$f_2(1270)$	1275.50	88 (18)	1273.01	2.0e-03
$f_1(1285)$	1281.90	89 (25)	1286.20	-3.4e-03
$\eta(1295)$	1294.00	90 (27)	1301.05	-5.4e-03
$\pi(1300)$	1300.00	90 (20)	1304.57	-3.5e-03
$a_2(1320)$	1318.20	91 (548)	1317.80	3.0e-04
$f_0(1370)$	1370.00	95 (14)	1372.27	-1.7e-03
$\pi(1400)$	1354.00	94 (15)	1360.06	-4.5e-03
$\eta(1405)$	1408.80	98 (14)	1413.85	-3.6e-03
$h_1(1415)$	1416.00	98 (14)	1413.85	1.5e-03
$f_1(1420)$	1426.30	99 (15)	1428.04	-1.2e-03
$a_0(1450)$	1474.00	102 (21)	1473.88	8.4e-05
$\rho(1450)$	1465.00	102 (19)	1470.88	-4.0e-03
$\eta(1475)$	1475.00	102 (19)	1470.88	2.8e-03
$f_0(1500)$	1506.00	105 (13)	1512.17	-4.1e-03
$f_2(1525)$	1517.40	105 (13)	1512.17	3.4e-03
$\pi_1(1600)$	1661.00	115 (8)	1657.33	2.2e-03
$a_1(1640)$	1655.00	115 (8)	1657.33	-1.4e-03
$\eta_2(1645)$	1617.00	112 (19)	1610.33	4.1e-03
$\omega(1650)$	1670.00	116 (18)	1666.36	2.2e-03
$\omega 3(1670)$	1667.00	116 (18)	1666.36	3.8e-04
$\pi_2(1670)$	1670.60	116 (646)	1671.85	-7.5e-04
$\phi(1680)$	1680.00	117 (25)	1680.22	-1.3e-04
$\rho_3(1690)$	1688.80	117 (14)	1686.00	1.7e-03
$\rho(1700)$	1720.00	120 (12)	1723.10	-1.8e-03
$f_0(1710)$	1704.00	119 (16)	1708.85	-2.8e-03
$\pi(1800)$	1810.00	126 (18)	1814.24	-2.3e-03
$\phi_3(1850)$	1854.00	129 (15)	1849.40	2.5e-03
$\eta_2(1870)$	1842.00	128 (18)	1835.51	3.5e-03
$\pi_2(1880)$	1874.00	131 (19)	1877.62	-1.9e-03
$f_2(1950)$	1936.00	135 (15)	1933.98	1.0e-03
$f_2(2010)$	2011.00	140 (17)	2004.33	3.3e-03
$a_4(2040)$	1995.00	139 (24)	1990.36	2.3e-03
$f_4(2050)$	2018.00	141 (14)	2018.77	-3.8e-04
$\phi(2170)$	2159.00	151 (15)	2158.84	7.2e-05
$f_2(2300)$	2297.00	161 (19)	2298.83	-7.9e-04
$f_2(2340)$	2345.00	164 (23)	2340.98	1.7e-03

name	PDG mass	N	nuons mass	rerr
--- Strange Mesons				
K^+	493.68	32 (14243)	493.65	4.5e-05
K^0	497.61	32 (15540)	497.31	6.0e-04
$K^*(892)$	891.66	61 (24)	892.52	-9.6e-04
$K_1(1270)$	1253.00	86 (16)	1246.49	5.2e-03
$K_1(1400)$	1403.00	97 (15)	1403.36	-2.6e-04
$K^*(1410)$	1414.00	98 (21)	1417.60	-2.5e-03
$K^*_2(1430)$	1425.00	99 (21)	1431.83	-4.8e-03
$K(1680)$	1718.00	119 (21)	1714.42	2.1e-03
$K_2(1770)$	1773.00	123 (14)	1772.01	5.6e-04
$K^*_3(1780)$	1779.00	124 (16)	1785.91	-3.9e-03
$K^*_2(1820)$	1819.00	126 (16)	1814.24	2.6e-03
$K_4(2045)$	2048.00	142 (20)	2041.47	3.2e-03
--- Charmed Mesons				
D^+	1869.66	130 (1739)	1871.04	-7.4e-04
D^0	1864.84	130 (1739)	1864.12	3.8e-04
$D^*(2007)^0$	2006.85	140 (17)	2004.33	1.3e-03
$D^*(2010)^+$	2010.26	140 (11)	2012.95	-1.3e-03
$D^*_0(2300)$	2340.00	164 (23)	2340.98	-4.2e-04
$D^0_1(2420)$	2420.10	170 (17)	2425.10	-2.1e-03
$D^0_1(2430)$	2412.10	169 (14)	2411.05	4.3e-04
$D^*_2(2460)^0$	2461.10	173 (14)	2467.34	-2.5e-03
$D^*_3(2750)^+$	2763.10	193 (23)	2763.59	-1.8e-04
--- Charmed Strange Mesons				
D^+_s	1968.35	137 (17)	1970.71	-1.2e-03
D^{*+}_s	2112.20	147 (12)	2112.25	-2.4e-05
$D^*_{s0}(2317)^+$	2317.80	162 (16)	2324.24	-2.8e-03
$D^*_{s1}(2460)^+$	2459.50	172 (9)	2466.34	-2.8e-03
$D^*_{s1}(2536)^+$	2535.10	177 (7)	2537.52	-9.6e-04
$D^*_{s2}(2573)^+$	2569.10	179 (7)	2565.78	1.3e-03
$D^*_{s1}(2700)^+$	2708.30	189 (13)	2706.94	5.0e-04
--- Bottom Mesons				
B^+	5279.34	372 (33)	5284.74	-1.0e-03
B^0	5279.65	374 (16)	5281.64	-3.8e-04
B^*	5324.70	377 (27)	5323.79	1.7e-04
$B_1(5721)^+$	5725.90	403 (33)	5719.54	1.1e-03
$B_1(5721)^0$	5726.10	406 (21)	5731.16	-8.8e-04
$B^*_2(5747)^+$	5737.20	404 (20)	5732.96	7.4e-04
$B^*_2(5747)^0$	5739.50	407 (23)	5745.56	-1.1e-03
$B^*_J(5970)^+$	5964.00	420 (70)	5957.69	1.1e-03
$B^*_J(5970)^0$	5971.00	423 (25)	5969.54	2.4e-04
--- Bottom Strange Mesons				
B^s_0	5366.88	380 (32)	5366.04	1.6e-04
B^*_s	5415.40	384 (16)	5422.09	-1.2e-03
$B_{s1}(5830)^0$	5828.70	413 (29)	5829.38	-1.2e-04
$B^*_{s2}(5840)^0$	5839.86	414 (37)	5843.44	-6.1e-04

name	PDG mass	N	nuons mass	rerr
--- Bottom Charmed Mesons				
B^+_c	6274.47	443 (22)	6280.20	-9.1e-04
$B_c(2S)^+$	6871.20	485 (21)	6867.14	5.9e-04
--- CCbar Mesons				
$\eta_c(1S)$	2983.90	210 (30)	2984.60	-2.3e-04
$J/\psi(1S)$	3096.90	218 (45)	3096.28	2.0e-04
$\chi_{c0}(1P)$	3414.71	241 (37)	3417.56	-8.3e-04
$\chi_{c1}(1P)$	3510.67	248 (29)	3515.71	-1.4e-03
$h_c(1P)$	3525.38	249 (32)	3529.81	-1.3e-03
$\chi_{c2}(1P)$	3556.17	251 (21)	3557.68	-4.2e-04
$\eta_c(2S)$	3637.50	257 (34)	3641.37	-1.1e-03
$\psi(2S)$	3686.10	260 (27)	3683.41	7.3e-04
$\psi(3770)$	3773.70	266 (25)	3767.05	1.8e-03
$\psi(3823)$	3822.20	270 (24)	3823.41	-3.2e-04
$\psi(3842)$	3842.71	271 (23)	3837.53	1.3e-03
$\chi(3872)$	3871.69	273 (22)	3865.07	1.7e-03
$Z_c(3900)$	3888.40	275 (17)	3893.33	-1.3e-03
$\chi(3915)$	3921.70	277 (32)	3921.29	1.1e-04
$\chi_{c2}(3930)$	3922.50	277 (32)	3921.29	3.1e-04
$\chi(4020)$	4024.10	284 (20)	4019.37	1.2e-03
$\psi(4040)$	4039.00	285 (19)	4033.43	1.4e-03
$\chi(4140)$	4146.80	293 (14)	4145.85	2.3e-04
$\psi(4160)$	4191.00	296 (23)	4187.92	7.4e-04
$\psi(4230)$	4220.00	298 (18)	4216.15	9.1e-04
$\chi_{c1}(4274)$	4274.00	302 (25)	4271.63	5.5e-04
$\psi(4360)$	4368.00	309 (25)	4370.24	-5.1e-04
$\psi(4415)$	4421.00	313 (16)	4425.92	-1.1e-03
$Z_c(4430)^+$	4478.00	315 (34)	4484.18	-1.4e-03
$\psi(4660)$	4630.00	328 (14)	4636.30	-1.4e-03
--- BBbar Mesons				
$\eta_b(1S)$	9398.70	667 (29)	9395.31	3.6e-04
$\Upsilon(1S)$	9460.30	672 (37)	9465.85	-5.9e-04
$\chi_{b0}(1P)$	9859.44	700 (40)	9859.49	-5.0e-06
$\chi_{b1}(1P)$	9892.78	703 (28)	9898.28	-5.6e-04
$h_b(1P)$	9899.30	703 (28)	9898.28	1.0e-04
$\chi_{b2}(1P)$	9912.21	704 (25)	9914.51	-2.3e-04
$\Upsilon(2S)$	10023.26	712 (29)	10027.81	-4.5e-04
$\Upsilon(1D)$	10163.70	722 (41)	10167.44	-3.7e-04
$\chi_{b0}(2P)$	10232.50	727 (40)	10238.70	-6.1e-04
$\chi_{b1}(2P)$	10255.46	728 (40)	10252.26	3.1e-04
$\chi_{b2}(2P)$	10268.65	729 (40)	10265.92	2.7e-04
$\Upsilon(3S)$	10355.20	735 (37)	10351.11	3.9e-04
$\chi_{b1}(3P)$	10513.40	747 (23)	10518.72	-5.1e-04
$\chi_{b2}(3P)$	10524.00	747 (23)	10518.72	5.0e-04
$\Upsilon(4S)$	10579.40	751 (32)	10575.24	3.9e-04
$Z_b(10610)^+$	10607.20	754 (35)	10604.59	2.5e-04
$Z_b(10650)^+$	10652.20	758 (32)	10656.82	-4.3e-04
$\Upsilon(10860)$	10885.20	773 (42)	10885.34	-1.3e-05
$\Upsilon(11020)$	11000.00	781 (38)	10997.90	1.9e-04

found ok if diff=|massPDG - massNuons| < 8 MeV, very good if diff < 5 MeV , veryvery good if diff < 1 MeV relerrm = 1.42e-03

findall_0.root nparticles = 116093 ==> nmesonsPDG = 135, nmfoundok = 135, nmverygood = 106, nmveryverygood = 67

Figure 15. PDG mesons masses compared to nuons.

Important Remark 1. One must be very careful with the affirmation that masses show a linear behaviour in function of a given integer. For example, when fitting the 268 particles (masses from 100 MeV/c^2 to 11,000 MeV/c^2) with a number of nuons going from 32 to 782, the distance between adjacent masses will be in average around 14.3 MeV/c^2. The precision to compute the masses must be better than 14.3/2 MeV/c^2. See the bottom of the mesons and baryons tables where it is shown that 50 per cent of the masses are calculated with a precision better that 1 MeV/c^2.

name	PDG mass	N	nuons mass	rerr
--- N Baryons				
p	938.27	64 (13447)	938.29	-2.2e-05
n	939.57	64 (13696)	939.50	6.5e-05
N(1440)	1440.00	100 (20)	1442.55	-1.8e-03
N(1520)	1515.00	105 (13)	1512.17	1.9e-03
N(1535)	1530.00	106 (19)	1526.76	2.1e-03
N(1650)	1650.00	115 (15)	1652.49	-1.5e-03
N(1675)	1675.00	117 (25)	1680.22	-3.1e-03
N(1680)	1685.00	117 (25)	1680.22	2.8e-03
N(1700)	1720.00	120 (13)	1723.10	-1.8e-03
N(1710)	1710.00	119 (16)	1708.85	6.8e-04
N(1720)	1720.00	120 (13)	1723.10	-1.8e-03
N(1875)	1875.00	131 (19)	1877.62	-1.4e-03
N(1880)	1880.00	131 (19)	1877.62	1.3e-03
N(1895)	1895.00	132 (20)	1891.46	1.9e-03
N(1900)	1920.00	134 (14)	1919.77	1.2e-04
N(2060)	2100.00	147 (10)	2102.68	-1.3e-03
N(2100)	2100.00	147 (10)	2102.68	-1.3e-03
N(2120)	2120.00	148 (12)	2117.24	1.3e-03
N(2190)	2180.00	153 (11)	2186.02	-2.8e-03
$N(2220)^+$	2250.00	158 (14)	2256.42	-2.9e-03
$N(2250)^-$	2280.00	160 (20)	2284.39	-1.9e-03
N(2600)	2600.00	182 (14)	2593.00	2.7e-03
--- Δ Baryons				
Δ(1232)	1232.00	85 (20)	1230.51	1.2e-03
Δ(1600)	1570.00	109 (17)	1568.00	1.3e-03
Δ(1620)	1610.00	112 (19)	1610.33	-2.0e-04
Δ(1700)	1710.00	119 (16)	1708.85	6.8e-04
Δ(1900)	1860.00	130 (720)	1864.12	-2.2e-03
Δ(1905)	1880.00	131 (19)	1877.62	1.3e-03
Δ(1910)	1900.00	133 (21)	1905.83	-3.1e-03
Δ(1920)	1920.00	134 (14)	1919.77	1.2e-04
Δ(1930)	1950.00	136 (14)	1948.01	1.0e-03
Δ(1950)	1930.00	135 (15)	1933.98	-2.1e-03
Δ(2200)	2200.00	154 (17)	2200.13	-6.1e-05
Δ(2420)	2450.00	172 (12)	2453.26	-1.3e-03
--- Λ Baryons				
Λ(1232)	1115.68	77 (2459)	1117.46	-1.6e-03
Λ(1405)	1405.10	97 (16)	1399.70	3.8e-03
Λ(1520)	1519.00	105 (13)	1512.17	4.5e-03
Λ(1600)	1600.00	111 (24)	1595.64	2.7e-03
Λ(1670)	1674.00	117 (25)	1680.22	-3.7e-03
Λ(1690)	1690.00	118 (14)	1694.63	-2.7e-03
Λ(1800)	1800.00	125 (15)	1793.38	3.7e-03
Λ(1810)	1790.00	125 (15)	1793.38	-1.9e-03
Λ(1820)	1820.00	127 (22)	1821.76	-9.7e-04
Λ(1830)	1825.00	127 (22)	1821.76	1.8e-03
Λ(1890)	1890.00	132 (20)	1891.46	-7.7e-04
Λ(2100)	2100.00	147 (10)	2102.68	-1.3e-03
Λ(2110)	2090.00	146 (17)	2089.06	4.5e-04
Λ(2350)	2350.00	165 (15)	2354.83	-2.1e-03

name	PDG mass	N	nuons mass	rerr
--- Σ Baryons				
Σ^+	1189.37	82 (682)	1190.45	-9.1e-04
Σ^-	1197.45	82 (682)	1190.45	5.8e-03
Σ^0	1192.64	82 (735)	1188.48	3.5e-03
$\Sigma(1385)3/2^+$	1382.80	96 (13)	1389.86	-5.1e-03
$\Sigma(1385)3/2^0$	1383.70	96 (18)	1385.96	-1.6e-03
$\Sigma(1660)1/2^+$	1660.00	115 (9)	1657.33	1.6e-03
$\Sigma(1670)3/2^-$	1675.00	116 (646)	1671.85	1.9e-03
$\Sigma(1750)1/2^-$	1750.00	121 (27)	1743.17	3.9e-03
$\Sigma(1775)5/2^-$	1775.00	123 (11)	1772.01	1.7e-03
$\Sigma(1910)5/2^+$	1910.00	133 (13)	1913.32	-1.7e-03
$\Sigma(1915)5/2^+$	1915.00	133 (13)	1913.32	8.8e-04
$\Sigma(2030)7/2^+$	2030.00	141 (13)	2027.19	1.4e-03
$\Sigma(2250)7/2^+$	2250.00	157 (13)	2253.32	-1.5e-03
--- Ξ Baryons				
Ξ^0	1314.86	91 (697)	1314.99	-1.0e-04
Ξ^-	1321.71	91 (648)	1317.80	3.0e-03
$\Xi(1530)3/2^0$	1531.80	106 (19)	1526.76	3.3e-03
$\Xi(1530)3/2^-$	1535.00	106 (20)	1530.33	3.0e-03
Ξ(1690)	1690.00	117 (14)	1686.00	2.4e-03
$\Xi(1820)3/2^-$	1823.00	127 (20)	1828.61	-3.1e-03
Ξ(1950)	1950.00	136 (14)	1948.01	1.0e-03
Ξ(2030)	2025.00	141 (13)	2027.19	-1.1e-03
--- Ω Baryons				
Ω^-	1672.45	116 (646)	1671.85	3.6e-04
$\Omega(2012)^-$	2012.40	140 (11)	2012.95	-2.7e-04
$\Omega(2250)^-$	2252.00	157 (13)	2253.32	-5.9e-04
--- Exotic Baryons				
$\#P_c(4312)^+$	4311.90	303 (38)	4315.30	-7.9e-04
$\#P_c(4380)^+$	4380.00	308 (34)	4385.32	-1.2e-03
$\#P_c(4440)^+$	4440.00	312 (35)	4441.77	-4.0e-04
$\#P_c(4457)^+$	4457.30	313 (33)	4455.53	4.0e-04
--- New LHCB baryons				
$\Omega_b(6316)^-$	6315.64	446 (31)	6321.99	-1.0e-03
$\Omega_b(6330)^-$	6330.30	447 (32)	6336.06	-9.1e-04
$\Omega_b(6340)^-$	6339.71	447 (32)	6336.06	5.8e-04
$\Omega_b(6350)^-$	6349.88	448 (33)	6349.81	1.1e-05
$\Sigma_c(2923)^0$	2923.04	206 (17)	2928.69	-1.9e-03
$\Sigma_c(2939)^0$	2938.55	207 (16)	2943.17	-1.6e-03
$\Sigma_c(2965)^0$	2964.88	209 (24)	2970.48	-1.9e-03
Xi_cc (Doubly charmed)				
Ξ_{cc}^{++}	3621.20	254 (23)	3625.04	-1.1e-03

name	PDG mass	N	nuons mass	rerr
--- Charmed Baryons				
Λ_c^+	2286.46	159 (19)	2281.76	2.1e-03
$\Lambda_c(2595)^+$	2592.25	181 (11)	2594.03	-6.9e-04
$\Lambda_c(2625)^+$	2628.11	183 (11)	2621.86	2.4e-03
$\Lambda_c(2860)^+$	2656.10	185 (20)	2650.14	2.2e-03
$\Lambda_c(2880)^+$	2681.63	187 (10)	2678.47	1.2e-03
$\Lambda_c(2940)^+$	2939.60	205 (17)	2933.60	2.0e-03
$\Sigma_c(2455)^+$	2452.90	171 (9)	2451.95	3.9e-04
$\Sigma_c(2455)^0$	2453.75	172 (12)	2453.26	2.0e-04
$\Sigma_c(2520)^+$	2517.50	176 (18)	2523.30	-2.3e-03
$\Sigma_c(2520)^0$	2518.41	177 (17)	2523.27	-1.9e-03
$\Sigma_c(2800)^+$	2792.00	195 (9)	2792.62	-2.2e-04
$\Sigma_c(2800)^0$	2806.00	197 (20)	2803.18	1.0e-03
Ξ_c^+	2467.94	172 (9)	2466.34	6.5e-04
Ξ_c^0	2470.90	173 (14)	2467.34	1.4e-03
$\Xi_c'^+$	2578.40	180 (13)	2579.70	-5.1e-04
$\Xi_c'^0$	2579.20	181 (19)	2578.90	1.2e-04
$\Xi_c(2645)^+$	2645.56	185 (20)	2650.14	-1.7e-03
$\Xi_c(2645)^0$	2646.38	186 (20)	2649.05	-1.0e-03
$\Xi_c(2790)^+$	2792.40	195 (9)	2792.62	-7.8e-05
$\Xi_c(2790)^0$	2794.10	196 (19)	2789.07	1.8e-03
$\Xi_c(2815)^+$	2816.74	197 (10)	2820.32	-1.3e-03
$\Xi_c(2815)^0$	2820.25	198 (24)	2816.91	1.2e-03
$\Xi_c(2970)^+$	2966.34	207 (8)	2962.31	1.4e-03
$\Xi_c(2970)^0$	2970.90	209 (24)	2970.48	1.4e-04
$\Xi_c(3055)$	3055.90	215 (22)	3054.30	5.2e-04
$\Xi_c(3080)^+$	3077.20	215 (9)	3074.91	7.4e-04
$\Xi_c(3080)^0$	3079.90	217 (17)	3082.45	-8.3e-04
Ω_c^0	2695.20	189 (9)	2691.01	1.6e-03
$\Omega_c(2770)^0$	2765.90	194 (9)	2760.77	1.9e-03
$\Omega_c(3000)^0$	3000.41	211 (12)	2998.38	6.8e-04
$\Omega_c(3050)^0$	3050.20	215 (22)	3054.30	-1.3e-03
$\Omega_c(3065)^0$	3065.46	216 (18)	3068.43	-9.7e-04
$\Omega_c(3090)^0$	3090.00	218 (45)	3096.28	-2.0e-03
$\Omega_c(3120)^0$	3119.10	220 (24)	3124.53	-1.7e-03
--- Bottom Baryons				
Λ_b^0	5619.51	398 (32)	5619.47	7.1e-06
$\Lambda_b(5912)$	5912.20	419 (34)	5913.24	-1.8e-04
$\Lambda_b(5920)$	5919.92	419 (34)	5913.24	1.1e-03
$\Lambda_b(6146)$	6146.20	436 (49)	6152.26	-9.9e-04
$\Lambda_b(6152)$	6152.50	436 (49)	6152.26	4.0e-05
Σ_b^-	5810.56	410 (8)	5816.79	-1.1e-03
Σ_b^+	5830.32	411 (34)	5827.98	4.0e-04
$\Sigma_b^*(6097)$	6095.80	430 (40)	6098.00	-3.6e-04
Ξ_b^-	5797.00	409 (30)	5803.38	-1.1e-03
Ξ_b^0	5791.90	411 (35)	5791.80	1.8e-05
$\Xi_b'(5935)^-$	5935.02	418 (50)	5929.84	8.7e-04
$\Xi_b(5945)^0$	5952.30	422 (28)	5955.31	-5.1e-04
$\Xi_b(5955)^-$	5955.33	420 (70)	5957.69	-4.0e-04
$\Xi_b(6227)^-$	6226.90	439 (19)	6223.67	5.2e-04
Ω_b^-	6046.10	426 (34)	6041.64	7.4e-04

found ok if diff=|massPDG - massNuons| < 8 MeV, very good if diff < 5 MeV, veryvery good if diff < 1 MeV
findall_0.root nparticles = 116093 ===> nbaryonsPDG = 133, nbfoundok = 133, nbverygood = 111, nbveryverygood = 76

Figure 16. PDG baryons masses compared to nuons.

Important Remark 2. When looking at this linearity, one could also think that one should be able to determine this frequency from the PDG tables directly by making a Fourier Transform. Unfortunately, this does not work because there are by definition missing masses (not yet found!). Charged and neutral versions of a particle have substantially different masses, or particles masses like resonances have a large mean error.

4. Charge Density in the Neutron

Building experiments to understand the charge distribution/density in the nucleon has always been a challenge for physicists. The standard way to investigate the internal proton structure has always been via beams of lighter objects $(\nu, \mathrm{e}, \mu, \pi)$ or e-p collisions. This task is particularly difficult as the interpretation of results depends mainly on the assumed (quark/gluon) model of the proton. For the neutron case the task is even more difficult as it is hard for the time being to realise a e-n or ν, n, π or μ, n collider. In general the understanding of the neutron structure has been made via e, ν, μ beams into deuterium or carbon targets. In this case the estimation of the neutron structure is made by subtracting the *better known* proton results.

However, in 2010 a very interesting experiment BLAST [20] has been conducted at the MIT/BATES accelerator. An electron beam (few GeV) is colliding with a deuterium jet. This experiment has published a very interesting article [20] estimating the charge density inside the neutron. The results show a slightly positive core (max at 0.17e) and a small negative crown vanishing slowly after several fermis. It would be nice to see other experiments confirming this result. This result presents a nice challenge for the nuon model. A simple program npCharge shoots electrons into neutrons taken from a data base of several thousand neutrons generated by the program findall that computes the masses of all particles. The electrons are sent through the neutron at random distances from the centre (as in the experiment) and at each step (40 steps in total) the charge density is estimated. In the left of **Figure 17** one can see the result (black points with errors) and the result from BLAST superimposed (red line). In the right the average charge is shown, and of course, expected to be 0 on average.

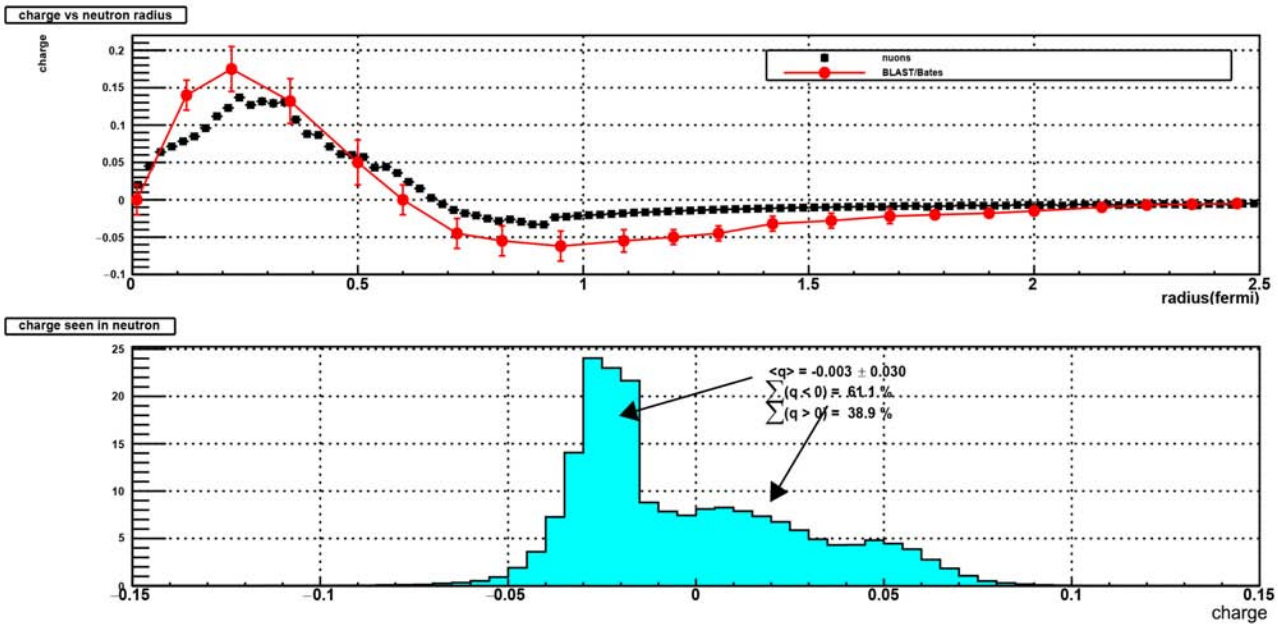

Figure 17. Charge Density vs radius (left). Average charge (right).

5. Testing the Model: Current and Future

In addition to the static tests presented above, the proposed model can be tested with many different experiments with different physics processes and energies. The most obvious tests are with:

- Elastic scattering with proton-proton or proton-antiproton
- Diffraction processes, e.g. proton-proton
- Deep inelastic scattering, e.g. electron-proton
- Highly inelastic collisions with production of jets in proton-proton collisions
- HeavyIons collisions

So far the model has been tested with proton-proton, proton-antiproton elastic scattering, electron-proton, positron-proton deep inelastic scattering and highly inelastic collisions that are described in the following sections.

6. Comparison with p-p and p-$\bar{p}$ Elastic Experiments

p-p and p-$\bar{p}$ elastic scattering experiments offer nice ways to measure the proton/antiproton shape and near surface constituents. Many results have been obtained with collider experiments starting with the ISR [21] up to the recent data with TOTEM [13] at the LHC. The result of these experiments is always shown in terms of the four momentum transfer $t = -p^2\theta^2$. The histogram of t exhibits 3 domains: a first domain for the small values of t that is traditionally interpreted as the Coulomb scattering contribution when the 2 particles do not overlap or are far away. The shape of the t distribution in this area has an exponential behaviour with a very large slope.

The first slope for small values of t is due to the Coulomb forces when the particles do not overlap up to a very large distance *distmax*. Figure 18 shows the maximum radial distance *distmax* between the 2 protons as a function of the beam energy.

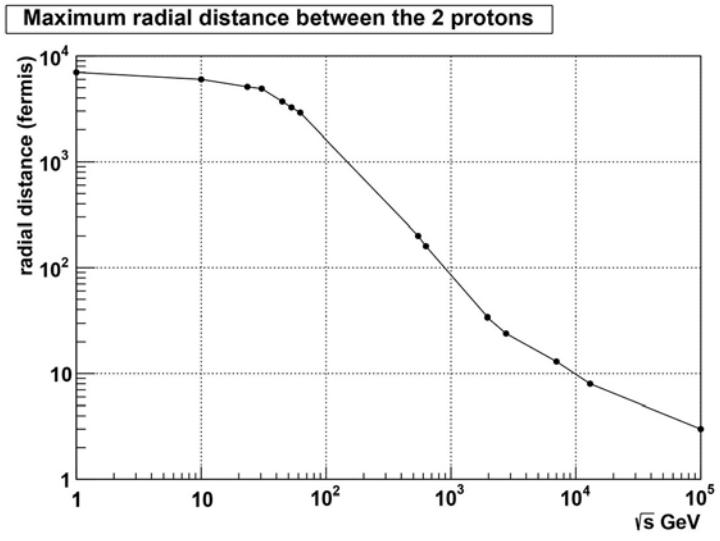

Figure 18. Maximum distance between the 2 protons center.

The large values of t are interpreted via the Strong Force contributions when the 2 particles interpenetrate. The third domain in the middle exhibits a dip and a maximum. The value of t at the dip is in general interpreted as being proportional to the inverse of the proton radius. As the position of the dip decreases when the energy increases, one usually says that the proton radius increases with the energy. The interpretation of the shape of the dip and associated maximum is interpreted via several mechanisms, e.g. the Pomeron-exchange [22] mechanism and Regge trajectories [23].

Using the nuon model, one reproduces extremely well the experimental results for all available data ranging from $\sqrt{s} = 27.43\,\text{GeV}$ at the ISR [21], 536 GeV at $\text{SP}\overline{\text{P}}\text{S}$ [24], 1960 GeV at the Tevatron [25] and 7 and 13 TeV at the LHC [13] (see **Figures 19-24**). The totem program has been written taking protons at random from the proton data base and colliding them with different impact distances. While the protons move, their internal nuons rotate and the necessary Lorentz transformations are taken into account. For example at 7 TeV, colliding 2 protons is like colliding 2 pancakes since their γ factor is about 3730. It is interesting to note that in the case of proton-antiproton scattering, the dip nearly vanishes in the experimental data and this behaviour is well reproduced by the model.

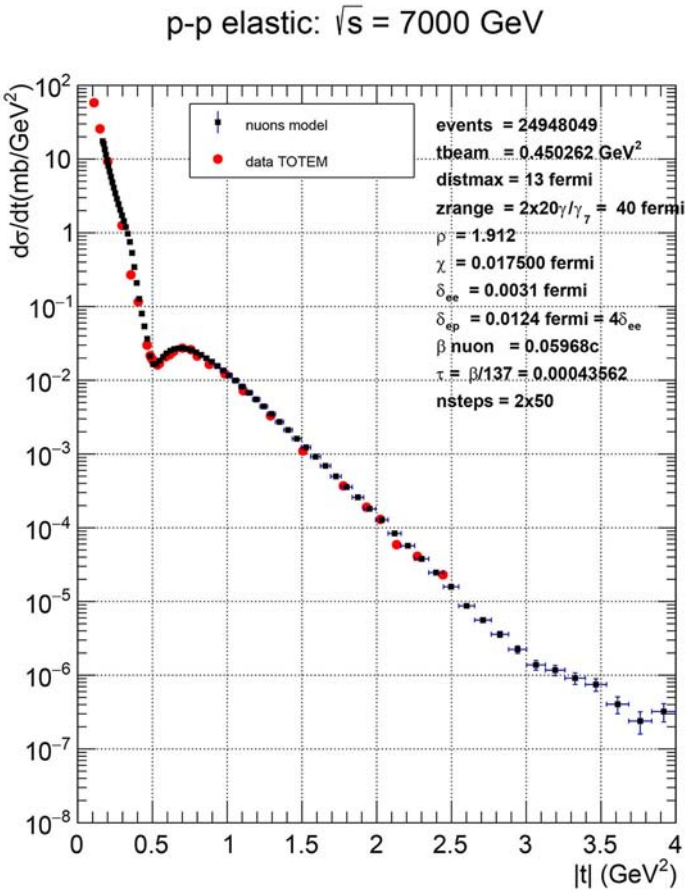

Figure 19. Momentum transfer distribution at LHC 7 TeV TOTEM.

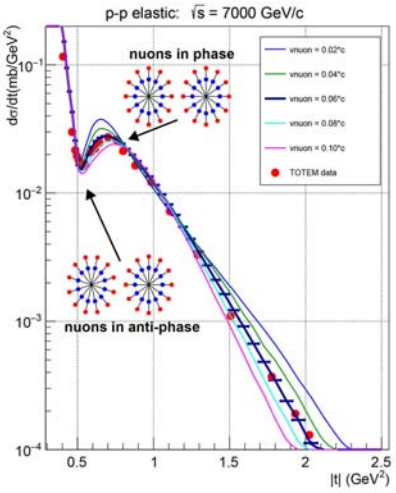

Figure 20. Momentum transfer distribution for various β at 7 TeV.

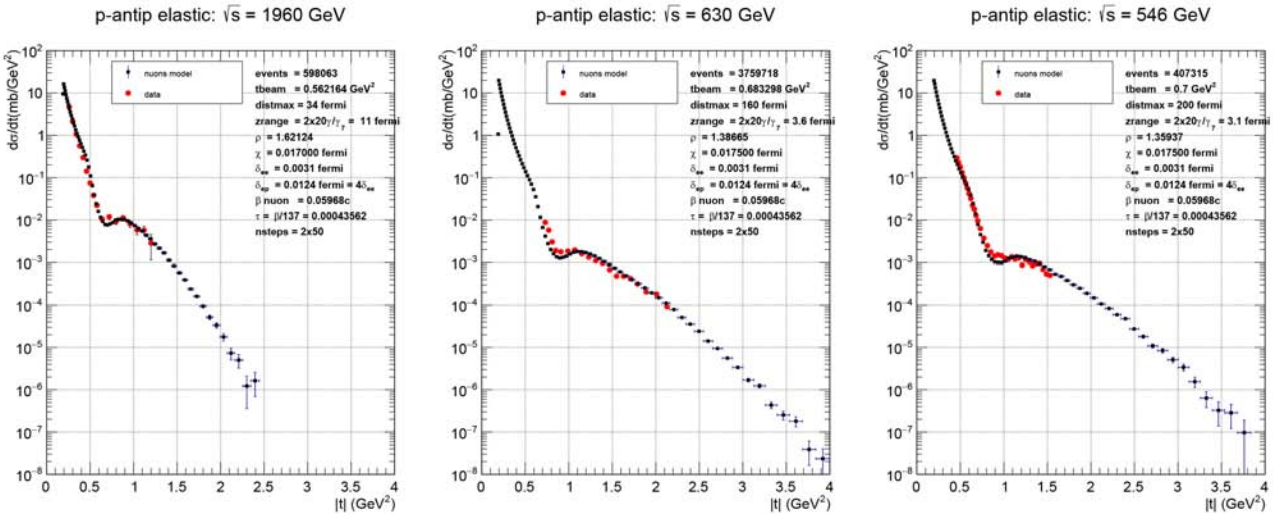

Figure 21. Tevatron (D_0) and SPS (UA4) proton-antiproton elastic scattering.

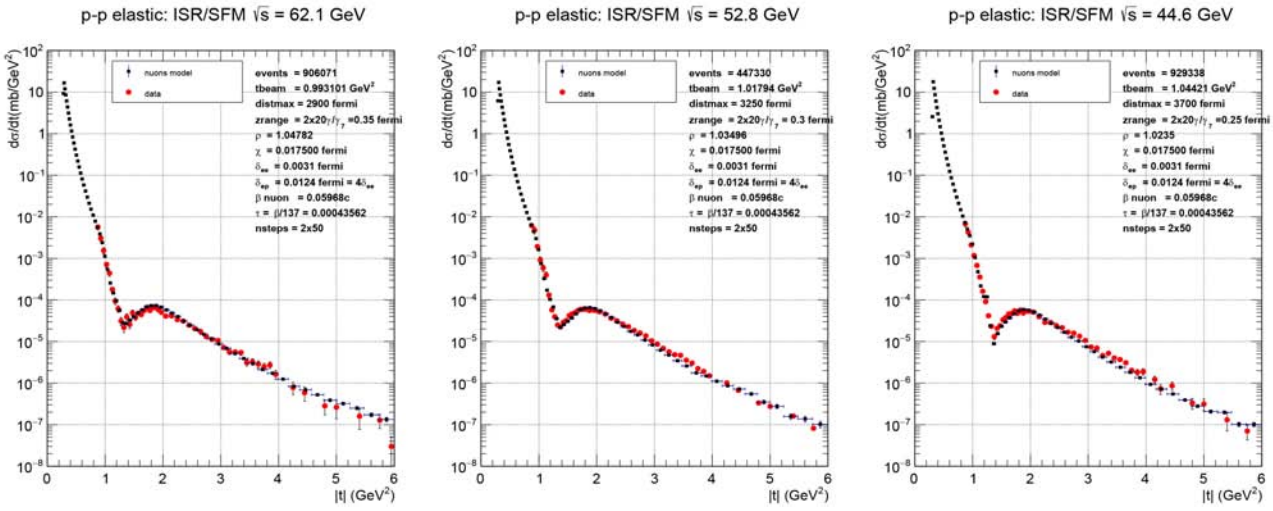

Figure 22. ISR proton-proton elastic scattering from $\sqrt{s} = 62.1 \rightarrow 44.1\,\text{GeV}$.

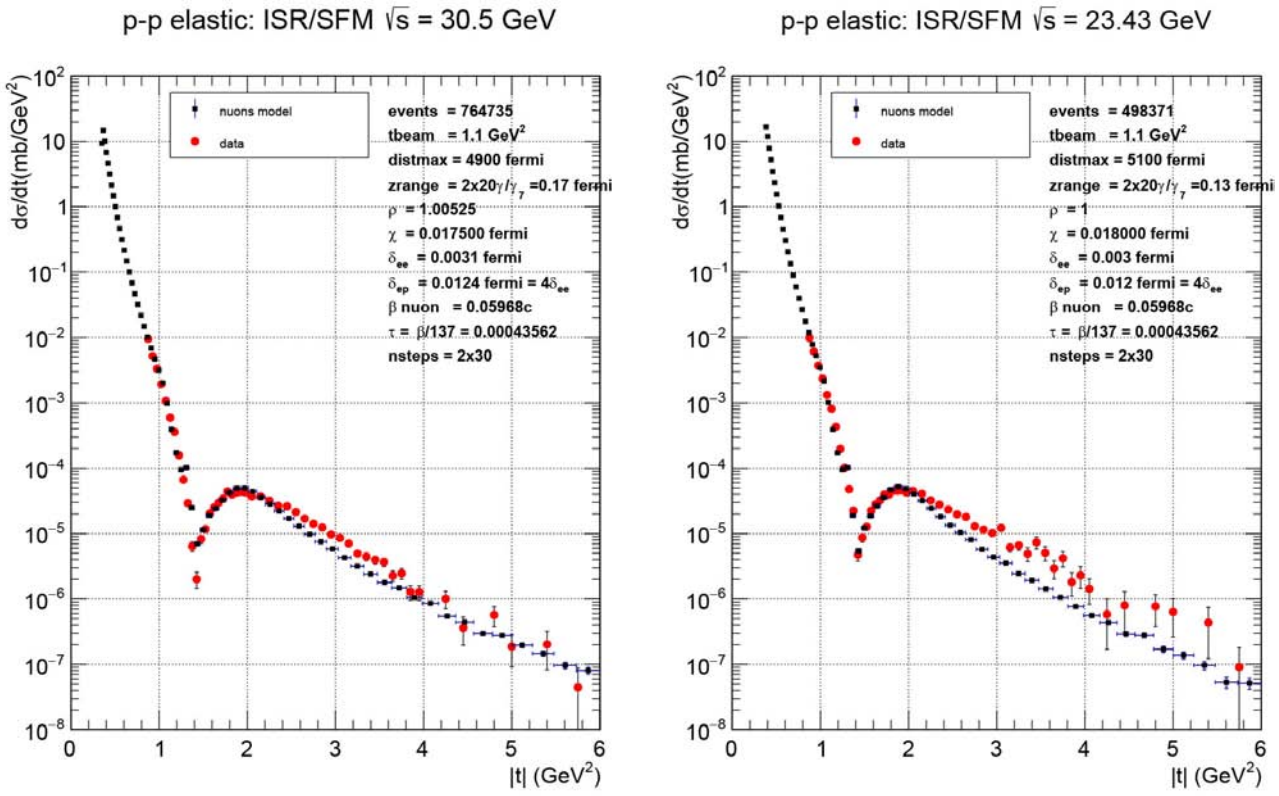

Figure 23. ISR proton-proton elastic scattering from $\sqrt{s} = 30.5 \rightarrow 23.43\,\text{GeV}$.

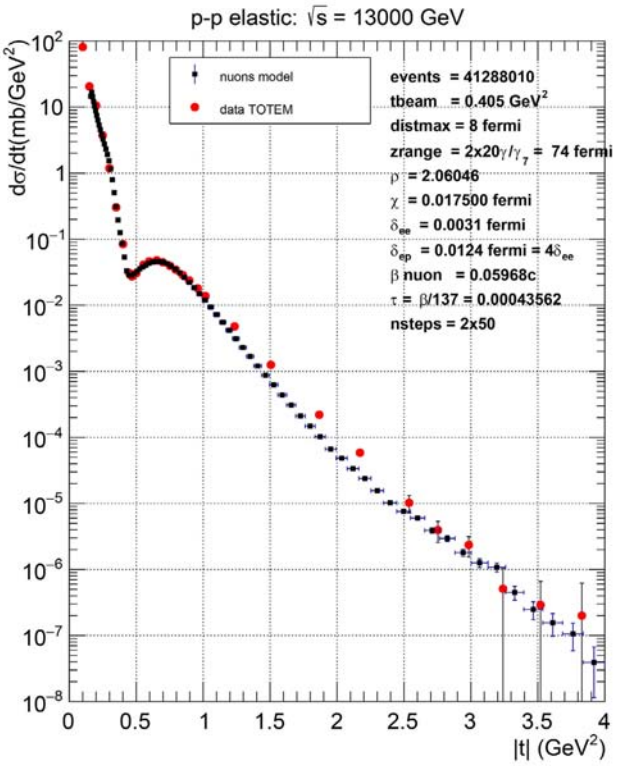

Figure 24. Nuons model prediction for the momentum transfer distribution at LHC 13 TeV compared to the TOTEM results.

The second slope for the high t values is also due to Coulomb interactions when the particles manage to interpenetrate with no destruction. The dip area is the case of the 2 particles tangent or with a very tiny interpenetration. This last case is interesting as we see several contributions generating this dip and maximum. The first contribution is the result of the of the 2 spinning particles and the nuons (such as the spokes of a bike wheel) that can be in phase or anti-phase. The best reproduction of the experimental results is obtained when the nuons are assumed to rotate around the axial nuons at a speed in the range $0.04c < kBeta < 0.10c$. We find that $kBeta = 0.06c$ is the best value for all energies from 21 GeV to 13 TeV. In Figure 20 we show the effect of varying $kBeta$ between 0.02 and 0.10 in the dip region at 7 TeV. The second major contribution to this dip/maximum is due to the fact that nearly tangent protons are not seen by the trigger of the experiment because the peripheral positrons collide and generate an inelastic interaction. One must also note that the shape of the *dip* is very sensitive to the position of the nuons inside the proton. If one smears the position of these nuons by more than one *millifermi*, about 50 per cent of the *dip* disappears. It would be very interesting to redo the p-p elastic experiments at the ISR energies with improved detector precision. In particular, the study of the precise cross-section around the *dip* region could carry more information about the proton structure.

In Figure 24 the predictions for the momentum transfer distribution at 13 TeV are presented, compared to the results from TOTEM at 13 TeV.

In Figure 25 the comparison with many experiments for proton-proton or proton-antiproton scattering ranging from the ISR energies to the latest LHC results.

7. Comparison with LHC p-p Collisions at 900 GeV and 7 TeV

Using the collide program, the case of inelastic collisions at the LHC has been simulated (900 GeV, 2.76 TeV, 7 TeV, 8 TeV and 13 TeV). See References CMS [26], ATLAS [27], ALICE [28]. The program collides protons at random impact distances. This simulation has two phases:

- Hard collisions between very close electrons/positrons in the colliding nuons producing jets. To describe this collision model, we take the average charged particle multiplicity that has been measured in great detail at the various e^+e^- colliders. For this work we have taken the parameters by P. V. Shlyapnikov [29] in the form $nch = 2.80829 - 0.518406 * \sqrt{sn} + 1.00586 * sn$ where sn is the center of mass energy available in the collision of electron/positrons from the 2 colliding nuons. The program generates a collision only when the distance $d12$ between the nuon components is less than a parameter $d12min$ that is around 0.1 fermi for collisions at 7 TeV, *i.e.* about 6 per cent of the proton radius. $d12min$ is about constant with the collision energy and represents the transversal move of a nuon rotating at about 0.06c when the proton travels about 1 fermi. The 3 cases described earlier (axial-axial, axial-radial and radial-radial) are processed with specific algorithms (see example in Figure 26).

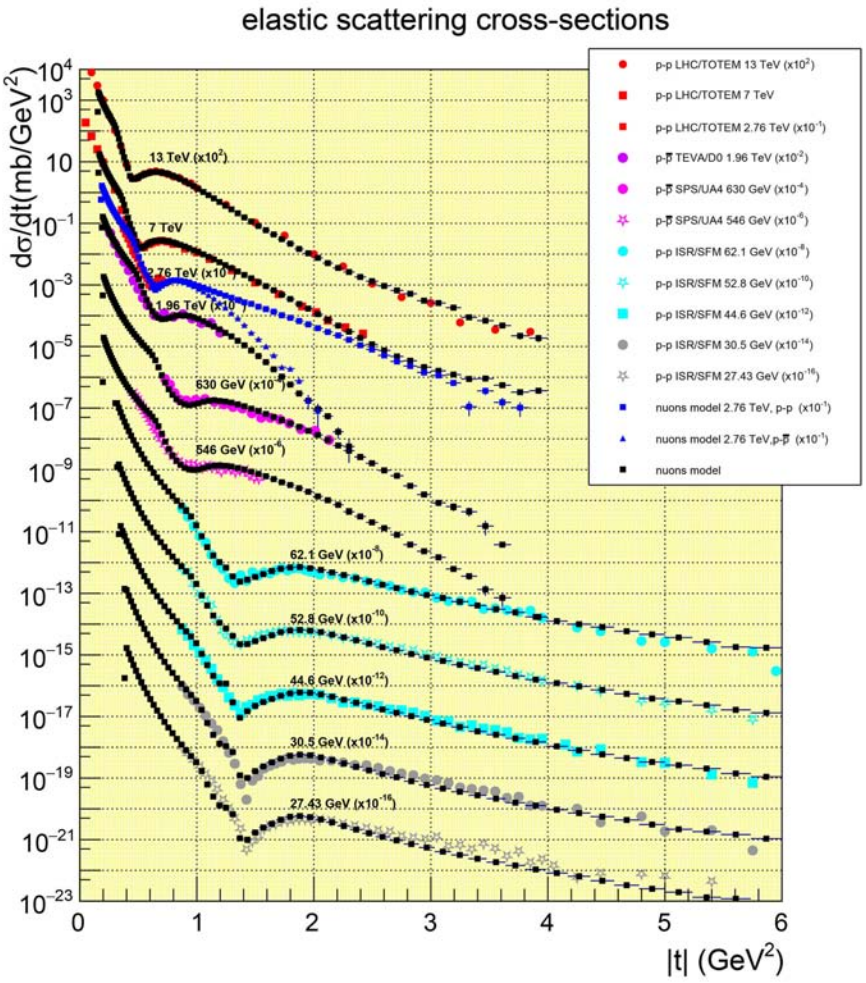

Figure 25. Nuons model compared to many experiments in a wide energy range.

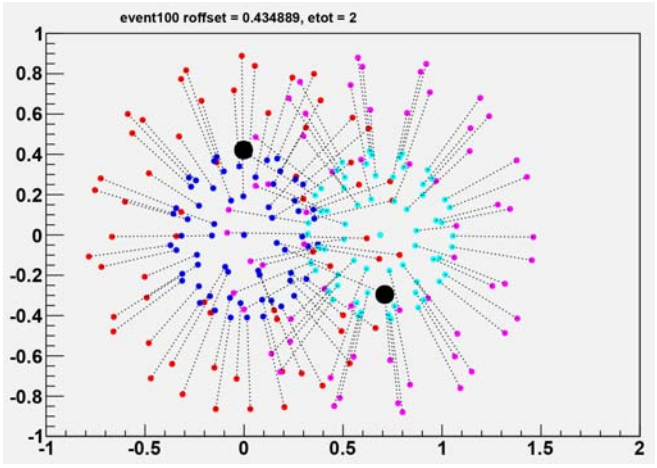

Figure 26. Example of p-p collision showing 2 colliding nuons.

In radial-radial collisions the corresponding collision energy is assumed to be 2 times the electron energy divided by $d12$ when the electrons rotate in the same direction or 0.5 times the electron energy divided by $d12$ otherwise.

In axial-radial collisions the collision energy is assumed to be 0.5*maxPt times the value of the Gaussian with $\sigma = kBeta$ at a distance $d12$.

In axial-axial collisions the collision energy is assumed to be maxPt * (the product of the two electron/positron gaussians of standard deviation *electron-Sigma* at a distance $d12/2$). The high Pt tracks and jets are generated by axial-axial collisions. If one smears the position of the axial nuons by just a few millifermi, then the high Pt tracks are not generated anymore (eg, no tracks with $Pt >$ 80 GeV/c for 7 TeV collisions).

- Soft collisions happening between the nuons left after all hard nuon collisions have been processed. When the original particle is destroyed the remaining nuons are candidates for a recombination. A hadronization model is included in the program to build particles such as $\mu, \pi, \mathrm{K}, \eta, \rho, \phi, \mathrm{p}, \Lambda, \Sigma, \Xi, \Omega$ with these remaining nuons.

We can also compare the ratio of soft to hard events with the experimental data or other Monte-Carlo systems. In a recent Alice paper [30] the ratio *soft/hard* events is indicated for 3 energies (see Table 1). An event is classified as soft when no tracks with a $P_T > 2\ \mathrm{GeV/c}$ is found in the range $-0.8 < \eta < 0.8$.

As shown in Figures 27-30, the P_T and η distributions are extremely well described by the model. Many additional plots are also available showing the good agreement for the number of generated particles, or distributions such as the ratios π/p, K/p. In Figure 31 the predictions at 13 TeV for the charged particle Pt distribution (top) and multiplicity distribution (bottom) are presented, compared to the results from CMS and ATLAS.

8. Particles Pt Distribution Peculiarities

The Particles Pt distribution was traditionally modeled with a power law with one single slope as a function of Pt. However with the recent LHC high statistics results, it is clear the slope of the power law changes drastically with Pt. In Figure 32 left we compare the slope as a function of particles Pt at 7 TeV with the CMS data and the predictions from Pythia8 and the NUONs model.

In Figure 32 right, we show the predictions of the NUONs model for the ratio of the Pt distribution divided by the Pt distribution for minimum bias events as a function of the event multiplicity.

Table 1. Ratio of the number "soft" to "hard" events for ALICE data, the nuon model and MC generators.

	0.9 TeV	2.76 TeV	7 TeV
ALICE (data)	5.70	3.54	2.36
NUONS	**5.84**	**3.16**	**2.03**
PHOJET	8.53	4.34	2.52
PERUGIA-0	5.6	3.26	2.06
PERUGIA-2011	6.78	3.64	2.29
PYTHIA8	7.28	3.92	2.37

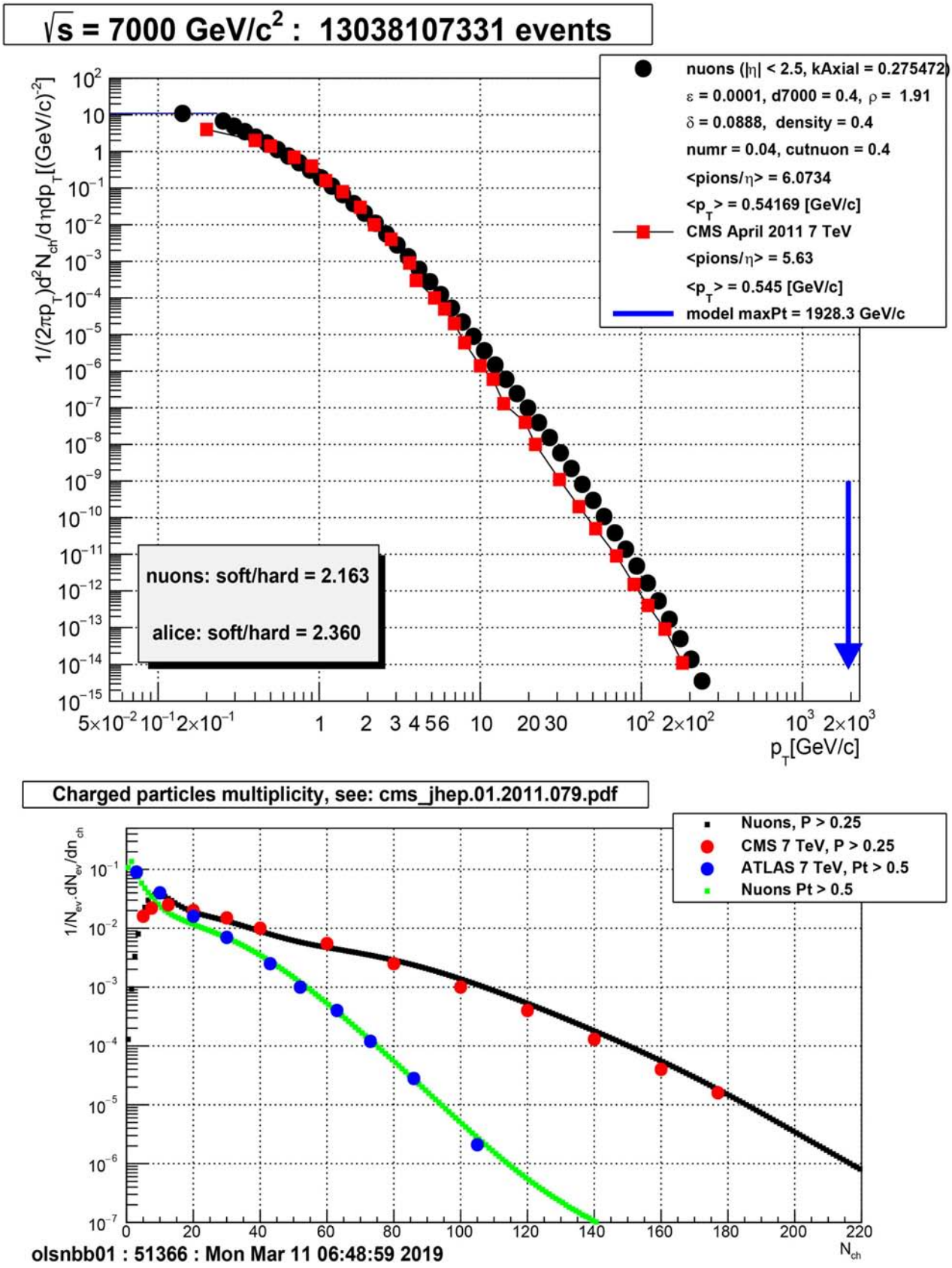

Figure 27. Pt and particle multiplicity distributions at 900 GeV compared with CMS results.

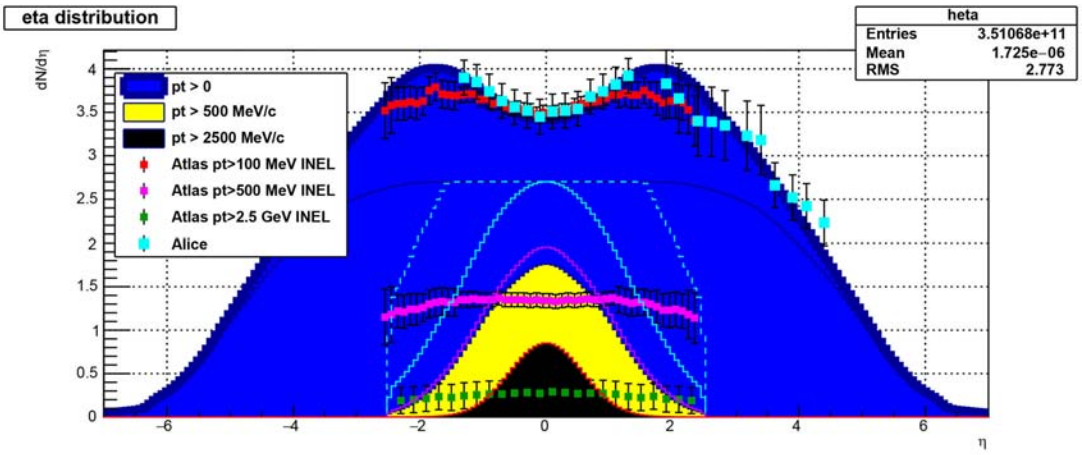

Figure 28. Pseudo-rapidity at 900 GeV compared with LHC results.

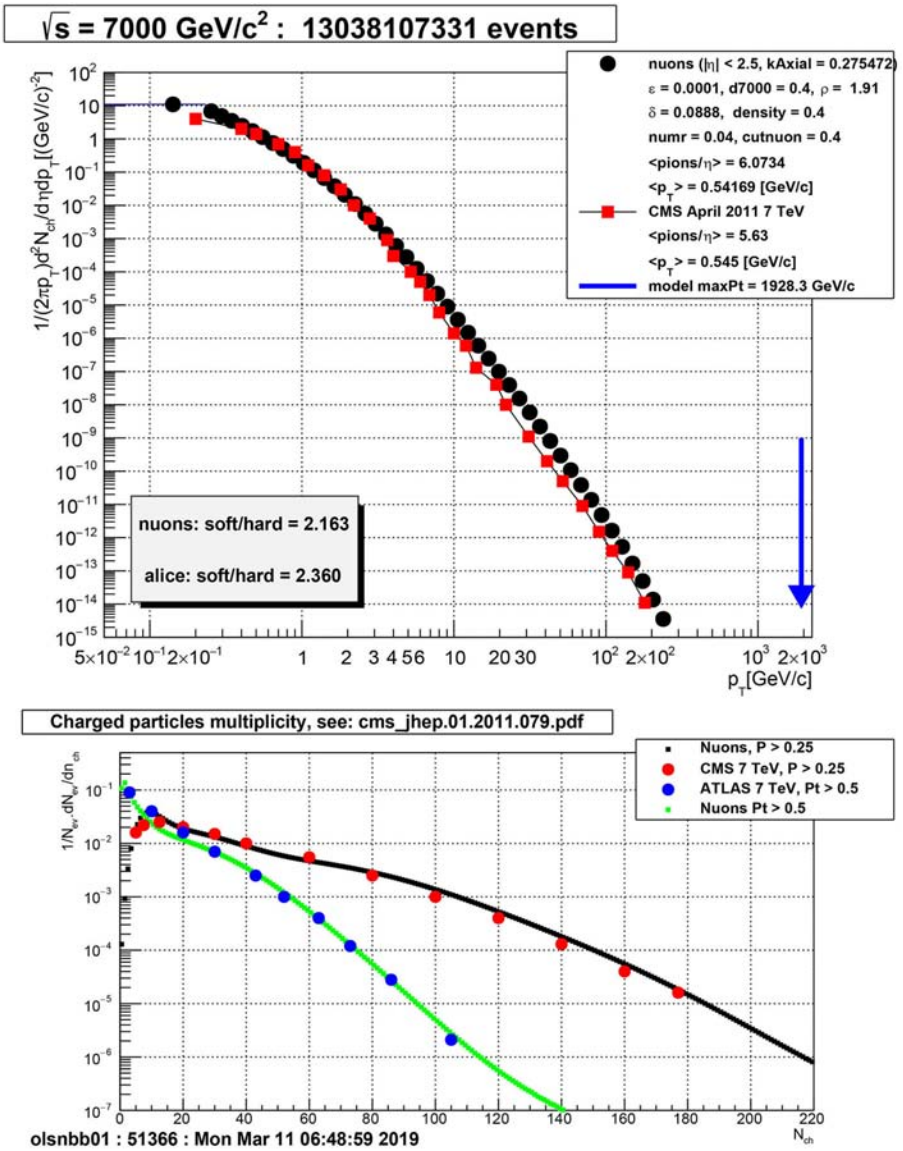

Figure 29. Pt and particle multiplicity distributions at 7 TeV compared with CMS results.

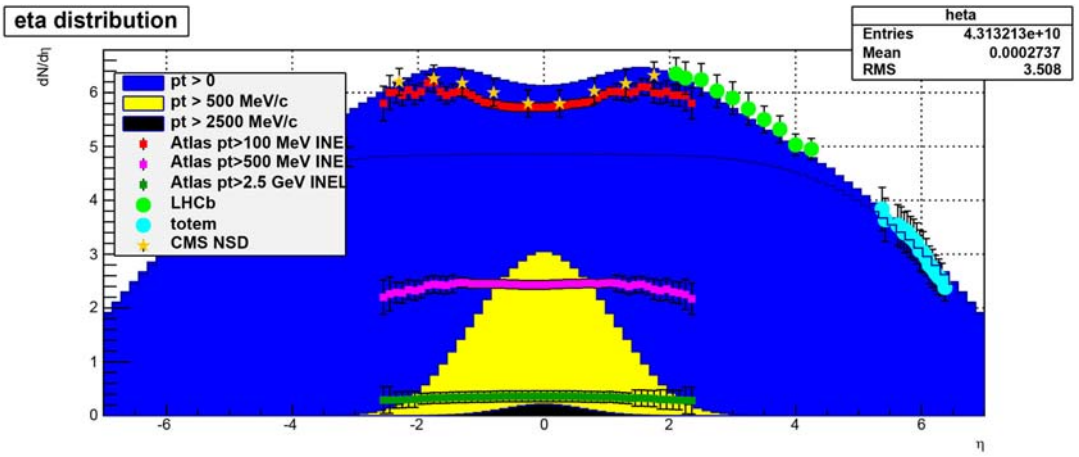

Figure 30. Pseudo-rapidity distribution at 7 TeV compared with LHC results.

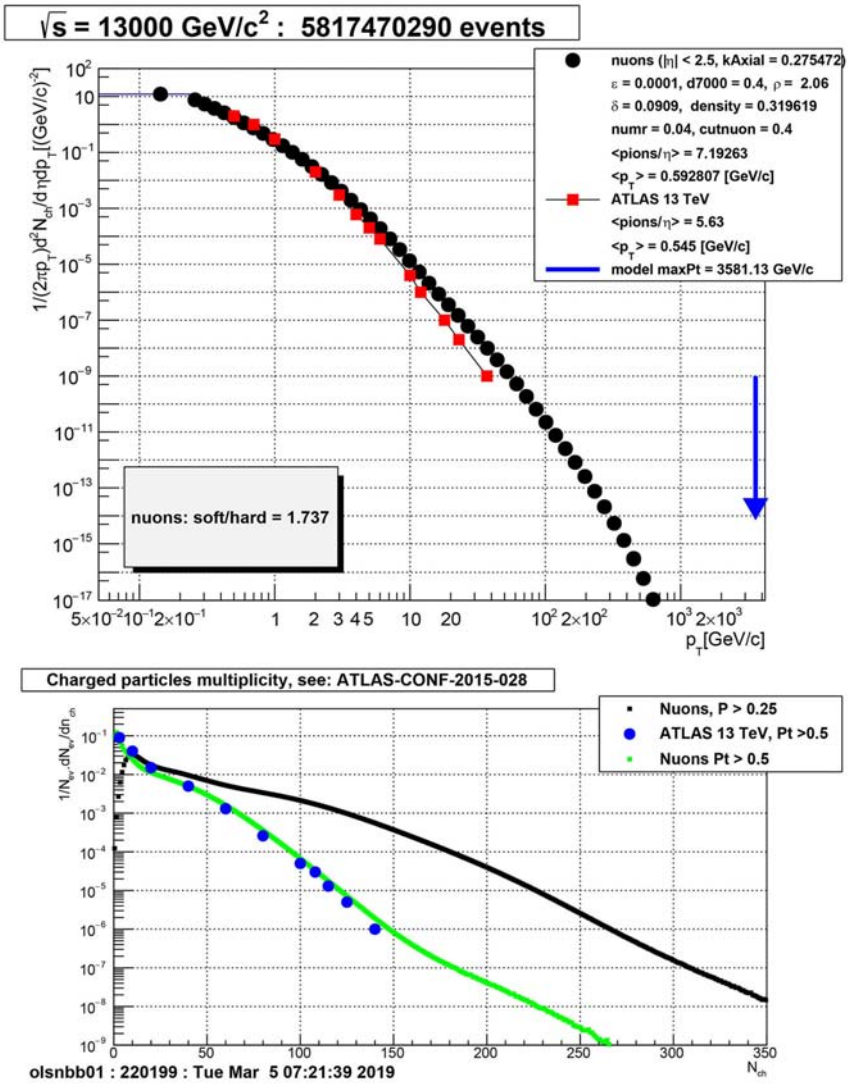

Figure 31. Nuons model predictions at 13 TeV for the charged particle Pt distribution (top) and multiplicity distribution (bottom) are presented, compared to the results from CMS [31] and ATLAS [32].

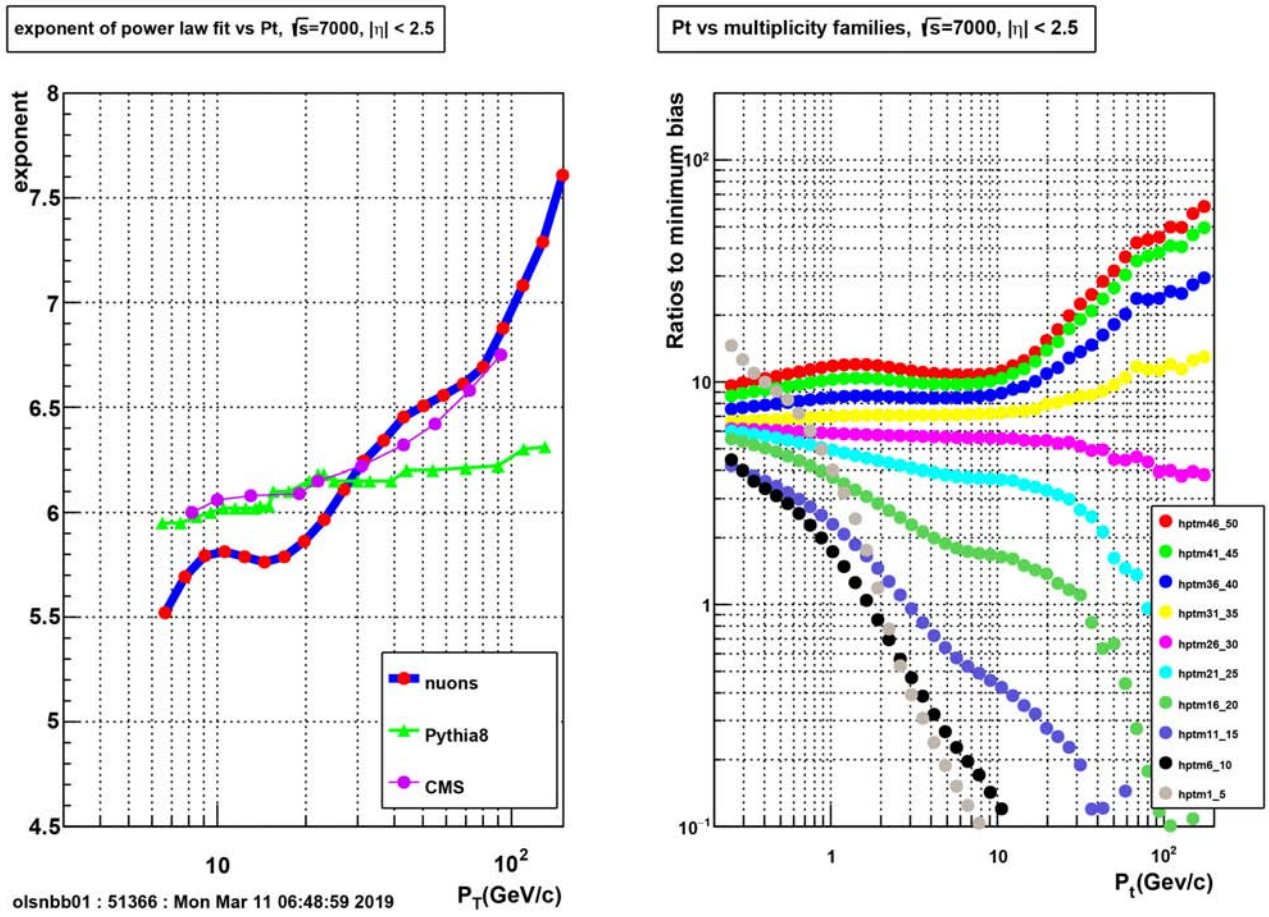

Figure 32. Left: Particles Pt cross-section slope compared with CMS results and Pythia8. Right: Particles Pt distribution divided by minimum bias Pt distribution for several event multiplicities.

While doing comparisons with many experimental data at various energies, one of the conclusions has been the lack of some variables facilitating the task. In the same way that in deep inelastic experiments, the Bjorken *x* variable had been introduced in the early days, it is proposed to introduce two new variables representing respectively the fraction of the event energy carried by one particle and the measured event energy:

$$Xt = 2Pt/\sqrt{s} \quad \text{and} \quad Xtev = \sqrt{\Sigma P^2 t}/\sqrt{s}$$

Using the two variables, one can now produce distributions like the one shown in Figure 33 where interesting shapes can be seen for the high values of *Xtev*. See the dip in the cross-section vs *Xt* for the 2 bottom curves xtev [0.051, 0.12] and xtev [0.12, 0.28]. It would be interesting to read a confirmation from the LHC experiments.

9. Jets Distribution at the LHC

Using the collide program one can investigate the jets distribution in p-p collisions at 7 TeV at the LHC. The program considers that a jet is produced whenever the distance between the electron and positron of 2 colliding nuons is less

than $d12min$ = 0.08 fermi (ie the hard collision parameter described above), the jet Pt above PtjetMin and the multiplicity above a threshold (e.g. 8 charged particles at 7 TeV). Multiple nuon collisions may happen (Multiple Parton Interactions) in a given proton proton collision, each one generating 1, 2 or more jets. Figure 34 illustrates one event with 2 jets generated by the collision of 2 axial nuons.

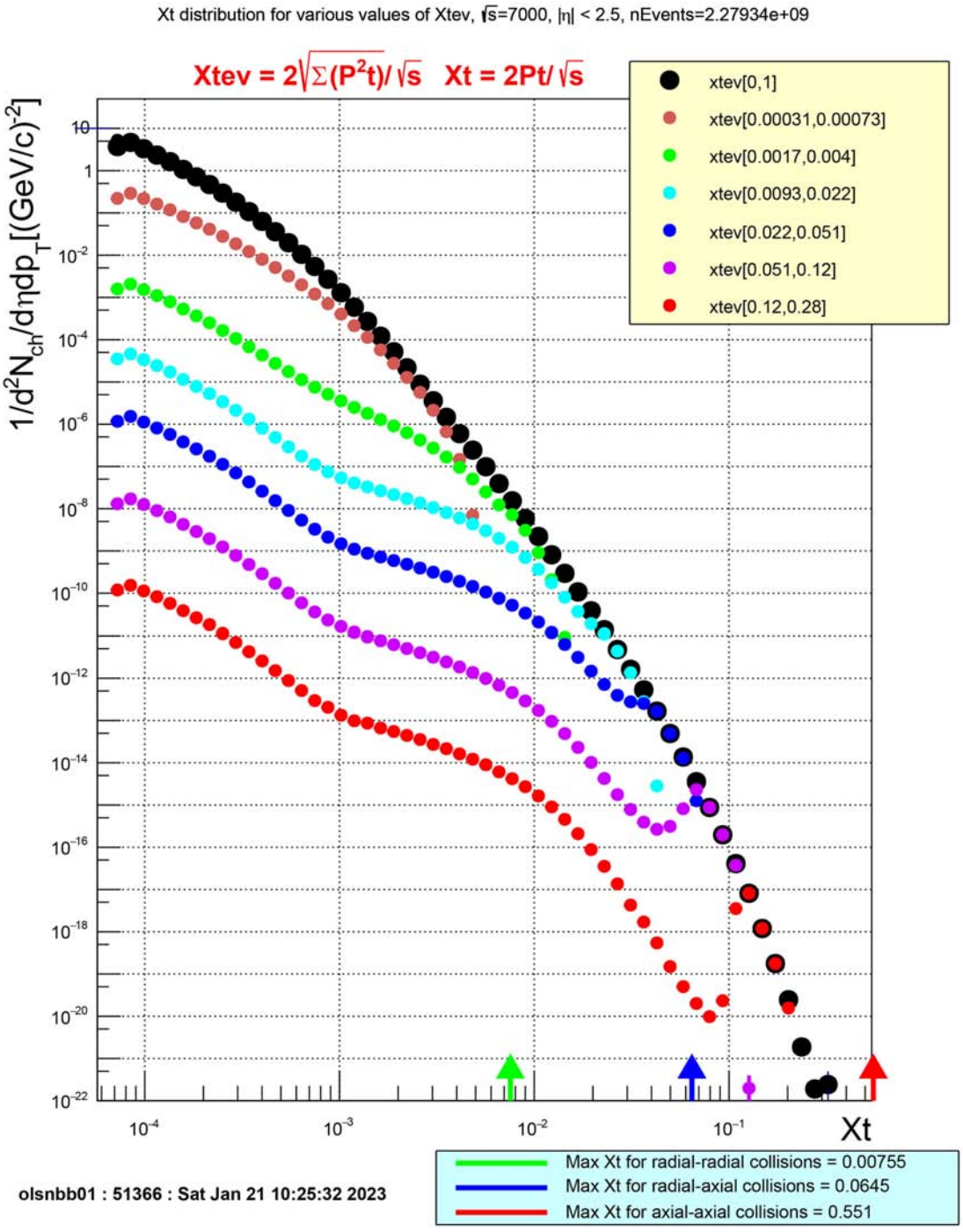

Figure 33. Left: Particles *Xt* cross-section for different values of *Xtev*.

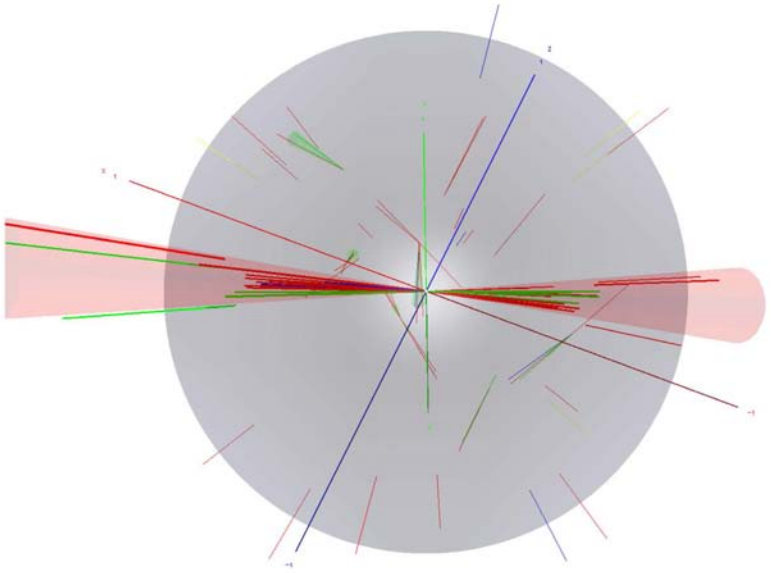

Figure 34. A 2-jet event generated by the collision of 2 axial nuons.

Figure 35 shows the inclusive Jet Multiplicity with the ratio of the n jet cross section to the $(n-1)$ jet cross-section compared to the ATLAS results [27].

Figure 36 shows various jets properties compared to results from CMS [33]. The distributions of jet pt, average pt of charged particles belonging to the underlying event or to jets, jet rates, and jet shapes are presented as functions of N[ch] and compared to the predictions of event generators. The CMS jet reconstruction requires tracks with $Pt > 0.25\,\text{GeV/c}$, $-2.4 < \eta < 2.4$, and a trigger condition with at least one track with $-4.65 < \eta 1 < -3.32$ and a track with $3.32 < \eta 2 < 4.65$. In the table only the results with Pythia6 tune Z2 are shown.

In **Figure 37** the jets inclusive Pt distribution (top) and 1st, 2nd, 3rd, 4th leading jet Pt distribution (bottom) are presented, compared to the results from ATLAS and CMS at 13 TeV.

In **Figure 38** the jets inclusive Pt distribution are compared to experimental results at energies ranging from 45 GeV to 13 TeV.

Using the same very low cuts as in the case used for the comparison with CMS [31], the **Figure 39** shows the number of collisions of different types per event as a function of the charged particles multiplicity. This plot may be compared with experimental results investigating Multiple Parton Interactions (MPI) versus the event multiplicity. For the medium and high multiplicity events, most collisions producing jets are from electron-electron radial collisions. All high multiplicity events have an axial-axial nuons collision. When running the program at different energies, one observes that the maximum number of collisions seems to reach a maximum value around 30. **Figure 40** shows (in linear scale in left pad) the number of collisions versus the particle multiplicity for different collision energies (from 900 GeV to 100 TeV). This plot indicates that the number of collisions is proportional to the multiplicity. The pad at the right of the same Figure shows the probability of having N collisions (MPI) per event.

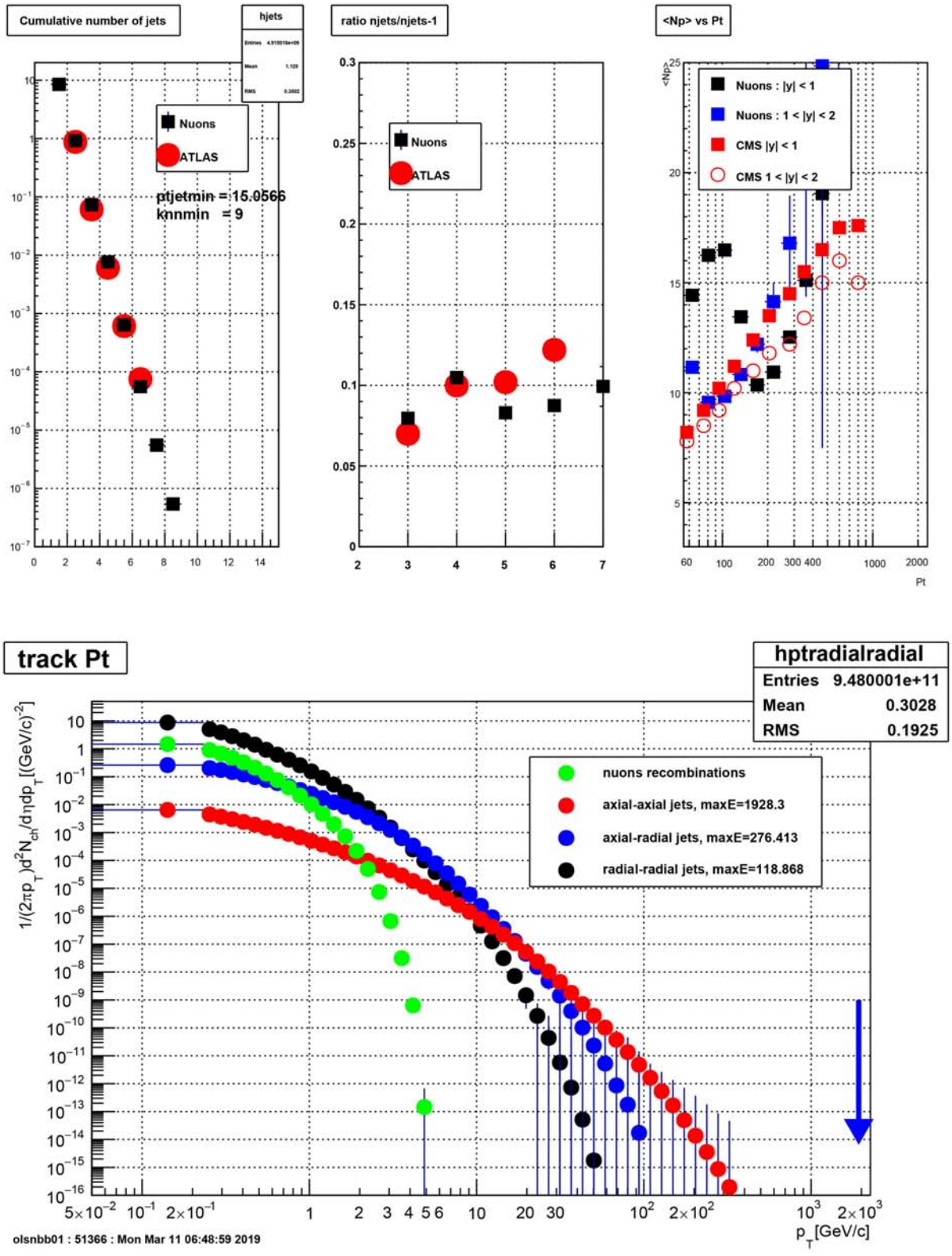

Figure 35. Jets with the Nuons model: Top left: Inclusive number of jets compared to ATLAS data. Top center: ratio 3/2, 4/3, 5/4, 6/5 compared to ATLAS. Top right: Average number of particles per jet as a function of the Pt of the jet compared to CMS data. The picture at the bottom shows the differential cross-section of charged particles versus Pt with a stack of the different contributions.

Jets compared to CMS data at $\sqrt{s}$ = 7000 GeV/c^2 : 13038107331 events

		$10< N_{ch}\leq 30$	$30< N_{ch}\leq 50$	$50< N_{ch}\leq 80$	$80< N_{ch}\leq 110$	$110< N_{ch}\leq 140$
events %	data	58.10	26.40	13.00	2.19	0.24
	nuon	57.49	25.83	14.36	2.12	0.19
p_T^{ch} particle	data	0.68 ± 0.01	0.75 ± 0.01	0.80 ± 0.01	0.85 ± 0.01	0.88 ± 0.01
	nuon	0.67	0.80	0.82	0.84	0.88
	pythia6Z2	0.67	0.74	0.80	0.85	0.90
p_T^{UE}	data	0.65 ± 0.01	0.71 ± 0.01	0.74 ± 0.01	0.76 ± 0.01	0.77 ± 0.01
	nuon	0.65	0.78	0.80	0.83	0.87
	pythia6Z2	0.65	0.70	0.74	0.76	0.77
p_T^{ij}	data	1.90 ± 0.02	1.64 ± 0.02	1.45 ± 0.01	1.32 ± 0.01	1.24 ± 0.01
	nuon	2.23	1.85	1.77	1.77	1.54
	pythia6Z2	1.86	1.62	1.44	1.33	1.29
p_T^{ijl}	data	3.65 ± 0.05	3.37 ± 0.04	3.15 ± 0.03	2.96 ± 0.03	2.86 ± 0.03
	nuon	3.61	3.24	3.12	3.12	2.87
	pythia6Z2	3.59	3.33	3.10	2.97	3.05
p_T^{ch} jet	data	6.85 ± 0.06	7.04 ± 0.09	7.18 ± 0.09	7.46 ± 0.11	7.81 ± 0.10
	nuon	7.44	7.78	7.62	7.74	8.09
	pythia6Z2	7.01	7.20	7.30	7.64	8.15
ch.jets/event pt>5	data	0.054 ± 0.004	0.287 ± 0.014	0.84 ± 0.03	2.13 ± 0.09	3.68 ± 0.15
	nuon	0.089	0.265	0.465	0.777	0.869
	pythia6Z2	0.067	0.304	0.87	2.12	3.95
ch.jets/event pt>30	data	$(3.2 \pm 0.5)10^{-5}$	$(3.4 \pm 0.4)10^{-4}$	$(1.5 \pm 0.1)10^{-3}$	$(4.3 \pm 0.4)10^{-3}$	$(1.0 \pm 0.1)10^{-2}$
	nuon	$(8.5 \pm 0.0)10^{-5}$	$(6.6 \pm 0.0)10^{-4}$	$(1.0 \pm 0.0)10^{-3}$	$(3.4 \pm 0.0)10^{-3}$	$(1.0 \pm 0.0)10^{-2}$
	pythia6Z2	$(2.7 \pm 0.3)10^{-5}$	$(3.5 \pm 0.2)10^{-4}$	$(1.4 \pm 0.2)10^{-3}$	$(5.7 \pm 0.4)10^{-3}$	$(2.1 \pm 0.1)10^{-2}$

Figure 36. Jets with the Nuons model compared to CMS data.

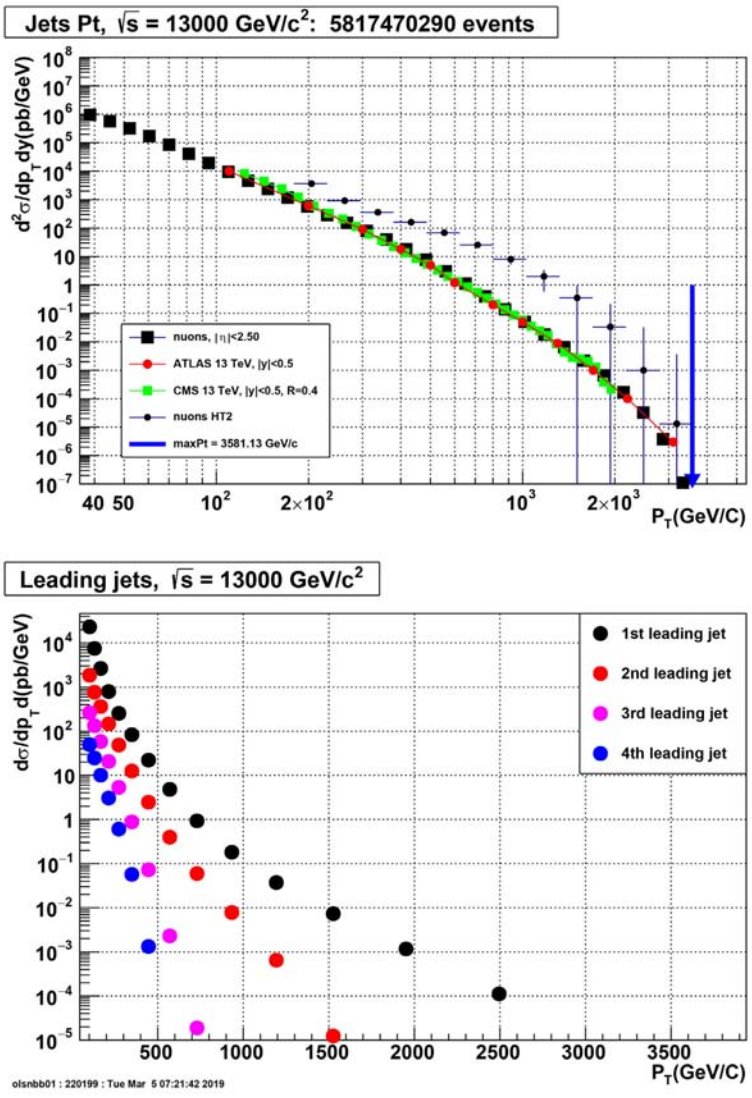

Figure 37. Nuons model predictions at 13 TeV for the charged particle Pt distribution (top) and multiplicity distribution (bottom) are presented, compared to the results from ATLAS and CMS at 13 TeV.

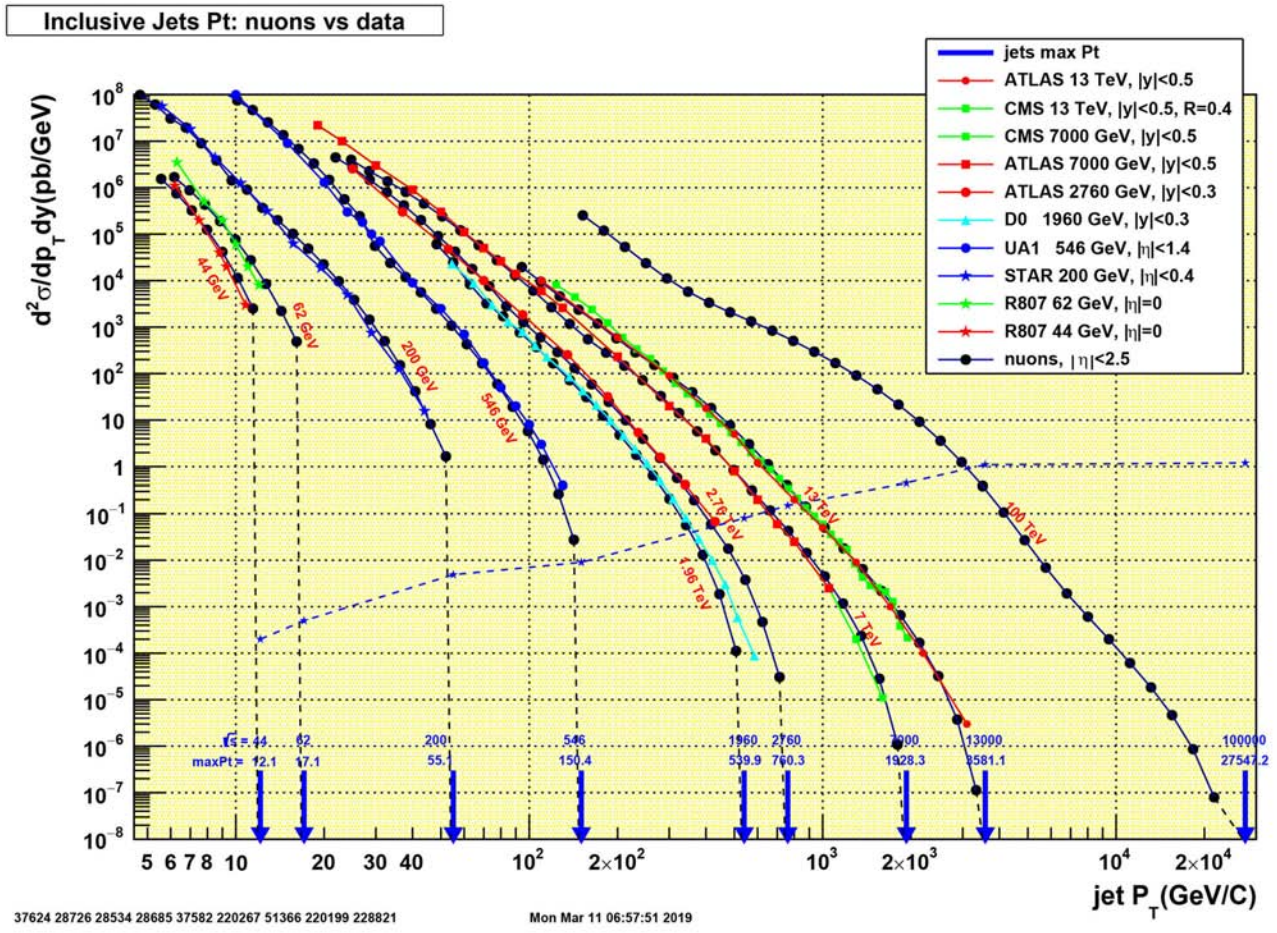

Figure 38. Nuons model predictions compared to experimental results at energies ranging from 45 GeV to 13 TeV. The arrows show the predictions for the jets Pt cut off.

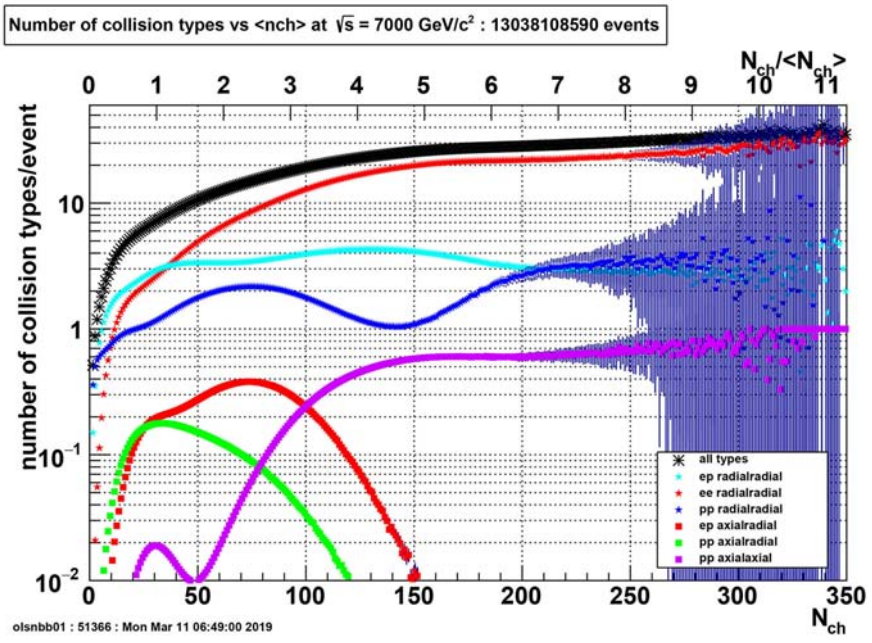

Figure 39. Number of collision types per event vs multiplicity at 7 TeV.

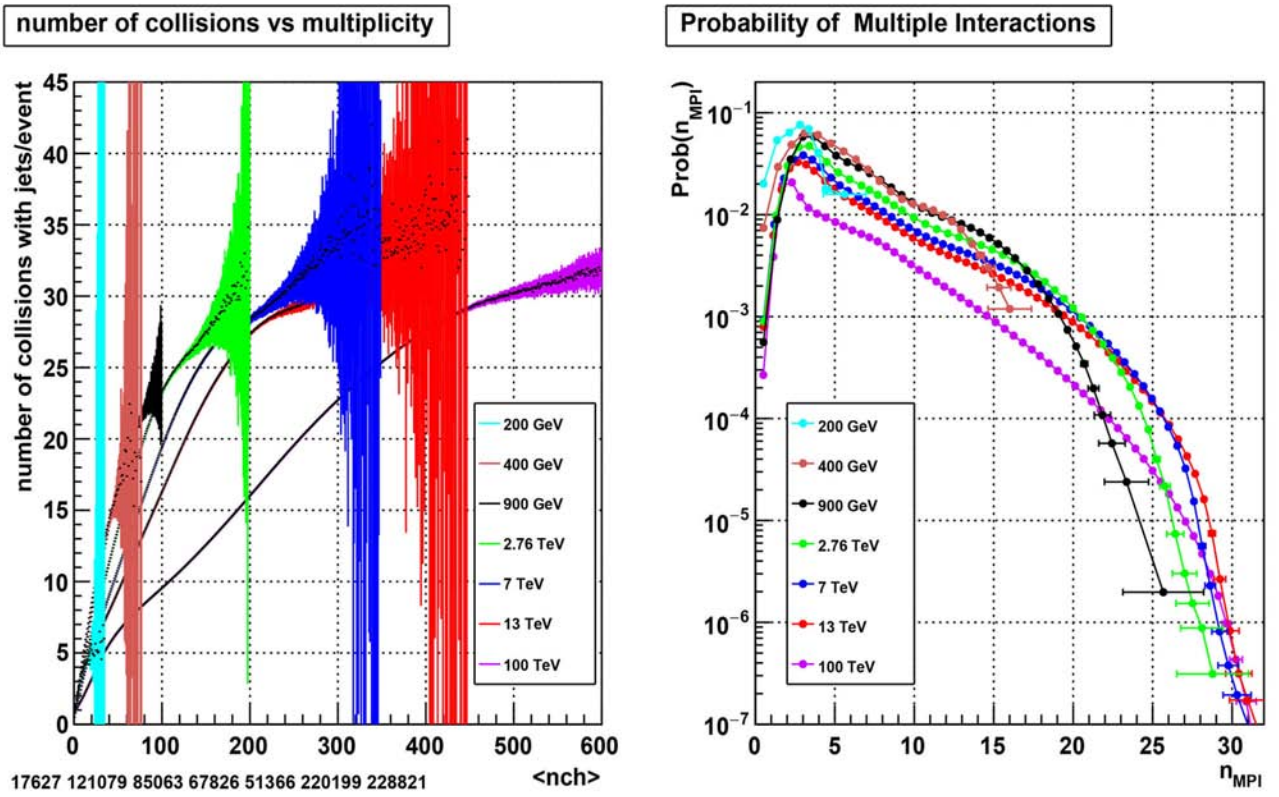

Figure 40. Left: Number of collisions per event vs multiplicity for different collision energies. Right: Probability for an event with N collisions.

10. Comparison with Electron-Proton and Positron-Proton Deep Elastic Experiments at HERA

Using the deep program, a variant of collide, the case of deep inelastic collisions at HERA has been simulated. The incoming electron or positron collides with one or more radial or axial components of the proton. The incoming electron or positron is generated at a distance d with the proton centre and progress step by step inside the proton with a sum of scattering angles depending on the distance with proton components If the incoming particle survives NC (Neutral Current case), the $Q2$ value is computed following the scattering angle. Otherwise CC (Charged Current case) the $Q2$ value is computed following the guidelines in the HERA [14] paper summarizing the combined results from the $H1$ and $ZEUS$ collaborations. The Charged Current case is triggered when the collision distance with one of the electrons or positrons of the proton is less than a distance $sigmaCC$ equal to 2 micro-fermi.

Since we are dealing with very high $Q2$ values, they correspond to the incoming particle (electron or positron) very close to the proton center. In this area, an incoming electron will see 3 attractive positrons and 2 repulsive electrons, and an incoming positron will see 3 repulsive positrons and 2 attractive electrons, see Figure 41. This simple fact explains by itself the difference in cross-sections for NC and CC cases (see Figure 42 and Figure 43).

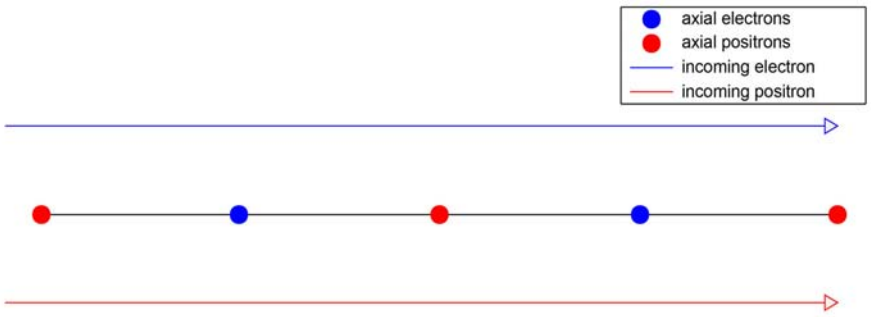

Figure 41. Picture showing why an electron has a larger scattering angle than a positron.

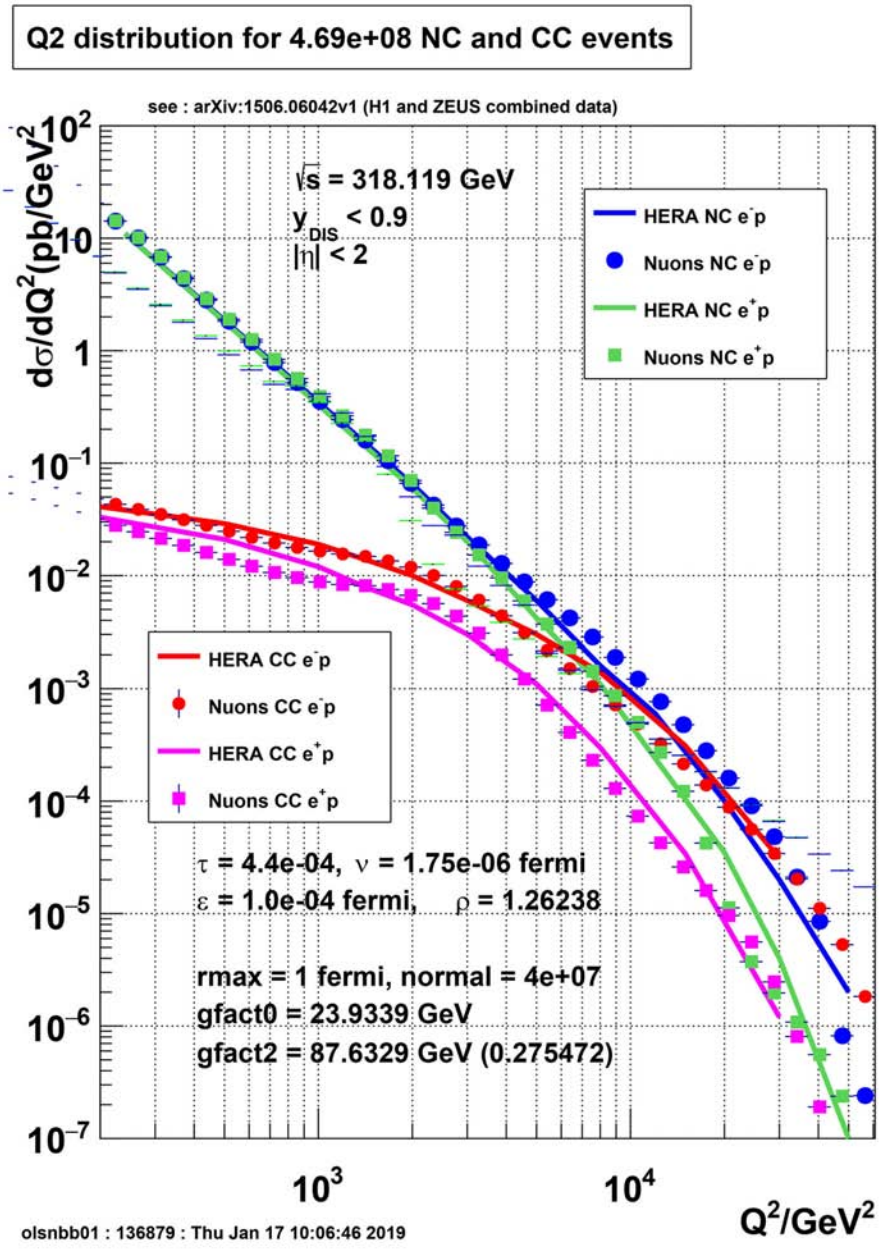

Figure 42. $Q2$ distribution for neutral and charged current events compared to HERA results.

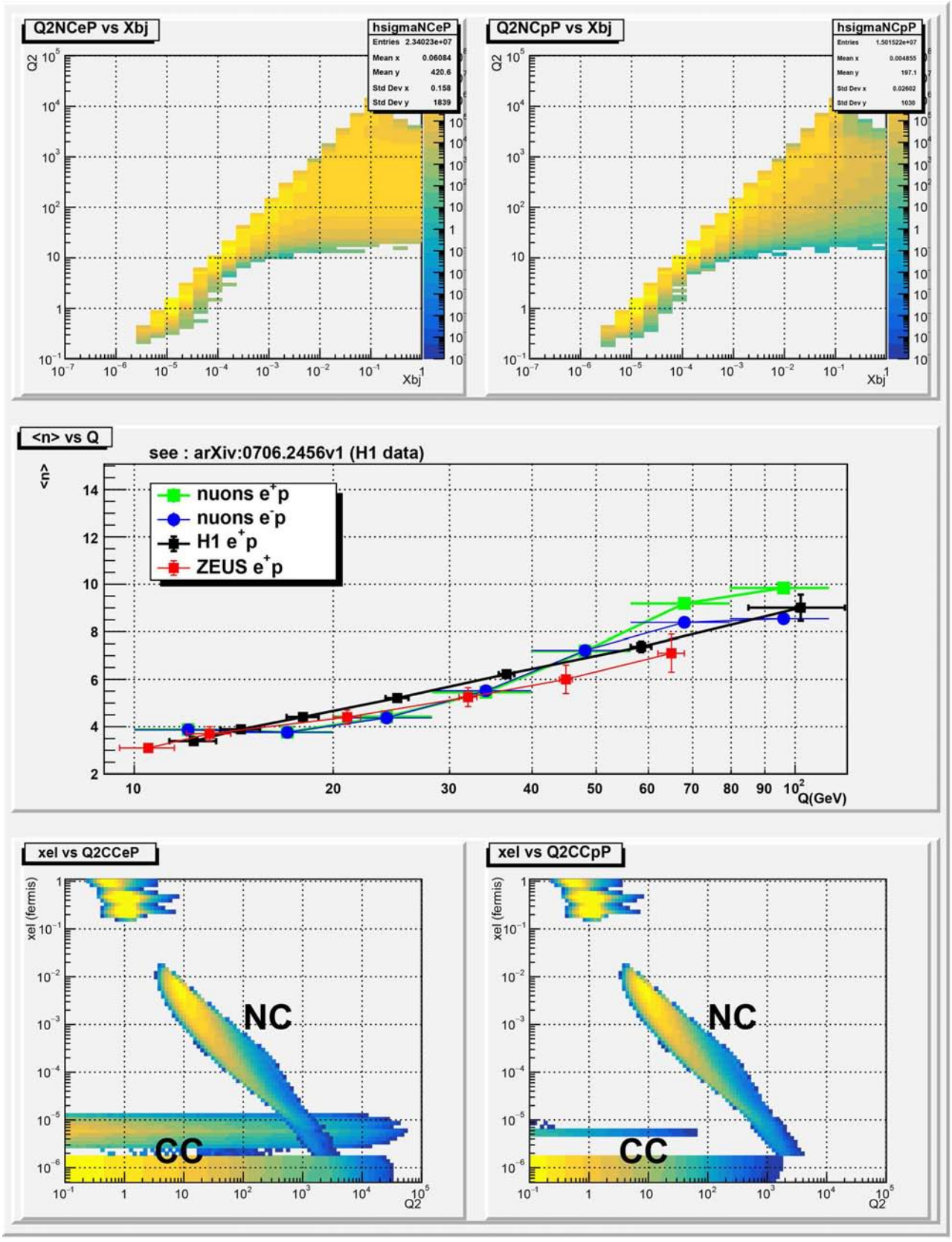

Figure 43. Top: $Q2$ vs x for electron-proton (left) and positron-proton (right). Center: Average Charged particles multiplicity vs Q compared to HERA results. Bottom: $Q2$ as a function of the distance (Fermi) electron-proton (left), or positron-proton (right).

It is fundamental for a better understanding of the central proton region to build as soon as possible new deep inelastic experiments to explore the center of mass energies ranging from 500 GeV to 5 TeV, and hence test all models up to a precision reaching the standard model quark or electron size.

11. Testing the Nuons Model with Heavy Ions Collisions

Two challenges were ahead to investigate these collisions:

Challenge 1: Which ion model? All experiments in this field use a theoretical model, typically the Glauber model to exploit the experimental data. This is somehow surprising, in particular when estimating the number of partners (colliding nucleons between the 2 ions). A model has been developed (see below) to build any ion (from deuterium to Uranium).

Challenge 2: Scarred by the CPU time necessary to make a collision? For instance the Lead ion with 82 proton and 126 neutrons, the nuons model has about 82 × 66 + 126 × 66 nuons, about 13,728 nuons per ion, *i.e.* 4 × 13,728 = 27,456 electrons or positrons and as many neutrinos and antineutrinos per ion! This challenge was nearly unthinkable 10 years ago, but the advent of new powerful and not too expensive processors is now making this goal possible.

The program collidenuc has been developed to solve these 2 challenges. The ion is built by gradual insertion of nucleons around a central nucleon, respecting the ratio protons/neutrons and the distance between proton-proton, proton-neutron and neutron-neutron, each nucleon having a skin (0.09 fermi for proton and 0.01 fermi for neutron). These numbers are based on the computed electromagnetic forces between nucleons. The program assumes also an ellipsoidal shape for the nucleus. In the case of a Lead nucleus, the radius is around 6.5 fermi. Once each nucleus has been built, it is filled with electrons and positrons taken from a data base of protons and neutrons previously generated by the program findall.

To generate a collision between the 2 nuclei, a double loop is performed to check if one of the 27,456 electrons or positrons in each nucleus can collide following the distance rules already explained in the proton-proton collide program. Figure 44 and Figure 45 show various parameters compared with results from the Alice experiment at 5 TeV/nucleon: -Number of charged particles versus the centrality of the collision; -Number of collision partners (Npartners) versus centrality; -Charged particles divided by number Npartners versus centrality; -Charged particles divided by number Npartners versus Npartners.

The same results are available for ions collisions at 2760 GeV and 1000 GeV.

12. Nuons Are Possible Candidates for Dark Matter and Dark Energy

Nuons are expected to behave like heavy sterile neutrinos. They are continuously produced in proton-nucleon collisions within galaxies, supernova explosions, etc. As these nuons are rarely interacting, they are produced isotropic-ally. In a

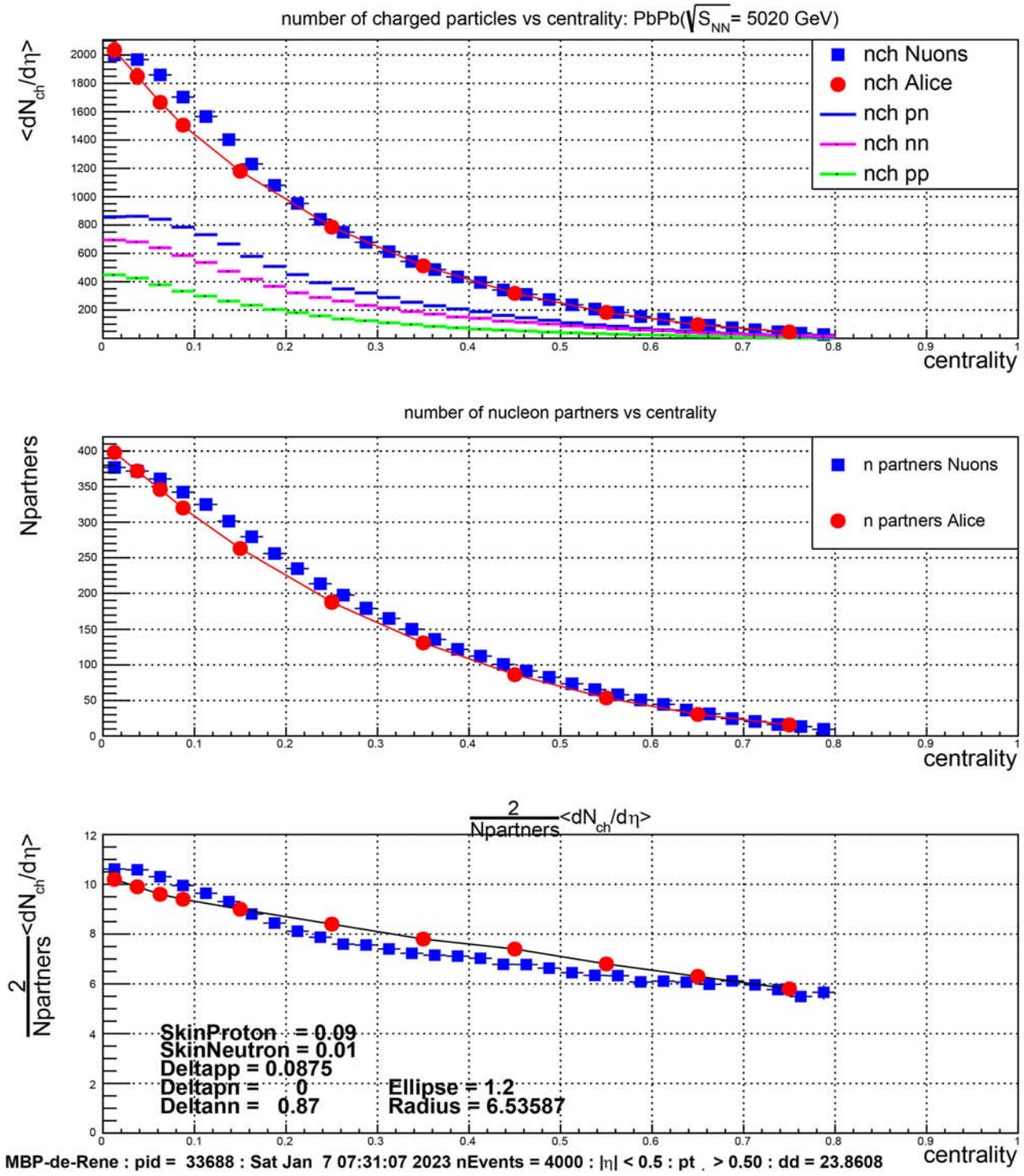

Figure 44. Top: Number of charged particles versus the centrality of the collision. Center: Number of collision partners (Npartners) versus centrality. Bottom: Charged particles divided by number Npartners versus centrality.

galaxy with a diameter of 1 million light years, they will happily fill the space between a galaxy and the surrounding galaxies after a few million years, adding a substantial amount of invisible matter to the galaxy. Recent results [34] confirm that the dark matter fills the space between galaxies in a uniform way. It would

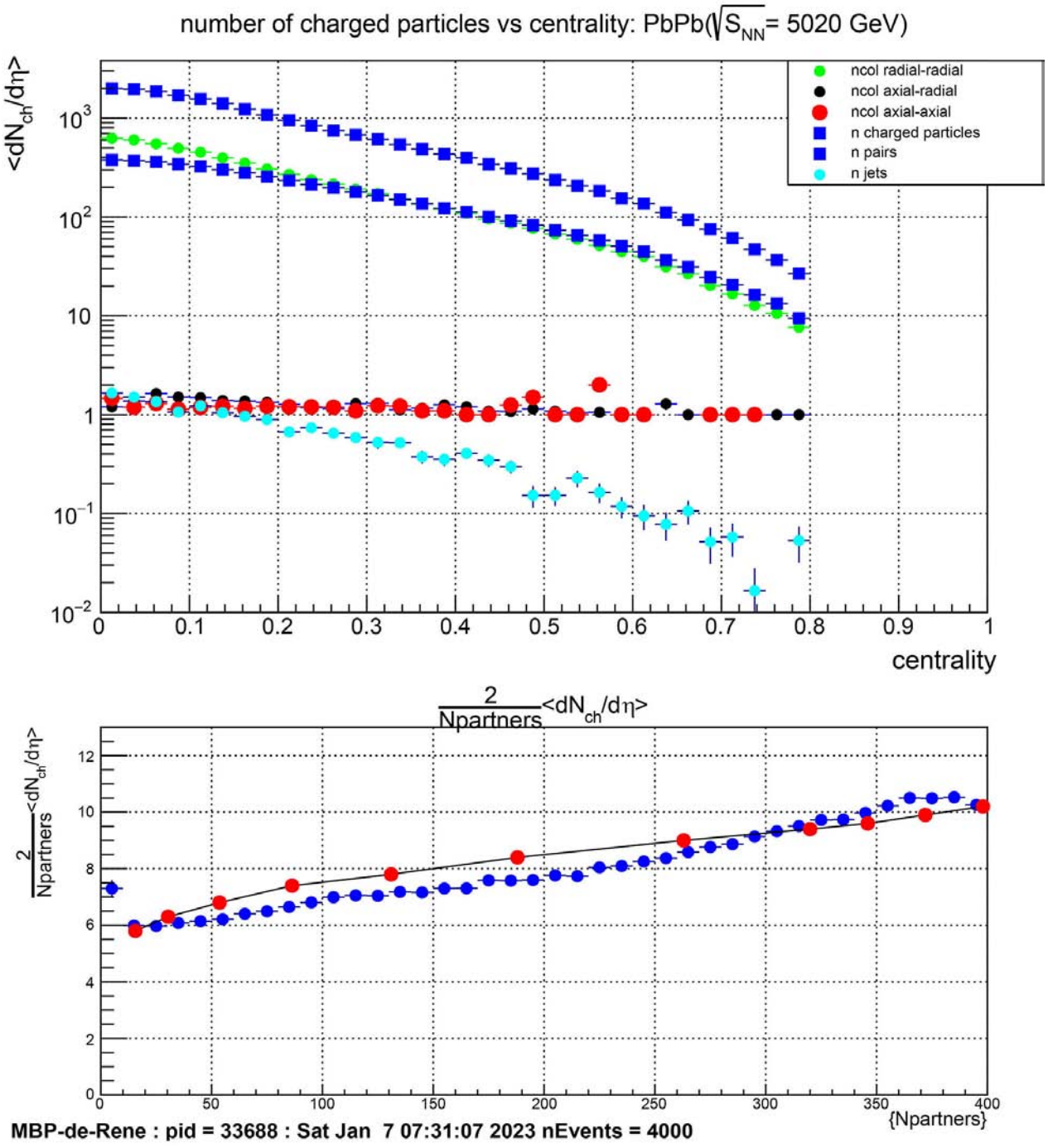

Figure 45. Top: Various types of collisions versus centrality. Bottom: Charged particles divided by number Npartners versus Npartners.

be interesting to estimate the number of nuons produced per unit of time in a galaxy to find out if the sum of their masses can contribute to 25 percent of the mass of the galaxy. These nuons emitted in the collisions can go through all galaxies after billions of light years. A growing number of nuons escape the visible universe and contribute more and more to the expansion of the universe, thanks to the usual gravitational laws. Well! just a guess!

13. Summary

A new model is proposed to describe particles with masses ranging from the muon to the Upsilon. Thanks to the introduction of the nuon as a building block at this scale, the masses of these particles are computed at 1/1000 precision or better and a linearity is observed between the mass and the number of nuon constituents. Particles can be built taking into account only Coulomb interactions and without introducing a strong force.

The model has been tested against many experimental results. The momentum transfer distribution for proton-proton elastic scattering agrees extremely well with the TOTEM data over 7 orders of magnitude as well as with previous results at lower energies. It reproduces the P_T distributions at all the LHC energies over 15 orders of magnitude as well as the pseudo-rapidity distributions in the $-7 < \eta < 7$ range and the particles multiplicity. The jets cross-section and internal jets properties agree extremely well with the recent data from ATLAS and CMS.

The simulation of electrons or positrons colliding protons reproduces very well the recent combined results of H1 and ZEUS at HERA about deep inelastic scattering.

The nuon model has been tested successfully against the heavy ions collisions results from LHC/Alice or BNL.

Conflicts of Interest

The author declares no conflicts of interest regarding the publication of this paper.

References

[1] Glashow, S.L. (1961) *Nuclear Physics*, **22**, 579-588. https://doi.org/10.1016/0029-5582(61)90469-2

[2] Weinberg, S. (1967) *Physical Review Letters*, **19**, 1264-1266. https://doi.org/10.1103/PhysRevLett.19.1264

[3] Salam, A. and Svartholm, N. (1968) Elementary Particle Physics Relativistic Groups and Analyticity. In: Svartholm, N., Ed., 8*th Nobel Symposium*, Almquvist and Wiksell, Stockholm, 367.

[4] Englert, F. and Brout, R. (1964) *Physical Review Letters*, **13**, 321-323. https://doi.org/10.1103/PhysRevLett.13.321

[5] Higgs, P.W. (1964) *Physical Review Letters*, **13**, 508-509. https://doi.org/10.1103/PhysRevLett.13.508

[6] Guralnik, G.S., Hagen, C.R. and Kibble, T.W.B. (1964) *Physical Review Letters*, **13**, 585-587. https://doi.org/10.1103/PhysRevLett.13.585

[7] Oerter, R. (2006) The Theory of Almost Everything: The Standard Model, the Unsung Triumph of Modern Physics. Plume, New York.

[8] Schumm, B.A. (2004) Deep Down Things: The Breathtaking Beauty of Particle Physics. Johns Hopkins University Press, Baltimore.

[9] Brun, R., *et al.* (1987) GEANT3: Detector Description and Simulation Tool. CERN

Program Library Long Writeup W5013, Geneva. https://cds.cern.ch/record/1119728

[10] Brun, R., *et al.* (1987) PAW—Physics Analysis Workstation. The Complete CERN Program Library. Version 1.07.

[11] Brun, R. and Rademakers, F. (1997) *Nuclear Instruments and Methods in Physics Research Section A*: *Accelerators*, *Spectrometers*, *Detectors and Associated Equipment*, **389**, 81-86. https://doi.org/10.1016/S0168-9002(97)00048-X

[12] Durr, S., *et al.* (2008) *Science*, **322**, 1224-1227. https://doi.org/10.1126/science.1163233

[13] Antchev, G., *et al.* (2011) *Europhysics Letters*, **95**, 41001.

[14] H1 and ZEUS Collaborations (2015) Combination of Measurements of Inclusive Deep Inelastic e + -p Scattering Cross Sections and QCD Analysis of HERA Data.

[15] James, F. (1988) MINUIT—Interpretation of the Errors on Parameters. CERN Program Library D506 Supplement.

[16] PDG. Particles Data Group, Data Taken from Review of Particle Physics. https://pdg.lbl.gov/2020/tables/contents_tables_mesons.html

[17] Koide, Y. (1983) *Physics Letters B*, **120**, 161.

[18] Greulich, K.O. (2010) *Journal of Modern Physics*, **1**, 300-302. https://doi.org/10.4236/jmp.2010.15042

[19] Paasch, K. (2017) On the Calculation of Elementary Particle Masses. https://hal.archives-ouvertes.fr/hal-01368054v3

[20] Smith, T.P. (2010) *Nature*, **98**, 478-485.

[21] Nagy, E., *et al.* (1979) *Nuclear Physics B*, **150**, 221-267. https://doi.org/10.1016/0550-3213(79)90301-8

[22] Nachtmann, O. (2003) Pomeron Physics and QCD.

[23] Collins, P.D.B. (1977) An Introduction to Regge Theory and High-Energy Physics. Cambridge University Press, Cambridge. https://doi.org/10.1017/CBO9780511897603

[24] UA4 Collaboration (1985) *Physics Letters B*, **155**, 197-202. https://doi.org/10.1016/0370-2693(85)90985-2

[25] D0 Collaboration (2010) Soft QCD Results from D0. https://arxiv.org/ftp/archiv/papers/1011/1011.6360.pdf

[26] The CMS Collaboration (2011) Charged Particle Transverse Momentum Spectra in pp Collisions at $\sqrt{s}$ = 0.9 and 7 TeV.

[27] Mateos, D.L. (2011) Measurement of Multi-JET Production Cross Section at a Center-of-Mass Energy of 7 TeV at the Large Hadron Collider with the Atlas Detector. Thesis, CERN-THESIS-2011-039.

[28] The ALICE Collaboration (2010) Transverse Momentum Spectra of Charged Particles in Proton-Proton Collisions at $\sqrt{s}$ = 900 GeV.

[29] Shlyapnikov, P.V. (1992) *Uspekhi Fizicheskikh Nauk*, **162**, 1-28. https://doi.org/10.3367/UFNr.0162.199206a.0001

[30] The ALICE Collaboration (2012) Transverse Sphericity of Primary Charged Particles in Minimum Bias Proton-Proton Collisions at $\sqrt{s}$ = 0.9, 2.76 and 7 TeV. CERN-PH-EP-2010-010, May.

[31] CMS Collaboration (2013) Jet and Underlying Event Properties as a Function of Particle Multiplicity in Proton-Proton Collisions at sqrt(s) = 7 TeV. CERN-PH-EP/2013-195.

[32] The ATLAS Collaboration (2011) *European Physical Journal C*, **71**, Article No. 1763.

[33] CMS Collaboration (2014) Charged Jet Cross Sections and Properties in Proton-Proton Collisions at sqrt(s) = 7 TeV. CERN-PH-EP/2014-254.

[34] Masaki, S., Fukugita, M. and Yoshida, N. (2012) *The Astrophysical Journal*, **746**, 38. https://doi.org/10.1088/0004-637X/746/1/38

Journal of Modern Physics, 2023, 14, 666-669
https://www.scirp.org/journal/jmp
ISSN Online: 2153-120X
ISSN Print: 2153-1196

On the Fine Structure and the Other Coupling Constants at the Planck Scale

Paolo Christillin

Università di Pisa, Pisa, Italy
Email: paolo.christillin@unipi.it

How to cite this paper: Christillin, P. (2023) On the Fine Structure and the Other Coupling Constants at the Planck Scale. *Journal of Modern Physics*, **14**, 666-669.
https://doi.org/10.4236/jmp.2023.145037

Received: January 13, 2023
Accepted: April 20, 2023
Published: April 23, 2023

Abstract

It is shown that the fine structure constant at Planck times α_P tends to one as well as those of the weak and strong interactions. This results by constraining them at the Planck force. That seems to provide interesting new results which confirm that at the beginning of space time (Planck scale) all fundamental forces converge to the same unit value.

Keywords

Fine Structure Constant, Fundamental Interactions Coupling Constants, Unification at Planck Scale

1. Introduction

It is well known that the smaller the energy into play, the more the interactions involved diversify. Undisputed examples are the electric and magnetic forces, seemingly two unrelated phenomena in the electron- and magneto-static domain, but successfully unified in higher energy electromagnetism. The same applies to electroweak interactions at the 100 GeV scale.

Thus conversely the higher the energy the more all interactions seem to unify.

The aim of the present note is to show that also electromagnetism determined by the fine structure α turns out to be one at the Planck scale as all other interactions as opposed to their present values[1] (Table 1).

2. GUT for Pedestrians

Planck units [1] are thought to represent the limits of our present theoretical

[1]The above numbers should be taken just as an indication, except for α_{em} determined from QED. All the other ones are determined from their ratio to the Coulomb potential. Thus for instance the strength of strong interactions is assumed to be given by the one pion Yukawa potential and therefore by $\alpha_{st} \simeq 14$ leaving open the problem of the treatment of the shorter ranged heavier mesons. Analogous comments about the weak interaction.

Table 1. Coupling constants of the fundamental interactions at present.

Interaction	Symbol	Value
strong	α_{st}	≥1
electromagnetic	α_{em}	1/137
weak	α_{wk}	10^{-8}
gravitational	α_{gr}	10^{-39}

treatment *i.e.* the origin of space time. As well known the units of mass, length and time where originally derived by Planck, whereas electromagnetism was not considered. This can probably be explained by the fact that mechanical quantities can be derived in two alternative ways: as the smallest quantum black hole and by explicitly re-scaling ordinary units. Thus the derivation of the Planck charge seems to be more questionable than that of the previous three mechanical units also because of the value of the Planck charge, which turns out to differ considerably from the elementary one.

Indeed [2]

$$q_P \simeq 11.7e \tag{1}$$

where e stands for the electric charge $\simeq 1.6\times10^{-19}$ C.

The implications of this result seem to have been however overlooked.

The Planck charge is derived by equating gravitational Planck force to the electric one

$$\frac{GM_P^2}{R_P^2} = \frac{1}{4\pi\varepsilon_0}\frac{q_P^2}{R_P^2} \tag{2}$$

Notice that the result does not depend on the Planck length *which implies that the same holds true also for the corresponding potentials.*

However from the explicit form of the Planck mass ($M_P = \sqrt{\frac{\hbar c}{G}}$) one immediately obtains

$$\hbar c = 1 = \frac{q_P^2}{4\pi\varepsilon_0} \tag{3}$$

Thus the result of Equation (1) is not at all fortuitous but just tell us that the fine structure constant at Planck scales is also unity as it can also trivially obtained by squaring Equation (1).

$$\alpha_P \simeq 137\alpha = 1 \tag{4}$$

So, in a sense, GM_P^2 plays the role of a Planck coupling constant which determines the fine structure one. This provides interesting results also for the weak and strong coupling constants at the Planck scale. As a matter of fact the relevant quantity being

$$\frac{g^2}{4\pi}\frac{1}{q^2-M^2}\rightarrow\frac{g^2}{4\pi}\exp -M/r \tag{5}$$

where M stands both the pion and for the weak boson mass, it is obvious that by the same considerations which led to Equation (2) (this time for the potential) one straightforwardly obtains

$$\frac{GM_P^2}{R_P}=\frac{g^2}{4\pi}\exp -M/r \tag{6}$$

where at the Planck radius the exponential can be safely approximated to 1 so that

$$GM_P^2=\frac{g^2}{4\pi}$$

Thus

$$\hbar c=1=\frac{g^2}{4\pi} \tag{7}$$

and

$$1=\alpha_{st}=\alpha_{wk}=\alpha_{em} \tag{8}$$

Thus gravitation, electromagnetism and strong interactions unify at the Planck scale. It is remarkable how the effect works respectively to increase and decrease the present values of the coupling constants.

The statement [2] "that at the Planck length scale it has been theorised that all the fundamental forces are unified but the exact mechanism of this unification remains unknown" gets here a partial rebuttal (**Figure 1**).

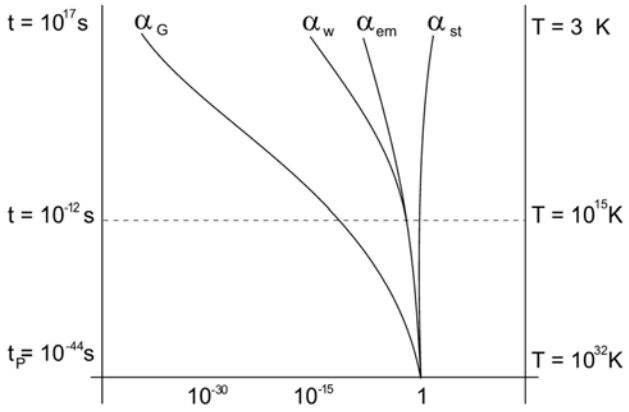

Figure 1. Time and temperature dependence of the different interactions. Not in scale. This shows how from the present very different values, the coupling constants tend to one at the Planck origin of space-time.

Needless to say the above results, as well as the description of a black hole, depend on the assumption of the validity of the Coulomb and Newton equations. This is anyhow in line with the theoretical instruments used in the derivation of

Planck units.

Similar conclusions have also been explicitly obtained in a description of gravitation below CMB as a QED black body [3] thus unifying gravitation and electromagnetism whose combined effect is a strong interaction one.

A related problem has been addressed by Pellis [4] with a different approach.

3. Conclusion

Therefore in addition to the unit Planck coupling constants $G, \hbar, c = 1$ also the coupling constants of the different interactions α appear in their own right with the same value.

Acknowledgements

I want to thank Luca Bonci for a careful reading of the manuscript and for help with the figure.

Conflicts of Interest

The author declares no conflicts of interest regarding the publication of this paper.

References

[1] Planck, M. (1899) *Sitzungsberichte der Koeniglich Preussischen Akademie der Wissenschaften zu Berlin*, **5**, 440-480.

[2] Wikipedia (2023) Planck Units. https://en.wikipedia.org/wiki/Planck_units

[3] Christillin, P. (2023) *Journal of Modern Physics*, **14**, 18-30. https://doi.org/10.4236/jmp.2023.141002

[4] Pellis, S. (2023) *Journal of High Energy Physics, Gravitation and Cosmology*, **9**, 245-294. https://doi.org/10.4236/jhepgc.2023.91021

Journal of Modern Physics, 2023, 14, 670-675
https://www.scirp.org/journal/jmp
ISSN Online: 2153-120X
ISSN Print: 2153-1196

The Perihelion Precession of the Planets Indicates a Variability of the Gravitational Constant

Hans Peter Weber

Deutsche Physikalische Gesellschaft, Bad Honnef, Germany
Email: weber@energie-know-how.de

How to cite this paper: Weber, H.P. (2023) The Perihelion Precession of the Planets Indicates a Variability of the Gravitational Constant. *Journal of Modern Physics*, **14**, 670-675.
https://doi.org/10.4236/jmp.2023.145038

Received: March 14, 2023
Accepted: April 20, 2023
Published: April 23, 2023

Abstract

The gravitational constant G according to the theory of NEWTON is the most imprecise constant of all physical constants. Moreover, there are a number of phenomena which suggest that this is caused by its invariant nature and the gravitation constant might be in fact a variable. In this article, a possible dependence of the gravitational constant on the distance between the two mass points is determined from the observed values of the perihelion displacement of the planets. However, to fit the observed measurements the $1/r^2$ dependence is modified to a $1/r^{2+1/R}$ dependence with "R" as the Rydberg constant. With the proposed new power function, the perihelion precessions of the planets are recalculated and then compared with previous observations as well as the postulated anomaly of Saturn.

Keywords

Gravitational Constant, Perihelion Precession of the Planets, Gravitational Equation with Variable G

1. The Gravitational Constant G

Newton's law of forces from 1686 has a weakness that causes the results of gravitational force calculations to be inaccurate [1]. Although the law takes into account the quadratic dilution of the lines of force in the case of a spherical propagation in space, it neglects the fact that the lines of force of the gravitational force field diminish potentially with increasing distance, so that gravitation is not only diluting according to its spatial extension, furthermore, additionally weakens accordingly to a potentially decreasing curve.

2. Observable Effects of Gravitation

At very large distances, the observable effects of gravity indicate a reduction of the gravitational attraction, whereas the gravitational attraction is larger at very small distances (e.g. in the atomic regime). This behavior of gravity is best represented by a power function. A similar perception of a modified gravity is published by [2] Nojiri, S. and Odintsov, S. (2007) as well as by [3] Hees *et al.* (2014). Another attempt to improve the concept of a gravitational constant or even eliminate the gravitational constant was undertaken by [4] E. G. Haug. He published several articles about this subject (papers of 2016 [4], 2018 [5], 2022 [6]). In his paper 2022 E. G. Haug proposes to eliminate the gravitational constant competely from the gravitations formula as Newton did not use it in his gravitations formula of 1686. He also attempted to improve the calculation of the perihelion precession of the planet Mercury (2020), however, he does not pursue his formula predictions of the perihelion precession of the other planets. This, however, is the main theme of this article of H. P. Weber.

There are a number of anomalies of gravity. The most spectacular is the perihelion precession of the planets. If Newton's law from 1686 were correct, the planetary orbits would describe an exact ellipse. However, this is not correct. The measured deviations, the perihelion precessions, are very small, but significant. The deviations sum up after hundred years to some extent, so reliable results of the observations are obtained. Most obvious are those with the planet Mercury near the sun with 43.11 arcsec per century.

Albert Einstein knew this problem with the gravitation since he dealt with it in the General Relativity Theory (GRT), which he developed mainly by including the gravitation. To solve the problem Einstein adapted the formulas of the GRT (*i.e.* the gravitation constant) to the orders of magnitude of the specific situation in our solar system accordingly, and could achieve thereby quite exact matching results with the measured values. He considered this also as a proof of the correctness of the GRT.

However, the GRT does not deliver useful results in every case. Some unresolved cases remain for the distance "r", for which the theory of relativity does not give results, or is invalid.

These are the cases below the Planck horizon and above the size of the solar system. Thus, for example, it was not possible so far to bring about the unification of the nuclear forces with gravitation.

In contrast to Einstein, this new approach tries to develop the gravitational formula with the help of a power function in such a way that the gravitation just shows the deviations which explain the observed perihelion precession of the planets. EINSTEINs formula $E = m * c^2$ is not disregarded, but the formula is enhanced with a variable which can now be applied to a wider range of cases for the gravitation.

The masses do not play any role, but gravitation depends on "r" itself. Thus the law of Newton has been modified in a manner that relativistic corrections are not necessary any more.

3. Mathematical Approach

The conventional formula of NEWTON is giving the gravitational force "F" as follows:

$$F = G\left(\frac{m_1 \cdot m_2}{r^2}\right) \tag{1}$$

The gravitational constant is modified in this article as follows

$$F = G_{var}\left(\frac{m_1 \cdot m_2}{r^2}\right) \tag{2}$$

$$G_{var} = \frac{k_1}{k_2} \text{ and } k_2 = \frac{1}{R}$$

It can also be written as:

$$F = G_{adj}\frac{1}{r^{1/R}}\left(\frac{m_1 \cdot m_2}{r^2}\right)$$

$$G = 6.67384 \times 10^{-11} = G_{conventional}$$

$$k_1 = G_{adj} = 6.67384 \times 10^{-11} \cdot 1.000024190$$

$$\text{Rydberg Constant} = R = 10973731.57 = 9.11267050E^{-08}$$

Here, the constant k_1 is the conventional gravitational constant adjusted about one meter (Correction = 1.00002419). This is a parallel shift to keep the perihelion precession centered.

The constant k_2 contains the Rydberg constant R, which adjusts the curve of Formula (4) (Figure 1) to better line-up the planets. The constants k_1 and k_2 were aligned to the perihelion shift of the planets.

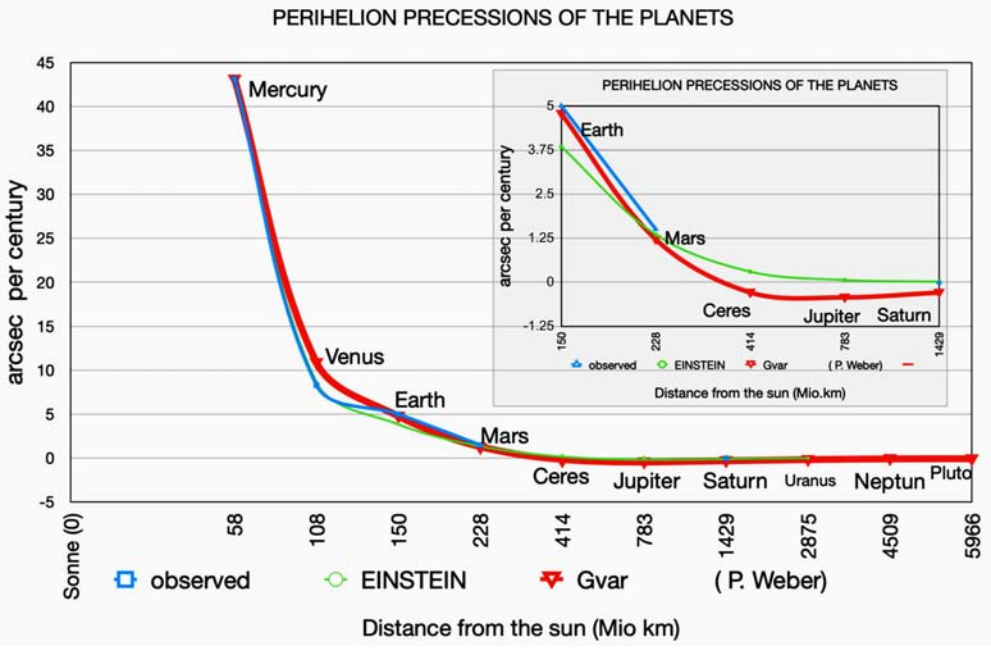

Figure 1. The perihelion precession of the planets.

4. The Perihelion Precessions of the Planetary Orbits

According to Newton, the orbit of the planets should describe exactly one ellipse in the course of one full rotation. In reality, however, the perihelion, the point of the ellipse facing away from the sun, shifts a small amount each year, so that the orbit becomes a rosette. In Table 1 three different values of the perihelion precession of the planets are listed as measured in angular seconds (arcsec) per century. In Column 1 values from the literature are given as comparison to the calculated values with conventional method approach using Einstein gravitational constant listed in Column 2 and with the new G_{var} given in Column 3.

4.1. Table 1, Column 1

The values in the Column 1 were taken from the literature. No values could be found for the planets outside the orbit of Mars, except data from Saturn with a perihelion precession of −0.006arcsec derived from the Cassini project of NASA. However, there are still unresolved uncertaincies of the interpretation of the measurements of the Saturn perihelion precession.

4.2. Table 1, Column 2

The values of the perihelion precession (PP) in Column 2 were calculated relativistically with Formula (3) using $G_{conventional}$ according to EINSTEIN. The "anomalous" percession of Jupiter and Saturn was investigated among others by [7] Pitjeva and Pitjev (2006) and [8] Iorio, L. (2009). Iorio's explanation failed as he tried to place a large mass in the outer solar system, which probably does not exist.

Table 1. Perihelion precessions of the planets.

	Column 1 Observed Precess.	Column 2 calculat. Precess.	Column 3 calculat. Precess.	Distance (million kms)
Planets	accord. to literature	accord. to EINSTEIN	new Gvar	
Mercury	43.11	42.99	42.66	58
Venus	8.3	8.63	10.7	108
Earth	5	3.84	4.7	150
Ikarus	9.8	10.06	3.2	
Mars	1.5	1.35	1.217	228
Ceres		0.3	−0.29	414
Jupiter		0.062	−0.43	780
Saturn	−0.006	0.0136	−0.2936	1429
Neptun		0.000347	−0.06835	4509

$$PP = \frac{6\pi \cdot G \cdot M}{msa \cdot a \cdot 1^{-e^2} \cdot c^2} \cdot 360000 \cdot \frac{180}{\pi} \tag{3}$$

G = gravitational constant (conventional), M = mass of the sun,
msa = major semi-axis of planet orbit, a = number of orbits per year,
e = Eccentricity, c = speed of light.

4.3. Table 1, Column 3

The values of the perihelion precession (PP) in Column 3 are calculated by the rotational velocity of the planets (v) with Formula (4) using once $G_{conventional}$ according to EINSTEIN and once with G_{var} of Formula (2) considering the eccentricity of the planetary orbits (arcsec per century).

$$v = \sqrt{\frac{G \cdot M}{r}} \tag{4}$$

5. Results and Conclusion

Comparing the two calculated perihelion deviations of Table 1, columns 2 and 3, we find that the planets Mercury to Mars show positive perihelion precessions with both types of calculations. However, the outer planets from Ceres to Pluto show only positive values with the Einstein formula. Calculated with G_{var}, the values of these planets in the red curve become negative!

6. Outlook

The "anomalous" precession values of the outer planets found by the Cassini probe are no anomalies but in fact conform with a variable gravitational G_{var}, and it is a necessity and quite reasonable to consider the gravitational constant as a variable. Thus, the law of Newton is modified in a manner that relativistic corrections are not necessary any more. The whole cosmos becomes mathematically analytically accessible with this approach. In [9] Weber, H. P. (2019) and in future publications different phenomena of the gravitation are calculated with the variable G_{var}. Emphasis will be given to the effects of the flexible G on the Planck units and the equivalence relations calculated on their basis. The author hopes having contributed to a better understandig of gravitational forces and is looking forward to a fruitful discussion on this new approach.

Conflicts of Interest

The author declares no conflicts of interest regarding the publication of this paper.

References

[1] Newton, I. (1686) Philosophiae Naturalis Principia Mathematica. Joseph Streater for the Royal Society, London. https://doi.org/10.5479/sil.52126.39088015628399

[2] Nojiri, S. and Odintsov, S.D. (2007) *International Journal of Geometric Methods in Modern Physics*, **4**, 115-145. https://doi.org/10.1142/S0219887807001928

[3] Hees, A., Folkner, W.M., Jacobson, R.A. and Park, R.S. (2014) *Physical Review D*, **89**, Article 102002. https://Journals.aps.org/prd/abstract/10.1103/PhysRevD.89.102002 https://doi.org/10.1103/PhysRevD.89.102002

[4] Haug, E.G. (2016) *Physics Essays*. https://hal.science/hal-03234242

[5] Haug, E.G. (2020) *Journal of High Energy Physics, Gravitation and Cosmology*, **6**, 238-243. https://doi.org/10.4236/jhepgc.2020.62017

[6] Haug, E.G. (2022) *Journal of Modern Physics*, **13**, 179-205. https://doi.org/10.4236/jmp.2022.132014

[7] Pitjeva, E.V. (2006) Limitations on Some Physical Parameters from Position Observations of Planets. 26*th Meeting of the IAU*, Prague, 22-23 August 2006.

[8] Iorio, L. (2009) *The Astronomical Journal*, **137**, 3615. https://doi.org/10.1088/0004-6256/137/3/3615

[9] Weber, H.P. (2019) Schwierige Materie. 144.

Journal of Modern Physics, 2023, 14, 676-691
https://www.scirp.org/journal/jmp
ISSN Online: 2153-120X
ISSN Print: 2153-1196

From Generalized Hamilton Principle to Generalized Schrodinger Equation

Xiangyao Wu[1*], Benshan Wu[1], Hong Li[2], Qiming Wu[1]

[1]Institute of Physics, Jilin Normal University, Siping, China
[2]Institute for Interdisciplinary Quantum Information Technology, Jilin Engineering Normal University, Changchun, China
Email: *wuxy2066@163.com

How to cite this paper: Wu, X.Y., Wu, B.S., Li, H. and Wu, Q.M. (2023) From Generalized Hamilton Principle to Generalized Schrodinger Equation. *Journal of Modern Physics*, **14**, 676-691.
https://doi.org/10.4236/jmp.2023.145039

Received: September 2, 2022
Accepted: April 21, 2023
Published: April 24, 2023

Abstract

The Hamilton principle is a variation principle describing the isolated and conservative systems, its Lagrange function is the difference between kinetic energy and potential energy. By Feynman path integration, we can obtain the standard Schrodinger equation. In this paper, we have given the generalized Hamilton principle, which can describe the heat exchange system, and the nonconservative force system. On this basis, we have further given their generalized Lagrange functions and Hamilton functions. With the Feynman path integration, we have given the generalized Schrodinger equation of nonconservative force system and the heat exchange system.

Keywords

Generalized Hamilton Principle, Nonconservative Systems, Thermodynamic System, Generalized Schrodinger Equation

1. Introduction

In quantum mechanics, each classical physical quantity corresponds to an operator, and the operator has a real eigenvalue, which is guaranteed by the Hermitian operator. The Hermitian operator has always been generally considered to represent observable measurements. In fact, in quantum mechanics, it is only necessary to guarantee the observability of the mechanical quantity, but not to guarantee that its operator must be Hermitian, that is, observable measurement may also be non-Hermitian. In 1947, in order to solve the divergence problem in the field theory, Pauli used the indeterminate metric to put forward the theory of the non-Hermitian operator and its self-consistent inner product, which was derived from a field quantization method proposed by Dirac [1] [2]. In order to maintain the unitary nature of the S matrix, Lee and Wick applied the non-

Hermitian view to quantum electrodynamics [3]. Later, in different fields, numerous studies have proved that under certain conditions, the non-Hermitian Hamiltonian quantum has a real number energy spectrum [4] [5] [6] [7]. In 1998, the author Bender proposed the space-time inverse symmetry (PT symmetry) quantum mechanics, which made the non-Hermitian quantum mechanics have a great leap forward [8] [9]. The non-Hermitian *PT* symmetric Hamilton do not violate the physical principles of quantum mechanics and have real eigenvalues. Over the past decade *PT* symmetric quantum theory has been developed into a variety of studies, including field theory and high-energy particle physics. Recently, preliminary studies on *PT* symmetric systems under optical structures have been carried out.

The quantum theory of non-Hermitian is described dissipative systems and open systems, their unique properties have attracted fast growing interest in the last two decades [10] [11] [12] [13], especially those empowered by parity-time symmetry. While the non-Hermitian quantum theories is still under intense investigation, its application in different fields has led to a plethora of findings, ranging from nonlinear dynamics [14], atomic physics [15], photonics [16], acoustics [17], microwave [18], electronics [19], to quantum information science [20].

The Hamilton principle is a variation principle describing the isolated and conservative systems, its Lagrange function is the difference between kinetic energy and potential energy. By Feynman path integration, we can obtain the standard Schrodinger equation. In this paper, we have given the generalized Hamilton principle, which can describe the heat exchange system, and the non-conservative force system. On this basis, we have further given their generalized Lagrange functions and Hamilton functions. With the Feynman path integration, we have given the generalized Schrodinger equation of nonconservative force system and the heat exchange system.

2. The Hamilton Principle for the Conservative System

In a mechanical system, the constraints that limit its position and speed can be written as equations

$$f\left(\boldsymbol{r}_i, \dot{\boldsymbol{r}}_i, t\right) = 0, \quad \left(i = 1, 2, \cdots, h\right) \tag{1}$$

the number of constraints equations are h. For the mechanical system of N free particles, their degree of freedom is $3N$, when they are restricted by h constraints of Equation (1), we can select $3N-h$ generalized coordinates $q_1, q_2, \cdots, q_{3N-h}$, the position vector $\boldsymbol{r}_i$ can be written as

$$\boldsymbol{r}_i = \boldsymbol{r}_i\left(q_1, q_2, \cdots, q_{3N-h}, t\right), \quad \left(i = 1, 2, \cdots, N\right) \tag{2}$$

the generalized coordinates q_i constitute the configuration space of $3N-h$ dimension

$$\boldsymbol{q} = \left[q_1, q_2, \cdots, q_{3N-h}\right], \tag{3}$$

the virtual displacement are

$$\delta \boldsymbol{q} = \left[\delta q_1, \delta q_2, \cdots, \delta q_{3N-h}\right], \tag{4}$$

the generalized velocity is

$$\dot{\boldsymbol{q}} = \frac{\mathrm{d}\boldsymbol{q}}{\mathrm{d}t} = \left[\dot{q}_1, \dot{q}_1, \cdots, \dot{q}_{3N-h}\right], \tag{5}$$

where $\dot{q}_i = \dfrac{\mathrm{d}q_i}{\mathrm{d}t}$.

With Equation (2), we have

$$\delta \boldsymbol{r}_i = \sum_j \frac{\partial \boldsymbol{r}_i}{\partial q_j} \delta q_j, \tag{6}$$

with Equation (6), we can calculate the virtual work of active force $\boldsymbol{F}_i$, it is

$$\delta\omega = \sum_i^N \boldsymbol{F}_i \cdot \delta r_i = \sum_i \boldsymbol{F}_i \cdot \sum_j \frac{\partial \boldsymbol{r}_i}{\partial q_j} \delta q_j = \sum_j \left(\sum_i \boldsymbol{F}_i \cdot \frac{\partial \boldsymbol{r}_i}{\partial q_j} \right) \delta q_j = \sum_j Q_j \delta q_j, \tag{7}$$

the generalized force Q_j is

$$Q_j = \sum_i \boldsymbol{F}_i \cdot \frac{\partial \boldsymbol{r}_i}{\partial q_j}, \tag{8}$$

if the generalized force Q_j is conservative force, the Equation (7) becomes

$$\delta\omega = \sum_j Q_j \delta q_j = -\delta U, \tag{9}$$

where U is the potential energy.

In rectangular coordinates, there is

$$\boldsymbol{F} = -\nabla U, \tag{10}$$

and the component is

$$F_i = -\frac{\partial U}{\partial x}. \tag{11}$$

In the following, we should study the system motion from time t_1 to t_2, the T is the system kinetic energy, there is

$$\int_{t_1}^{t_2} T\mathrm{d}t = \int_{t_1}^{t_2} T\left(q_i, \dot{q}_i, t\right)\mathrm{d}t, \tag{12}$$

where $T = \sum_i \dfrac{1}{2} m_i \boldsymbol{v}_i^2$.

The variation of Equation (12) is

$$\delta \int_{t_1}^{t_2} T\mathrm{d}t = \int_{t_1}^{t_2} \delta T\mathrm{d}t = \int_{t_1}^{t_2} \sum_i m_i \boldsymbol{v}_i \cdot \delta \boldsymbol{v}_i \mathrm{d}t, \tag{13}$$

with $\boldsymbol{v}_i = \dfrac{\mathrm{d}\boldsymbol{r}_i}{\mathrm{d}t}$, we have

$$\delta \boldsymbol{v}_i = \frac{\mathrm{d}\left(\delta \boldsymbol{r}_i\right)}{\mathrm{d}t} \tag{14}$$

the Equation (13) becomes

$$\delta \int_{t_1}^{t_2} T\mathrm{d}t = \int_{t_1}^{t_2} \sum_i m_i \boldsymbol{v}_i \cdot \frac{\mathrm{d}\left(\delta \boldsymbol{r}_i\right)}{\mathrm{d}t} \mathrm{d}t = \sum_i m_i \boldsymbol{v}_i \cdot \delta \boldsymbol{r}_i \Big|_{t_1}^{t_2} - \int_{t_1}^{t_2} \sum_i m_i \dot{\boldsymbol{v}}_i \cdot \delta \boldsymbol{r}_i \mathrm{d}t \tag{15}$$

i.e.,

$$\delta\int_{t_1}^{t_2} T\mathrm{d}t + \int_{t_1}^{t_2}\sum_i m_i\dot{\boldsymbol{v}}_i\cdot\delta\boldsymbol{r}_i\mathrm{d}t = \sum_i m_i\dot{\boldsymbol{v}}_i\cdot\delta r_i\Big|_{t_1}^{t_2} \tag{16}$$

with $\boldsymbol{F}_i = m_i\dot{\boldsymbol{v}}_i$ and $\delta\omega = \sum_i \boldsymbol{F}_i\cdot\delta r_i$, we have

$$\delta\int_{t_1}^{t_2} T\mathrm{d}t + \int_{t_1}^{t_2}\sum_i \boldsymbol{F}_i\cdot\delta\boldsymbol{r}_i\mathrm{d}t = \sum_i m_i\dot{\boldsymbol{v}}_i\cdot\delta r_i\Big|_{t_1}^{t_2} \tag{17}$$

and

$$\delta\int_{t_1}^{t_2} T\mathrm{d}t + \int_{t_1}^{t_2}\delta\omega\mathrm{d}t = \sum_i m_i\dot{\boldsymbol{v}}_i\cdot\delta r_i\Big|_{t_1}^{t_2}, \tag{18}$$

if the variation of two endpoints are zero, there are

$$\delta q_j\Big|_{t_1} = \delta q_j\Big|_{t_2} = 0 \tag{19}$$

and

$$\delta\boldsymbol{r}_i\Big|_{t_1} = \delta\boldsymbol{r}_i\Big|_{t_2} = 0 \tag{20}$$

the Equation (18) becomes

$$\delta\int_{t_1}^{t_2} T\mathrm{d}t + \int_{t_1}^{t_2}\delta\omega\mathrm{d}t = 0, \tag{21}$$

as the kinetic energy T is determined by the speed of each moment, there is

$$\delta\int_{t_1}^{t_2} T\mathrm{d}t = \int_{t_1}^{t_2}\delta T\mathrm{d}t. \tag{22}$$

When the active force F is conservative force, the work it does can be expressed as potential energy U, it is

$$\int_{t_1}^{t_2}\boldsymbol{F}\cdot\delta\boldsymbol{r}\mathrm{d}t = \int_{t_1}^{t_2}\delta\omega\mathrm{d}t = -\int_{t_1}^{t_2}\delta U\mathrm{d}t = -\delta\int_{t_1}^{t_2} U\mathrm{d}t, \tag{23}$$

the Equation (21) becomes

$$\delta\int_{t_1}^{t_2}\left(T-U\right)\mathrm{d}t = 0, \tag{24}$$

i.e.,

$$\delta\int_{t_1}^{t_2} L\mathrm{d}t = 0, \tag{25}$$

or

$$\delta S = 0. \tag{26}$$

where the Lagrange function $L = T - V$, and the action $S = \int_{t_1}^{t_2} L\mathrm{d}t$. The Equation (25) or (26) is the Hamilton principle for the conservative system.

3. The Generalized Hamilton Principle for the Nonconservative System

When the active forces include both conservative force F_1 and nonconservative force F_2, we have

$$\delta\omega = \boldsymbol{F}_1\cdot\delta\boldsymbol{r} + \boldsymbol{F}_2\cdot\delta\boldsymbol{r} = \delta\omega_1 + \delta\omega_2, \tag{27}$$

and

$$\int_{t_1}^{t_2} \boldsymbol{F}_1 \cdot \delta \boldsymbol{r} \mathrm{d}t = \int_{t_1}^{t_2} \delta \omega_1 \mathrm{d}t = -\int_{t_1}^{t_2} \delta U \mathrm{d}t = -\delta \int_{t_1}^{t_2} U \mathrm{d}t, \tag{28}$$

substituting Equations (27) and (28) into (21), there are

$$\delta \int_{t_1}^{t_2} (T-U) \mathrm{d}t + \int_{t_1}^{t_2} \delta \omega_2 \mathrm{d}t = 0, \tag{29}$$

and

$$\int_{t_1}^{t_2} \delta (T-U) \mathrm{d}t + \int_{t_1}^{t_2} \delta \omega_2 \mathrm{d}t = 0, \tag{30}$$

or

$$\int_{t_1}^{t_2} \delta (T-U+\omega_2) \mathrm{d}t = 0, \tag{31}$$

we define generalized Lagrange function $\overline{L}$, it is

$$\overline{L} = T - U + \omega_2 = L + \omega_2, \tag{32}$$

the Equation (31) becomes

$$\int_{t_1}^{t_2} \delta \overline{L} \mathrm{d}t = \int_{t_1}^{t_2} \delta (L+\omega_2) \mathrm{d}t = \int_{t_1}^{t_2} (\delta L + \delta \omega_2) \mathrm{d}t = 0. \tag{33}$$

The Equation (33) is called the generalized Hamilton principle for the nonconservative force system, it is different from the Hamilton principle (25) for the conservative force system, the Equation (33) contains the work of nonconservative force, and the variation is inside the integral sign.

From Equation (7), we can give the work of nonconservative forces $F_{2i} (i = 1, 2, \cdots, N)$, it is

$$\delta \omega_2 = \sum_{i=1}^{N} \boldsymbol{F}_{2i} \cdot \delta \boldsymbol{r}_i = \sum_j \left(\sum_i \boldsymbol{F}_{2i} \cdot \frac{\partial \boldsymbol{r}_i}{\partial q_j} \right) \delta q_j = \sum_i \left(\sum_{j=1}^{N} \boldsymbol{F}_{2j} \cdot \frac{\partial \boldsymbol{r}_j}{\partial q_i} \right) \delta q_i, \tag{34}$$

when there is a single nonconservative force F_2, there is

$$\delta \omega_2 = \sum_i \boldsymbol{F}_2 \cdot \frac{\partial \boldsymbol{r}}{\partial q_i} \delta q_i = \sum_i F_{2i} \delta q_i. \tag{35}$$

So, when there are both conservative force F_1 and nonconservative force F_2 for the system, the generalized Lagrange function is

$$\overline{L} = T - U + \omega_2 = L + \int \boldsymbol{F}_2 \cdot \mathrm{d}\boldsymbol{r}, \tag{36}$$

the generalized action is

$$\overline{S} = \int_{t_1}^{t_2} \overline{L} \mathrm{d}t. \tag{37}$$

and the generalized Hamilton principle is

$$\int_{t_1}^{t_2} \delta \overline{L} \mathrm{d}t = \int_{t_1}^{t_2} (\delta L + \delta \omega_2) \mathrm{d}t = 0. \tag{38}$$

when there is only nonconservative force F_2, and there is not conservative force F_1 for the system, the generalized Hamilton principle is

$$\int_{t_1}^{t_2} \delta \overline{L} \mathrm{d}t = \int_{t_1}^{t_2} (\delta T + \delta \omega_2) \mathrm{d}t = 0, \tag{39}$$

and the generalized Lagrange function is

$$\bar{L} = T + \omega_2 = T + \int \boldsymbol{F}_2 \cdot \mathrm{d}\boldsymbol{r}. \tag{40}$$

4. The Generalized Hamilton Principle for the Heat Exchange System

In the mechanical, the change rate of energy is

$$\frac{\mathrm{d}E}{\mathrm{d}t} = \boldsymbol{F} \cdot \boldsymbol{v}. \tag{41}$$

For a microcosmic particle, when it exchanges heat Q with the outside world, there is

$$\frac{\mathrm{d}E}{\mathrm{d}t} = \frac{\mathrm{d}Q}{\mathrm{d}t}, \tag{42}$$

and the radiant force should be produced, it is

$$\boldsymbol{F} \cdot \boldsymbol{v} = \frac{\mathrm{d}Q}{\mathrm{d}t}, \tag{43}$$

when the microcosmic particle absorb heat, $\frac{\mathrm{d}Q}{\mathrm{d}t} > 0$, the radiant force is $\boldsymbol{F} = -k\boldsymbol{v}$. When the microcosmic particle deliver heat, $\frac{\mathrm{d}Q}{\mathrm{d}t} < 0$, the radiant force is $\boldsymbol{F} = k\boldsymbol{v}$. The Equation (43) should be changed to the following formula

$$\boldsymbol{F} \cdot \boldsymbol{v} = -\frac{\mathrm{d}Q}{\mathrm{d}t}, \tag{44}$$

i.e.,

$$\boldsymbol{F} \cdot \mathrm{d}\boldsymbol{r} = \boldsymbol{F} \cdot \boldsymbol{v}\mathrm{d}t = -\mathrm{d}Q, \tag{45}$$

then

$$\int \boldsymbol{F} \cdot \mathrm{d}\boldsymbol{r} = -\int \mathrm{d}Q = -Q, \tag{46}$$

the radiant force is a nonconservative force, When a microcosmic particle exchanges heat with the outside world, its generalized Lagrange function is

$$\bar{L} = T - U + \int \boldsymbol{F} \cdot \mathrm{d}\boldsymbol{r} = L - Q, \tag{47}$$

the generalized Hamiltonian function for the heat exchange system is

$$\bar{H} = p\dot{q} - \bar{L} = T + U + Q, \tag{48}$$

and the generalized Hamilton principle for the heat exchange system is

$$\int_{t_1}^{t_2} \delta \bar{L} \mathrm{d}t = \int_{t_1}^{t_2} \left(\delta L - \delta Q\right) \mathrm{d}t = 0. \tag{49}$$

5. The Generalized Lagrange Equation and Generalized Hamilton Function for the Nonconservative System

1) The generalized Lagrange equation for the nonconservative system

For the nonconservative system, the generalized Lagrange function is

$$\bar{L} = T - U + \omega_2 = L + \omega_2 = L + \int \boldsymbol{F}_2 \cdot \mathrm{d}\boldsymbol{r}, \tag{50}$$

i.e.,

$$\bar{L} = L\left(q_i, \dot{q}_i, t\right) + \omega_2\left(\boldsymbol{r}\left(q_i\right), t\right), \tag{51}$$

the variation of $\bar{L}$ is

$$\begin{aligned}\delta\bar{L} &= \delta L\left(q_i, \dot{q}_i, t\right) + \delta\omega_2\left(\boldsymbol{r}\left(q_i\right), t\right)\\ &= \frac{\partial L}{\partial q_i}\delta q_i + \frac{\partial L}{\partial \dot{q}_i}\delta\dot{q}_i + \boldsymbol{F}_2 \cdot \delta\boldsymbol{r}\\ &= \frac{\partial L}{\partial q_i}\delta q_i + \frac{\partial L}{\partial \dot{q}_i}\delta\dot{q}_i + \boldsymbol{F}_2 \cdot \frac{\partial \boldsymbol{r}}{\partial q_i}\delta q_i\\ &= \frac{\partial L}{\partial q_i}\delta q_i + \frac{\partial L}{\partial \dot{q}_i}\delta\dot{q}_i + F_{2i} \cdot \delta q_i,\end{aligned} \tag{52}$$

where $\delta\omega_2 = \boldsymbol{F}_2 \cdot \delta\boldsymbol{r}$, $\delta\boldsymbol{r} = \frac{\partial \boldsymbol{r}}{\partial q_i}\delta q_i$ and $\boldsymbol{F}_2 \cdot \frac{\partial \boldsymbol{r}}{\partial q_i} = F_{2i}$.

Substituting Equation (52) into the generalized Hamilton principle (38), there is

$$\int_{t_1}^{t_2} \delta\bar{L}\mathrm{d}t = \int_{t_1}^{t_2}\left(\frac{\partial L}{\partial q_i}\delta q_i + \frac{\partial L}{\partial \dot{q}_i}\delta\dot{q}_i + F_{2i} \cdot \delta q_i\right)\mathrm{d}t = 0. \tag{53}$$

Obviously, there is

$$\int_{t_1}^{t_2} \frac{\partial L}{\partial \dot{q}_i}\delta\dot{q}_i\mathrm{d}t = -\int_{t_1}^{t_2} \frac{\mathrm{d}}{\mathrm{d}t}\frac{\partial L}{\partial \dot{q}_i}\delta q_i\mathrm{d}t \tag{54}$$

substituting Equation (54) into (53), we have

$$\frac{\mathrm{d}}{\mathrm{d}t}\frac{\partial L}{\partial \dot{q}_i} - \frac{\partial L}{\partial q_i} = F_{2i}. \tag{55}$$

The Equation (55) is the generalized Lagrange equation for the nonconservative system.

2) The generalized Hamilton function for the nonconservative system

When L and w_2 do not include time, the time derivative of $\bar{L}$ is

$$\begin{aligned}\frac{\mathrm{d}\bar{L}}{\mathrm{d}t} &= \frac{\partial L}{\partial q_i}\dot{q}_i + \frac{\partial L}{\partial \dot{q}_i}\ddot{q}_i + \frac{\partial w_2}{\partial \boldsymbol{r}} \cdot \frac{\partial \boldsymbol{r}}{\partial q_i}\dot{q}_i\\ &= \frac{\partial L}{\partial q_i}\dot{q}_i + \frac{\partial L}{\partial \dot{q}_i}\ddot{q}_i + \boldsymbol{F}_2 \cdot \frac{\partial \boldsymbol{r}}{\partial q_i}\dot{q}_i\\ &= \left(\frac{\partial L}{\partial q_i} + F_{2i}\right)\dot{q}_i + \frac{\partial L}{\partial \dot{q}_i}\ddot{q}_i\\ &= \frac{\mathrm{d}}{\mathrm{d}t}\frac{\partial L}{\partial \dot{q}_i}\dot{q}_i + \frac{\partial L}{\partial \dot{q}_i}\ddot{q}_i\\ &= \frac{\mathrm{d}}{\mathrm{d}t}\left(\frac{\partial L}{\partial \dot{q}_i}\dot{q}_i\right),\end{aligned} \tag{56}$$

where $w_2 = \int \boldsymbol{F}_2 \cdot \mathrm{d}\boldsymbol{r}$ and $\boldsymbol{F}_2 = \frac{\partial w_2}{\partial \boldsymbol{r}}$.

With Equation (56), we have

$$\frac{\mathrm{d}}{\mathrm{d}t}\left(\frac{\partial L}{\partial \dot{q}_i}\dot{q}_i - \bar{L}\right) = 0, \tag{57}$$

or

$$\frac{\partial L}{\partial \dot{q}_i}\dot{q}_i - L - w_2 = \bar{H} = constant, \tag{58}$$

as

$$\frac{\partial L}{\partial \dot{q}_i}\dot{q}_i - L = T + U = H, \tag{59}$$

then

$$\bar{H} = T + U - w_2 = H - w_2. \tag{60}$$

The $\bar{H}$ is called the integral of generalized energy, or generalized Hamilton function for the nonconservative force system.

3) The invariance of $\bar{L}$ and the conserved quantity

With Equations (52) and (55), we have

$$\begin{aligned}\delta\bar{L} &= \frac{\partial L}{\partial q_i}\delta q_i + \frac{\partial L}{\partial \dot{q}_i}\delta\dot{q}_i + F_{2i}\cdot\delta q_i \\ &= \left(\frac{\partial L}{\partial q_i} + F_{2i}\right)\delta q_i + \frac{\partial L}{\partial \dot{q}_i}\delta\dot{q}_i \\ &= \frac{\mathrm{d}}{\mathrm{d}t}\frac{\partial L}{\partial \dot{q}_i}\delta\dot{q}_i + \frac{\partial L}{\partial \dot{q}_i}\delta\dot{q}_i \\ &= \frac{\mathrm{d}}{\mathrm{d}t}\left(\frac{\partial L}{\partial \dot{q}_i}\delta q_i\right) = 0.\end{aligned} \tag{61}$$

By the invariance of $\bar{L}$ ($\delta\bar{L} = 0$), we can obtain the conserved quantity for the nonconservative system

$$\frac{\partial L}{\partial \dot{q}_i}\delta q_i = constant. \tag{62}$$

It is the same as the conservative system.

6. The Generalized Lagrange Equation and Generalized Hamilton Function for the Heat Exchange System

1) The generalized Lagrange equation for the heat exchange system

In Equation (47), the generalized Lagrange function for the heat exchange system is

$$\bar{L} = T - U - Q = L - Q, \tag{63}$$

In Section 8 (Equation (91)), we have given the microcosmic heat $Q = TS$, the Equation (63) becomes

$$\bar{L} = L - TS. \tag{64}$$

i.e.,

$$\bar{L} = L(q_i, \dot{q}_i, t) - ST(q_i, \dot{q}_i, t), \tag{65}$$

When L and T do not include time, the variation of $\bar{L}$ is

$$\delta\bar{L} = \frac{\partial L}{\partial q_i}\delta q_i + \frac{\partial L}{\partial \dot{q}_i}\delta\dot{q}_i - S\frac{\partial T}{\partial q_i}\delta q_i, \tag{66}$$

substituting Equation (66) into the generalized Hamilton principle (38), there is

$$\begin{aligned}\int_{t_1}^{t_2}\delta\bar{L}\mathrm{d}t &= \int_{t_1}^{t_2}\left(\frac{\partial L}{\partial q_i}\delta q_i + \frac{\partial L}{\partial \dot{q}_i}\delta\dot{q}_i - S\frac{\partial T}{\partial q_i}\delta q_i\right)\mathrm{d}t \\ &= \int_{t_1}^{t_2}\left(\frac{\partial L}{\partial q_i} - \frac{\mathrm{d}}{\mathrm{d}t}\frac{\partial L}{\partial \dot{q}_i} - S\frac{\partial T}{\partial q_i}\right)\delta q_i\mathrm{d}t = 0,\end{aligned} \tag{67}$$

as the δq_i is arbitrary, we obtain

$$\frac{\partial L}{\partial q_i} - \frac{\mathrm{d}}{\mathrm{d}t}\frac{\partial L}{\partial \dot{q}_i} - S\frac{\partial T}{\partial q_i} = 0 \tag{68}$$

The Equation (68) is the generalized Lagrange equation for the heat exchange system.

2) The generalized Hamilton function for the heat exchange system

When L and T do not include time, the time derivative of $\bar{L}$ is

$$\begin{aligned}\frac{\mathrm{d}\bar{L}}{\mathrm{d}t} &= \frac{\partial L}{\partial q_i}\dot{q}_i + \frac{\partial L}{\partial \dot{q}_i}\ddot{q}_i - S\frac{\partial T}{\partial q_i}\dot{q}_i \\ &= \left(\frac{\partial L}{\partial q_i} - S\frac{\partial T}{\partial q_i}\right)\dot{q}_i + \frac{\partial L}{\partial \dot{q}_i}\ddot{q}_i \\ &= \frac{\mathrm{d}}{\mathrm{d}t}\frac{\partial L}{\partial \dot{q}_i}\dot{q}_i + \frac{\partial L}{\partial \dot{q}_i}\ddot{q}_i \\ &= \frac{\mathrm{d}}{\mathrm{d}t}\left(\frac{\partial L}{\partial \dot{q}_i}\dot{q}_i\right),\end{aligned} \tag{69}$$

With Equation (69), we have

$$\frac{\mathrm{d}}{\mathrm{d}t}\left(\frac{\partial L}{\partial \dot{q}_i}\dot{q}_i - \bar{L}\right) = 0, \tag{70}$$

or

$$\frac{\partial L}{\partial \dot{q}_i}\dot{q}_i - L + TS = \bar{H} = constant, \tag{71}$$

as

$$\frac{\partial L}{\partial \dot{q}_i}\dot{q}_i - L = T + U = H, \tag{72}$$

then

$$\bar{H} = T + U + Q = H + Q = H + TS. \tag{73}$$

The $\bar{H}$ is called the integral of generalized energy, or generalized Hamilton function for the heat exchange system.

3) The invariance of $\bar{L}$ and the conserved quantity

In Equations (66) and (68), we have

$$\begin{aligned}\delta\bar{L} &= \frac{\partial L}{\partial q_i}\delta q_i + \frac{\partial L}{\partial \dot{q}_i}\delta\dot{q}_i - S\frac{\partial T}{\partial q_i}\delta q_i \\ &= \left(\frac{\partial L}{\partial q_i} - S\frac{\partial T}{\partial q_i}\right)\delta q_i + \frac{\partial L}{\partial \dot{q}_i}\delta\dot{q}_i \\ &= \frac{\mathrm{d}}{\mathrm{d}t}\frac{\partial L}{\partial \dot{q}_i}\delta q_i + \frac{\partial L}{\partial \dot{q}_i}\delta\dot{q}_i \\ &= \frac{\mathrm{d}}{\mathrm{d}t}\left(\frac{\partial L}{\partial \dot{q}_i}\delta q_i\right) = 0.\end{aligned} \tag{74}$$

By the invariance of $\bar{L}$ ($\delta\bar{L} = 0$), we can obtain the conserved quantity for the heat exchange system

$$\frac{\partial L}{\partial \dot{q}_i}\delta q_i = constant. \tag{75}$$

It is the same as the conservative system.

In the above, we have given the generalized Hamilton principle for the non-conservative force and the heat exchange system. On this basis, we further given the generalized Lagrange function and generalized Hamilton function for the nonconservative force and the heat exchange system. With the results, we shall study the non-Hermitian quantum theory for the nonconservative force and the heat exchange microcosmic system.

7. The Non-Hermitian Quantum Theory for the Nonconservative Force System

With the generalized Hamilton principle and generalized Lagrange function, we will deduce the non-Hermitian quantum theory for the nonconservative force system by the approach of path integral, the path integral formula is

$$\Psi(\boldsymbol{r},t') = \int \exp\left[\frac{i}{\hbar}\int_t^{t'} \bar{L}\left(\dot{\boldsymbol{r}}(\tau),\boldsymbol{r}(\tau),\tau\right)\mathrm{d}\tau\right] D\left[\boldsymbol{r}(t)\right]\Psi(\boldsymbol{r}',t)\mathrm{d}\boldsymbol{r}', \tag{76}$$

In Equation (76), the generalized Lagrange function $\bar{L}$ is

$$\bar{L} = T - U + \omega_2 = L + \omega_2 = L + \int \boldsymbol{F}\cdot\mathrm{d}\boldsymbol{r}, \tag{77}$$

where the force $\boldsymbol{F}$ is the nonconservative force, the Equation (76) gives the wave function at a time t' in terms of the wave function at a time t. In order to obtain the differential equation, we apply this relationship in the special case that the time t' differs only by an infinitesimal interval ε from t. For a short interval ε the action is approximately ε times the Lagrangian for this interval, we have

$$\Psi(\boldsymbol{r},t+\varepsilon) = \int \frac{\mathrm{d}\boldsymbol{r}'}{A^3}\exp\left[\frac{i\varepsilon}{\hbar}\bar{L}\left(\frac{\boldsymbol{r}-\boldsymbol{r}'}{\varepsilon},\frac{\boldsymbol{r}+\boldsymbol{r}'}{2},\frac{t'+t}{2}\right)\right]\Psi(\boldsymbol{r}',t), \tag{78}$$

where A is a normalization constant.

Substituting Equation (77) into (78), there is

$$\Psi(\boldsymbol{r},t+\varepsilon) = \int \frac{\mathrm{d}\boldsymbol{r}'}{A^3}\exp\left[\frac{i\varepsilon}{\hbar}\left(\frac{m}{2}\left(\frac{\boldsymbol{r}-\boldsymbol{r}'}{\varepsilon}\right)^2 - V\left(\frac{\boldsymbol{r}+\boldsymbol{r}'}{2},\frac{t'+t}{2}\right) + \int_{\boldsymbol{r}'}^{\boldsymbol{r}}\boldsymbol{F}\cdot\mathrm{d}\boldsymbol{r}''\right)\right]\Psi(\boldsymbol{r}',t). \tag{79}$$

In macroscopic field, the frictional force and adhere force are non-conservative force, and the non-conservative force $\boldsymbol{F}$ is directly proportional to velocity $\boldsymbol{v}$, their directions are opposite, *i.e.* $\boldsymbol{F}=-k\boldsymbol{v}$. In microcosmic field, atomic and molecular can also suffer the action of non-conservative force. In the experiment of Bose-Einstein condensates, the atomic Rb^{87}, Na^{23} and Li^{7} can be cooled in laser field, since they get the non-conservative force from the photons.

Substituting $\boldsymbol{F}=-k\boldsymbol{v}$ into Equation (79), we get

$$\Psi(\boldsymbol{r},t+\varepsilon)=\int\frac{\mathrm{d}\boldsymbol{r}'}{A^3}\exp\left[\frac{i\varepsilon}{\hbar}\left(\frac{m}{2}\left(\frac{\boldsymbol{r}-\boldsymbol{r}'}{\varepsilon}\right)^2-V\left(\frac{\boldsymbol{r}+\boldsymbol{r}'}{2},\frac{t'+t}{2}\right)\right.\right.\\\left.\left.-k\int_{r'}^{r}\left(\frac{\boldsymbol{r}-\boldsymbol{r}'}{\varepsilon}\right)\cdot\mathrm{d}\boldsymbol{r}''\right)\right]\Psi(\boldsymbol{r}',t). \tag{80}$$

The quantity $\frac{(\boldsymbol{r}-\boldsymbol{r}')^2}{\varepsilon}$ appear in the exponent of the first factor. It is clear that if $\boldsymbol{r}'$ is appreciably different from $\boldsymbol{r}$, this quantity is very large and the exponential consequently oscillates very rapidly as $\boldsymbol{r}'$ varies, when this factor oscillates rapidly, the integral over $\boldsymbol{r}'$ gives a very small value. Only if $\boldsymbol{r}'$ is near $\boldsymbol{r}$ do we get important contributions. For this reason we make the substitution $\boldsymbol{r}'=\boldsymbol{r}+\boldsymbol{\eta}$ with the expectation that appreciable contribution to the integral will occur only for small $\boldsymbol{\eta}$, we obtain

$$\Psi(\boldsymbol{r},t+\varepsilon)=\int\frac{\mathrm{d}\boldsymbol{\eta}}{A^3}\exp\left[\frac{i\varepsilon}{\hbar}\left(\frac{m}{2}\left(\frac{\boldsymbol{\eta}}{\varepsilon}\right)^2-V\left(\boldsymbol{r}+\frac{\boldsymbol{\eta}}{2},t+\frac{\varepsilon}{2}\right)-k\int_{r'}^{r}\frac{-\boldsymbol{\eta}}{\varepsilon}\cdot\mathrm{d}\boldsymbol{r}''\right)\right]\Psi(\boldsymbol{r}+\boldsymbol{\eta},t) \tag{81}$$

Now we have

$$\int_{r'}^{r}\boldsymbol{\eta}\cdot\mathrm{d}\boldsymbol{r}''=\int_{r'}^{r}|\boldsymbol{\eta}||\mathrm{d}\boldsymbol{r}''|\cos\theta=|\boldsymbol{\eta}|\int_{r'}^{r}|\mathrm{d}\boldsymbol{r}''|\cos\theta=|\boldsymbol{\eta}|^2 \tag{82}$$

so that

$$k\int_{r'}^{r}\frac{-\boldsymbol{\eta}}{\varepsilon}\cdot\mathrm{d}\boldsymbol{r}''=-\frac{k}{\varepsilon}|\boldsymbol{\eta}|^2=-\frac{k}{\varepsilon}\boldsymbol{\eta}^2 \tag{83}$$

substituting Equation (83) into (81), we have

$$\Psi(\boldsymbol{r},t+\varepsilon)=\int\frac{\mathrm{d}\boldsymbol{\eta}}{A^3}\exp\left[\frac{i\varepsilon}{\hbar}\left(\frac{m}{2}\frac{\boldsymbol{\eta}^2}{\varepsilon^2}-V\left(\boldsymbol{r}+\frac{\boldsymbol{\eta}}{2},t+\frac{\varepsilon}{2}\right)+\frac{k}{\varepsilon}\boldsymbol{\eta}^2\right)\right]\Psi(\boldsymbol{r}+\boldsymbol{\eta},t)\\=\int\frac{\mathrm{d}\boldsymbol{\eta}}{A^3}\mathrm{e}^{\frac{im\boldsymbol{\eta}^2}{2\hbar\varepsilon}}\mathrm{e}^{-\frac{i\varepsilon}{\hbar}V\left(\boldsymbol{r}+\frac{\boldsymbol{\eta}}{2},t+\frac{\varepsilon}{2}\right)}\mathrm{e}^{+\frac{i}{\hbar}k\boldsymbol{\eta}^2}\Psi(\boldsymbol{r}+\boldsymbol{\eta},t) \tag{84}$$

After more complex calculation, we have

$$i\hbar\frac{\partial\Psi(\boldsymbol{r},t)}{\partial t}=\left(-\frac{\hbar^2}{2m}\nabla^2+V-i\hbar\frac{3k}{m}\right)\Psi(\boldsymbol{r},t)=\hat{H}\Psi(\boldsymbol{r},t), \tag{85}$$

the Hamiltonian H is

$$\hat{H}=-\frac{\hbar^2}{2m}\nabla^2+V-i\hbar\frac{3k}{m}. \tag{86}$$

Obviously, the Hamiltonian H is non Hermitian. The Detailed derivation can

see the Ref. [21].

8. The Non-Hermitian Quantum Theory for the Thermodynamics

In classical mechanics, the energy of a macroscopic object is

$$E = \frac{p^2}{2m} + V(r). \tag{87}$$

For a microcosmic particle, when it exchanges heat Q with the outside world, with Equation (48) or (73), the particle total energy should be the sum of kinetic energy, potential energy and thermal energy, it is

$$E = \frac{p^2}{2m} + V(r) + Q. \tag{88}$$

In thermodynamics, for the infinitely small processes, the entropy is defined as

$$\mathrm{d}S = \frac{\mathrm{d}Q}{T}. \tag{89}$$

For the finite processes, it is

$$Q - Q_0 = TS - TS_0. \tag{90}$$

At temperature T, when a particle has the microcosmic entropy S, it should has the thermal potential energy Q, it is

$$Q = TS, \tag{91}$$

the Equation (88) becomes

$$E = \frac{p^2}{2m} + V(r) + TS. \tag{92}$$

the Equation (92) is the classical total energy of a microcosmic particle. In quantum theory, it should become operator form. it is

$$\hat{H} = \frac{\hat{p}^2}{2m} + \hat{V}(r) + T\hat{S}. \tag{93}$$

where $\hat{H} = i\hbar\frac{\partial}{\partial t}$, $\hat{p}^2 = -\hbar^2\nabla^2$ and $\hat{S}$ is the microcosmic entropy operator.

At the i-th microcosmic state, the classical microcosmic entropy S_{Fi} and S_{Bi} for Fermion and Bose systems are

$$S_{Fi} = -k_B\left[n_i \ln n_i + (1-n_i)\ln(1-n_i)\right], \tag{94}$$

and

$$S_{Bi} = -k_B\left[n_i \ln n_i - (1+n_i)\ln(1+n_i)\right], \tag{95}$$

where k_B is the Boltzmann constant, n_i is the average particle numbers of particle in the i-th state. For the Fermion (Bose), the $n_i \le 1$ ($n_i \ge 1$).

In quantum theory, the classical microcosmic entropy should become operator. The microcosmic entropy operator depends on temperature, but it has no

the dimension of temperature, and it is non-Hermitian operator because it has to do with heat exchange. So, the microcosmic entropy operator includes the temperature operator $T\frac{\partial}{\partial T}$. Moreover, it has to do with the state distribution. For the Fermion and Bose systems, the microcosmic entropy operator $\hat{S}_{Fi}$ and $\hat{S}_{Bi}$ of a particle in the *i*-th state can be written as

$$\hat{S}_{Fi} = -k_B\left[n_i \ln n_i + (1-n_i)\ln(1-n_i)\right]T\frac{\partial}{\partial T} = S_{Fi}T\frac{\partial}{\partial T}, \tag{96}$$

and

$$\hat{S}_{Bi} = -k_B\left[n_i \ln n_i - (1+n_i)\ln(1+n_i)\right]T\frac{\partial}{\partial T} = S_{Bi}T\frac{\partial}{\partial T}. \tag{97}$$

We can prove the following operator relation:

$$\hat{T}^{+} = \hat{T} = T, \tag{98}$$

$$\left(-i\frac{\partial}{\partial T}\right)^{+} = -i\frac{\partial}{\partial T} \tag{99}$$

$$\left[\hat{T}, \frac{\partial}{\partial T}\right] = -1. \tag{100}$$

With Equations (98) - (100), we find the operator $T\frac{\partial}{\partial T}$ is non-Hermitian, the microcosmic entropy operators (96) and (97) are also non-Hermitian, it leads to the total Hamilton operator (93) is non-Hermitian and space-time inversion (*PT*) symmetry

$$\hat{H}^{+} \neq H, \quad (PT)H(PT)^{-1} = H. \tag{101}$$

This is because the particle (atom or molecule) exchanges energy with the external environment, it is an open system, its Hamiltonian operator should be non-Hermitian.

9. The Schroding Equation with Temperature

With the canonical quantization, $E = i\hbar\frac{\partial}{\partial t}$, $\boldsymbol{p} = -i\hbar\nabla$, substituting Equation (96) into (93), we can obtain the Schroding equation with temperature

$$i\hbar\frac{\partial}{\partial t}\psi(\boldsymbol{r},t,T) = \left(-\frac{\hbar^2}{2m}\nabla^2 + V(r) + \sum_i S_{Fi}T^2\frac{\partial}{\partial T}\right)\psi(\boldsymbol{r},t,T), \tag{102}$$

By separating variables

$$\psi(\boldsymbol{r},t,T) = \Psi(\boldsymbol{r},T)f(t), \tag{103}$$

we obtain

$$i\hbar\frac{\mathrm{d}f(t)}{\mathrm{d}t} = E_n f(t), \tag{104}$$

$$\left(-\frac{\hbar^2}{2m}\nabla^2 + V(r) + f_n S_{Fi}T^2\frac{\partial}{\partial T}\right)\psi_n(\boldsymbol{r},T) = E_n\psi_n(\boldsymbol{r},T). \tag{105}$$

By separating variables $\Psi_n(\boldsymbol{r},T)=\Psi_n(\boldsymbol{r})\phi(T)$, the Equation (105) can be written as

$$-\frac{\hbar^2}{2m}\nabla^2\Psi_n(\boldsymbol{r})+V(r)\Psi_n(\boldsymbol{r})=E_{1n}\Psi_n(\boldsymbol{r}), \tag{106}$$

$$f_n S_{Fi} T^2 \frac{\partial}{\partial T}\phi(T)=E_{2n}\phi(T) \tag{107}$$

where $E_n=E_{1n}+E_{2n}$, E_{1n} is the eigenenergy obtained by the Schroding Equation (106), E_{2n} is the eigenenergy obtained by the temperature Equation (107), the n expresses the n-th energy level, n_i is the average particle numbers of the i-th state in the n-th energy level, and f_n is the degeneracy of the n-th energy level.

For Equation (107), by the dimensional analysis, the energy E_{2n} can be written as

$$E_{2n}=f_n S_{Fi} T_0=-k_B f_n\left[n_i\ln n_i+(1-n_i)\ln(1-n_i)\right]T_0, \tag{108}$$

and $\phi(T)$ satisfies equation

$$T^2\frac{\partial}{\partial T}\phi(T)=\phi(T)T_0, \tag{109}$$

the temperature wave function $\phi(T)$ is

$$\phi(T)=A\mathrm{e}^{-\frac{T_0}{T}}, \tag{110}$$

where A is the normalization constant, and T_0 must be the temperature constant, because the energy E_{2n} cannot be the function of variable T, such as the hydrogen atom level is not the function of coordinate variable $\boldsymbol{r}$. The general solution of Equation (102) is

$$\psi(\boldsymbol{r},t,T)=\sum_n C_n\Psi_n(\boldsymbol{r})\phi_n(T)\mathrm{e}^{-\frac{i}{\hbar}E_n t}. \tag{111}$$

For a free particle, its momentum is $\boldsymbol{p}$, and is in the environment of temperature T, because it is in the determinate state, *i.e.*, the average particle numbers $n_i=\delta_{ij}$, the free particle plane wave solution and total energy are

$$\psi(\boldsymbol{r},t,T)=A\mathrm{e}^{\frac{i}{\hbar}\left(\boldsymbol{p}\cdot\boldsymbol{r}-Et+i\frac{T_0}{T}\hbar\right)}, \tag{112}$$

and

$$E=\frac{p^2}{2m}. \tag{113}$$

By the accurate measurement the hydrogen atom spectrum, we can determine the temperature constant T_0. The hydrogen atom has only one electron outside the nucleus, the degeneracy of the n-th energy level is $f_n=n^2$.

When the electron jumps from m-th energy level to the n-th energy level $(m>n)$, the transition frequency without temperature correction (the theoretical calculation with Schroding equation) is

$$\nu_{mn}^{th} = \frac{E_m - E_n}{h}, \tag{114}$$

the transition frequency with temperature correction is

$$\nu_{mn}(T) = \nu_{mn}^{exp} = \frac{E_m(T) - E_n(T)}{h}, \tag{115}$$

the energy levels $E_m(T)$ and $E_n(T)$ are

$$E_m(T) = E_m - k_B f_m \left[m_i \ln m_i + (1-m_i)\ln(1-m_i) \right] T_0, \tag{116}$$

and

$$E_n(T) = E_n - k_B f_n \left[n_i \ln n_i + (1-n_i)\ln(1-n_i) \right] T_0. \tag{117}$$

The average particle numbers of every state in the m-th and n-th energy levels are $m_i = \frac{1}{m^2}$ and $n_i = \frac{1}{n^2}$.

With Equations (114) and (115), we obtain the temperature constant T_0, it is

$$T_0 = \frac{h\left(\nu_{mn}^{exp} - \nu_{mn}^{th}\right)}{k_B\left[\ln\frac{m^2}{n^2} - \left(m^2-1\right)\ln\left(1-\frac{1}{m^2}\right) + \left(n^2-1\right)\ln\left(1-\frac{1}{n^2}\right)\right]}, \tag{118}$$

where h is the Planck constant, by measurement transition frequency ν_{mn}^{exp}, we can determine the temperature constant T_0. When the electron jumps from the first excited state ($m=2$) to ground state ($n=1$), the T_0 is

$$T_0 = \frac{h\left(\nu_{21}^{exp} - \nu_{21}^{th}\right)}{k_B\left[4\ln 4 - 3\ln 3\right]}. \tag{119}$$

The theory should be tested by the experiments.

10. Conclusion

The Hamilton principle is a variation principle describing the isolated and conservative systems, its Lagrange function is the difference between kinetic energy and potential energy. By Feynman path integration, we can obtain the standard Schrodinger equation. In this paper, we have given the generalized Hamilton principle, which can describe the heat exchange system, and the nonconservative force system. On this basis, we have further given their generalized Lagrange functions and Hamilton functions. With the Feynman path integration, we have given the generalized Schrodinger equation of nonconservative force system and the heat exchange system.

Fund

This work was supported by the Scientific and Technological Development Foundation of Jilin Province (No. 20190101031JC).

Conflicts of Interest

The authors declare no conflicts of interest regarding the publication of this paper.

References

[1] Pauli, W. (1943) *Reviews of Modern Physics*, **15**, 175. https://doi.org/10.1103/RevModPhys.15.175

[2] Dirac, P.A.M. (1942) *Proceedings of the Royal of London. Series A. Mathematical and Physical Sciences*, **180**, 1-40. https://doi.org/10.1098/rspa.1942.0023

[3] Lee, T.D. and Wick, G.C. (1969) *Nuclear Physics B*, **9**, 209-243. https://doi.org/10.1016/0550-3213(69)90098-4

[4] Harms, B.C., Jones, S.T. and Tan, C.I. (1980) *Nuclear Physics B*, **171**, 392-412. https://doi.org/10.1016/0550-3213(80)90377-6

[5] Andrianov, A.A. (1982) *Annals of Physics*, **140**, 82-100. https://doi.org/10.1016/0003-4916(82)90336-0

[6] Hollowood, T. (1992) *Nuclear Physics B*, **384**, 523-540. https://doi.org/10.1016/0550-3213(92)90579-Z

[7] Harms, B.C., Jones, S.T. and Tan, C.I. (1980) *Physics Letters B*, **91**, 291-295. https://doi.org/10.1016/0370-2693(80)90452-9

[8] Bender, C.M. and Boettcher, S. (1998) *Physical Review Letters*, **80**, 5243. https://doi.org/10.1103/PhysRevLett.80.5243

[9] Bender, C.M., Boettcher, S. and Meisinger, P.N. (1999) *Journal of Mathematical Physics*, **40**, 2201. https://doi.org/10.1063/1.532860

[10] El-Ganainy, R., Makris, K.G., Khajavikhan, M., Musslimani, Z.H., Rotter, S. and Christodoulides, D.N. (2018) *Nature Physics*, **14**, 11. https://doi.org/10.1038/nphys4323

[11] Ozdemir, S.K., Rotter, S., Nori, F. and Yang, L. (2019) *Nature Materials*, **18**, 783. https://doi.org/10.1038/s41563-019-0304-9

[12] Konotop, V.V., Yang, J. and Zezyulin, D.A. (2016) *Reviews of Modern Physics*, **88**, Article ID: 035002. https://doi.org/10.1103/RevModPhys.88.035002

[13] Miri, M.A. and Alu, A. (2019) *Science*, **363**, 42. https://doi.org/10.1126/science.aar7709

[14] Ge, L. and Wan, W. (2020) Nonlinear and Novel Phenomena in Non-Hermitian Photonics. In: Kevrekidis, P.G., Cuevas-Maraver, J. and Saxena, A., Eds., *Emerging Frontiers in Nonlinear Science*, Springer, Cham, 227-248. https://doi.org/10.1007/978-3-030-44992-6_10

[15] Peng, P., Cao, W., Shen, C., Qu, W., Wen, J., Jiang, L. and Xiao, Y. (2016) *Nature Physics*, **12**, 1139. https://doi.org/10.1038/nphys3842

[16] Feng, L., El-Ganainy, R. and Ge, L. (2017) *Nature Photonics*, **11**, 752-762. https://doi.org/10.1038/s41566-017-0031-1

[17] Christensen, J., Willatzen, M., Velasco, V.R. and Lu, M.-H. (2016) *Physical Review Letters*, **116**, Article ID: 207601. https://doi.org/10.1103/PhysRevLett.116.207601

[18] Chen, H.-Z., *et al.* (2020) *Nature Physics*, **16**, 571. https://doi.org/10.1038/s41567-020-0807-y

[19] Assawaworrarit, S., Yu, X. and Fan, S. (2017) *Nature*, **546**, 387. https://doi.org/10.1038/nature22404

[20] Kawabata, K., Ashida, Y. and Ueda, M. (2017) *Physical Review Letters*, **119**, Article ID: 190401. https://doi.org/10.1103/PhysRevLett.119.190401

[21] Wu, X.-Y., Zhang, B.-J., *et al.* (2009) *International Journal of Theoretical Physics*, **48**, 2027-2035.

Scientific Research Publishing

Journal of Modern Physics, 2023, 14, 692-721
https://www.scirp.org/journal/jmp
ISSN Online: 2153-120X
ISSN Print: 2153-1196

Cosmological Inconstant, Supernovae 1a and Decelerating Expansion

Russell Bagdoo

Saint-Bruno-de-Montarville, Quebec, Canada
Email: rbagdoo@gmail.com

How to cite this paper: Bagdoo, R. (2023) Cosmological Inconstant, Supernovae 1a and Decelerating Expansion. *Journal of Modern Physics*, **14**, 692-721.
https://doi.org/10.4236/jmp.2023.145040

Received: March 11, 2023
Accepted: April 21, 2023
Published: April 24, 2023

Abstract

In 1998, two groups of astronomers, one led by Saul Perlmutter and the other by Brian Schmidt, set out to determine the deceleration—and hence the total mass/energy—of the universe by measuring the recession speeds of type la supernovae (SN1a), came to an unexpected conclusion: ever since the universe was about 7 billion years old, its expansion rate has not been decelerating. Instead, the expansion rate has been speeding up. To justify this acceleration, they suggested that the universe does have a mysterious dark energy and they have emerged from oblivion the cosmological constant, positive this time, which is consistent with the image of an inflationary universe. To explain the observed dimming of high-redshift SN1a they have bet essentially on their distance revised upwards. We consider that an accelerated expansion leads right to a "dark energy catastrophe" (*i.e.*, the chasm between the current cosmological vacuum density value of 10 GeV/m^3 and the vacuum energy density proposed by quantum field theory of ~10^{122} GeV/m^3). We suppose rather that the universe knows a slowdown expansion under the positive pressure of a dark energy, otherwise called a variable cosmological constant. The dark luminosity of the latter would be that of a "tired light" which has lost energy with distance. As for the low brilliance of SN1a, it is explained by two physical processes: The first relates to their intrinsic brightness—supposedly do not vary over time—which would depend on the chemical conditions which change with the temporal evolution; the second would concern their apparent luminosity. Besides the serious arguments already known, we strongly propose that their luminosity continually fades by interactions with cosmic magnetic fields, like the earthly PVLAS experiment which loses much more laser photons than expected by crossing a magnetic field. It goes in the sense of a "tired light" which has lost energy with distance, and therefore, a decelerated expansion of the universe. Moreover, we propose the "centrist" principle to complete the hypothesis of the cosmological principle of homogeneity and isotropy considered verified. Without denying the Copernican

principle, he is opposed to a "spatial" theoretical construction which accelerates the world towards infinity. The centrist principle gives a "temporal" and privileged vision which tends to demonstrate the deceleration of expansion.

Keywords

Variable Cosmological Constant, SN1a, Dark Energy Catastrophe, Theory of Relation, Deceleration of the Expansion, PVLAS Experiment, Tired Light, Centrist Principle

1. Introduction

The aim of this paper is to propose the earthly experience *Polarizzazione del Vuoto con LASer* (PVLAS) [1] [2] amalgamated to the radiation of the SN1a, and show that it corroborates the interpretation of the theory of Relation according to which the observation of the distant SN1a leads to a deceleration of the expansion and a variable cosmological constant.

We consider that the light of the SN1a loses its brightness through the intergalactic magnetic fields, in the same way that the laser of the earthly PVLAS experiment loses photons by going through a magnetic field. This experiment tends to demonstrate that the weakening of the apparent luminosity of the SN1a is due to a physical process rather than a distance to revise upward as required by the theory of inflation. This physical process is added to some of the main propositions already known in opposition to the acceleration of the expansion. It leans toward a very low density of matter and a flat universe, in accordance with the results of the weighing of clusters of galaxies and those from the cosmic microwave background (CMB). It implies a deceleration of the expansion and appeals to a "variable" cosmological constant which derives from the theory of Relation of which we present some aspects. The basic assumption of this new theory excludes the original phase of exponential growth of the cosmic inflation. Rather, it appeals to a relativistic big bang [3] [4], stemming from a previous universe, with a primeval dark energy with a density of at least 10^{60} times greater than the current vacuum energy, whose high temperature "substance" would quickly have begun to disintegrate into ordinary matter and dark matter, decay that would have continued during the history of the universe, especially with each broken symmetry, whenever the forces of interaction between particles change their nature. The "full" initial quantum becomes the quantum vacuum of space through a variable cosmological constant, which is nothing else than the dark energy which is transformed into common and dark matter. In this way, the "dark energy catastrophe" is stemmed and the reconciliation between particle physicists and cosmologists takes place.

But in order to demonstrate the deceleration of the universe, the paper also proposes a "centrist principle" which would coexist with the Copernican principle. The centrist-quantum vision reinforces the whole edifice of knowledge of

the big bang. The concept of the center of the world reappears and the center is brought back to the rank of a privileged coordinate system. This quantum center gives rise to a cosmological time which does not separate from the space of expansion. The arrow of time generates epochs which are separated by temporal lengths. Each epoch has a different coordinate system because temperature and density change from epoch to epoch. The Copernican-relativist vision where the center is reduced to the rank of any coordinate system only applies to an era in itself. That is what made think that the theory of relativity is primarily a local theory and not a global one.

The second section presents the prevailing theory of inflation which is, in physical cosmology, a theory of exponential expansion of space in the early universe. The third section presents the distant Type 1a supernovae whose observations indicated in 1998 the unexpected result that the universe appears to be undergoing accelerated expansion. The fourth section introduces the "dark energy catastrophe" which is the disagreement as much as 120 orders of magnitude between the small observed value of the cosmological constant and the theoretical large value of vacuum energy density suggested by quantum field theory. The fifth section describes a variable cosmological constant within the framework of the theory of Relation. The sixth section shows two ways to explain the low luminosity of SN1a: greater distance and physical process. The seventh section, in order to explain the weakening of the apparent luminosity of SN1a, suggests comparing the laser of the terrestrial experiment PVLAS which loses photons by crossing a magnetic field to the rays of SN1a which lose their luminosity by interactions with cosmic magnetic fields. The eighth section proposes a "centrist principle" intended to demonstrate the deceleration of the universe. It would oppose the Copernican principle while coexisting with it.

2. Inflationary Scenarios

Before discussing the theory of inflation currently prevailing, let us mention that the cosmology, which exists hardly since the XXth century, grounded on the laws of physics as we know them, and on the observations done from the smallest to the largest scales, has made up the standard model. This one is an archeology of the universe by the thought which goes back up to the big bang, and which appears as an apotheosis of physics. However, in the late 70, some pieces fit together very poorly in the puzzle of the standard big bang theory. For example, observations show that on a large scale the matter is widely distributed in a rather homogeneous way. How then to understand the formation of large structures (clusters of galaxies, superclusters), which show an extreme heterogeneity of the universe today? The physical process at the origin of the small density fluctuations was missing. There were also the riddles of a very flat universe, broken symmetries and magnetic monopoles [5].

In 1980, a new hypothesis, issuing from particle theory, claimed its ability to solve these conundrums, while preserving the success of the standard theory.

The universe would have known very early in the cosmic chronology a dazzling phase of expansion, the inflation [6] [7]. One can imagine there are several tens of billions of years, a universe whose energy was carried by a field, which was perched away from its minimum energy state. Because of its negative pressure, the field drove an enormous burst of inflationary expansion. The space, driven by something akin to the current dark energy, would have dilated with a gigantic factor, say 10^{100} [8]. Then, some 10^{-35} sec later, as the field slid down its potential energy bowl, the burst of expansion ended, and the field released its trapped energy to the production of ordinary matter and radiation. For many billions of years, these familiar constituents of the universe exerted an ordinary attractive gravitational pull that slowed the spatial expansion. But as the universe grew and thinned out, the gravitational pull diminished. About 7 billion years ago, ordinary gravitational attraction became weak enough for the gravitational repulsion of the universe's cosmological constant to become dominant, and since then the rate of spatial expansion has been continually increasing [9].

After twenty years of works, the inflationary universe scenario was able to make macroscopic random fluctuations of energy, inevitable at the quantum scale. With this theory, the most infinitesimal initial irregularities in the distribution of energy can be grown enormously and create future centers of condensation of matter. These will in turn become the seeds from which the matter will gradually be structured on scales larger and larger.

Despite this sketch of cosmic evolution, at the end of the XXth century, views on inflation had failed in forming a definitive scenario. Some astrophysicists were ready to raise arms and declare false the theory of inflation (and even the big bang). Most of the astronomers who had measured the mass of distant clusters of galaxies were convinced that matter represented only 20% - 40% of the critical density of the universe, and that the latter should be close to the critical density that makes it flat but could not find the remaining 80% - 60% [10].

3. Supernovae 1a

In 1998, a revolution took place in the world of the cosmology. The astronomers of the Supernova Cosmology Project and of the High-z Supernova Search Team announced that the rate of the cosmic expansion accelerates instead of slowing down [11]. The astronomers used old stars thermonuclear explosions—SN1a—to measure the rate of expansion of the universe. They expected to measure a deceleration of the expansion, slowed by the gravitational force attraction of the matter content of the universe. They were stunned to notice that the recession of galaxies, instead of slowing down as the universe grows older, seems to accelerate.

This announcement was consistent with measurements from previous studies, which evaluated the density of matter at 27%, of which the largest part (~22%) comes from the dark matter, still unknown but which exerts a gravitational influence on observable galaxies [12]. Once this value was determined, researchers had only to consider the contributions of Cobe satellite and Boomerang balloon

[13], and of course the theoretical framework of the big bang's models. These stipulate that the sum of the three cosmological parameters [density of matter, noted Ω_M (baryonic matter + dark matter), density of curvature, noted Ω_K and the density of dark energy which takes the role of the cosmological constant, noted Ω_Λ] must be equal to unity for critical density universe ($\Omega = 1$). However, the results of Boomerang have fixed the density curve. Its value is null.

The meticulous analysis of the data led the astronomers to argue so: the recession velocity of a supernova depends on the difference between the gravitational attraction of ordinary matter and the gravitational pull of the dark energy from the cosmological constant; taking the density of matter, whether visible or invisible, equals to about 27% of the critical density, they concluded that the accelerated expansion they had demonstrated could be explained by a push towards outside due to a cosmological constant which dark energy contribute about 73% of the critical density.

These two combined values bring the total density of mass/energy of the universe to exactly the 100% value predicted by the inflationary cosmology! [6] [14]. Measurements of SN1a and the theory of inflation were complementary and confirmed themselves mutually, independently.

4. The "Dark Energy Catastrophe"

However, the concordance of all the experiments which conducts to a space almost flat, ever expanding, startled more than a cosmologist. At the dawn of the XXIth century, astrophysicists discover that all their theories are based only on observation of visible 5% of the total energy and 95% of the universe are completely foreign to them. This does not prevent them from continuing to build their theoretical edifice. If the experimental indications of a non-zero value for the cosmological constant come not only from the SN1a, but also of independent measures on the fluctuations of cosmic background radiation, what is its value?

The acceleration is very slow, which tells us that the value of the vacuum energy, though nonzero, is extremely tiny. The theoretical problem with the observed vacuum energy is that it is far smaller than anyone would estimate. According to particle theorists estimates, energy should be much bigger. But if it was, it would justly not be able to lead to this acceleration of SN1a so difficult to measure. With a huge energy, the universe would have collapsed long ago (if negative) or quickly expanded into the great void (if positive). That is what we call the "dark energy catastrophe".

Thus, these fascinating measures also present a significant enigma. At this is added the challenge of revealing the nature of dark energy, characterized by the cosmological constant.

The vacuum energy is precisely the favorite candidate but effectively, if so, the quantum physicists would prefer to see it multiplied by at least 10^{60} so that this vision of the cosmos suits to the standard model of the physics of particles [15]. Several models are possible, but the predicted value in most cases is 10^{122} times

above the limits prescribed by astronomical observation. The cosmological constant is comparable to the inverse square of a length. For the physicists of the infinitesimal, this length is interpreted as the distance scale at which the gravitational effects due to the vacuum energy become manifest on the geometry of space-time. They consider that this scale is the Planck length, or 10^{-33} cm. For the astronomers, the cosmological constant is a force of cosmic repulsion which affects the rate of expansion on the scale of the radius of the observable universe, which is 10^{28} cm. The ratio of both lengths is 10^{61}, which is the square root of 10^{122}.

The vacuum of the physicists is full of energy. Its energy fluctuations give birth to pairs of particles. During the history of the universe, whenever the interaction forces between particles change their nature, thus in every symmetry breaking, the vacuum cashed energy. Today, the vacuum energy, which constitutes the essence of the cosmological constant, should be much larger than the value predicted by the cosmologists.

The observed SN1a seem to say that these remaining two thirds of the critical density seem to exist in the form of a mysterious "dark energy" and to bolster up the inflationnaire cosmology. But their rate of acceleration may mean that the contribution of dark energy to the critical density is about 73%, two-thirds which miss so that the universe is flat, as predicted by the inflation theory, nevertheless this last one, as well as the model of particles or strings, have to explain why the universe's vacuum energy is as small as we know it must be. Their best models of unification, expected to make correct predictions in the field of elementary particles, lead to some absurd cosmological consequences, and they have no answer to this problem [16]. Thus, for theoretical physicists, the hope of reconciling their models and those of their colleagues' cosmologists flew away. Some physicists believe that there is no true explanation.

The so-called theories of quintessence were born to dissipate this conception: the cosmological constant is replaced by a variable field during the time, very high in the phases of the early universe, in agreement with the calculations of physicists, but falls very low during the cosmic evolution, according to the value measured by astronomers today. The quintessence field would evolve naturally towards an "attractor" conferring it a low value, regardless of its original value. Physicists consider that many different initial conditions would lead to a similar universe—the one which is precisely observed! But these theories require extra dimensions [8] [17].

Even if astronomers and cosmologists are probably right about the low predicted value of vacuum energy, and that it belongs especially to particle physicists of better understand the theories of unification and the true nature of the vacuum energy, we estimate that both groups are conceptually wrong. Physicists are deluded into believing that, if there was great energy at the beginning, there should be still a great energy today. On the other hand, cosmologists are mistaken in believing that the vacuum energy was always the same, almost zero. For them, there is no real empty vacuum in nature: constantly, particles are created

and annilihated virtually, what explains the presence of energy. To be connected to this low density of the vacuum energy which has never changed, they need a constant energy density that models the presence of a permanent cosmological constant.

In fact, if astronomers take the observations of supernovae and the microwave background and apply the theory of general relativity to them, they have a universe that corresponds to the magic omega number of 1; if particle physicists apply quantum theory to them, they get an answer that is about 122 orders of magnitude higher. Unraveling all this gibberish amounts in fact to tackling the problem of reconciling the physics of the immensely large-general relativity—and that of the infinitely small-quantum mechanics. The dark energy catastrophe is for the moment this abyss between the value of the density of the current cosmological vacuum which is worth 10 GeV/m^3 (or ~10 protons/m^3) and the energy density of the vacuum proposed by the quantum field theory which is ~10^{122} GeV/m^3 (~10^{122} protons/m^3).

5. A Variable Cosmological Constant within the Framework of the Theory of Relation

According to the theory of Relation, the force of gravity is not a force independent of the force of expansion. The two structures in our theory, the expansion structure and the condensation structure, represent the force of expansion and the force of gravity. Except that they are directly linked, one is engendering the other; the colossal energy of the force of expansion generating the force of gravity. It is the energy of the big bang that is transformed over the time of expansion into matter as we know it. There is not a coincidence infinitely improbable (and yet accidentally close to an infinite fraction near a point of equilibrium) between the immeasurable energy released at the time of universe creation and gravity, there is a natural transformation of energy (that of the cosmological constant which is also called dark energy) into matter. The fact that the expanding universe seems forever in a chaotic state of maximum entropy, and the fact that there are low entropy structures is not a big mystery; it is simply the transformation of the electromagnetic (em) energy of the big bang, which is continuously transformed into frozen matter, into gravitational energy. This is why the universe is decelerating.

A) Scenario of the theory of Relation

The question to know why the density of energy is so tiny finds answer within the framework of the theory of Relation [10]. This new theory uses a "cosmological inconstant", or a variable cosmological constant, which means a variable density energy during the cosmological time. It does not require the presence of extra dimensions: the universe has two complementary and interpenetrated structures and four dimensions (one of time and three of space). The structure of the condensation has the aspect of the Einstein's gravific space-time and electromagnetic matter, whereas the structure of the expansion has some aspects of

the Lorentz-Maxwell's flat em spacetime and ordinary matter.

Since the big bang, the em structure of the expansion—with the variable cosmological constant—is in decline, having abandoned his energy for the benefit of the increasing structure of the condensation, positive and gravitational. Throughout cosmological time, a perpetual annihilation of the negative energy-mass is transformed into a continual creation of positive energy-mass. The first structure of condensation represents the positive solution of Dirac's equation of energy, while the second structure of expansion express its negative energy solution which was eliminated by a mathematical trick [15] [18].

The negative energy-mass is assimilated to the cosmological constant or the dark energy. The variable density of dark energy takes the form of a variable cosmological constant directly related to the full energy that will become the minimal energy of vacuum. We can say that it starts with the energy of particle physicists, with 10^{120}, and leads to the almost zero energy of the astronomers, that is $\sim 10^{0}$.

Through the "principle of Compensation", the lost negative energy is transformed into positive energy [19]. Permanently, real positive particles (not virtual) are created, and all do not disappear (those corresponding to positive energy), hence the presence of a growing positive matter and a weakening vacuum energy. The principle says that the decreasing of the negative em energy-mass during the expansion induces a proportional and opposite increasing positive gravitational energy-mass. The em wave of spacetime is supported by an inhomogeneous vacuum filled of "minimal" negative energy perpetually in interaction with positive matter.

B) General characteristics of the theory of Relation

1) With the theory of Relation, it is not the dark matter which dominated from the beginning but an expansive dark energy. How does this anti-gravity manifest in the theory of Relation? It is as early as the big bang related to the density of the "full quantum" which existed in the earliest moments of the universe. This dark energy varies over time, hence the term "variable cosmological constant". The repulsive action of the full energy launches the universe starts in its infancy, between 10^{-35} and 10^{-32} sec, in a crazy phase of annihilation of dark energy and creation of ordinary and dark matter. Its huge negative dark energy is so transformed into positive energy/mass. It is at the same time energy, negative cosmological constant and arrow of time, because it creates space-time and matter. It is associated with the topological defects of the space bound to the various broken symmetries that the universe has experimented in the past. Dark energy empties its energy to reach the today's "quantum vacuum" or the cosmological "vacuum energy", which reconciles the particle physicist and the cosmologist.

2) The structure of expansion goes with dark energy. Globally, into the theory of Relation, our complex universe is dual: positive and negative. The negative part, which is a universe by itself, disintegrates, and "creates" our actual positive universe. The Compensation principle asserts that the permanent loss of nega-

tive energy of the expanding em wavelength of spacetime induces the positive gravific spacetime matter. Flat em spacetime can yield induced gravity to ordinary matter. Gravific spacetime matter produced by the expansion can flatten the em spacetime. The deep meaning of the Compensation principle is that when there is less em mass/charge repulsive force in the structure of expansion—going forward with the arrow of cosmological time—there is more mass/matter attractive force in the other structure [3] [19].

This said, according to general relativity, even in the absence of particles, the universe can carry energy known as vacuum energy, this energy has a physical consequence: it stretches or shrinks space. The positive vacuum energy accelerates the expansion of the universe, while the negative energy makes it collapse [20]. We do not contest this classification, but in the theory of Relation the positive vacuum energy and the negative vacuum energy have another meaning. The first structure of condensation represents the positive solution of Dirac's equation of energy**,** while the second structure of expansion express its negative energy solution [15]. (Let us say that in the expression $E = \pm mc^2$, $E = +mc^2$ represents the positive energy, while $E = -mc^2$ represents the negative energy. $E = -mc^2$ is considered just as a virtual energy, which is wrong, in our view).

So, in our theory, the negative vacuum energy means dark energy also known as cosmological constant, while the positive vacuum energy means the structure of condensation, with the positive matter which augments and the space which shrinks. It is the inverse of Einstein's classification.

3) The cosmological constant provokes the expansion of space and at the same time its positive pressure exerted inwards slows down its expansion. This is not the positive pressure that induced deceleration but the transformation of negative dark energy into positive ordinary energy that produces an "attractive" force of gravity. The repulsive force of gravity of the primeval universe is a colossal negative energy which would result from the presumable big crunch of a pre-universe. From 10^{-35} sec, we can say that full dark energy had brutally begun its transformation into "white" energy of the primordial vacuum.

The total energy of matter increases as the universe expands. Similarly, the total energy of the graviton increases with decelerated expansion of the universe because it takes energy to the cosmological constant. With the expansion of the universe, the loss of energy of photons becomes directly observable, because their wavelength lengthens—they undergo a redshift—and the more the wavelength of the photon lengthens, the less it has some energy.

Microwave photons of cosmic background radiation are thus redshifted during nearly fourteen billion years, which explains their long wavelength (in the field of the microwaves) and low temperature. In this sense, we have a "tired" dark energy, and the gravitons would have extracted some energy from the disintegrated dark energy. In short, as the expansion of the universe decelerates dark energy's negative cosmological constant gives energy to the gravitation of the positive matter, while the graviton takes energy to matter and radiation [9].

4) There is a transformation of the negative energy (the em spacetime wave, or

dark energy, namely the cosmological constant) into positive energy (ordinary matter + dark matter), and we have a gravitation (energy/mass) which increases with the cosmological time of expansion. The matter increases, so the total energy related to mass of the particle varies. There is creation of particles and therefore of energy/mass. (This does not violate the principle of equivalence: the "proper energy" of the particles is equal to their rest mass). What does not remain constant is the global mass which grows with the expansion. So, if R_U, t_o and M^o is the radius, the time and the mass of our universe:

$$R_U = t_o c = GM^o / c^2 \tag{1}$$

R_U, and M^o increase with time. The global mass continues to enlarge because the disintegration of the pre-universe after the big bang is not yet finished [3] [19] [21].

5) What is the contribution of dark energy to the critical density in the theoretical framework of the theory of Relation? The full dark energy transformed into white vacuum energy, born in about 10^{-32} sec after the big bang has left imprints on the CMB in the form of tiny density fluctuations resulting from small variations in temperature (the order of 0.001%) of this radiation. By scrutinizing these tiny fluctuations in temperature with telescopes perched on balloons or satellites (in particular, the WMAP satellite launched by NASA in 2001 [22]), astronomers have inferred that the amount of dark energy that was responsible for more than two thirds of the critical density. In addition to this evaluation of the density of energy, independently, physicists have determined the density of matter (visible and dark) of the universe. The apparent size of heterogeneities of the cosmic background on the bottom of the sky is partially determined by the overall geometry of the slice of space which separates us from it. This apparent size provides an indirect measure of the total density of the universe, and it appears that the quantities of dark and ordinary matter account for less than a third of the found value [9] [10].

Conscientious French researchers declared that to explain that the universe is Euclidian, such as was predicted by the WMAP satellite, we do not need the hypothesis of dark energy and that the density of matter, alone, is sufficient. It is however necessary to put the hand on this missing matter. This claim does not correspond to the theory of inflation [6]. In its framework, the concordance of the experiments is consistent with a very low-density matter and the apparent abnormal recession of SN1a led to a positive cosmological constant, sign of an accelerated expansion [23]. Its theoretical framework is consistent with the results of weighing of clusters, deriving from the study of the cosmic microwave background: an energy density of 73% and a matter density of 27%. This gives

$$73\% + 27\% = 100\% \tag{2}$$

and involves a constant density of dark energy, that is to say a positive cosmological constant, during time, since at least 6 billion years.

Nevertheless, it seems to us that the inflation does not correspond to the

theory of Relation, no more than a universe dominated by matter that would sound the death knell of dark energy. In the relationary cosmology, there is a negative "variable" cosmological "constant", in which dark energy density is reduced in favor of the density of matter consistent with the results of weighing galaxy clusters. We obtain

$$\underset{\text{Dark energy}}{(73\%-20\%)}+\underset{\text{Ordinary and dark matter}}{(27\%+20\%)}=100\% \tag{3}$$

This expression means that the energy without mass (without positive mass) of the cosmological constant that contributes about 73% of the critical density would decrease over time towards 50%. What is lost of the immaterial dark energy becomes mass, joins the 27% coming from ordinary and dark matter, and keep the positive matter growing bigger. This compensatory balance maintains constantly the total mass/energy of the universe at the full 100%. Such a process implies a continuous creation of matter throughout the cosmological time, translates a slowing down expansion and explains a variable cosmological constant (~73% → ~50%) which continues to fill the missing mass (~27% → ~50%).

Dark energy in the framework of the theory of Relation—with a variable cosmological constant with a maximum of dark energy at the beginning and a minimum of matter/mass—can not only reconcile the model of physicists but also resolves the same endemic difficulties that claims to solve the positive cosmological constant.

For example, the presence of a negative cosmological constant equal to about 73% of the critical mass allows, as well than a positive constant, to settle an annoying paradox: the present universe is very heterogeneous if one judge by the distribution of matter, nevertheless the expansion seems perfectly uniform in all directions. By using both constants, the contradiction disappears with an energy distributed in a homogeneous way and which would govern the expansion... Except that, in parallel, the dark energy of the positive constant carries back into the past the beginning of the cosmic expansion. If its value was large enough it could even repel it to infinity (big bang eliminated). Whereas dark energy of the variable negative constant can back up until Planck's time and space time and space, starting from the vacuum energy of the cosmologists to the full energy of the physicists [3] [21]. The Compensation principle reveals a hidden, evolutionary, variable symmetry which explains the above value but close to the zero of the current cosmological constant [19].

6. Distances on the Rise or Physical Process to Explain the Low Luminosity of the SN1a?

To explain the low brightness of distant SN1a, scientists had two choices: either a physical process weakened their radiation, or their distance should be revised upwards.

In 1998, the results of the weighing of galaxy clusters, those from the study of cosmic microwave background and the latter resulting from the observation of

distant SN1a, formed parts of a cosmic puzzle which matched to present the image of a nearly flat universe with a matter, whether dark or ordinary, which represented only ~27% of the critical density of the universe. Two international teams clamored that the luminosity of distant SN1a were 25% weaker than their close colleagues [11] [24]. When we observe such a supernova in another galaxy, it is enough to compare its visible magnitude with its intrinsic magnitude (brightness if is next to us) to know its distance. By decomposing through a spectrograph the light of those stars taken by the expansion of the universe, astronomers determine the redshift, and consequently their receding velocity. These two values, bound by the expansion which depends itself on the contents of the universe, showed a redshift higher upper to the predictions. Astronomers were quick to conclude that they are more distant than previously expected: it was a matter of distance [25] [26].

The results on supernovae gibe with the inflationary cosmology. Everything was held so that the expansion accelerates through a positive cosmological constant. Although the case appears heard for most astronomers, it seems problematic if not erroneous. The astronomers had considered *a priori* that the luminosity of SN1a is almost always the same: 5 billion times the Sun. But is the intrinsic magnitude of SN1a really constant?

This one is indeed known only due to the explosion models developed by astrophysicists. However, some mechanisms ruling the explosion are still misunderstood and some features of these models are still unprecise, what could modify the fragile value of the intrinsic magnitude that they predict. It is unclear, for example, if the explosion is due to a deflagration propagating slower than sound or to a supersonic boom. Such an uncertainty incites certain cosmological theories to postulate a variation of the constants of the nature, of which the constant of gravitation, although no observation or experiment showed some variation of G. A variable cosmological constant would be, however, more likely to change the value of the energy (and hence of the intrinsic magnitude) released by a supernova. Indeed, this energy depends among others on the reaction speed of some elements synthesized during the explosion such the nickel. If the cosmological constant, or the density of dark energy, does not have the same value at the instant of the supernova as it does today (contrary to what is usually assumed), the reaction rate and the chemical composition involving nickel would not be those envisaged by astrophysicists. There would be an evolution of the system overtime and the measures of luminosity of supernovae would then be corrected.

On the other hand, the result of the observations of the satellite XMM-Newton of Agency's European Space X-ray observatory (ESA) around 2003-2004 implies a decelerating expansion and excludes a distance in the increase to explain the excessive paleness of distant supernovae 1a [27] [28]. This is consistent with the theory of Relation.

Within the framework of the theory of the inflation, the concordance of the

experiments goes in the direction of a very low matter density and the apparent abnormal recession of SN1a led to a positive cosmological constant. The choice of a physical process that weakens the radiation of supernovae was quickly dismissed and astronomers opted for the scenario of an accelerated dark energy which would have taken the upper hand during the second half of the history of the universe. This scenario is difficult to check, unless we observe clusters of galaxies today and in the past when the universe was only half its current age. Indeed, in a world dominated by this strange energy which accelerates expansion, clusters would have a very hard time forming. Galaxies too far apart would not even be able to assemble. Very early in the history of such a universe, no more clusters of galaxies would form. Those we see today would have been formed in the distant past. The question to be answered to determine the existence of dark energy was simple: yes or no, were clusters of galaxies formed in the second half of the life in the universe? It turns out that the XMM-Newton has returned data about the nature of the universe indicating that the universe must be a high-density environment, in clear contradiction to the "concordance model" relying on the theory of inflation. In a survey of distant clusters of galaxies, the results of the satellite revealed that today's clusters of galaxies are superior to those present in the universe around seven thousand million years ago. Such a measure logically inclines toward a decelerated expansion.

For his part, the American astrophysicist Bradley Schaefer obtained a result of the relation distance/luminosity which determines an inconstancy of the density of dark energy [29]. His idea was to use some gamma ray bursts (GRBs) as distance indicators which would mark out the distant Universe. Hundreds of times brighter than supernovae, GRBs can indeed be detected at distances much greater than these. So they would probe the dynamics of the expansion in an age of the universe very old and still poorly known. In this purpose, he began to analyze gamma-ray bursts detected by satellites Swift and Hete 2. Schaefer said he established the distance of 52 GRBs to about 12.8 billion light years. He compared the intrinsic intensity of the 52 gamma flashes with the intensity seen from Earth, determined their distance and established a relationship between this one and their luminosity. He found that the bursts to the same distances as the distant supernovae are fainter and therefore further that if the current expansion of the universe was decelerating, thus confirming the acceleration recorded using SN1a. In contrast, the most distant bursts at distances much greater than those where SN1a can be observed with present techniques seem rather more brilliant and therefore closer than expected if the acceleration was due to a cosmological constant. Since the brightness of 52 GRBs measured until the borders of the universe is too intense for the accelerating expansion is due to the cosmological constant, Schaefer concluded that the density of dark energy, instead of being constant, had to vary.

This finding does not seem to stand out from the current framework of accelerated expansion and from increase of distance to explain the low luminosity of the distant SN1a [30] [31]. The fact remains that astronomers know—while ac-

knowledging not knowing enough about the secrets of exploding supernovae to be sure of their luminosity—that the synthesis of heavy elements in stars was different in the past from what it is today. It is therefore likely that the bursts due to the older stars have had at their disposal a larger reservoir of energy at that time. Ultimately, if the most distant bursts are the brightest, this is due rather to the evolution of objects that are at the origin than to the expansion.

Let us underline that Jayant V. Narlikar showed at the beginning of the years two thousand that the observed SNIa explosions, that were looking fainter than their luminosity in the Einstein-deSitter model, could be explained by the presence in galaxies of a certain type of dusts, forming needles. The absorption of light by the inter-galactic metallic dust would extinguishe radiation travelling over long distances. The galactic dusts would be produced by condensation of iron rejected by previous generations of supernovae. Explanation which has the merit of being based on facts, since laboratory experiments show that indeed this type of condensation produces needle-shaped [32] [33].

If the question of the absorption of light by the metallic dust ejected from the explosions of supernovae is generally ignored in the standard approach, which of a process of "tired light" which would weaken the luminosity is completely ruled out. The tired light is a theory proposed by Albert Einstein to reconcile its hypothesis of static universe with the observation of the expansion of the universe. Einstein had emitted the hypothesis that light could, for an unspecified reason, lose energy in proportion to the distance traveled, hence the name of "tired light". The term was coined by Richard Tolman—as an interpretation of Georges Lemaître and Edwin Hubble who believed that the cosmic redshift was caused by the stretching of light waves as they travel in the expanding space. Fritz Zwicky in 1929 suggested, as an alternative explanation to an expansion which derived from the observation of a redshift proportional to the distance of the galaxies, that the shift was caused by photons which gradually lose energy with the distance, probably because of the resistance to the gravitational field between the source and the detector [34]. Obviously, the ideas of Einstein and Zwicky, in a supposed static universe, were quickly ruled out.

With the theory of Relation, a form of "tired light" is indistinguishable from the assumption of a decelerated expansion of the universe with a variable cosmological constant. We are talking about the presently undetectable radiation of dark energy. Note that the tired light of this theory has nothing to do with the traditional model of light tired of the static universe in irreconcilable contradiction with the expanding universe. In the case of primeval photons, the tired light is also connected to the expansion of the universe. Today the distribution of these photons presents a blackbody spectrum from the hot and dense phase experienced by the early universe. Due to the expansion, of a thermal imbalance with a temperature that decreases with cosmic time, the blackbody spectrum of CMB observed by the COBE satellite in early 1990 is similar but not identical to that of the recombination, approximately 380 000 years after the big bang. The photons

during the expansion would have lost energy (collected elsewhere), changed frequency without being deformed, as evolve the cells of a living body between the early youth and the advanced age [19] [35].

6.1. The Effect of Dark Matter on the Expansion of the Universe

According to most cosmologists, dark matter, which contributes about 24% - 25% of the content of the universe, has coexisted since the big bang with ordinary matter (4% - 5%) and dark energy (72% - 70%). They postulated that even before the epoch of radiation, and in later epochs, dark matter was the dominant species [36]. It gathered the cosmic structures and held them together. The more dark matter there is, the more gravity there is. Gravity keeps galaxies relatively close together and objects in them should be brighter because they are closer. In the case of a slowing of the expansion, one expects to find that the most distant supernovae are a little brighter than their close sisters. When 16 supernovae from the *High-z Supernova Search Team*, added to the 42 from the *Supernova Cosmology Project* (SCP) were detected at distances amounting to billions of light-years, their luminosity was not stronger but, on the contrary, 25% lower than that of their close counterparts. To explain this phenomenon, the scientists deduced that the speed of expansion was increasing: the expansion of the universe was accelerating.

The theory of Relation does not share the vision of an accelerating expansion under the pressure of a dark energy and dark matter preponderant from the origin of the history of the universe. We have previously suggested that there was almost no dark matter at the beginning of the universe [3] [19], that it appeared gradually in the cosmos, and we have tried to understand the nature of this major constituent of the universe [37] [38]. We assume that there was much less dark matter a few billion light years ago. Gravity therefore bound planets, stars and galaxies less strongly. The latter were more distant from each other and the objects in them must have been less bright because they are more distant. The latter were further apart from each other and the objects in them must have been less bright because they are more distant. In the case of an expansion at a steady rate, the remote SN1a discovered should be less bright than expected. This was the case. This suggests that they are closer and that the expansion is decelerating.

6.2. Acceleration of Expansion beyond a Reasonable Doubt; Rejection of Physical Processes That Can Explain the Pallor of SN1a

To determine simultaneously the distance at which a luminous object is and its speed of distance, it is necessary to know the luminous intensity of the emitted waves, called intrinsic luminosity, and to compare them with the received waves, called apparent luminosity. The latter decreases as the square of the distance from the source. As for the speed of distance, it is determined by the wavelengths received and their shift is due to the Doppler effect. Until the observation of type 1a supernovae about 9 billion light-years away at the edge of the un-

iverse, everything seemed normal: the more distant a supernova was, the weaker its luminosity was following a roughly linear curve. In the case of a slowing down of the expansion, we should have noticed that the most distant supernovae were a little more luminous than their close counterparts. In other words, these supernovae should have been a little less far away than if the expansion had kept a constant pace and appear comparatively brighter. The opposite was the surprise, the brightness was 25% lower. Astronomers concluded that they must be further away, as if the universe had stretched a little further than expected, and that the expansion was accelerating.

Two physical processes that could have caused this decline in apparent luminosity were quickly ruled out.

First process: a part of this light would have been absorbed on its way by matter in the form of gas or dust.

This explanation was dismissed by saying that, since these dusts absorb more blue light than red light, these supernovae should have had an "excess of red", which was not the case.

However, we mentioned Narlikar in section 6 who explains this non-excess of red by the presence of an interstellar metallic dust in the shape of a needle capable of absorbing all wavelengths. If one considers the absorption by the inter-galactic metallic dust which weakens radiation travelling over long distances, then the observed faintness of the extra-galactic SN1a can be explained in the framework of the Einstein-deSitter model, without any dark energy. Non-exotic metallic dust, since it was produced by laboratory experiments [32] [33].

Second process: supernovae were less luminous in the past than they are today.

The astronomers also ruled out this hypothesis, because the lack of luminosity remains the same, whether the supernova is old or not.

Let us recall that Henrietta Leavitt's cepheids were also intended to play the role of "standard candle", and that they had to be split into several classes with different properties. Even if nature makes classes of stars, it does not make two identical supernovae. We know that the first supernovae were of a different chemical composition from the following ones since the generations of stars had not yet succeeded one another to manufacture the heavy elements. This suggests a non-uniformity of SN1a; intrinsic luminosities whose absolute magnitude varies according to properties. How can they say that the supernovae of the past with a different composition from the following are the same as those of now?

In order to find out what could stretch space in this way, Einstein's cosmological constant was unearthed, which allows, mathematically, to introduce into space a negative pressure force that accelerates the expansion. This positive constant calls for a huge constant—in the form of dark energy—which would imply that the universe would have expanded so fast that no structure at all could have formed. In fact, general relativity applied to supernova observations and cosmic

microwave background leads to an almost zero value. The existence of galaxies seems to accommodate this limit. For its part, quantum theory also requires a huge cosmological constant. The limits it predicts for accelerating the expansion and obtaining galaxies are of the order of 120 orders of magnitude greater than the value calculated by general relativity.

This prediction, already qualified as the worst prediction ever made by a scientific theory, indicates that something remains deeply misunderstood. This model of the big bang, which is that of a "preposterous universe", must be revised in its foundations. Hence the theory of Relation.

7. Supernovae and Pvlas Experiment

Aside from negative pressure dark energy, there are astrophysical processes that could affect the measurements and explain why distant supernovae have been observed to be fainter than what is expected in a matter dominated universe [39]. We are discussing here a less exposed argument, although touched upon, the PVLAS experiment [1] [2]. This is a physical process supported by an earthly experiment likely to explain the dimming of the apparent luminosity of SN1a. The general idea is that the latter lose their luminosity through interactions with cosmic magnetic fields, just as the laser of the PVLAS experiment loses photons when crossing a magnetic field [40] [41] [42].

On one hand, we have the Italian physicists of the PVLAS experience who studied in 2000, in a laser device, the way a magnetic field affects the propagation of a beam of "polarized light". The waves of this type of light oscillate on the same plane, characterized by an angle. Theoretical models predict a slight modification of this angle, because a small number of photons are deflected by the magnetic field and disappear from the beam. Except that the variation that the Italian physicists observed was ten thousand times greater than expected. They spent the next five years to verify this result, so much the stakes were potentially important. They acquired in 2006 the certainty that the strange phenomenon they had observed at the beginning of the millennium is not the result of a bias.

On the other hand, we can briefly say that supernova has roughly the volume of the Earth, the mass of the Sun and luminosity five billion times that of this last one. And therefore, one can easily conceive that the light emitted by a SN1a can be as brilliant and coherent than the laser, if not more.

Laser light has special and exceptional qualities which rank it in a separate category. At first, this light is extremely intense: much more than the Sun. It is monochromatic and pure, that is to say of a single color and the same energy for all the photons of the beam. It is temporally and spatially "coherent" because the time interval between the passage of a crest of a wave and that of the next is always the same. Finally, it is directive: the laser beam is very narrow and spreads very little. The SN1a constitute, despite differences, the candidate who can best resemble the laser light [43] [44].

In 1916, Einstein remarked that an electron located in a low energy level can absorb a quantized energy $h\nu$ and jump into an upper level; if the same energy

$h\nu$ is then received by the atom, it cannot be any more absorbed because the electron is already in the high energy level; Einstein then anticipated that the atom will behave as if it still wanted to absorb this energy: as it could not do, the excited electron will return to the fundamental state by emitting the energy $h\nu$: we say that this energy is stimulated—the total energy emitted by the atom is thus $h\nu$ not captured + $h\nu$ stimulated = $2h\nu$ [45] [46] [47]. We can compare a SN1a, which corresponds to the explosion of a white dwarf star after the accretion of matter and wave carrying the energy $nh\nu$ extracted from a close giant star, to an atomic system with "scales" of energy.

The SN1a form a relatively homogeneous class of objects, both in their mechanisms of explosion and in their spectroscopic and photometric observed characteristics. Their standardisable character authorizes to use them to build a diagram of Hubble permitting the determination of the cosmological parameters [48]. Due to the low dispersion of their maximum of luminosity in the spectral band B and their important luminosity which allows observing them at very high-redshifts, they have become the "standard candles" to measure great distances and constrain the cosmological parameters. Their maximum luminosity presents 40% dispersal, which is still largely homogeneous. Like laser, which is a macroscopic quantum object, a SN1a emits photons which have almost all the same wavelength, are almost all in phase, move all according to parallel paths. Their luminous waves are waves where the radiation emitted by atoms is synchronized between them [49] [50].

The light from supernovae, assimilated to a laser beam, suggests a supernova-amplifier of em waves based on stimulated emission, which would cross through cosmic magnetic fields by losing some energy-luminosity, like the PLVAS lasers [51]. The radiation of the supernovae which inevitably passes through the magnetic fields of galaxy clusters, stars, and interstellar space, gives up photons, which would be transformed into dark matter. The brightness of an em energy that loses photons and frequency in the long run, without its speed of light being affected, can only wane.

We would so obtain, corroborated by the PVLAS experiment, a kind of tired light that weakens the brightness of supernovae. If the most distant supernovae are fainter than expected, this would come from the fact that, at such distances, losses of luminosity by "tired energy" were able to finally be detected. And this observational bias could constitute a method to establish a distance-luminosity relation in the distant universe, predict a change in the density of dark energy and play a crucial role in the determination of the constancy or not of the density of dark energy.

Since the confirmation of the experience PVLAS, physicists have been particularly obsessed with the creation of axions in order to demonstrate the existence of dark matter. Is it the fear of a bad incidence on their conclusions that prevented the astronomers from imagining that a similar physical process can weaken the luminosity of the "cosmic probes"?

8. The "Centrist" Cosmological Principle and the Deceleration of the Expansion of the Universe

The cosmological principle states that all points and directions in the universe are more and less equivalent, and thus that the universe is, at least on large scales, homogeneous and isotropic. Given the cosmological principle, the Copernican principle concludes that there is no center of the universe [52]. Adopted by the theory of relativity, and then became the cornerstone of the building of the standard big bang, the Copernican cosmological principle leads—in agreement with the interpretation of contemporary astronomers—to the acceleration of the expansion of the universe.

The theory of Relation finds that the cosmological principle suffers from incompletion, and it is this insufficiency which led, in our opinion, to the blunder of the acceleration of the expansion of the universe. Karl Popper criticized the cosmological principle on the grounds that it makes "our lack of knowledge a principle of knowing something". According to him, cosmological principles were dogmas that should not have been proposed [53]. Recent findings have suggested that violations of the cosmological principle exist in the universe [54]. Evidence from galaxy clusters [55], quasars [56], type Ia supernovae [57] and anisotropies in the cosmic microwave background (temperature fluctuations and variations in the densities) suggests that isotropy is violated on large scales. A number of observations have been reported to be in violations of homogeneity of the cosmic microwave background over cosmological scales [58]. It is not the purpose of this section to debate whether the expansion could have been anisotropic—occurring in some preferred directions and allowing contraction in another direction—or inhomogeneous with some regions denser than others.

8.1. The "Centrist" Principle

Instead, the theory of Relation proposes to include a "centrist principle" into the cosmological principle, in addition to the Copernican principle. This principle can be confused with a new geocentrism that Physics has been striving to reject since Copernicus. In fact, it translates a neo-geocentrism: our representation of the universe cannot avoid, in order to be coherent, to include a privileged center from where the history of the world originates.

The existence of the universe is subordinated to the existence of a Word (*i.e.*, a generator of things) in this universe. This Word is the original center of the universe, namely the big bang, an extremely condensed state that has been expanding for about fifteen billion years. This privileged central point gave birth to all the points of the universe. It is quite relative, if not false, that every point in the universe is central and gives birth to the universe.

Unlike the Copernican principle, which uses a spatial length (or "spatial space") with an everywhere simultaneous factitious time, the centrist cosmological principle leads to the deceleration of the expansion of the universe. If astronomers had remembered that into space "seeing far means seeing early", they

would have been aware of using a temporal length with acceleration to the past, to the beginning. And that the reversal towards us, towards the direction of expansion, towards "here and now" of the current epoch means a slowdown of the expansion of the universe.

8.2. The "Centrist" Cosmological Principle and Temporal Length

The temporal length (or "temporal space") of theory of Relation is characterized by a space-time with an irreversible cosmological time during expansion. The "centrist" cosmological principle concerns the spherical symmetry around the point of the singular origin which will be called the big bang (but which is the point of Planck supposed to mark the origin of theoretical time at the first millionth of a second approximately after the creation event). Centrism therefore refers to the beginning of the universe which becomes the center of the observable and unobservable universe. The cosmos at different times keeps the same center evolving to form the arrow of expansion, so snapshots taken at different times look like different sized enlargements of earlier snapshots. We formulate the cosmological hypothesis that the observers of an epoch occupy a privileged position to observe the center of the universe. This assumption is called the *centrist principle*. It implies a cosmological history where the energy of electromagnetic radiation which resulted in the cosmic microwave background radiation must be taken into consideration; case discussed by the theory of Relation which questioned the expansion of the universe from a hot state of thermal equilibrium to the universe we observe today, about 15 billion years after the big bang. The theory of Relation uses an equation of the universe with an irreversible cosmological time that unites Planck's time with present time [3] [21].

With theory of Relation, the starting matter-energy of expansion is at the speed of light. Then the speed of expansion decreases as energy is transformed into matter. There is a rapid deceleration at first and then more and more slowly. Light always propagates at speed c but the wavelength increases and the frequency decreases to form the cosmic microwave background (CMB). Although energy transforms into matter throughout the expansion, the hypotheses of homogeneity and isotropy can be considered, even approximately, to be valid since the matter-energy density of the Planck era. Spacetime of the theory of Relation offers a spatio-temporal framework with stratified epochs of locked states. This supposes, for each of the overlapping epochs, the invariance of the laws in the displacements of each of the coordinate systems. Any point arbitrarily chosen at an epoch is equivalent to any other choice from the point of view of the fundamental laws of physics; all observers are Copernicans since they occupy no privileged place.

But by recentering the big bang point as the center of the world, these observers are no longer equally qualified to serve as the origin of the coordinate system since there would be a particular origin to which to compare the positions of other objects [59]. The observer at the origin of an electromagnetic space-time

"sees" towards the future all the Copernican observers, who everywhere here and now "see" him at the very beginning. The finite speed of light means that we always look at the universe as it was in the past, rather than as it is in the present. According to the Copernican cosmological principle, "here and then" is the same as "there and then" (then meaning previously), which means that from any point in the present epoch time has the same past no matter the distance to the past. In this sense only, one can speak of temporal length for relativity. In the theory of Relation, "here and then" and its spatially opposite equivalent "there and then" imply a real temporal distance since the time of this spacetime has everything to do with the past, as advent and fading, in connection with the continuing succession to the past, and vice versa to the future [60].

This makes that the travel backward through expansion time goes from the currently estimated speed of the expansion to the speed of light of the beginning. There is an increase in speed going towards the beginning and the observed apparent brightness of SN1a, weaker than expected, only accentuates the acceleration towards the origin (assuming only the distance is involved). If, conversely, we position ourselves at the origin to follow the expansion towards the present epoch that is part of the horizon, we can only go from c towards the lower present speed by following the arrow of cosmological time. Thus interpreted, the pallor of the SN1a only accentuates this deceleration.

The centrist principle incorporates the concepts of isotropy and homogeneity of the cosmological principle. Like the Copernican principle, the centrist principle adopts the paradigm of the cosmological principle. The Copernican principle does not claim that the center does not exist, only that we are not there. From this principle, we should expect that we are not at the center of anything, much less some universal cataclysm. The centrist principle says that the center exists and that we can imagine being at the center: a special place, if only for the sole reason that it is unique.

Imagine being near the region of the early universe where the big bang happened and watching as it expands. By the cosmological principle, this volume must be completely representative of the universe as long as it is sufficiently large for true isotropy to prevail. In the beginning, the density and temperature were very high, and everything was in the state of electromagnetic radiation. This light at several billion degrees absolute was gradually transformed into matter, *i.e.*, elementary particles. The universe was opaque: radiation and matter were constantly exchanging energy. As the universe expanded, cooled and diluted, there came a time when radiation stopped interacting with matter and the universe became transparent. The universe was opaque: matter and radiation constantly exchanged energy. As the universe expanded, cooled, and rarefied, there came a point at which the matter ceased to interact with the radiation, and the universe became transparent. Since the decoupling, the cosmic radiation has evolved independent of the matter: these cosmic photons are neither created nor destroyed; they simply stream through space in all directions. They constitute a cosmic background radiation (CBR) as a relic from a hot, dense phase in the

early history of the universe. The CBR provides evidence for the big bang, can tell us about the conditions in the very early universe and is also the best evidence we have that the picture adheres to the cosmological principle. A truly homogeneous and isotropic big bang should produce a relic cosmic background that is a perfect blackbody in all directions, excluding any possible interactions with matter lying between its distant source and our radio antennas [61].

According to the centrist principle, temporal space is isotropic and homogeneous. We can imagine the expansion of the universe as an arrow of time [62] [63] made up of epoch-points in the direction of the future (line in the direction of movement). The density of matter changes with time, and the space of this arrow (it constitutes the radius of the universe) has asymmetries since it does not remain identical to itself if a translation or a rotation is carried out. The existence of homogeneous and isotropic spaces defines a class of privileged, central and fundamental observers, those whose universe line straddles this arrow of time at all points. These observers are a mathematical and theoretical construction, and their existence is necessary insofar as they define and measure the theoretical reference time of this temporal arrow, called cosmological time. In theory of Relation, the measured cosmological time depends on the state of motion of the expansion of the universe. Any observer will have to determine his movement in relation to these central observers.

Allow us the following technical remark. As each point represents an epoch, the matter remains isotropic and homogeneous for this point-epoch. The line of spatial space of this point is perpendicular to the line of the universe constituted by the arrow of time which runs from the past to the future: such a space for a particular epoch is Copernican, has symmetries since it remains identical to itself if a translation or a rotation is done. Relativity applies for each era in particular: the density of matter is the same at all points, no observer occupies a privileged position in space and a theoretical cosmic time of reference makes it possible to measure the movement of one observer in relation to another.

The centrist cosmological principle is therefore a generalization of the universe as a whole from the non-Copernican point of view: any creature or observer at the beginning occupies the privileged place in the universe. The reappearance of the concept of the center of the world leads to that of its limits: our universe is not infinite and with the deceleration of expansion the universe is heading towards a tipping point, towards a big crunch.

8.3. The "Copernican" Cosmological Principle and Spatial Length

The cosmological assumption that we do not occupy a privileged position in space is called the *Copernican principle* [64]. According to this principle, space is isotropic and homogeneous. The density of matter is therefore the same at all points but may possibly change over time. Such a space therefore has symmetries since it remains identical to itself if one performs a translation or a rotation.

According to the Copernican cosmological principle of the theory of relativity,

"here and now" is the same as "there and now". This means that time has the same present whatever the distance, which implies that time does not express becoming or the past and has the appearance of duration, that is to say that it has an aspect of conservation, permanence, and stability. We can speak here of a spatial distance since the time of this space-time has nothing to do with the continuous succession. The time of this space-time is perfectly reversible just like this space-time itself.

The Copernican principle is a cornerstone of general relativity and much of astronomy: not only do we not live in a special part of the universe, but there are no special parts of the universe—everything is the same everywhere. There is equivalence between "here and now" and "there and now"; equivalence between "here and then" and "there and then". The observers are spatially opposed but the time is the same, as if it did not exist, which means that the speed of the expansion goes from ~0 to ~c, towards the horizon, towards infinity. If we reverse the positions, we cannot go from ~c to 0. We go from ~0 to ~c again and always since "here and now" is the same as "there and now". It is a spatial space directed from all sides towards the infinity of the horizon: if, in addition, an excessive pallor is added to the SN1a, this only further confirms the acceleration of the expansion of the universe towards the big freeze.

8.4. Einstein and the Copernican Cosmological Principle of Homogeneity and Isotropy

The cosmological principle of homogeneity and isotropy, in accordance with the Copernican principle, was implicitly formulated by Albert Einstein in 1917 when he was looking for solutions to the equations of general relativity describing the universe considered as static. The observations were limited to the Milky Way because no object located in our galaxy had been identified as such. It has the consequence that Man does not occupy a privileged position in the spatially homogeneous universe; that is to say that his general appearance does not depend on the position of the observer.

After much trial and error—de Sitter, Friedmann, Lemaître and the proof of expansion by Hubble in the late 1920s—Einstein presents in his 1945 memoir entitled *On the Cosmological Problem* (appendix to the second edition of *The Meaning of Relativity*) [65], the conception of a uniform distribution of matter on a very large scale in the universe and the explanation by general relativity of an isotropic recession of the galaxies, in agreement with all the relativist cosmologists of the time and in good understanding with the investigation of Hubble and its successors.

In fact, the Copernican cosmological principle concerns spatial space. But as far as temporal space is concerned, Einstein quickly understood the difficulty of a cosmic history and a singular origin that we will call big bang**.** He never considered the case where the energy of radiation should be taken into consideration, a case that has since been discussed by cosmologists who wonder about the structure of the early universe. For the creator of the theory of general relativity,

this singular origin (big bang) is a mirage which results from the fact that one unduly extends the domain of validity of spatial space to the domain of temporal space, because, beyond a certain density of matter-energy, the hypotheses of homogeneity and isotropy can no longer be considered, even approximately, as valid.

8.5. The Big Bang and the Centrist Principle

In keeping with the theory of Relation, the Copernican cosmological principle is unacceptable with regard to the dynamic theory of the big bang. This principle implies that the spacetime of relativity and the spacetime of the big bang theory are interchangeable concepts when they are not. And therein lays the physical flaw: they respond to specifically different realities, since one can conceive of a space-time whose reversible time is a perpetual "now", whether here or there at the other end of the world, and a space-time whose arrow of time going from cause to effect is irreversible. This arrow of time is due to the initial conditions: the universe began in a state of low entropy and the arrow is determined by the inexorable increase in entropy, an increase which is observed in all macroscopic occurrences. What provides a past and a future for the universe is that it began in a state of low entropy; it makes the past distinct from the future. The cosmic time of general relativity has nothing to do with the cosmological time of the big bang that we find in the formula of the theory of Relation.

Above, we imagined being near the region of the early universe where the big bang occurred and watching its expansion. Observations indicate that the universe has many special epoch-points in the arrow of time and evolves with cosmological time. The universe of our epoch is filled with numberless galaxies, organized into huge structures stretching over millions of parsecs. The galactic spectra provided redshifts giving the information that the galaxies were nearly all receding. There is a systematic increase of redshift with distance and nearly all cosmologists agree that the data present support for the interpretation that the major contribution to the redshifts of distant objects is the cosmological redshift due to the expansion of space itself. From the centrist principle, we should expect that we are at the center of everything, even more of a universal bang, unlike the Copernican principle that we are not at the center of anything, much less some universal explosion. The Hubble flow, *i.e.* the overall motion of galaxies away from one another, due to the general expansion of the universe is quite clearly consistent with the cosmological principle [61]. Only by appealing to the cosmological principle can we affirm that the same laws of physics discovered on Earth also apply to distant galaxies, and that all objects, regardless of the temporal or spatial distance separates, are composed of the same fundamental substances that we find on Earth and in its vicinity.

The Copernican cosmological principle theoretically leads in relativity to the equivalence during expansion between temporal length and spatial length. But this equivalence is in fact only valid for the spatial length that leads to the spatial infinity since the temporal length to the past means nothing given that this time

is both a "now" without change and a change without time direction. Einstein distinguished well between spatial space and temporal space but preferred to consider the latter as a mirage without reality, which is a mistake. The other fault comes from current cosmologists who wanted to be more Einsteinian than Einstein himself by no longer distinguishing the difference between spatial space and temporal space. They employed the "*perfect*" Copernican cosmological principle which implies that temporal space is the equivalent of spatial space [66]. They stated that the universe is identical to itself in each of its points and at all epochs, a different hypothesis from Einstein's cosmological principle which states that all points in the universe possess the same properties at a given epoch. In our opinion, this double aberration which perverts the cosmological principle constitutes the major contemporary cosmological error.

8.6. The Expansion of the Universe: One Foot on the Accelerator, One Foot on the Brake

Here we are again with a center, no longer of the Earth or the Milky Way, but of the universe. This suggests a privileged direction. Which? Undoubtedly, that of the irreversible arrow of cosmological time which points from the past towards the future during the expansion. And this "temporal" cosmology undeniably presupposes a "centrist" cosmological principle. One can have the vision of a central and privileged observer using an "irreversible" space-time which opposes an observer who uses a "reversible" space-time where "here and there" always have the same "now": "spatial" cosmology which uses the Copernican principle is not equivalent to "temporal" cosmology which uses the centrist principle.

When spatially opposed observers of an epoch, for whom reversible cosmic time is the same for all, claim to have the same past, they fall straight on the arrow of the single time that crosses all epochs and defines the entire observable universe. The irreversibility of this central arrow, as shown by the basic equation of the theory of Relation [3] [21] is inscribed at all levels, from the simplest of quantum objects—the hydrogen atom—to the universe itself, born of an entropic explosion. One then no longer flounders in the Copernican principle which has become synonymous with the cosmological principle; one has the obligation to graft the centrist principle as well to the cosmological principle so that irreversibility has a fundamental meaning within physics.

The centrist principle rehabilitates the standard cosmological model from before 1998 which predicted a deceleration. The expansion that decelerates from the original center towards us means that one could explain the unexpected pallor of the distant SN1a compared to the brightness of the closer SN1a simply because the former are closer to the center with a higher speed, and that the second are closer to us with a lower speed. A drop in speed coming towards us would explain the difference in brilliance. The experimental discovery in 1998 of the acceleration of the expansion of the universe by dint to the observation of distant supernovae was precipitated and erroneous because cosmologists speak of an expansion which they are at the same time unable to describe correctly since

they do not make a distinction between "spatial space" and "temporal space". They do not know if it is a spatial expansion towards infinity or a temporal ascent towards the origin.

All in all, here we are with an expansion of the universe which has, in accordance with interpretations of the cosmological principle, both one foot on the accelerator and one foot on the brake, like Schrödinger's cat in a state at the same time dead and alive. One of the predictions of the basic equation of the theory of Relation is that the expansion of the universe can only decelerate.

9. Discussion and Conclusions

Since its discovery during the late 90's, the dimming of distant SNIa apparent luminosity has been mostly ascribed to the influence of a mysterious dark energy component. The discovery was able to confirm the ideas of inflation and the acceleration of the expansion. Cosmology has achieved its inflationary version of a standard model, called the "cosmic concordance", within the strongly tested framework of the hot big bang model. However, in this paper we argue that the official declaration of the astronomers in 1998, to the effect that the expansion of the universe accelerates, was precipitated and erroneous. Furthermore, a drawback to their conclusion: The dark energy component or a positive cosmological constant represents, in the current "concordance" model, about 73% of the energy density of the universe. Nevertheless, a cosmological constant is usually interpreted as the vacuum energy and current particle physics cannot explain such an amplitude approaching zero. No theoretical model, not even the most modern, such as supersymmetry or string theory, is able to explain the presence of this mysterious dark energy in the amount that our observations require. On the other hand, if dark energy were the size that theories predict, the universe would have expanded with such a fantastic velocity that it would have prevented the existence of everything we know in our cosmos. This negative pressure fluid remains a serious weakness known as the cosmological constant problem. We dubbed it the "dark energy catastrophe" [23] [30] [31] [64].

We propose the theory of Relation with a variable cosmological constant, which explains the early universe as well as the state of the current universe, and which leads to a deceleration of the expansion, what has the merit to resolve the paradox of the cosmological constant. The expansion of the universe is so likened to a positive pressure and to a negative cosmological constant. It has decelerated steadily throughout cosmological time due to the presence of dark energy that varies down in favor of a matter/mass which does not stop growing since the beginning.

The accelerated cosmic expansion of the universe is mostly based on the apparent faintness of the distant SN1a. Two means were available to explain the wanness: revise the distance on the rise, which means acceleration, and the physical process which means a deceleration. The astronomers hurried to accredit the distance on the rise which was consistent with the theory of inflation.

They have disregarded arguments brought by several physicists-theorists and experimentalists (XXM-Newton) that foster physical processes.

We subject an argument susceptible to explain by a physical process the decline of the visible luminosity of SN1a. It is about the PVLAS experiment which revealed a loss of intensity of the luminosity of laser radiation in a magnetic field. Further to this experiment, physicists have struggled to discover the mysterious particle of the dark matter which would explain the loss of photons. They seemed to be obsessed by this single issue, without even considering that light from distant quasars and supernovae could also lose brightness when it passes through the inevitable cosmic magnetic fields. If the loss of photons experience PVLAS was ten thousand times greater than expected, and if it is appropriated to compare this laser experience with the radiation of SN1a, we can therefore hardly doubt that this is a physical process of "tired light" which increases the redshift, weakens the apparent brightness of SN1a, what indicates a deceleration of the expansion which excludes the increase in distance.

We bring the philosophical "centrist" assumption. It is opposed to the philosophical Copernican assumption which postulates that there is no privileged point of view in the universe. The Copernican principle has spawned the cosmological principle of isotropy and homogeneity, which has never been tested, on which is built the big bang edifice and is based relativity. The resulting interpretation leads to negative pressure dark energy or a positive cosmological constant, implying the worst prediction in physics: the discrepancy of ~122 orders of magnitude between the energy density of the vacuum observed by astronomers and that predicted from the calculation of particle physicists. We think it is necessary to consider a centrist principle that coexists with the Copernican principle, in order to include the arrow of irreversible time of expansion that marks the history of our universe. A Copernican observer from any point of a particular epoch uses reversible cosmic time that gives all the space to a spatial space directed towards the horizon (towards the future). One of the aspects of this time implies that physical causality ignores any dissymmetry between future and past, any distinction between "cause" and "effect". This same Copernican observer becomes a "centrist" observer when he gives way to a temporal space that uses an irreversible cosmological time that accelerates through all epochs towards the original radial center. (This going back in time corresponds to the contraction phase while the opposite, the current expansion phase, is our reality).

Relativity has contributed a great deal by clarifying that the change in mass depends on the relative magnitudes of space and time; that time is a sequence of events which follow one another in a determined place, like a succession, in space, of points on a line. But it has obscured a great deal by accustoming us to consider as an illusion the idea that time is a succession of states which embrace the universe; to estimate, like a geocentric point of view of the Middle Ages, the world which, in its duration, would be composed of a continuous succession of locked epochs, like slices, as if the history of events were stratified. The instanta-

neous events of each epoch form a state, or a stratum. The "now" epoch represents one of these strata extending through the history of the universe. The ordered succession of these strata forms the whole of reality [67]. It is partly the interpretation of the succession of events of spatial order with a relative and local time (which we do not reject), to the detriment of a succession of events of temporal order with a universal time, which has led to the scientific catastrophe of our time.

This is why the theoretical model of the theory of Relation proposes an irreversible spacetime resulting from the original quantum universe and whose course of cosmological time—with a history, a past directed towards the future—flows until the current epoch. Irreversibility, entropy and temperature are related to the direction of the arrow of this time. Now such an expansion which originates from a hot state of electromagnetic radiation can only gradually transform its light into matter, which elucidates the mystery of dark energy, and slow down. To see far is to see early.

Conflicts of Interest

The author declares no conflicts of interest regarding the publication of this paper.

References

[1] Wikipedia, PVLAS. https://en.wikipedia.org/wiki/PVLAS

[2] Ejlli, A., Della Valle, F., Gastaldi, U., Messineo, G., Pengo, R., Ruoso, G. and Zavattini, G. (2020) *Physics Reports*, **871**, 1-74. https://doi.org/10.1016/j.physrep.2020.06.001

[3] Bagdoo, R. (2019) *Journal of Modern Physics*, **10**, 310-343. https://doi.org/10.4236/jmp.2019.103022

[4] Bagdoo, R. (2009) *The General Science Journal*, 7.

[5] Cohen-Tannoudji, G. and Spiro, M. (1986) La matière-espace-temps. Fayard, Paris, 316, 325.

[6] Wikipedia, Inflation (Cosmology). https://en.wikipedia.org/wiki/Inflation_(cosmology)

[7] Tsujikawa, S. (2003) Introductory Review of Cosmic Inflation.

[8] Greene, B. (2005) The Fabric of the Cosmos. First Vintage Books Edition, 301.

[9] Peter, P. (2009) *Dossier Pour la Science*, No. 62, 75-76.

[10] Jodra, S. (2001) *Ciel & Espace*, No. 370, 44-46.

[11] Riess, A.G., *et al.* (1998) *The Astronomical Journal*, **116**, 1009-1038. https://doi.org/10.1086/300499

[12] Thuan, T.X. (2003) Origines. Éditions Fayard, Paris, folio essais, 95, 96.

[13] Khalatbari, A. (2002) *Ciel & Espace*, No. 384, 30.

[14] Cramer, J.G. (2001) *Analog Science Fiction & Fact Magazine*. https://www.npl.washington.edu/av/altvw104.html

[15] Baruch, J.-O. (2003) *La Recherche*, No. 361, 37.

[16] O'Raifeartaigh, C., O'Keeffe, M., Nahm, W. and Mitton, S. (2017) *The European Physical Journal H*, **43**, 1-45.

[17] Luminet, J.-P. (2005) L'Univers chiffonné. Éditions Fayard, Paris, folio essais, 87, 320-322.

[18] Wikipedia, Quantum Field Theory. https://en.wikipedia.org/wiki/Quantum_field_theory

[19] Bagdoo, R. (2020) *Journal of Modern Physics*, **11**, 616-647. https://doi.org/10.4236/jmp.2020.115041

[20] Randall, L. (2006) Warped Passages. Harper Perennial, New York, 198.

[21] Bagdoo, R. (2019) *Journal of Modern Physics*, **10**, 922-952. https://doi.org/10.4236/jmp.2019.108061

[22] NASA, Wilkinson Microwave Anisotropy Probe. https://map.gsfc.nasa.gov https://www.nasa.gov/topics/universe/features/wmap-complete.html

[23] Cérélier, M.-N. (2007) The Accelerated Expansion of the Universe Challenged by an Effect on the Inhomogeneities.

[24] Perlmutter, S., *et al.* (1999) *The Astrophysical Journal*, **517**, 565. https://doi.org/10.1086/307221

[25] Haït, J.-F. (2006) *Ciel & Espace*, No. 429, 34.

[26] Fay, S. (2007) *Ciel & Espace*, No. 443, 44-45.

[27] Khalatbari, A. (2004) *Ciel & Espace*, No. 405, 34.

[28] Fay, S. and Henarejos (2005) *Ciel & Espace*, No. 422, 27.

[29] Schaefer, B.E. (2007) *The Astrophysical Journal*, **660**, 16-46. https://doi.org/10.1086/511742

[30] Fay, S. (2006) *Ciel & Espace*, No. 432, 35-37.

[31] Kaiser, N. and Hudson, M.J. (2015) *Monthly Notices of the Royal Astronomical Society*, **450**, 883-895. https://doi.org/10.1093/mnras/stv693

[32] Narlikar, J.V. (2004) *La Recherche*, No. 372, 66.

[33] Vishwakarma, R.G. and Narlikar, J.V. (2005) *International Journal of Modern Physics D*, **14**, 345-354. https://doi.org/10.1142/S0218271805006547

[34] Zwicky, F. (1929) *Proceedings of the National Academy of Sciences of the United States of America*, **15**, 773-779. https://doi.org/10.1073/pnas.15.10.773

[35] Shao, M.-H. (2013) *Physics Essays Publication*, **26**, 183-190. https://doi.org/10.4006/0836-1398-26.2.183

[36] Bertone, G. (2014) Le Mystère de la Matière Noire. Dunod, Paris, 95.

[37] Bagdoo, R. (2020) *Journal of Modern Physics*, **11**, 168-195. https://doi.org/10.4236/jmp.2020.112011

[38] Bagdoo, R. (2022) *International Journal of Fundamental Physical Sciences* (*IJFPS*), **12**, 35-61. https://doi.org/10.14331/ijfps.2022.330154

[39] Östman, L. and Mörtsell, E. (2005) *Journal of Cosmology and Astroparticle Physics*, **0502**, 005. https://doi.org/10.1088/1475-7516/2005/02/005

[40] Zavattini, *et al.* (2006) *La Recherche*, No. 397, 12.

[41] Zavattini, E., *et al.* (2006) *Physical Review Letters*, **96**, Article ID: 110406. https://doi.org/10.1103/PhysRevLett.96.110406

[42] Adler, S.L. (1971) *Annals of Physics*, **67**, 599-647. https://doi.org/10.1016/0003-4916(71)90154-0

[43] Wikipedia, Laser. https://en.wikipedia.org/wiki/Laser

[44] Brotherton, M. (1970) Fonctionnement et utilisation des masers et lasers. Dunod,

Paris, 3, 56.

[45] Maitte, B. (1981) La lumière. Édition du Seuil, Paris, 296.

[46] Hartmann, F. (1974) Les Lasers, Presses Universitaires de France, Que sais-je, 16.

[47] Brown, R. (1969) Les Lasers. Larousse, Paris, 19.

[48] Le Du, J. (2008) Standardisation spectroscopique des supernovæ de type 1a dans le cadre du sondage supernovæ legacy survey. Thèse, Université de la Méditérranée, Marseille. https://inis.iaea.org/search/search.aspx?orig_q=RN:48007277

[49] Weschler, M. How Lasers Work, HowStuffWorks. https://science.howstuffworks.com/laser-weapon.htm

[50] Park, D. (1968) Aspects de la physique contemporaine, Les lasers. Dunod, Paris, 143-146.

[51] Appell, D. (2008) *Scientific American*, **298**, 100-102. https://doi.org/10.1038/scientificamerican0508-100

[52] Coles, (1998) The New Cosmology. Icon Books, London, 11, 12, 14.

[53] Kragh, H. (2012) "The Most Philosophically of All the Sciences": Karl Popper and Physical Cosmology. http://philsci-archive.pitt.edu/9062/1/Popper_%26_cosmology_PhilSci.pdf

[54] ESA Science & Technology (2013) Simple but Challenging: The Universe According to Planck. https://sci.esa.int/web/planck/-/51551-simple-but-challenging-the-universe-according-to-planck

[55] Billings, L. (2020) *Scientific American*. https://www.scientificamerican.com/article/do-we-live-in-a-lopsided-universe1/

[56] Secrest, J.S., *et al.* (2021) *The Astrophysical Journal Letters*, **908**, L51. https://doi.org/10.3847/2041-8213/abdd40

[57] Javanmardi, B., *et al.* (2015) *The Astrophysical Journal Letters*, **810**, 47. https://doi.org/10.1088/0004-637X/810/1/47

[58] European Space Agency (2013) Simple but Challenging: The Universe According to Planck. https://sci.esa.int/web/planck/-/51551-simple-but-challenging-the-universe-according-to-planck

[59] Nottale, L. (1998) La relativité dans tous ses états. Hachette, New York, 13-15.

[60] Jolivet, R. (1965) Traité de philosophie, logique-cosmologie. Emmanuel Vitte, Lyon, Paris, 345-356.

[61] Hawley, J.F. and Holcomb, K.A. (1998) Foundations of Modern Cosmology. Oxford University Press, Oxford, 148, 152, 153, 273, 277, 338, 453, 454.

[62] Carroll, S.M. (2008) *Scientific American*, **298**, 48. https://doi.org/10.1038/scientificamerican0608-48

[63] Coveney, and Highfield, R. (1992) The Arrow of Time. Fawcett Columbine Book, New York.

[64] Uzan, J.-P. (2018) Big Bang. Flammarion, Paris, 104-112, 180-183, 236-238.

[65] Merleau-Ponty, J. (1993) Einstein, Champs Flammarion, Paris, 224, 280.

[66] Wikipedia, Cosmological Principle. https://en.wikipedia.org/wiki/Cosmological_principle

[67] Eddington, A.S. (1924) Vues générales sur la théorie de la Relativité. Gauthier-Villars, Paris, 48, 69, 86.

Journal of Modern Physics, 2023, 14, 722-740
https://www.scirp.org/journal/jmp
ISSN Online: 2153-120X
ISSN Print: 2153-1196

Propagation Characteristics of Ultrasonic Guided Waves in Grouted Rockbolt Systems with Bond Defects under Different Confining Conditions

Shuisheng Yu[1*], Jin Chen[2], Yawei Wang[1], Honghao Yang[1], Shucan Lu[1]

[1]School of Architectural Engineering, Zhongyuan University of Technology, Zhengzhou, China
[2]School of Economics and Management, Zhongyuan University of Technology, Zhengzhou, China
Email: *yuss.1987@163.com

How to cite this paper: Yu, S.S., Chen, J., Wang, Y.W., Yang, H.H. and Lu, S.C. (2023) Propagation Characteristics of Ultrasonic Guided Waves in Grouted Rockbolt Systems with Bond Defects under Different Confining Conditions. *Journal of Modern Physics*, **14**, 722-740.
https://doi.org/10.4236/jmp.2023.145041

Received: March 16, 2023
Accepted: April 23, 2023
Published: April 26, 2023

Abstract

A rockbolt acting in the rock mass is subjected to the combined action of the pull-out load and confining pressure, and the bond quality of the rockbolt directly affects the stability of the roadway and cavern. Therefore, in this study, confining pressure and pull-out load are applied to grouted rockbolt systems with bond defects by a numerical simulation method, and the rockbolt is detected by ultrasonic guided waves to study the propagation law of ultrasonic guided waves in defective rockbolt systems and the bond quality of rockbolts under the combined action of pull-out load and confining pressure. The numerical simulation results show that the length and location of bond defects can be detected by ultrasonic guided waves under the combined action of pull-out load and confining pressure. Under no pull-out load, with increasing confining pressure, the low-frequency part of the guided wave frequency in the rockbolt increases, the high-frequency part decreases, the weakening effect of the confining pressure on the guided wave propagation law increases, and the bond quality of the rockbolt increases. The existence of defects cannot change the strengthening effect of the confining pressure on the guided wave propagation law under the same pull-out load or the weakening effect of the pull-out load on the guided wave propagation law under the same confining pressure.

Keywords

Grouted Rockbolt Systems, Bond Defect, Pull-Out Load, Confining Pressure, Ultrasonic Guided Wave

1. Introduction

The occurrence environment of a deep rock mass is complex when it is in a state of "three highs and one disturbance" (high ground stress, high seepage pressure, high earth temperature and mining disturbance) [1]. A rockbolt acting in the rock mass is always subjected to the combined action of the pull-out load and confining pressure. The construction quality of the rockbolt (such as the quality of the rockbolt bond, whether the length of the rockbolt is consistent with the design length, whether the mortar is full, that is, whether the rockbolt has played the expected role, etc.) directly affects the stability of the roadway, chamber and slope. The construction of rockbolts is a concealed project, with the rockbolt and grouted agent being hidden [2] [3], the length of the rockbolt being insufficient [4] [5] or whether it contains natural joints [6] [7] [8]. The bond quality of the rockbolt and its defects are closely related to the stability and safety of the surrounding rock and roadway slope, so it is necessary to detect the bond defects and quality of the rockbolt under the combined action of pull-out load and confining pressure.

In the detection of bond defects and quality, Xu *et al.* [3] determined the location of bond defects by means of experiments and numerical simulations from a mechanical point of view. Lin *et al.* [4] used the impact echo method to detect the bond length, and their results showed that the method could detect the bond length well when it was clear whether the rockbolt was grouted or not. The attenuation and group velocity of ultrasonic guided waves in rockbolts were studied by Cui *et al.* [9], and the influence of insufficient rockbolts and mortar on grouted rockbolts was confirmed and verified by experiments. Zhang *et al.* [10] used the Hilbert-Huang signal processing method to analyse the detection signals of various complete bond and defective bond models. This method could clearly identify the defects and the reflected signals at the bottom of the rockbolt to more accurately deduce the defect position and bond length. Zhang *et al.* [11] used self-designed nondestructive testing experimental systems for bond quality to detect whether bond systems have defects and determined the number of defects by using the multiscale entropy method. Wang *et al.* [12] used ultrasonic guided wave technology to detect the initial corrosion of reinforced concrete with defects. Their results showed that the method could identify debonding and crack propagation at the interface between the steel bar and concrete. Liu *et al.* [13] used the finite element method to simulate the propagation process of ultrasonic guided waves in defective rockbolts, used the improved adaptive noise complete ensemble empirical mode decomposition (ICEEMDAN) method to process the reflected signals of ultrasonic guided waves, and obtained the arrival time of the reflected wave of defects according to the peak value of the decomposed natural mode function, thus determining the location and length of bond defects. Liu *et al.* [14] analysed the influence of tensile stress on the propagation characteristics of ultrasonic guided waves in steel cables based on a fast Fourier transform, and their results showed that the energy transfer of ultrasonic guided waves increased with increasing tensile force. Yu *et al.* [15] used a rockbolt pull-out and stress

wave detection test device to pull out the rockbolt and detect its bond quality under different loads and then used the wavelet transform to carry out wavelet multiscale and frequency spectrum analysis on the detection signal, determined the debonding length of the rockbolt under the pull-out load and evaluated the bond quality of the rockbolt. Ivanovic and Neilson [16] used a magnetostrictive nondestructive testing method to evaluate the effective length of a rockbolt under a pull-out load without considering the defects in the grouted rockbolt system. Yu *et al.* [17] used ultrasonic guided waves to detect bond defects under different pull-out loads to determine bond quality but did not consider confining pressure. Yu *et al.* [18] used ultrasonic guided waves to detect rockbolts under different pull-out loads and confining pressures and studied the bond quality of rockbolts but did not consider the influence of bond defects.

Based on the above research, it can be seen that there is relatively little research on the detection and propagation law of bond quality by using ultrasonic guided waves, especially under the combined action of pull-out load and confining pressure. However, the stress change in the rock mass is one of the important factors affecting the bond strength of the rockbolt and the propagation of stress waves in the rockbolt. Therefore, a numerical simulation method was used to realize the influence of stress in rockbolt support by applying confining pressure in this study. Fully grouted rockbolt systems with bond defects under the combined action of pull-out load and confining pressure were detected to determine the location of bond defects and the influence of pull-out load and confining pressure on the propagation law of ultrasonic guided waves and to evaluate the bond quality of rockbolts.

2. The Establishment of the Numerical Model and Experimental Verification

Defects often appear in grouted rockbolt systems, and the existence of defects always affects structural safety. Therefore, the bond quality of grouted rockbolt systems with defects is studied under pull-out load and confining pressure.

In the numerical simulation, the size of the sample refers to the sample size of the laboratory test in reference [19]. A hollow cylinder concrete sample was used to simulate the surrounding rock, with an outer diameter of 150 mm, an inner diameter of 40 mm and a length of 1500 mm. hollow cylinder cement mortar was used to simulate the grouted agent, with an outer diameter of 40 mm and an inner diameter of 25 mm. The rockbolt diameter was 25 mm, the length was 2500 mm, the B-end of the grouted rockbolt was 700 mm away from the A-end, the defect-end was 700 mm away from the B-end of the grouted rockbolt system, and the defect length was 100 mm. The dimension parameters of the grouted rockbolt system are shown in **Figure 1**.

2.1. Modelling of the Concrete, Cement Mortar, and Rockbolt

The concrete damage plasticity model (CDPM) used herein to simulate the

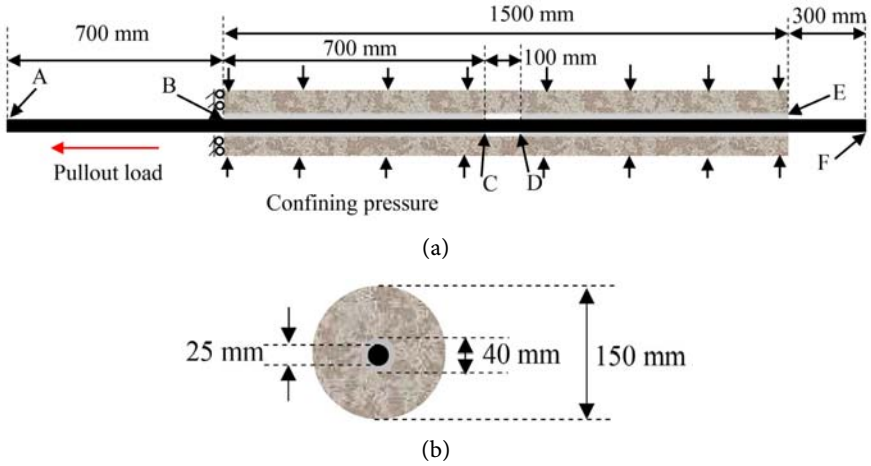

Figure 1. Grouted rockbolt systems model with one bond defect. (a) Size of grouted rockbolt systems; (b) Diameter of grouted rockbolt systems.

mechanical behaviour of quasibrittle materials (*i.e.*, the concrete and cement mortar) was proposed for ABAQUS by Lee and Fenves (1998) [20]. The CDPM considers isotropic damaged elasticity in combination with isotropic tensile and compressive plasticity to represent the inelastic behaviour of concrete [21]. The model exhibits multiple advantages, including its simplicity and numerical stability.

We introduced a damage variable into the CDPM and used the damage plasticity to determine the uniaxial tension and compression constitutive relationships of our concrete (cement mortar) specimens. The concrete (cement mortar) elastic modulus was reduced to simulate the degradation of the concrete unloading stiffness under elevated levels of strain. The CDPM assumes that concrete (cement mortar) failure results from tensile cracking and crushing.

Based on test results in the reference [15], the rockbolt experiences elastic ascent, yielding, hardening and complete slip without breaking. Therefore, the rockbolt is set as an elastoplastic material in ABAQUS. The material parameters of the rockbolt, concrete and cement mortar are presented in **Table 1**.

2.2. Modelling of Bond Behaviour

The interface bond behaviour can be modelled by cohesive elements [22] [23] [24] or surface-based cohesive behaviour [19] [25] [26] using the traction-separation law in Abaqus. The interface thickness of our specimen is negligibly small, and we sought to reduce the calculation time, so we modelled the interface bond behaviour between the rockbolt (concrete) and cement mortar by the surface-based cohesive behaviour in this study.

The damage laws for the cohesive behaviour in shear directions (see **Figure 2**) are defined according to the following steps: 1) linear elastic shear stress-slip relations by defining the elastic bond stiffness; 2) damage initiation criteria, which can be defined by the maximum bond shear stress; and 3) damage evolution laws for the exponential softening branch of the bond [27].

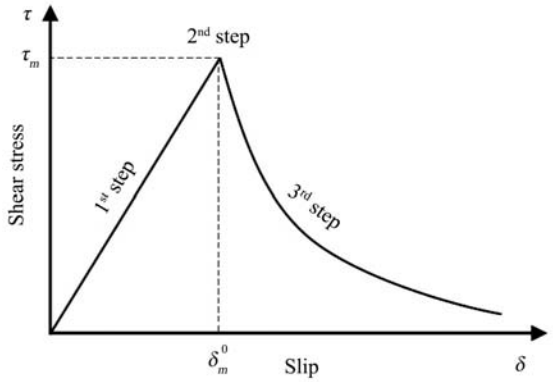

Figure 2. Damage law for the cohesive behavior [27].

Table 1. Material properties of the rockbolt, concrete and cement mortar [15].

Ingredient	Density (kg/m³)	Elastic modulus (GPa)	Poisson's ratio
Rockbolt	7850	210	0.3
Cement mortar	2100	20	0.19
Concrete	2300	33	0.23

The uncoupled constitutive relation of the traction-separation behaviour as expressed in Abaqus is as follows:

$$T=\begin{Bmatrix} t_n \\ t_s \\ t_t \end{Bmatrix}=\begin{bmatrix} k_{nn} & 0 & 0 \\ 0 & k_{ss} & 0 \\ 0 & 0 & k_{tt} \end{bmatrix}\begin{Bmatrix} \delta_n \\ \delta_s \\ \delta_t \end{Bmatrix}=K\delta \tag{1}$$

where t_n is the nominal stress in the normal direction; t_s and t_t are the nominal stresses in two local shear directions; k_{nn}, k_{ss} and k_{tt} are the corresponding stiffness coefficients; and δ_n, δ_s and δ_t are the corresponding displacements.

k_{nn}, k_{ss} and k_{tt} are given by [22]:

$$k_{ss}=k_{tt}=\tau_m/\delta_m^0 \tag{2}$$

$$k_{nn}=100k_{ss}=100k_{tt} \tag{3}$$

where τ_m is the maximum shear strength and δ_m^0 is the slip value at the maximum shear strength, namely, the effective displacement at the initiation of the damage.

The stress components of the traction-separation model are affected by the damage.

$$t_n=(1-d)\overline{t}_n \tag{4}$$

$$t_s=(1-d)\overline{t}_s \tag{5}$$

$$t_t=(1-d)\overline{t}_t \tag{6}$$

where $\overline{t}_n$, $\overline{t}_s$ and $\overline{t}_t$ are the stress components predicted by the elastic traction-separation behaviour for the current strains without damage. d is the dam-

age variable. For exponential softening,

$$d = 1 - \left\{ \frac{\delta_m^0}{\delta_m^{\max}} \right\} \left\{ 1 - \frac{1 - \exp\left(-\alpha \left(\frac{\delta_m^{\max} - \delta_m^0}{\delta_m^f - \delta_m^0} \right) \right)}{1 - \exp(-\alpha)} \right\} \tag{7}$$

where δ_m^f is the effective displacement at complete failure. $\delta_m^{\max}$ is the maximum value of the effective displacement attained during the loading history. α is a nondimensional material parameter that defines the rate of damage evolution.

In the numerical model, the grouted rockbolt systems are simulated by four-node bilinear axisymmetric quadrilateral elements with reduced integration (CAX4R). The interface at the loaded end of the concrete is fixed during the test for the boundary condition in the grouted rockbolt systems. On the basis of extensive trials, a mesh size of 2 mm for the rockbolt and cement mortar and a mesh size of 5 mm for the concrete are deemed adequate to obtain sufficiently accurate results. The stiffness matrix is singular when the damage value, scalar stiffness degradation (SDEG), is equal to 1. Therefore, the maximum damage value was limited to 0.9998 to avoid the occurrence of a singular stiffness matrix [27].

2.3. Numerical Test Procedure

Conventional rockbolts acting in deep rock masses have a stress variation of 10 - 15 MPa during service [28]. Therefore, in the numerical simulations, the confining pressures are 0, 5, 10 and 15 MPa, which are used to study the effect of confining pressure on the propagation law of ultrasonic guided waves and to determine the bond quality of rockbolts under confining pressure.

The testing procedure was as follows. First, the grouted rockbolt was maintained without pull-out force and confining pressure, the ultrasonic guided wave was excited at the A-end. Next, the 5 MPa, 10 MPa and 15 MPa confining pressure was applied, respectively, the rockbolt was detected by ultrasonic wave in absence of pull-out load. Rockbolts with bond defects are often subjected to the combined effect of axial and radial loads during service. Therefore, the propagation law of guided waves in grouted rockbolt systems is explored considering the combined effect of confining pressure and pull-out load in two cases: 1) the same pull-out load with different confining pressures and 2) the same confining pressure with different pull-out loads. When the pull-out load keep unchanged, the confining pressure was increased to 5 MPa, 10 MPa and 15 MPa, and the above steps were repeated. When the confining pressure keep unchanged, the pull-out load was increased to 25 kN, 50 kN, 75 kN and 100 kN, the ultrasonic guided wave was tested according to the above steps. According to the results of ultrasonic guided wave testing, the bond quality of rockbolt under the combined action of pull-out load and confining pressure were analyzed.

2.4. Experimental Verification

The ultrasonic guided wave is used for detection in the numerical simulation, and the cut-off frequency of the guided wave in the grouted rockbolt free of loading is 22 kHz. Therefore, the input waveform of the ultrasonic guided wave was the sine wave with 10 cycles and 22 kHz frequency obtained by the Hanning window (**Figure 3**) [15]. The ultrasonic guided wave was excited at the A-end, and the wave was received at the F-end. The comparison between the numerical and experimental results is shown in **Figure 4** [15]. The signal received at the other end was in good agreement with the experimental result, which indicated that the numerical model could simulate the guided wave propagation in grouted rockbolt systems.

3. Propagation of Ultrasonic Guided Wave in Grouted Rockbolt Systems with Bond Defects

3.1. Influence of Confining Pressure on Guided Wave Propagation in Absence of Pull-Out Load

The ultrasonic guided wave signal was excited at the A-end (**Figure 1**). **Figure 5** displays the propagation of ultrasonic guided waves in grouted rockbolt systems

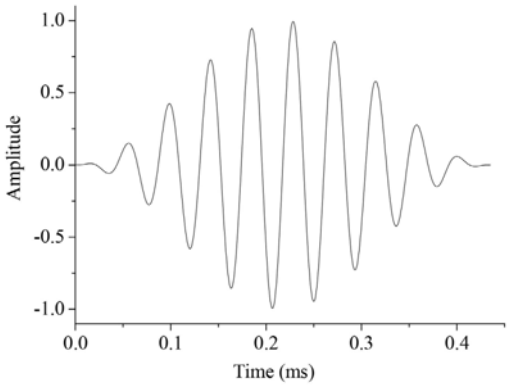

Figure 3. Excitation signal input for the numerical simulation [15].

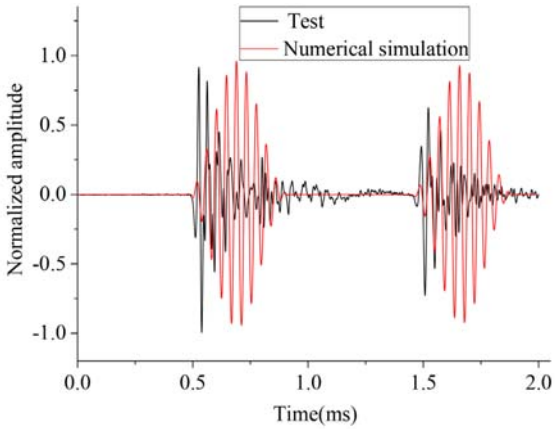

Figure 4. Comparison of numerical and test results of wave propagation in free rockbolt [15].

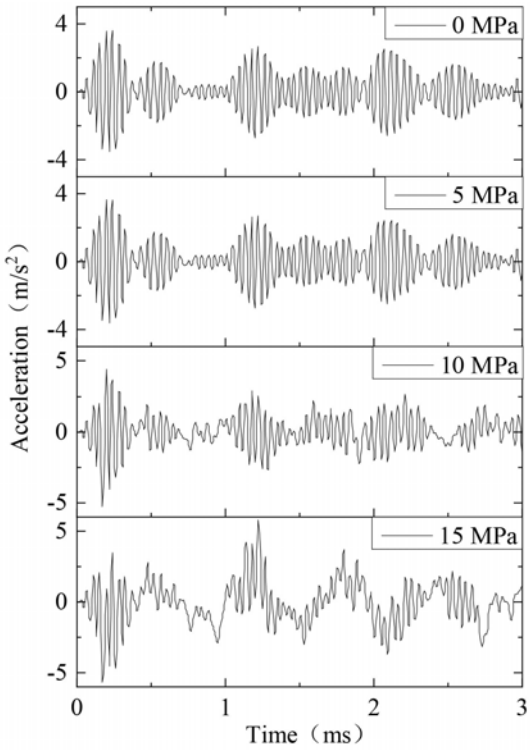

Figure 5. The influence of confining pressure on guided wave propagation in absence of pull-out load.

with bond defects in the absence of a pull-out load. The law of guided wave propagation gradually deteriorates with increasing confining pressure, and this phenomenon is the same as the propagation law of guided waves in grouted rockbolt systems without bond defects [18], while the echo wave packet at the bond defects fluctuates with increasing confining pressure, and the presence of bond defects cannot change the weakening effect of the confining pressure on the propagation law of guided waves.

The variation of frequency in the guided wave with the confining pressure in absence of pull-out load is shown in **Figure 6**. In the grouted rockbolt systems with bond defect, the low frequency part of the guided wave frequency in the rockbolt increases and the high frequency part decreases with the increase of the confining pressure. In **Figure 7**, the ratio Q of the maximum amplitude of guided wave at low frequency to that at high frequency increases exponentially with the increase of the confining pressure, indicating that the presence of bond defects cannot change the trend of the Q value with the confining pressure.

The propagation process of guided waves in grouted rockbolt systems with bond defects under different confining pressures without a pull-out load is shown in **Figure 8**. The wave propagation is relatively good without confining pressure, and the wave propagation arrives at the B-end of the rockbolt at 0.3 ms and then continues to spread along the rockbolt and reach the bond defect. In the bond defect, part of the guided wave continues to spread, and the other part is reflected back to the loading end; the peak echo energy arrives at the loading end at 1.2

ms. Under a 5 MPa confining pressure, the wave propagation is slightly less regular due to the effect of the confining pressure, but at 0.7 ms, the peak wave energy can be clearly seen when arriving at the bond defect from the propagation cloud map, and then part of the guided wave is reflected back to the loading end, and part continues to propagate to the distal end of the grouted rockbolt systems. As the confining pressure increases to 10 MPa and 15 MPa, the law of guided wave propagation becomes increasingly worse, which further indicates that the confining pressure has a weakening effect on guided wave propagation without a pull-out load.

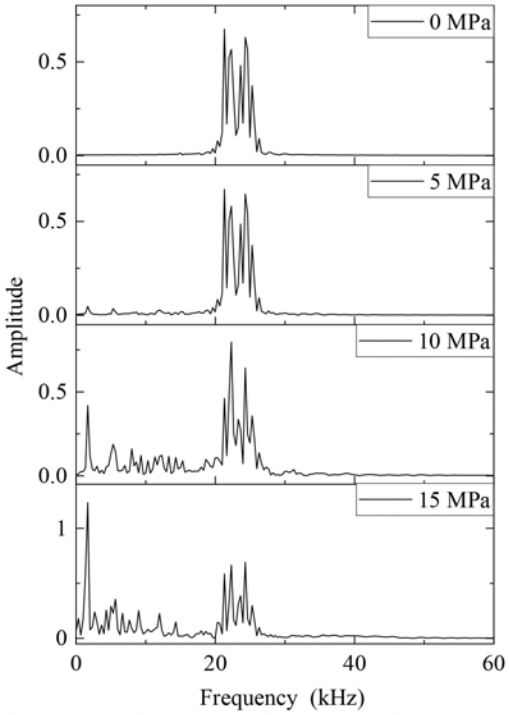

Figure 6. The change of frequency with confining pressure in absence of pull-out load.

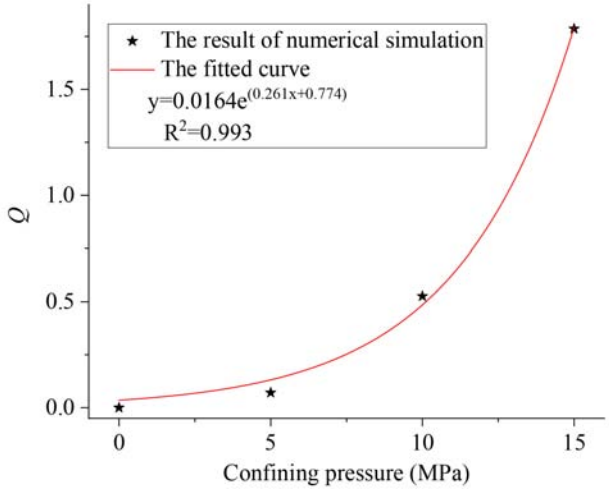

Figure 7. The relationship of Q and confining pressure without pull-out load.

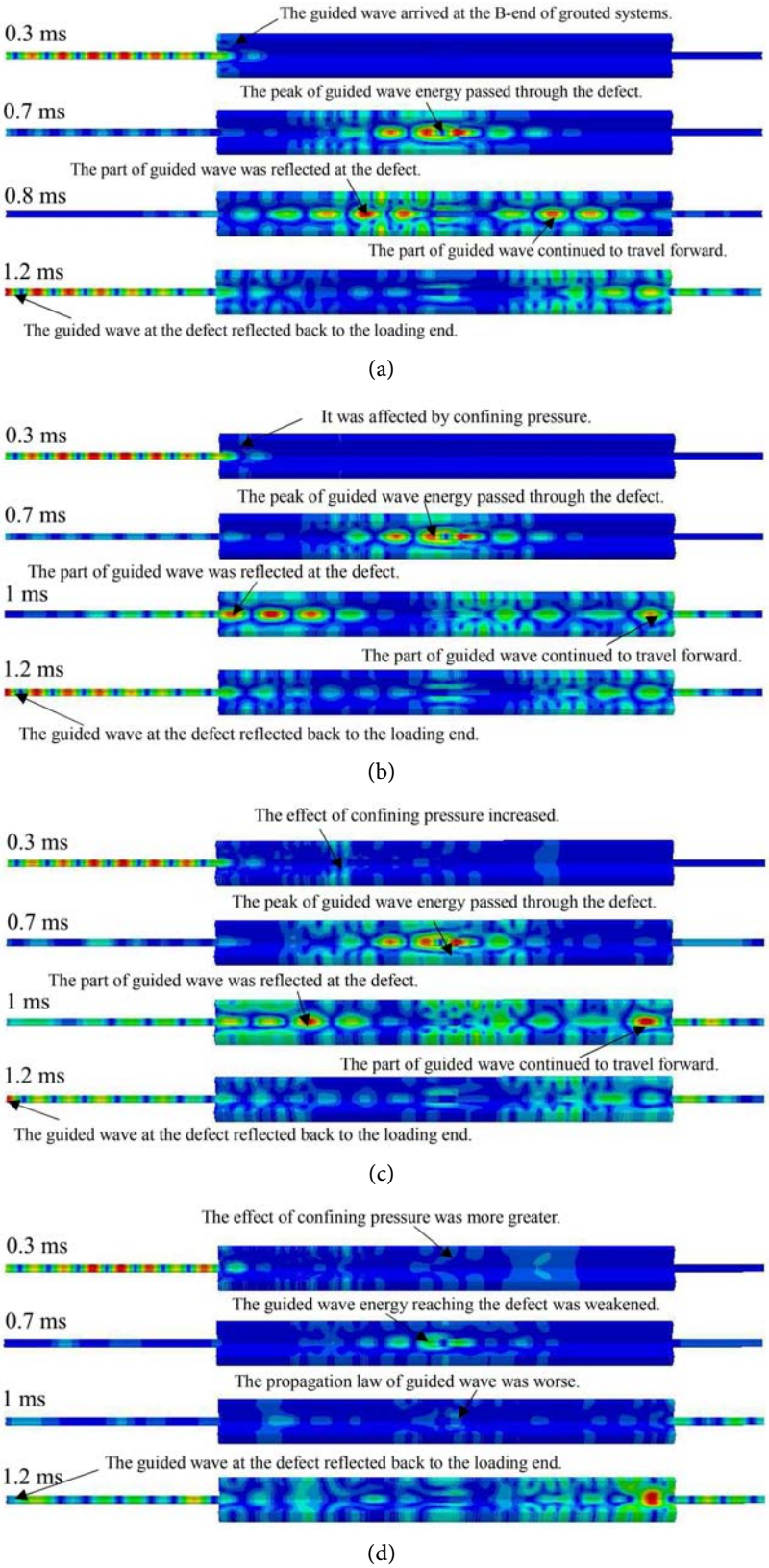

Figure 8. The guided wave propagation in grouted rockbolt systems under different confining pressure and in absence of pull-out load. (a) 0 MPa; (b) 5 MPa; (c) 10 MPa; (d) 15 MPa.

3.2. Effect of Confining Pressure on Guided Wave Propagation under Pull-Out Load

3.2.1. Under the Same Pull-Out Load and Different Confining Pressures

When the pull-out load is 50 kN, the propagation law of the guided wave under different confining pressures is shown in Figure 9. Under the same pull-out load, when the confining pressure is 0 MPa, the concrete is less restrictive, the rockbolt has a longer debonding length, and the guided wave propagation is more disordered due to the increased interference. With increasing confining pressure, the radial force of rockbolt systems increases, and the adhesion between the rockbolt and cement mortar increases, which leads to the restriction of the rockbolt, so the debonding length of the rockbolt gradually decreases, the bond quality increases, the law of guided wave propagation increases, and the echoes at the bond defects are gradually visible. Therefore, the confining pressure has a strengthening effect on the guided wave propagation law compared with the pull-out load, and the larger the confining pressure is, the stronger the strengthening effect is under the same pull-out load.

Under the action of a 50 kN pull-out load, the change in frequency in the guided wave with the confining pressure is shown in Figure 10. With the increase in the confining pressure, the low frequency part of the guided wave frequency in the rockbolt decreases, while the high frequency part increases, and the Q value (Figure 11) decreases exponentially with the increase in the confining pressure. This indicates that the confining pressure plays a strengthening role in the law of guided wave propagation under the same pull-out load.

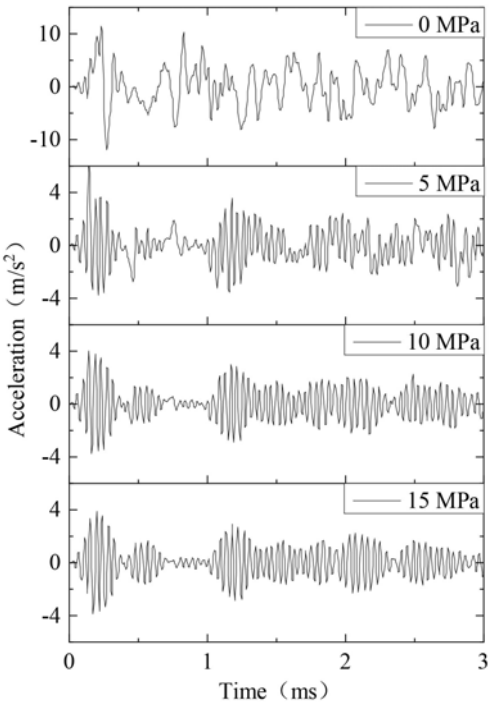

Figure 9. The influence of confining pressure on guided wave propagation law under 50 kN pull-out load.

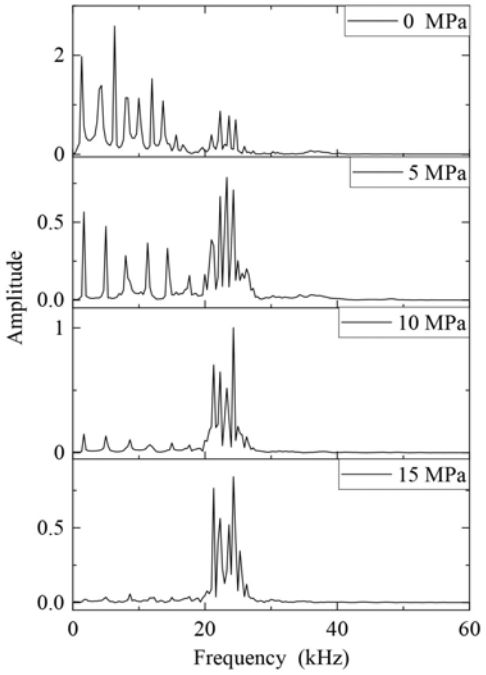

Figure 10. The change of frequency with the confining pressure under 50 kN pull-out load.

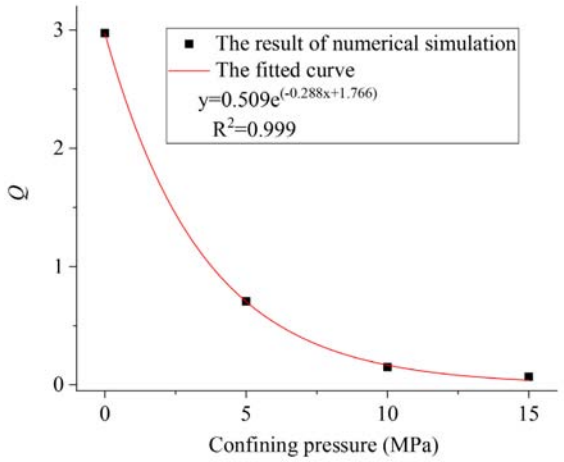

Figure 11. The relationship of Q and confining pressure under pull-out load.

Figure 12 displays a three-quarter model of the cylinder sample (The two-dimensional axisymmetric model was rotated around the symmetry axis to obtain the three-dimensional model in Abaqus) and shows the propagation process of the guided wave under different confining pressures when the pull-out load is 50 kN. When there is no confining pressure, the propagation process of the guided wave under the pull-out load of 50 kN is not very regular, but with the increase in the confining pressure, it can be clearly seen gradually that the peak energy of the guided wave reaches the bond defect, and the reflected wave occurs at the bond defect. At 1.2 ms, the return wave at the bond defect reaches the loading end, and the law of the guided wave propagation is enhanced. The guided

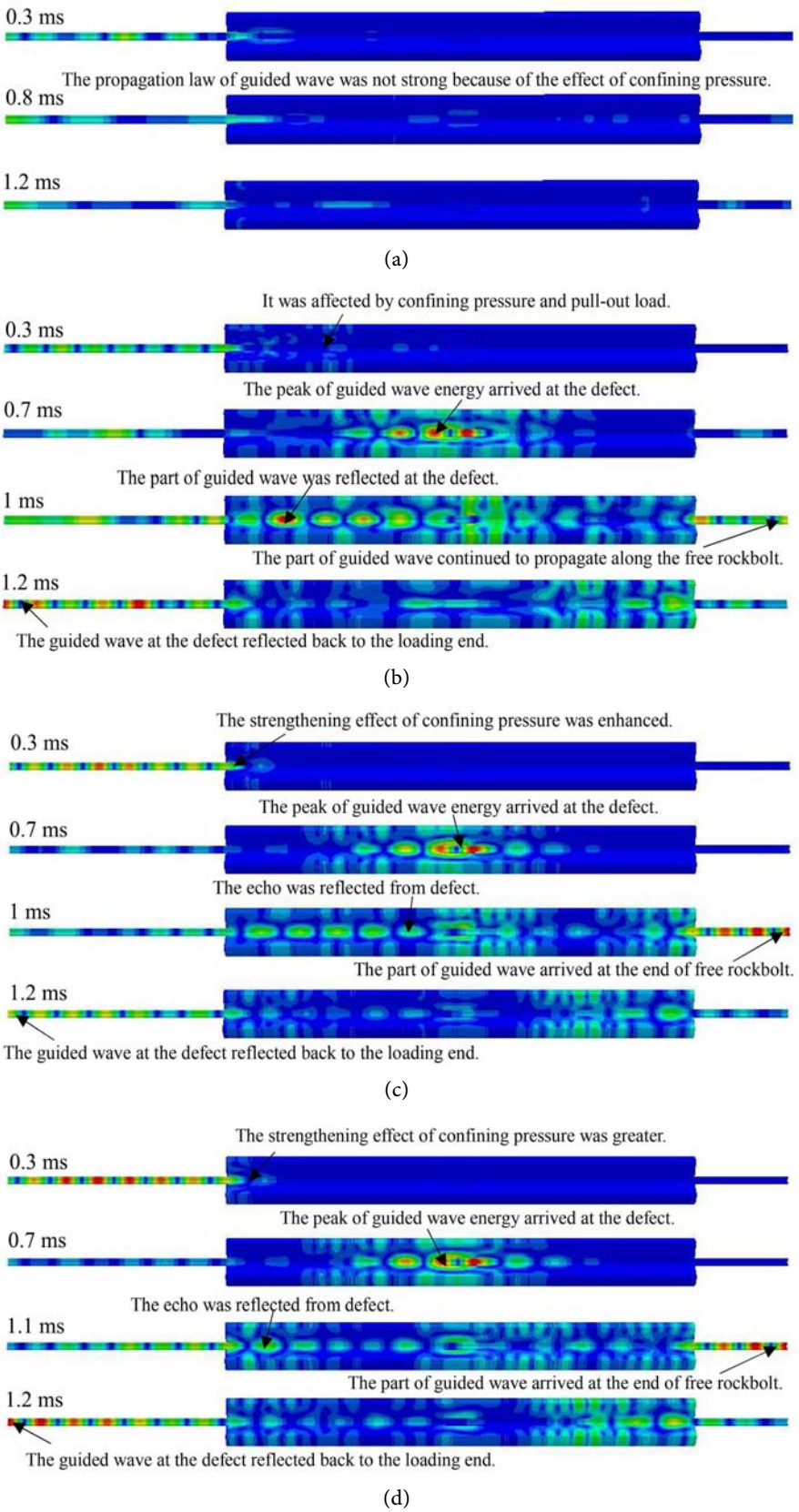

Figure 12. The influence of confining pressure on guided wave propagation process under 50 kN pull-out load. (a) 0 MPa; (b) 5 MPa; (c) 10 MPa; (d) 15 MPa.

wave propagation cloud map further reflects the strengthening effect of the confining pressure on the guided wave propagation law under the pull-out load under the same confining pressure and different pull-out loads.

3.2.2. Under the Same Confining Pressure and Different Pull-Out Loads

When the confining pressure is 10 MPa, the propagation law of the guided wave under different pull-out loads is shown in Figure 13. Without a pull-out load, the propagation law of the guided wave is affected by the confining pressure, and the wave packet oscillates slightly. The confining pressure weakens the guided wave propagation, but the echo at the bond defect is still clearly visible. However, when the pull-out load increases to 50 kN and 75 kN, the law of guided wave propagation gradually weakens, and the bond quality of the rockbolt also worsens, especially under the 75 kN pull-out load, and the echo at the bond defect can hardly be seen. The above phenomenon reflects that the pull-out load under the same confining pressure has a weakening effect on the guided wave propagation law, and the larger the pull-out load is, the more obvious the weakening effect is, resulting in the less obvious bond defect echo received at the A-end.

Figure 14 shows the variation in the frequency of the guided wave with the drawing load under a confining pressure of 10 MPa. When there is no pull-out load, the confining pressure weakens the law of guided wave propagation, and the Q value is relatively large. When the pull-out load increases to 50 kN, the high-frequency part of the guided wave increases, and the low-frequency part decreases. This is mainly due to the combined effect of the confining pressure and the pull-out load, and the strengthening effect of the confining pressure is

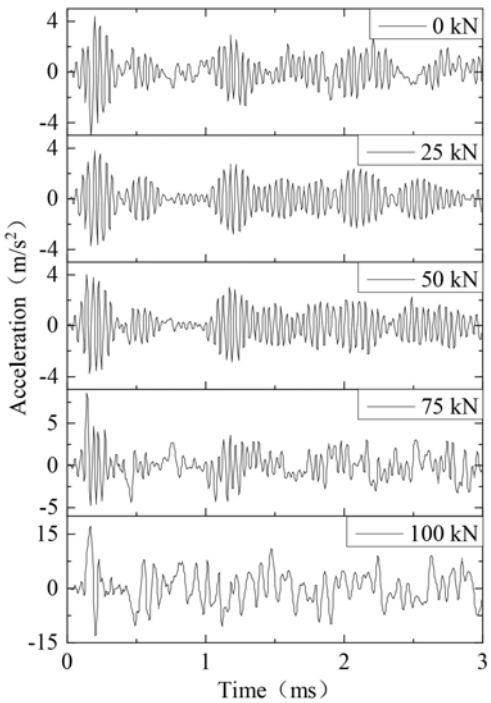

Figure 13. The influence of pull-out load on guided wave propagation law under 10 MPa confining pressure.

stronger than the weakening effect of the pull-out load, which dominates, leading to the reduction in the Q value (see Figure 15). When the pull-out load increases to 75 kN and 100 kN, the high frequency part decreases, the low frequency part increases, and the frequency in the guided wave shifts to the low frequency. It can be seen in Figure 15 that the Q value decreases first and then increases with increasing pull-out load in a quadratic polynomial function relationship, and the rockbolt anchoring bond quality decreases.

Figure 16 displays the propagation process of the guided wave under different pull-out loads under the action of a 10 MPa confining pressure. At first, the guided wave is only affected by the confining pressure. In the cloud chart, the guided wave propagation process is relatively good. At 0.7 ms, the peak of the

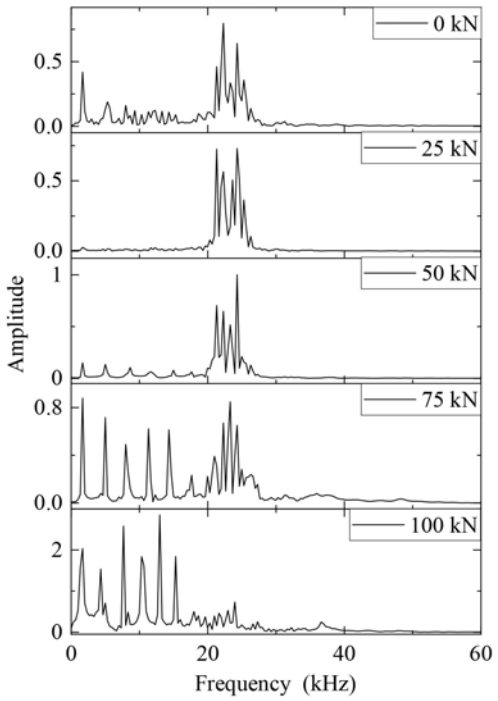

Figure 14. The change of frequency with pull-out load under 10 MPa confining pressure.

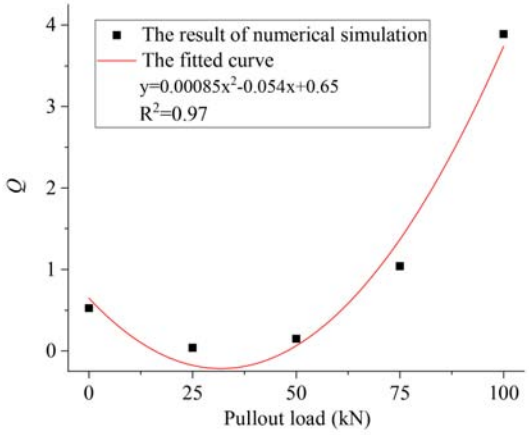

Figure 15. The relationship of Q and pull-out load under 10 MPa confining pressure.

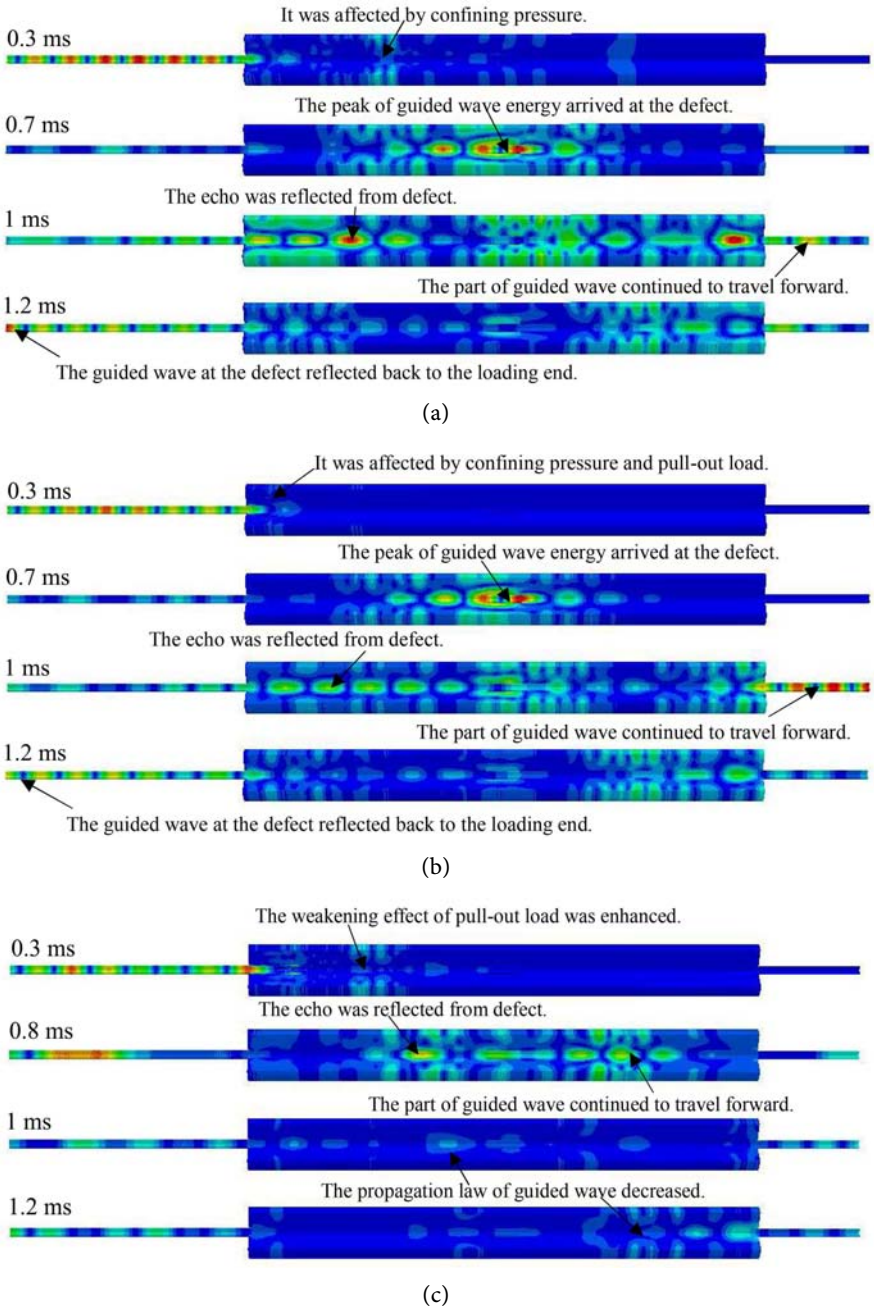

Figure 16. The influence of pull-out load on guided wave propagation process under 10 MPa confining pressure. (a) 0 kN; (b) 50 kN; (c) 75 kN.

guided wave energy reaches the bond defect, and then part of the energy is reflected back to the loading end of the anchorage systems at the bond defect, while part of the energy continues to propagate to the far end of the anchorage systems. However, under the action of 50 kN and 75 kN pull-out loads, some rockbolts debonded, and the adhesion between the rockbolts and cement mortar weakened. At the same time, under the action of confining pressure, the friction resistance between the rockbolts and cement mortar increases at the debonding point of the rockbolts, resulting in increased energy dissipation of the guided

wave in the process of propagation, and the law of guided wave propagation weakens. Therefore, under the same confining pressure, with the increase in the pull-out load, the rock bond quality of the rock rod will gradually deteriorate.

4. Conclusions

In this study, the propagation law of guided waves in grouted rockbolt systems with bond defects under the combined action of confining pressure and pull-out load is studied by numerical simulation, the propagation law of guided waves under the combined action of different pull-out loads and confining pressure is analysed, the bond quality of the rockbolt is determined, and the following conclusions are obtained:

1) In the absence of a pull-out load, with increasing confining pressure, the guided wave propagation law gradually worsens, and the echo wave packet at the bond defect also fluctuates with increasing confining pressure. The existence of a bond defect cannot change the weakening effect of the confining pressure on the guided wave propagation law.

2) Under the same pull-out load, with increasing confining pressure, the radial stress of the grouted rockbolt systems increases, and the bond between the rockbolt and cement mortar increases, resulting in reinforcement of the restraint of the rockbolt, and the law of guided wave propagation also increases gradually. The confining pressure plays a strengthening role in guided wave propagation.

3) Under the same confining pressure, with increasing pull-out load, part of the rockbolt debonding occurs, and the adhesion between the rockbolt and cement mortar weakens. However, at the debonding point of the rockbolt, the confining pressure increases the friction resistance between the rockbolt and the cement mortar, resulting in an increase in the energy dissipation of the guided wave in the propagation process and the weakening effect of the propagation law of the guided wave.

Acknowledgements

This work is funded by the National Science Foundation of China (Grant No. 52104157). This support is gratefully acknowledged.

Data Availability

The data used to support the findings of this study are included within the article.

Conflicts of Interest

The authors declare no conflicts of interest.

References

[1] He, M.C., Xie, H.P., Peng, S.P. and Jiang, Y.D. (2005) *Chinese of Journal Rock Mechanics and Engineering*, **24**, 2803-2813.

[2] Xu, F., Wang, K., Wang, S.G., Li, W.W., Liu, W.Q. and Du, D.S. (2018) *Construction and Building Materials*, **185**, 264-274. https://doi.org/10.1016/j.conbuildmat.2018.07.050

[3] Xu, C., Li, Z.H., Wang, S.Y., Wang, S.R., Tang, C.A., *et al.* (2018) *Rock Mechanics and Rock Engineering*, **51**, 861-871. https://doi.org/10.1007/s00603-017-1373-1

[4] Lin, Y.F., Ye, J.W. and Lo, C.M. (2022) *Construction and Building Materials*, **316**, Article ID: 125904. https://doi.org/10.1016/j.conbuildmat.2021.125904

[5] Cui, Y. and Zou, D.H. (2012) *Journal of Applied Geophysics*, **79**, 64-70. https://doi.org/10.1016/j.jappgeo.2011.12.010

[6] Srivastava, L.P. and Singh, M. (2015) *Engineering Geology*, **197**, 103-111. https://doi.org/10.1016/j.enggeo.2015.08.004

[7] Ghadimi, M., Shahriar, K. and Jalalifar, H. (2015) *Tunnelling and Undergroud Space Technology*, **50**, 143-151. https://doi.org/10.1016/j.tust.2015.07.014

[8] Nie, W., Zhao, Z.Y., Ma, S.Q. and Guo, W. (2018) *Tunnelling and Underground Space Technology*, **71**, 15-26. https://doi.org/10.1016/j.tust.2017.07.005

[9] Cui, Y. and Zou, D.H. (2006) *Journal of Applied Geophysics*, **59**, 337-344. https://doi.org/10.1016/j.jappgeo.2006.04.003

[10] Zhang, J.K., Li, K., Zhang, H., Wang, N., Guo, Q.L. and Zhao, L.Y. (2021) *Chinese of Journal Rock Mechanics and Engineering*, **40**, 1460-1472. http://rockmech.whrsm.ac.cn/EN/10.13722/j.cnki.jrme.2020.0630

[11] Zhang, L., Huang, Z.M., Bai, L., Ma, Z.G., Mao, X.B. and Chen, Z.Q. (2021) *Journal of China University Mining Technology*, **50**, 1077-1086.

[12] Wang, Y.K. Mukherjee, A. and Castel, A. (2022) *Construction and Building Materials*, **360**, Article ID: 129346. https://doi.org/10.1016/j.conbuildmat.2022.129346

[13] Liu, L.L., Zhu, J., Zhang, S.H. and Sun, P.H. (2022) *Earth Sciences*.

[14] Liu, X.C., Wu, B., Qin, F., He, C.F. and Han, Q. (2017) *Ultrasonics*, **73**, 196-205. https://doi.org/10.1016/j.ultras.2016.08.014

[15] Yu, S.S., Zhu, W.C. and Niu, L.L. (2022) *International Journal of Coal Science and Technology*, **9**, 8-15. https://doi.org/10.1007/s40789-022-00482-4

[16] Ivanovic, A. and Neilson, R.D. (2013) *International Journal of Rock Mechanics and Mining Science*, **64**, 36-43. https://doi.org/10.1016/j.ijrmms.2013.08.017

[17] Yu, S.S., Niu, L.L., Chen, J., Wang, Y.W. and Yang, H.H. (2022) *Advances in Materials Science and Engineering*, **2022**, Article ID: 3282211. https://doi.org/10.1155/2022/3282211

[18] Yu, S.S., Niu, L.L. and Chen, J. (2022) *Shock and Vibration*, **2022**, Article ID: 7012510. https://doi.org/10.1155/2022/7012510

[19] Yu, S.S., Zhu, W.C., Niu, L.L., Zhou, S.C. and Kang, P.H. (2021) *Tunnelling and Underground Space Technology*, **85**, 56-66. https://doi.org/10.1016/j.tust.2018.12.001

[20] Lee, J. and Fenves, G.L. (1998) *Journal of Engineering Mechanics*, **124**, 892-900. https://doi.org/10.1061/(ASCE)0733-9399(1998)124:8(892)

[21] Dassault Systemses Simulia (2014) ABAQUS Theory Manual & Users Manuals Version 6.11.

[22] Henriques, J., Silva, L.S. and Valente, I.B. (2013) *Engineering Structures*, **52**, 747-761. https://doi.org/10.1016/j.engstruct.2013.03.041

[23] Park, K., Ha, K., Choi, H. and Lee, C. (2015) *Cement and Concrete Composites*, **63**, 122-131. https://doi.org/10.1016/j.cemconcomp.2015.07.008

[24] Chang, C., Wang, G.Z., Liang, Z.Z., Yang, J.H. and Tang, C.A. (2017) *Construction and Building Materials*, **135**, 665-673. https://doi.org/10.1016/j.conbuildmat.2017.01.031

[25] Henriques, J., Gentili, F., Simoes da Silva, L. and Simoes, R. (2015) *Engineering Structures*, **87**, 86-104. https://doi.org/10.1016/j.engstruct.2014.12.039

[26] Yang, W.R., He, X.J. and Dai, L. (2017) *Composite Structures*, **161**, 173-186. https://doi.org/10.1016/j.compstruct.2016.11.041

[27] Rezazadeh, M., Carvelli, V. and Veljkovic, A. (2017) *Construction and Building Materials*, **153**, 102-116. https://doi.org/10.1016/j.conbuildmat.2017.07.092

[28] Martin, L.B., Tijani, M., Hassen, F.H. and Noiret, A. (2013) *International Journal of Rock Mechanics and Mining Science*, **63**, 50-61. https://doi.org/10.1016/j.ijrmms.2013.06.007

Scientific Research Publishing

Journal of Modern Physics, 2023, 14, 741-754
https://www.scirp.org/journal/jmp
ISSN Online: 2153-120X
ISSN Print: 2153-1196

Ontology of Relativistic Mass

Edwin Eugene Klingman

Cybernetic Micro Systems, Inc., San Gregorio, CA, USA
Email: klingman@geneman.com

How to cite this paper: Klingman, E.E. (2023) Ontology of Relativistic Mass. *Journal of Modern Physics*, **14**, 741-754.
https://doi.org/10.4236/jmp.2023.145042

Received: March 17, 2023
Accepted: April 24, 2023
Published: April 27, 2023

Abstract

The term "relativistic mass" defined by equation $m = \gamma m_0$ with $\gamma = \left(1 - v^2/c^2\right)^{-1/2}$ has a somewhat controversial history, based on special relativity theory, mathematics, logic, intuition, experiment, and ontology. Key is the ontological framework, specifically whether the framework does or does not include gravity. This paper examines both cases, with detailed analysis of gravitomagnetism and of relativistic mass in collisions.

Keywords

Spacetime Ontology, Comparative Ontology, Local Absolute Space, Relativistic Mass, C-Field Circulation, Hidden Energy Reservoir, Transverse Mass, Longitudinal Mass

1. Introduction

The term "relativistic mass", defined by equation $m = \gamma m_0$ with $\gamma = \left(1 - v^2/c^2\right)^{-1/2}$, has a somewhat controversial history; some physicists believe that mass changes with velocity; others do not.

Trupp [1] claims "*According to the Theory of Special Relativity, the mass of a body has increased when it has gathered speed* (where mass resists acceleration)." Okun [2] states "*The terminology* [relativistic mass] *has no rational justification today*", while Rindler [3] and others retained it as a useful concept. This is a key disagreement about a very major aspect of physics, affecting our understanding of ontology, that is, the nature of physical reality. A physical theory provides a logico-mathematical model of reality that *assumes* an ontology; often, different theories assume different ontologies. Different theories have varied degrees of success, and this has caused many physicists to dismiss ontology as "unknowable". An anonymous reviewer seemed to confirm this: "*Eventually, strange and unintuitive as 4D is, one quits thinking about ontology.*" However, since the

nature of physical reality should be of significance to physicists, this paper presents an ontological analysis of relativistic mass. This paper is not an analysis of Einstein's special relativity of space-time; my recent paper [4] compares *space-time relativity* to *energy-time theory* on a feature-by-feature basis and presents a table of the results.

Analysis proceeds in terms of an ontological framework—specifically whether gravity is included or not. Special relativity excludes gravity, with frames in constant relative motion, unaccelerated with respect to each other, with no privileged frame. An observer in each frame feels himself to be at rest with a *rest mass*, m_0, regardless of his relative velocity with respect to the other frame.

Thyssen [5] claims "*special relativity leaves the debate on the dimensionality of the world underdetermined*." *i.e.*, it is uncertain whether time has a unique dimension and space has three dimensions D^{3+1} or space-time is a 4D reality, however, one can develop physics for a D^{3+1} universe (*presentism*) or a 4D universe (*eternalism*) in terms of Hestenes multi-vector $X=(ct+\boldsymbol{x})$ based on one's choice of basic assumptions: *local absolute space and time* D^{3+1} or *relative space-time* 4D and corresponding choice of how to apply the Lorentz transformation. The *energy-time* theory D^{3+1} formulation $X=(t+\boldsymbol{x})$ is Lorentz compatible, but, based on metaphysical assumptions of local absolute space and time and inertial mass, yields $m=\gamma m_0$, as opposed to relativistic 4D rotations mixing 3-space and time: $x'=\gamma(v,c)(x-vt)$, $t'=\gamma(v,c)(t-vx/c^2)$.

The non-intuitive mixing of time and space in 4D is problematic in relativity, where primed coordinates (x',t') apply in one frame: unprimed coordinates (x,t) in another. Relativity problems are always posed in terms of two or more inertial reference frames, each with its own universal time dimension, related by the Lorentz transformation. An alternate ontology, D^{3+1}, represents all of space and a universal time dimension covering all of space right now. Two physical frames of interest, one at rest, the other in motion, each have their own spatial map but share a common time. Speed of light is with respect to local absolute space, whereas relativity assumes $c=constant$ in all frames. Rindler, a major relativist, noted: "*Each inertial frame now has the properties with which the ether frame had been credited.*" The assumption $c=constant$ is necessary for Lorentz to work, but per Rindler: "*Light propagates the same in all inertial frames… It is not for us to ask how!*" If it made sense, we *could* ask how; Rindler admits *it doesn't make sense*.

Beginning with photon relation $x=\pm ct$ we can derive $c^2t^2-x^2-y^2-z^2=0$; for another photon $c^2t'^2-x'^2-y'^2-z'^2=0$. Constant c allows us to relate these two frames in relative motion $v\neq 0$ via the Lorentz group $(x',y',z',t')=L(v,c)(x,y,z,t)$ and inverse transformation: $L^{-1}(v,c)=L(-v,c)$. This group symmetry, characteristic of geometry, is represented by *rotations*; rotation from $\boldsymbol{x}$ to $\boldsymbol{x}'$ can be reversed by an inverse rotation from $\boldsymbol{x}'$ to $\boldsymbol{x}$. Sobczyk [6] develops a theory of linear algebra based on such null vectors with property $v^2=0$. In physics they produce the invariants about which physical theories can be formed.

Einstein concluded, circa 1918, that gravity functioned as the *ether*, but failed to update relativity, which banishes the medium of ether, replacing it with the proclamation that the local space-time coordinate frame accomplishes the required invariance. The gravitational field is assumed present everywhere in space, and, having energy, the field is *material* and is the medium through which electromagnetic waves and gravitomagnetic waves propagate. Light propagation in this local medium is compatible with both Michelson-Morley and Michelson-Gale experiments [7] but violates Einstein's axiom of constant c in all frames and his claim that one cannot detect the speed of the local frame from within the frame.

This paper is organized as follows:

The Introduction discusses ideas about relativistic mass, key to *ontology*—the physical reality of the universe—briefly describing two alternate ontologies. Section 2 traces Voight's decision to vary space and time in analyzing the Doppler effect, instead of varying the dynamic frequency and momentum aspects of the (acoustic) physics of reality. Section 3 treats *relativistic mass* as *Lorentzian mass* in a Galilean framework. Section 4 applies a concept from the quantum theory of fields, super-selection rules, to formulate a Hamiltonian in terms of spin-$\frac{1}{2}$ particles and spin-1 helical C-field circulation. In Section 5, the Lenz Law nature of the gravitomagnetic field is discussed. Section 6 asks "*How weak is the C-field*?" Local gravity holds the moon to the earth and promises pain when anyone jumps from a high place. Gravity is *not* weak; what about the C-field? Section 7 defines C-field energy and asks how this energy is to be accounted for. Section 8 treats the issue of relativistic mass in collisions. Section 9 summarizes the paper.

2. Voight's Transformation

The source of the idea that time and space change with local velocity appears to be Voight's 1887 analysis of the Doppler effect, based on the generalized wave function: $\psi = \psi_0 \sin\left(\boldsymbol{k}\cdot\boldsymbol{r} - \omega t\right)$, where the phase angle is a D^{3+1} product of $\{\boldsymbol{k},\omega\}$ with $\{\boldsymbol{r},t\}$. Voight chose parameters of space and time to vary for two observers, rather than the momentum and frequency aspects of the wave carrying the Doppler shift. His coordinate-based analysis underlies Einstein's relativistic interpretation of space and time, with associated concepts: "time-dilation" and "length contraction". The corresponding space-time ontology derived from Lorentz is based on 4D-geometry; the ability to transfer from one 4D frame (x,y,z,t) to another frame (x',y',z',t'), with basic motion fixed by uniform velocity $\boldsymbol{v}$ between the frames. Einstein's lack of acceleration removes *force* from the picture; the transformation from an event in one frame to its corresponding event in the other frame is independent of mass, so mass does not appear in the Lorentz transformation.

In energy-time theory [8] the *clock slowing* mechanism is explained using Galilean transformation; arguments exist against length contraction, which has

never been measured and, per Rindler, probably never will be. In space-time theory t' is the *time dimension* in the primed frame, different from the t dimension in the unprimed frame; incompatible with physicists' intuition, while the energy-time definition of t' is that of time *measurement*, not time dimension.

Time-dilation, the key "proof" of relativity, can be derived in the ontology of local absolute space and time, by assuming that mass is a function of velocity $m = m(v)$. When one frame is accelerated with respect to another, clocks in the accelerated frame effectively gain mass and hence resist acceleration. All clocks are based on some form of simple harmonic oscillator, in which a restoring force returns a displaced mass to its equilibrium position, where it overshoots and is displaced in the opposite direction; the increase in inertia causes mass to accelerate more slowly, so clocks do run slower when moving. That mass will be minimum when $v = 0$ implies a preferred frame in which mass is minimized. The *space-time symmetry principle* forbids preferred frames, so rest mass is not associated with *any* frame, but with *every* frame. Any observer in a moving frame sees rest mass m_0; in D^{3+1}-ontology only the rest frame S has $m \equiv m_0$ while 4D-ontology assigns velocity zero to *every* object at the origin of any S' inertial reference frame: $m \equiv m_0$; when relativists transform (x, y, z, t) and $(x, y, z, t)'$ they reset rest mass:

$$\begin{matrix} \text{Rest} \\ \begin{bmatrix} x = 0 \\ \dot{x} = 0 \\ m = m_0 \end{bmatrix} \end{matrix} \Rightarrow \begin{matrix} \text{Moving} \\ \begin{bmatrix} x' = 0 \\ \dot{x}' = 0 \\ m' = m_0 \end{bmatrix} \end{matrix} \tag{1}$$

Einstein essentially invented "slices" of physical reality in which the objects of interest move with uniform velocity with respect to each other. He *excluded from his theory* periods of physical acceleration necessary to provide the relative velocity to objects initially at rest in a local frame and he mapped 4D-ontology into "slices" of D^{3+1}-ontology as seen in **Figure 1**. The velocity curve shows constant relative velocity of relativity as shaded regions, while the acceleration portions of the curve exist only in D^{3+1}-ontology, between the slices.

Recognition of the *relativistic reset* $m(v) \to m_0$ of mass as the basis of the inertial reference frame, *automatically excludes all inter-frame kinetic energy*; allowing the observer to switch from one frame to the other and to retain the relevant *rest mass* in accordance with *space-time symmetry*, the key postulate that *there is no preferred frame*. This enables geometric transformation from one frame to the other and back, but makes it is impossible to tell which inertial frame is stationary and which is moving. In other words, the relativistic approach effectively *resets* the rest mass in each frame, while causing parameters of space and time to vary from observer to observer according to Lorentz transformation. So, relativity, based on ontologically questionable assumptions, always contains paradoxes, places where logic breaks down. Per Susskind [9]:

"*Special relativity…is counter-intuitive…full of paradoxical phenomena*."

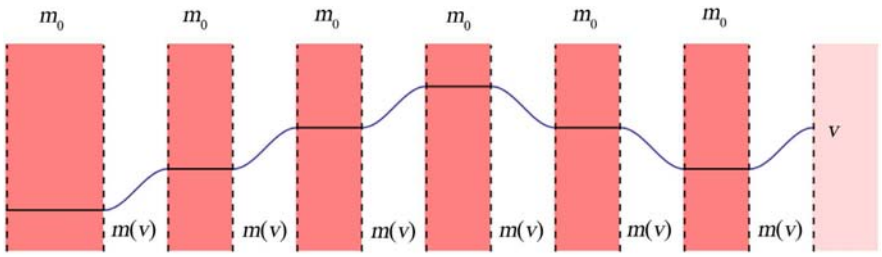

Figure 1. Map 4D-ontology onto "slices" of D^{3+1}-ontology.

3. Relativistic Mass = Lorentzian Mass

4D *time-space*-rotation is thus established at the expense of kinetic energy according to Lorentz transformation, while according to *energy-time theory* inertial mass is transformed by inertial factor γ to Lorentzian mass, $m = \gamma m_0$; *time and space are Galilean in nature*. Lucas and Hodgson [10] say of inertial mass: "*If we insist on retaining Newtonian dynamics, and Newtonian definitions of velocity and acceleration, then we can still obtain relativistically correct results if we pay the price of allowing the mass to depend on the velocity.*"

$$\begin{array}{cc} \text{Space-time theory} & \text{Energy-time theory} \\ \left\{\begin{array}{c} m' = m_0 \\ x' = \gamma(v)(x - vt) \\ t' = \gamma(v)(t - vx) \end{array}\right\} & \left\{\begin{array}{c} m' = \gamma(v) m_0 \\ x' = x - vt \\ t' = t \end{array}\right\} \end{array} \tag{2}$$

Einstein's relativity states the equivalence of inertial frames of reference. Weinberg [11] distinguishes this from the Galilean principle of relativity, obeyed by Newtonian mechanics, by the transformation connecting coordinate systems in different inertial frames. Of course, physics is fundamentally independent of coordinate systems—they can have no effect on physical reality. Per Weinberg: "*A symmetry transformation is a change in our point of view that does not change the results of possible experiments.*" Although the mathematics of the Poincare group is simpler than that of the Galilean group, Weinberg notes:

"*…there is nothing to prevent us from formally enlarging the Galilean group, by adding one more generator to its Lie algebra, which commutes with all the other generators, and whose eigenvalues are the masses of the various states.*"

In Equations (2), *energy-time theory* is seen to consist of the Galilean transformation and a generator whose eigenvalues are the masses of the various states in relative motion. This is the formal explanation of *relativistic mass*.

Weinberg [12] also points out that since $\mathrm{d}\tau = \mathrm{d}t/\gamma$ we obtain:

$$m\frac{\mathrm{d}}{\mathrm{d}t}[\gamma v] = q\left[\boldsymbol{E} + \frac{\boldsymbol{v}}{c} \times \boldsymbol{B}\right]. \tag{3}$$

"*It is a special feature of electromagnetic force that the only changes in the equation of motion introduced by special relativity is the replacement off mass m in the momentum with* $m = \gamma m_0$, [*and thus*] *treat* γm_0 *as a relativistic mass.*"

In other words, the concept of relativistic mass is conceptually useful. Weinberg also points out that, based on Maxwell's equations, "*we have no a priori knowledge of the Lorentz transformation properties of the electric and magnetic fields*."

The use of relativistic mass, $m = \gamma m_0$ in *energy-time theory* obviates the need for Lorentz transformation on space and time. This is ontologically correct at the level of special relativity, which does *not* incorporate gravitation. *Energy-time theory*, like special relativity, does *not* include a theory of gravity. When, however, one adds the primordial field theory to energy-time theory then kinetic energy of the moving mass is shown to represent storage of energy in the C-field circulation, and mass is invariant, as claimed.

4. Super-Selection Rules

Weinberg, in *The Quantum Theory of Fields*, observes that it may not be possible to prepare a system in a state represented by $\Psi_A + \Psi_B$. "It is widely believed to be impossible to prepare a system in a superposition of two states whose total angular momenta are integers and half-integers, respectively." In such cases, there is a "superselection rule" between the different classes of states. In this section we invoke a *superselection rule* explanation of relativistic mass. Elsewhere, I derive a fermion from the primordial field with spin-$\frac{1}{2}$, while the field circulation induced by particle motion has $U(1)$ symmetry, and hence integer spin. According to the superselection rule, these states are not super-imposable into one state, and must be developed separately. In other words, the mass/energy of the moving particle is a function of two classes of energy:

$$E = f\left(mc^2, mv^2\right) \tag{4}$$

where mc^2 has been shown to have half-integral spin, and where mv^2 will be seen to have integral spin representing momentum-induced circulation of the C-field. In *energy-time theory* the Hamiltonian is derived for *relativistic mass* $m = \gamma m_0$, with $E = mc^2$ and $\boldsymbol{p} = m\boldsymbol{v}$:

$$\begin{aligned} &E = \left(m_0^2c^4 + c^2p^2\right)^{1/2} \Rightarrow E^2 = m_0^2c^4 + c^2p^2 = m_0^2c^4 + c^2\gamma^2m_0^2v^2 \\ &\Rightarrow E^2 = \gamma^2m_0^2c^4 \end{aligned} \tag{5}$$

Dividing both sides by $m_0^2c^4$ we obtain:

$$\frac{E^2}{m_0^2c^4} = 1 + \gamma^2\frac{v^2}{c^2} \Rightarrow \gamma^2 = 1 + \gamma^2\frac{v^2}{c^2} \Rightarrow \gamma = \frac{1}{\sqrt{1 - v^2/c^2}} \tag{6}$$

In other words, separating the energies according to spin thus yields:

$$E = \sqrt{\left(m_0c^2\right)^2 + \left(cp\right)^2} = m_0c^2\sqrt{1 + v^2/c^2} \sim \underbrace{m_0c^2}_{\text{spin-}\frac{1}{2}} + \underbrace{\frac{m_0}{2}v^2}_{\text{spin-1}}, \tag{7}$$

which is the way orthogonal entities must be added. Energy-time theory, supporting the concept of relativistic mass, retains the Lorentz γ-factor, but applies

it to inertial mass, rather than to abstract space and time. In D^{3+1}-ontology the velocity $\boldsymbol{v}$ of an object is with respect to rest frame *S*, *local absolute space*, and any change of $\boldsymbol{v}$ is via accelerating force: $m\boldsymbol{a} = \mathrm{d}\boldsymbol{p}/\mathrm{d}t = \mathrm{d}\left(\gamma m_0 \boldsymbol{v}\right)/\mathrm{d}t$ while in 4D-ontology the momentum relation $\boldsymbol{p} = \gamma m_0 \boldsymbol{u}$ is applied where $\boldsymbol{u}$ is the velocity of the object in a reference frame, *not* the velocity of the reference frame relative to another.

5. The Lenz Law Nature of the Gravitomagnetic Field

Energies involved in relativistic mass include rest mass mc^2 and momentum $\boldsymbol{p}$. Circa 1893, Heaviside [13] extended Newtonian gravity, based on analogy with Maxwell's equations, with a key equation describing the circulation of the gravitomagnetic field, which we call the C-field:

$$\nabla \times \boldsymbol{C} = -\boldsymbol{p} + \frac{\partial \boldsymbol{G}}{\partial t} \tag{8}$$

In (8) we let physical constants $c = g = \hbar = 1$ where c is the speed of light and g is Newton's gravitational constant, with $\boldsymbol{G}$ being the gravitational field. Instead of momentum, $\boldsymbol{p}$ is momentum density:

$$\boldsymbol{p} = \frac{\boldsymbol{P}}{\int \mathrm{d}^3 x} = \frac{m}{\int \mathrm{d}^3 x}\boldsymbol{v} = \rho \boldsymbol{v} \tag{9}$$

For momentum used in the Hamiltonian, we have $\boldsymbol{P} = m_0 \boldsymbol{v} = \int \mathrm{d}^3 x \nabla \times \boldsymbol{C}$. That is, momentum is the volume integral of the C-field circulation induced by the momentum density $\boldsymbol{p}$. Temporarily ignore change in gravitational field, $\frac{\partial \boldsymbol{G}}{\partial t}$, and consider only $\nabla \times \boldsymbol{C} = -\boldsymbol{p}$. The force $\boldsymbol{F}$ that accelerates rest mass $\boldsymbol{F} = m_0 a = \mathrm{d}\boldsymbol{p}/\mathrm{d}t$ gives rise to a change in circulation of the C-field:

$$\frac{\mathrm{d}}{\mathrm{d}t}\left(\nabla \times \boldsymbol{C}\right) = \frac{-\frac{\mathrm{d}\boldsymbol{P}}{\mathrm{d}t}}{\int \mathrm{d}^3 x} \tag{10}$$

The negative sign in Equation (8) is associated with the direction of circulation, that is, momentum density $\boldsymbol{p}$ induces a left-handed circulation about the momentum. However, in the force formula, any negative sign associated with change in momentum density $\mathrm{d}\boldsymbol{p}/\mathrm{d}t$ will have the same meaning as current flow in Lenz's Law of electromagnetic theory. As a reminder of the physics of Lenz's Law, consider the classic distributor found on gasoline engines. The collapsing magnetic field induced by flowing electric current is interrupted by mechanically breaking the connection. Lenz's Law states that the direction of the electric current induced in a conductor by a changing magnetic field is such that the magnetic field created by the induced current opposes changes in the initial magnetic field. When the current conductor is broken, the change in current is immediate, and this large derivative (rate of change) induces a strong force to keep current flowing in the inductor. Since electric "force" is the "emf" electric field or induced *electro-motive force*, a sufficiently strong emf will ionize atoms

and produce a "spark". This spark is timed to ignite the fuel in the cylinder near top-dead-center, thus driving the piston down for the power stroke.

In other words, the current flowing in the coil (inductor) induces a magnetic field that is sustained by the continued current flow. When the flow is interrupted, the collapsing magnetic field causes an electric force that attempts to keep the current flowing. The dual of electric current density flow in electromagnetism is mass density flow in gravitomagnetism: $\boldsymbol{J} \Leftrightarrow \boldsymbol{P}$ therefore:

$$\nabla \times \boldsymbol{B} \sim \boldsymbol{j} \quad \text{and} \quad \nabla \times \boldsymbol{C} \sim -\boldsymbol{p} \tag{11}$$

implies

$$\frac{\mathrm{d}}{\mathrm{d}t}(\nabla \times \boldsymbol{B}) \sim \frac{\mathrm{d}\boldsymbol{j}}{\mathrm{d}t} \quad \text{and} \quad \frac{\mathrm{d}}{\mathrm{d}t}(\nabla \times \boldsymbol{C}) \sim -\frac{\mathrm{d}\boldsymbol{p}}{\mathrm{d}t}. \tag{12}$$

Thus, the gravitomagnetic dual of Lenz's Law is such that change in momentum (force $\mathrm{d}\boldsymbol{P}/\mathrm{d}t$) induces a C-field circulation. For a charged particle we might use electric field $\boldsymbol{E}$ to accelerate the particle, inducing both B-field and C-field circulations. If charges are balanced, $\sum q = 0$, then we can mechanically accelerate the mass, producing only C-field circulation. When all forces are removed, the mass will essentially "coast" forever, that is, *momentum is conserved*. Yet, according to Feynman [14]: *the reason why things coast for ever has never been found out*: "*The law of inertia has no known origin*." But, from the above analogy, a decrease in momentum will generate a corresponding decrease in C-field circulation, and this will, in turn, generate a force that compensates for the initial decrease, thereby maintaining momentum. Thus, acceleration increases the C-field circulation, while deceleration is opposed by the existing circulation. The same physical reasoning applies to a particle "tunneling" through a finite potential barrier. The change in momentum as the particle begins to penetrate the barrier is opposed by the corresponding force associated with the change in circulation. The particle is effectively accelerated by the collapsing C-field circulation until the circulation disappears.

6. How Weak Is the C-Field?

A potentially major impediment to understanding gravitomagnetic circulation as kinetic energy, and hence as "relativistic mass", is the label "weak field approximation", based on derivation of Heaviside's equations from Einstein's nonlinear field equations in curved space-time. For weak fields the higher order terms in the approximation can be ignored and higher order terms dropped, leaving the "linear" Heaviside equations. For those physicists, probably the majority, who believe that curved space-time is the true nature of gravity, this is a convincing argument. Yet, physicists such as Clifford Will, working with *gravitomagnetic post-Newtonian* physics, have remarked upon the unexpected effectiveness of the equations in strong-field problems [15]. And Einstein's gauge field tensor can be derived from Heaviside's equations [16].

The ontology of gravitational field versus curved space-time is treated in [17] and [18]. The ontology of the gravitomagnetic field can explain century old pa-

radoxes associated with curved space-time ontology. The gravitational field underlies the "ontology of relativistic mass".

The existence of the C-field was proved in 2011 via the *Gravity Probe B* experiment [19] where the results confirmed general relativity to within a few percent. But this too may give the impression of "weak field", largely because the experiment was performed in orbit and the density of the Earth as seen from orbit is relatively low. Contrast this with the density of atomic nuclei seen from nuclear distances. The key parameter in $\nabla \times \boldsymbol{C} \sim \rho \boldsymbol{v}$ is mass density ρ. For a macro-object in motion, a mass, the relevant C-field circulation energy is the sum of the energy for each nucleus times the number of nuclei of which the mass is constituted.

Finally, as analyzed in "*Quasi-Local Mass*", energy-density is *not defined* in general relativity; this too probably accounts for the fact that many physicists are oblivious to the ontology of the C-field circulation, conceiving of it instead as "frame dragging" in curved space time.

For the moment, take both ontologies seriously. Assume, per general relativity, a twisting of the local spacetime fabric with respect to the undisturbed background of reality. Contrast this with the circulating flow of the gravitomagnetic C-field. A 2D rubber sheet is often used to illustrate curved space time, but this perspective is lacking. Consider the images in **Figure 2** [20] and [21]; in 2a a superluminal jet source is postulated to be a black hole spinning near the extreme theoretical limit. In 2b the spin of Earth is shown "dragging" curved space around it. Since the Earth has been spinning daily for billions of years; this "rubber band" concept of space-time would imply that the rubber sheet must be wrapped up infinitely tight, a paradoxical idea. On the other hand, *the C-field conception is based on circulation of the energy in the field*, and simply contributes to the angular momentum of a spinning object; the circulating field surrounds the object. We next look at the energy of the field.

What has yet to be measured is the strength of the C-field at the atomic and nuclear level. Since Heaviside's equations are density based, one expects the greatest C-field strength at the nuclear level. Erroneous belief in the "weak field approximation" has prevented consideration of this realm of physics.

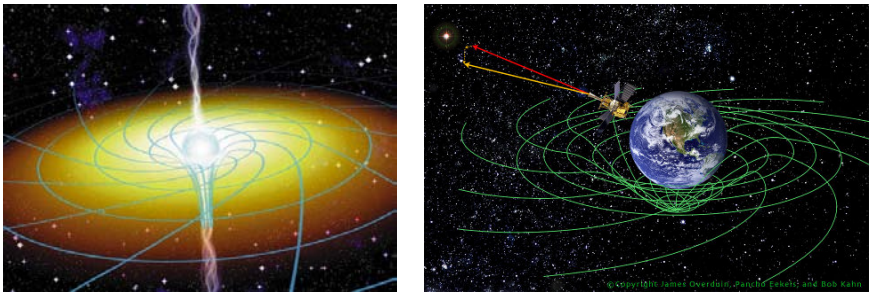

(a) (b)

Figure 2. Images of "frame dragging" in general relativity. (a) NASA image of frame dragging around a black hole, and (b) Frame dragging as measured by Gravity Probe B.

7. The Energy of the C-Field

The energy density of any physical field is proportional to the square of the field strength, for example, the energy density of the electromagnetic field is $\sim\left(E^2+B^2\right)$. The formula for C-field energy density is:

$$\left(\frac{c^2}{g}\right)(\boldsymbol{C}\cdot\boldsymbol{C}) \quad = \text{C-field energy density} \tag{13}$$

If we multiply energy density by local volume, we obtain the dimensional relation:

$$\int \mathrm{d}^3x\left(\frac{c^2}{g}\right)(\boldsymbol{C}\cdot\boldsymbol{C}) \Rightarrow \left(l^3\right)\cdot\left(\frac{m}{l}\frac{1}{t^2}\right)=\frac{ml^2}{t^2}\approx mv^2 . \tag{14}$$

The C-field has been shown to be real, and therefore to have finite energy density, but this local energy density has not been treated in any standard treatment of kinetic energy (of motion). Thus, we seem to be faced with two choices:

If C-field energy is not kinetic energy, then it must be added to kinetic energy in any real physical situation, else C-field circulation energy is kinetic energy; no new energies need be accounted for.

An alternative gravitomagnetic approach is dual to geometric algebra-based treatments of Maxwell's equations; Arthur [22] develops D^{3+1} and 4D models in detail. We follow his treatment of D^{3+1}-Maxwell equation $\left(\nabla+\partial_t\right)F=J$ with F the field tensor and J the source, $J=\rho\left(1+v\right)$. Multiply both sides by $\left(\nabla-\partial_t\right)$ to obtain:

$$\left(\nabla^2-\partial_t^2\right)F=\left(\nabla-\partial_t\right)J . \tag{15}$$

In source-free space $J=0$ and Equation (15) becomes the wave equation, which, in terms of a plane wave, reduces to $\left(-k^2+\omega^2\right)F=0$. Making use of natural units $g=c=\hbar=1$ and the quantum equivalents: momentum $p=\hbar k$ and $E=\hbar\omega=\hbar C$, we obtain:

$$\left(-k^2+\omega^2\right)\Rightarrow -p^2+C^2=0 \tag{16}$$

For unit mass this implies

$$p^2=C^2 \tag{17}$$

/ \ <energy densities>

kinetic C-field

In other words, kinetic energy, is again seen to be physically represented by energy of gravitomagnetic circulation induced by momentum $\boldsymbol{p}$. Almost every energy in physics is associated with a potential or energy field—kinetic energy may be unique in having no field correlate. Heaviside theory of gravitomagnetism implies that the essentially undefined mechanism of storage of *energy of motion* is actually C-field circulation energy, bringing our most basic energy into agreement with all other field energies.

8. Relativistic Mass in Collisions

The chiral nature of C-field circulation (left-handed) implies that particles mov-

ing in opposite directions generate C-fields circulating in opposite directions. If these particles collide, counter-rotating C-fields should effectively cancel each other, that is, the relativistic mass of each cancels out. Does this happen? A recent paper by Trupp, dealing with "*The Interaction between an Accelerated Mass in Straight Motion and a Hidden Energy Reservoir as a Strict Mathematical Consequence of Special Relativity*", states:

"*The total energy of two objects that undergo a symmetrical, elastic, head-on collision is therefore not conserved, thus requiring the involvement of a hidden reservoir of energy.*"

He claims that "*an apparent disappearance of energy has been noticed in particle physics already, but its consequences have been ignored*". This recalls Cannoni's statement [23] that the *law of velocity addition* is known to be violated in relativistic colliders. It appears as if violations of Einstein's special relativity are essentially ignored in the literature, rather than the usual approach in which any experiment that contradicts a theory is typically considered to invalidate the theory. Additionally, paradoxical elements of relativity are downplayed. Einstein, Lorentz, and others distinguish between "transverse mass" and "longitudinal mass". R. C. Tolman [24] observed that:

"*If, however, mass is a quantity to which a conservation law applies, the mass of a body cannot well be different in different directions…*"

For a particle with momentum $\boldsymbol{p}_z$ in the *z*-direction a longitudinal force $\boldsymbol{F}_L = \frac{\mathrm{d}\boldsymbol{p}_z}{\mathrm{d}t}$ is applied in the *z*-direction, acting in the same direction as the original force that resulted in $\boldsymbol{p}_z = \nabla \times \boldsymbol{C}$. From the above discussion of Lenz's Law, we observe that any further acceleration or deceleration in this direction will be opposed by existing C-field circulation, and this resistance to further acceleration is interpreted as increased (relativistic) mass.

On the other hand, a transverse force $\boldsymbol{F}_T = \frac{\mathrm{d}\boldsymbol{p}_y}{\mathrm{d}t}$ is orthogonal to momentum $\boldsymbol{p}_z$ and therefore orthogonal to $\nabla \times \boldsymbol{C}$. In this case local C-field circulation will not resist acceleration by $\boldsymbol{F}_T$ and thus will not be interpreted as other than rest mass, *i.e.*, relativistic mass is directional. This does not lead us, as it led Einstein and others, to distinguish between *transverse mass* and *longitudinal mass*.

This demonstrates the power of ontology to resolve issues. Equations of motion that are ontologically unexplained or otherwise inappropriate can lead to confusion: "*the mass of a body cannot well be different in different directions.*" In energy-time ontology and Heaviside-based gravity the mass of the body is always the same (rest) mass in all directions, but a body in motion has direction-dependent momentum, and correspondingly direction-dependent circulating field-based resistance to acceleration.

In his analysis, Trupp concludes that Epstein [25] was correct when he postulated that the only way to avoid the inconsistency of two different masses is the following:

"…*when a body is accelerated by means of an external, technical force, an additional, hidden force turns up.*"

This "hidden" force is the Lenz-Law-like force associated with $\boldsymbol{p}_z = \nabla \times \boldsymbol{C}$. This direction dependent force, $\frac{\mathrm{d}}{\mathrm{d}t}(\nabla \times \boldsymbol{C}) \sim -\frac{\mathrm{d}\boldsymbol{p}}{\mathrm{d}t}$ is hidden from previous special relativity experiments and hidden theoretically by the erroneous *weak field approximation* of general relativity.

Trupp states initially that he is by no means attempting to modify or refute the basic assumptions of special relativity; he chooses to analyze a "fixed acceleration", a very artificial construct, which, nevertheless leads him to conclude that:

"*The energy of the hidden, work-performing force is fed from a hidden reservoir in space.*"

He states the relativistic mass or energy generated by Epstein's hidden force is not converted into elastic energy in a head-on collision, but

"*flows off into the unknown where it had come from.*"

We are not committed to the proposition that special relativity should not be refuted, and do not argue Trupp's details. It is obvious from the rest of our paper that the "*hidden reservoir in space*" is C-field circulation, which stores the energy as angular momentum (equal to linear momentum, in agreement with partitioning of energy).

In other papers I have shown that the C-field resolves other century-old paradoxes built into special and general relativity. Therefore, it is interesting that Trupp and others deduce that the nature of the resolution is *hidden*, a somewhat ontological deduction of the nature of reality.

9. Summary

It seems strange that an actual storage mechanism for kinetic energy is generally ignored. Yet, kinetic energy, *the energy of motion*, is typically the first introduction to energy in high school or even earlier. Young physicists simply learn the definition of such and absorb it before going on to learn of many other forms of energy, all of which are associated with some energy storage mechanism. If and when they encounter gravitomagnetic field energy, they are biased, both by the original acceptance of kinetic energy and the later biases of "weak field approximation" and of "frame dragging". It is hardly surprising that when physicists encounter *relativistic mass* and use the relativistic Hamiltonian to relate it to kinetic energy, it is with some degree of confusion. As noted above, *C-field energy is real*, and must either be *equated to* kinetic energy or *added to* kinetic energy. From thorough consideration of the density-based nature of C-field circulation, and the density of atomic and nuclear constituents of matter, it appears that equating momentum-induced C-field circulation energy to momentum associated kinetic energy is the most natural interpretation and is completely compatible with the ontology of relativistic mass.

Conflicts of Interest

The author declares no conflicts of interest regarding the publication of this paper.

References

[1] Trupp, A. (2022) *Journal of Modern Physics*, **13**, 16-33. https://doi.org/10.4236/jmp.2022.131002

[2] Okun, L. (2008) The Concept of Mass. https://arxiv.org/pdf/hep-ph/0602037.pdf

[3] Rindler, W. (1991) Introduction to Special Relativity. 2nd Edition, Oxford Science Pub, Oxford.

[4] Klingman, E. (2023) *Journal of Modern Physics*, **14**, 501-525. https://doi.org/10.4236/jmp.2023.144028

[5] Thyssen, P. (2019) *Foundations of Physics*, **49**, 1336-1354. https://doi.org/10.1007/s10701-019-00294-8

[6] Sobczyk, G. (2023) Geometric Algebras of Light Cone Projective Graph Geometries. *ICACGA* 2022: *International Conference of Advanced Computational Applications of Geometric Algebra*, Denver, 2-5 October 2022, 1-22. https://www.researchgate.net/publication/369033961

[7] Michelson, A. (1925) *The Astrophysical Journal*, **61**, 137. https://doi.org/10.1086/142878

[8] Klingman, E. (2020) *Journal of Modern Physics*, **11**, 1950-1968. https://doi.org/10.4236/jmp.2020.1112123

[9] Susskind, L. (2017) Special Relativity and Classical Field Theory. Basic Books, New York.

[10] Lucas and Hodgson (1990) Spacetime and Electromagnetism. Clarendon Press, Oxford.

[11] Weinberg, S. (2005) The Quantum Theory of Fields. Vol. 1, Cambridge University Press, Cambridge.

[12] Weinberg, S. (2021) Foundations of Modern Physics. Cambridge University Press, Cambridge. https://doi.org/10.1017/9781108894845

[13] Heaviside, O. (1893) *The Electrician*, **31**, 81-82.

[14] Feynman, R. (1965) The Character of Physical Law. The M.I.T. Press, Cambridge.

[15] Will, C. (2011) *Proceedings of the National Academy of Sciences of the United States of America*, **108**, 5938. https://doi.org/10.1073/pnas.1103127108

[16] Klingman, E. (2022) *Journal of Applied Mathematics and Physics*, **10**, 2292-2302. https://doi.org/10.4236/jamp.2022.107156

[17] Klingman, E. (2021) *Journal of Modern Physics*, **12**, 1190-1209. https://doi.org/10.4236/jmp.2021.129073

[18] Klingman, E. (2022) *Journal of Modern Physics*, **13**, 347-367. https://doi.org/10.4236/jmp.2022.134025

[19] Everitt, C., *et al.* (2011) *Physical Review Letters*, **106**, Article ID: 221101.

[20] Frame Dragging near Spinning Black Holes? https://heasarc.gsfc.nasa.gov/docs/xte/Snazzy/Overheads/frame.SM.html

[21] Frame Dragging as Measured by Gravity Probe B. Credit & © J. Overduin, P. Eekels, B. Kahn.

[22] Arthur, J. (2011) Understanding Geometric Algebra for Electromagnetic Theory. Wiley, Hoboken. https://doi.org/10.1002/9781118078549

[23] Cannoni, M. (2017) *International Journal of Modern Physics A*, **32**, Article ID: 1730002. https://doi.org/10.1142/S0217751X17300022

[24] Tolman, R. (1912) *Philosophical Magazine*, **23**, 375-380. https://doi.org/10.1080/14786440308637231

[25] Epstein, P. (1911) *Annalen der Physik*, **341**, 779-795. https://doi.org/10.1002/andp.19113411404

Journal of Modern Physics, 2023, 14, 755-776
https://www.scirp.org/journal/jmp
ISSN Online: 2153-120X
ISSN Print: 2153-1196

The Essence of Microscopic Particles and Quantum Theory

Xiangyao Wu[1], Benshan Wu[1], Qiming Wu[1], Hong Li[2]

[1]Institute of Physics, Jilin Normal University, Siping, China
[2]Institute for Interdisciplinary Quantum Information Technology, Jilin Engineering Normal University, Changchun, China
Email: wuxy2066@163.com

How to cite this paper: Wu, X.Y., Wu, B.S., Wu, Q.M. and Li, H. (2023) The Essence of Microscopic Particles and Quantum Theory. *Journal of Modern Physics*, **14**, 755-776.
https://doi.org/10.4236/jmp.2023.145043

Received: September 2, 2022
Accepted: April 25, 2023
Published: April 28, 2023

Abstract

In the paper, we have given the quantum equation of the gravitational field intensity $E_g(\mathbf{r},t)$ and electric field intensity $E(\mathbf{r},t)$ for the material particles, since the gravitational field intensity $E_g(\mathbf{r},t)$ and electric field intensity $E(\mathbf{r},t)$ is in direct proportion to the distribution function $\psi(\mathbf{r},t)$ of particle spatial position (wave function), these quantum equations are natural converted into the Schrodinger equation. In addition, we have proposed the new model about the photon and matter particles. For all particles, they are not point particles, but they have a very small volume. The photon has a vibration electric field in its very small volume. The neutral material particle, such as neutron, it has a vibration gravitational field in its very small volume. For the charge material particles, such as electron and proton, they have both vibration gravitational field and vibration electric field in their very small volume. With the model, we can explain the diffraction and interference of single slit and multiple-slit for the single photon and material particles, the volatility of all particles come from the superposition of their respective vibration field. After the vibration field of particle superposition, it shows up as a particle property. On this basis, We have obtained some new results, and realized the unification of both wave and particle and field and matter.

Keywords

Photon, Material Particles, Electromagnetic Field, Gravitational Field, Schrodinger Equation

1. Introduction

In 1900, the derivation of the black-body spectrum due to Planck is taken as the birth of quantum theory [1]. After Einstein proposed the light quantum hypo-

thesis and successfully explained the photoelectric effect, people accepted the theory that light has wave-particle duality. In 1922, D. E. Broglie argued that all particles, like photons, have wave-particle duality [2] [3]. Broglie further thinking matter wave theory, he thought the matter waves of wave mechanics and classical mechanics is similar to the relationship between wave optics and geometrical optics, the relationship between the analogy thought for later founded the schrodinger wave mechanics to lay the important foundation of schrodinger in material Broglie wave theory, on the basis of schrodinger quantum wave equation is given [4] [5] [6].

In the development of physics in the 20th century, Einstein and Bohr are the two greatest scientist. They both created the glory of modern physics, but they had their own unique and profound views on the basic problems of modern physics, which caused a long-term debate. Bohr think quantum own existence form, can be described by probability wave function, when the quantum system interact with the outside world, the wave function will collapse to a specific value can be observed, for quantum system, it is impossible to get something other than the probability, the laws of quantum mechanics is only spontaneously, must abandon the decisive principle of cause and effect. Bohr later put forward the famous correspondence principle and complementary principle, which further caused a great shock in the physics.

In 1935, Einstein, Podorsky and Rosen proposed the criterion of the completeness of physical theoretical system and the famous EPR paradox [7], which involves how to understand the reality of the micro world and demonstrates the incompleteness of the description of physical reality by quantum mechanics. In 1950s, Bohm proposed the quantum theory of hidden parameters inspired by EPR paradox [8]. In the 1960s, John Bell derived a quantitative Bell's inequality [9] [10], on the quantum correlation of distant particles from mathematics according to the quantum theory of hidden parameters. It was possible to design experiments to test the EPR paradox. Physicists completed experiment results are in violation of Bell's inequality and consistent with the predictions of quantum mechanics [11] [12] [13]. The above experiments only show that quantum theory is related at a distance and non-local, but do not determine whether quantum theory is deterministic or non-deterministic, that is to say, whether the causality of the microscopic world is established has not been determined, and the debate on the basis of quantum theory needs to go on. Einstein acknowledged that the internal system of quantum mechanics was self-consistent, but he insisted that quantum mechanics was not the final description of a complete microscopic system.

Although quantum mechanics has made many achievements in developing new technologies, many fundamental questions still exist and need to be studied. In order to understand the microscopic world, whether we need to introduce new concepts and ideas to explain why we should introduce the concept of probability into quantum mechanics, thereby unifying the ideas of determinism and proba-

bility theory.

In classical electrodynamics, charged particle is treated as point charge, which leads to infinite self-energy. Therefore, it is problematic to treat particles as points. From the point of view of quantum mechanics, the Compton wavelength is usually used to describe the distribution area of particle, and the concept of point particles should be abandoned.

According to De Broglie's idea of analogy, the relation between quantum mechanics and classical mechanics is similar to that between wave optics and geometric optics. In the paper, we have given the quantum equation of the gravitational field intensity $E_g(\boldsymbol{r},t)$ for matter particles, since the gravitational field intensity $E_g(\boldsymbol{r},t)$ relatives to the particle position distribution function $\psi(\boldsymbol{r},t)$, the quantum equation convert into the Schrodinger equation. In the paper, we have given the quantum equation of the gravitational field intensity $E_g(\boldsymbol{r},t)$ and electric field intensity $E(\boldsymbol{r},t)$ for the material particles, since the gravitational field intensity $E_g(\boldsymbol{r},t)$ and electric field intensity $E(\boldsymbol{r},t)$ is in direct proportion to the distribution function $\psi(\boldsymbol{r},t)$ of particle spatial position (wave function), these quantum equations are natural converted into the Schrodinger equation. In addition, we have proposed the new model about the photon and matter particles. For all particles, they are not point particles, but they have a very small volume. The photon has a vibration electric field in its very small volume. The neutral material particle, such as neutron, it has a vibration gravitational field in its very small volume. For the charge material particles, such as electron and proton, they have both vibration gravitational field and vibration electric field in their very small volume. With the model, we can explain the diffraction and interference of single slit and multiple-slit for the single photon and material particles, the volatility of all particles come from the superposition of their respective vibration field. After the vibration field of particle superposition, it shows up as a particle property. On this basis, we have obtained some new results, and realized the unification of both wave and particle and field and matter.

2. The Relationship between Quantum Equation of Photon and Maxwell's Equations

The Maxwell's equations are the macroscopic equation of electromagnetic field, which are description the change rule of electric and magnetic fields for a beam of light or a large number of photons. The single photon also has electric and magnetic fields, it satisfies the Maxwell's equations.

1) The Maxwell's equations in vacuum are

$$\nabla \times \boldsymbol{E} = -\frac{\partial \boldsymbol{B}}{\partial t} \tag{1}$$

$$\nabla \times \boldsymbol{B} = \mu_0 \varepsilon_0 \frac{\partial \boldsymbol{E}}{\partial t} \tag{2}$$

$$\nabla \cdot \boldsymbol{E} = 0 \tag{3}$$

$$\nabla \cdot \boldsymbol{B} = 0 \tag{4}$$

In the Ref. [14], we have given the quantum vector wave equation of photon, it is

$$i\hbar \frac{\partial}{\partial t}\boldsymbol{\psi} = c\hbar \nabla \times \boldsymbol{\psi} + V\boldsymbol{\psi}, \tag{5}$$

where the $\boldsymbol{\psi}$ is the vector wave function of photon, the V is the potential energy of photon in medium, it is

$$V = \hbar\omega(1-n), \tag{6}$$

where the n is the refractive index of photon in medium. when the photon is in the air or vacuum, the refractive index $n=1$, the potential energy $V=0$, *i.e.*, it is a free photon, the Equation (2) becomes

$$i\hbar \frac{\partial}{\partial t}\boldsymbol{\psi} = c\hbar \nabla \times \boldsymbol{\psi}. \tag{7}$$

In the Ref. [15], we have given the quantum spinor wave equations of free and non-free photons (see Appendix A and B), they are:

$$i\hbar \frac{\partial}{\partial t}\psi(\mathbf{r},t) = -ic\hbar\boldsymbol{\alpha}\cdot\nabla\psi(\mathbf{r},t), \tag{8}$$

and

$$i\hbar \frac{\partial}{\partial t}\psi(\mathbf{r},t) = -ic\hbar\boldsymbol{\alpha}\cdot\nabla\psi(\mathbf{r},t) + V\psi(\mathbf{r},t). \tag{9}$$

The photon spinor wave function ψ and the matrices $\boldsymbol{\alpha}$ are:

$$\psi(\mathbf{r},t) = \begin{pmatrix} \psi_1(\mathbf{r},t) \\ \psi_2(\mathbf{r},t) \\ \psi_3(\mathbf{r},t) \end{pmatrix}, \tag{10}$$

and

$$\alpha_x = \begin{pmatrix} 0 & 0 & 0 \\ 0 & 0 & -i \\ 0 & i & 0 \end{pmatrix}, \alpha_y = \begin{pmatrix} 0 & 0 & i \\ 0 & 0 & 0 \\ -i & 0 & 0 \end{pmatrix}, \alpha_z = \begin{pmatrix} 0 & -i & 0 \\ i & 0 & 0 \\ 0 & 0 & 0 \end{pmatrix}, \tag{11}$$

Using the method of separation variable $\psi(\mathbf{r},t) = \psi(\mathbf{r})f(t)$, the Equations (8) and (9) become

$$-ic\hbar\boldsymbol{\alpha}\cdot\nabla\psi(\mathbf{r}) = E\psi(\mathbf{r}), \tag{12}$$

and

$$\left[-ic\hbar\boldsymbol{\alpha}\cdot\nabla + V\right]\psi(\mathbf{r}) = E\psi(\mathbf{r}), \tag{13}$$

where E is the total energy of photon, Equations (9) and (13) are the spinor wave equations of time-dependent and time-independent of photon in medium, which can be used to study the quantum property of photon in medium.

Substituting Equations (10) and (11) into (9), we have

$$
\begin{aligned}
i\hbar\frac{\partial}{\partial t}\begin{pmatrix}\psi_1\\ \psi_2\\ \psi_3\end{pmatrix} &= -i\hbar c\begin{pmatrix} 0 & -i\dfrac{\partial}{\partial z} & i\dfrac{\partial}{\partial y}\\ i\dfrac{\partial}{\partial z} & 0 & -i\dfrac{\partial}{\partial x}\\ -i\dfrac{\partial}{\partial y} & i\dfrac{\partial}{\partial x} & 0\end{pmatrix}\begin{pmatrix}\psi_1\\ \psi_2\\ \psi_3\end{pmatrix}+\begin{pmatrix}V & 0 & 0\\ 0 & V & 0\\ 0 & 0 & V\end{pmatrix}\begin{pmatrix}\psi_1\\ \psi_2\\ \psi_3\end{pmatrix}\\
&= \hbar c\begin{pmatrix}\dfrac{\partial\psi_3}{\partial y}-\dfrac{\partial\psi_2}{\partial z}\\ \dfrac{\partial\psi_1}{\partial z}-\dfrac{\partial\psi_3}{\partial x}\\ \dfrac{\partial\psi_2}{\partial x}-\dfrac{\partial\psi_1}{\partial y}\end{pmatrix}+\begin{pmatrix}V & 0 & 0\\ 0 & V & 0\\ 0 & 0 & V\end{pmatrix}\begin{pmatrix}\psi_1\\ \psi_2\\ \psi_3\end{pmatrix}.
\end{aligned}
\tag{14}
$$

With Equation (14), we obtain

$$\hbar c\left(\frac{\partial\psi_3}{\partial y}-\frac{\partial\psi_2}{\partial z}\right)=i\hbar\frac{\partial}{\partial t}\psi_1-V\psi_1, \tag{15}$$

$$\hbar c\left(\frac{\partial\psi_1}{\partial z}-\frac{\partial\psi_3}{\partial x}\right)=i\hbar\frac{\partial}{\partial t}\psi_2-V\psi_2, \tag{16}$$

and

$$\hbar c\left(\frac{\partial\psi_2}{\partial x}-\frac{\partial\psi_1}{\partial y}\right)=i\hbar\frac{\partial}{\partial t}\psi_3-V\psi_3. \tag{17}$$

If we set $\boldsymbol{\Psi}=\psi_1\boldsymbol{i}+\psi_2\boldsymbol{j}+\psi_3\boldsymbol{k}$, the Equations (15)-(17) can be written as

$$i\hbar\frac{\partial}{\partial t}\boldsymbol{\psi}=c\hbar\nabla\times\boldsymbol{\psi}+V\boldsymbol{\psi}. \tag{18}$$

We can find the quantum vector wave Equation (5) and the quantum spinor wave Equation (9) are equivalent.

In Equation (7), if we set

$$\boldsymbol{\psi}=\frac{1}{\sqrt{2}}\left(\sqrt{\varepsilon_0}\boldsymbol{E}+i\frac{1}{\sqrt{\mu_0}}\boldsymbol{B}\right), \tag{19}$$

substituting Equation (19) into (7), we obtain

$$i\hbar\sqrt{\varepsilon_0}\frac{\partial}{\partial t}\boldsymbol{E}-\hbar\frac{1}{\sqrt{\mu_0}}\frac{\partial}{\partial t}\boldsymbol{B}=c\hbar\sqrt{\varepsilon_0}\nabla\times\boldsymbol{E}+ic\hbar\frac{1}{\sqrt{\mu_0}}\nabla\times\boldsymbol{B}, \tag{20}$$

comparing the real and imaginary parts of the both sides of Equation (20), we get

$$\nabla\times\boldsymbol{E}=-\frac{\partial\boldsymbol{B}}{\partial t}, \tag{21}$$

$$\nabla\times\boldsymbol{B}=\mu_0\varepsilon_0\frac{\partial\boldsymbol{E}}{\partial t}, \tag{22}$$

if we let $\nabla\cdot\boldsymbol{\psi}=0$, there is

$$\nabla\cdot\boldsymbol{E}=0, \tag{23}$$

$$\nabla \cdot \boldsymbol{B} = 0. \tag{24}$$

By the following quantum wave equation of photon and gauge condition

$$i\hbar \frac{\partial}{\partial t}\boldsymbol{\psi} = c\hbar \nabla \times \boldsymbol{\psi}, \tag{25}$$

$$\boldsymbol{\psi} = \frac{1}{\sqrt{2}}\left(\sqrt{\varepsilon_0}\boldsymbol{E} + i\frac{1}{\sqrt{\mu_0}}\boldsymbol{B}\right), \tag{26}$$

$$\nabla \cdot \boldsymbol{\psi} = 0. \tag{27}$$

We can obtain the Maxwell's wave Equations (1)-(4) in vacuum.

2) The Maxwell's equations in medium are

$$\nabla \times \boldsymbol{E} = -\frac{\partial \boldsymbol{B}}{\partial t} \tag{28}$$

$$\nabla \times \boldsymbol{B} = \mu\varepsilon \frac{\partial \boldsymbol{E}}{\partial t} \tag{29}$$

$$\nabla \cdot \boldsymbol{E} = 0 \tag{30}$$

$$\nabla \cdot \boldsymbol{B} = 0. \tag{31}$$

With Equations (5) and (6), we can obtain the quantum wave equation of photon in medium, it is

$$\begin{aligned} i\hbar \frac{\partial}{\partial t}\boldsymbol{\psi}\left(\bar{r},t\right) &= c\hbar \nabla \times \boldsymbol{\psi}\left(\bar{r},t\right) + V\boldsymbol{\psi}\left(\bar{r},t\right) \\ &= c\hbar \nabla \times \boldsymbol{\psi}\left(\bar{r},t\right) + \hbar\omega\left(1-n\right)\boldsymbol{\psi}\left(\bar{r},t\right). \end{aligned} \tag{32}$$

By the separation of variables

$$\boldsymbol{\psi}\left(\bar{r},t\right) = \boldsymbol{\psi}\left(\bar{r}\right) f\left(t\right), \tag{33}$$

substituting Equation (33) into (32), we have

$$c\nabla \times \boldsymbol{\psi}\left(\bar{r}\right) = n\omega \boldsymbol{\psi}\left(\bar{r}\right) \tag{34}$$

if we let

$$\boldsymbol{\psi} = \frac{1}{\sqrt{2}}\left(\sqrt{\varepsilon}\boldsymbol{E} + i\frac{1}{\sqrt{\mu}}\boldsymbol{B}\right), \tag{35}$$

with Equations (34) and (35), we get

$$\nabla \times \boldsymbol{E} = i\omega\mu \boldsymbol{H}, \tag{36}$$

$$\nabla \times \boldsymbol{H} = -i\omega\varepsilon \boldsymbol{E}, \tag{37}$$

by the gauge condition $\nabla \cdot \boldsymbol{\psi} = 0$, we have

$$\nabla \times \boldsymbol{E} = 0, \tag{38}$$

$$\nabla \times \boldsymbol{B} = 0. \tag{39}$$

Equations (36)-(39) are the Maxwell's wave equations for the monochromatic light in the medium.

By the following quantum wave equation of photon and gauge condition

$$c\nabla \times \boldsymbol{\psi}\left(\bar{r}\right) = n\omega \boldsymbol{\psi}\left(\bar{r}\right) \tag{40}$$

$$\boldsymbol{\psi} = \frac{1}{\sqrt{2}}\left(\sqrt{\varepsilon}\boldsymbol{E} + i\frac{1}{\sqrt{\mu}}\boldsymbol{B}\right), \tag{41}$$

$$\nabla \cdot \boldsymbol{\psi} = 0. \tag{42}$$

We can obtain the Maxwell's Equations (36)-(39) in medium.

The probability density $\rho_\gamma(\boldsymbol{r})$ of photon in space $\boldsymbol{r}$ is

$$\rho_\gamma(\boldsymbol{r}) = \left|\boldsymbol{\psi}(\boldsymbol{r})\right|^2 = \frac{1}{2}\left(\varepsilon \boldsymbol{E}^2 + \frac{1}{\mu}\boldsymbol{B}^2\right) = \varepsilon \boldsymbol{E}^2 = \rho_{EB}(\boldsymbol{r}). \tag{43}$$

From Equation (43), we find the probability density $\rho_\gamma(\boldsymbol{r})$ of photon is equal to the energy density $\rho_{EB}(\boldsymbol{r})$ of the electromagnetic field of photon, we can obtain the following results:

1) For a lot of photons, the electromagnetic field energy density $\rho_{EB}(\boldsymbol{r})$ is in direct proportion to the photon numbers $N(\boldsymbol{r})$ and the single photon probability density $\rho_\gamma(\boldsymbol{r})$, it is

$$\rho_{EB}(\boldsymbol{r}) \propto N(\boldsymbol{r}) \propto \rho_\gamma(\boldsymbol{r}). \tag{44}$$

2) For a single photon, it is not a point particle, instead, it has a very small distribution area Ω of electromagnetic fields, the whole distribution area represents a photon.

We define a concept of partial photon, which is described by the occupancy $P_\gamma(\boldsymbol{r})$, it is

$$P_\gamma(\boldsymbol{r}) = \frac{\varepsilon \boldsymbol{E}^2(\boldsymbol{r})}{\int_\Omega \varepsilon \boldsymbol{E}^2(\boldsymbol{r})\mathrm{d}^3\boldsymbol{r}}. \tag{45}$$

At space $\boldsymbol{r}$, the bigger the occupancy $P_\gamma(\boldsymbol{r})$, the bigger the photon component, there is

$$\int_\Omega P_\gamma(\boldsymbol{r})\mathrm{d}^3\boldsymbol{r} = 1. \tag{46}$$

Since the photon itself is a very small distribution area of electromagnetic fields, the each point in the region represents the partial photon, the photon is not positioned. The wave-particle duality of photon can be understood as: The entire electromagnetic field distribution area of photon represents a photon, which manifests as the particle nature of photon. The electromagnetic field energy density distribution of photon manifests as the wave nature of photon. With the Equation (43), the probability density $\left|\psi(\boldsymbol{r})\right|^2$ of photon is equal to its electromagnetic fields energy density, it is

$$\rho_\gamma(\boldsymbol{r}) = \left|\psi(\boldsymbol{r})\right|^2 = \rho_{EB}(\boldsymbol{r}) = \varepsilon_0 \boldsymbol{E}^2(\boldsymbol{r}), \tag{47}$$

with Equations (45)-(47), we have

$$\psi(\boldsymbol{r}) = \sqrt{\varepsilon_0}E(\boldsymbol{r})\mathrm{e}^{i\theta}. \tag{48}$$

where the θ is a phase factor. Photon is not a point particle, it exists in the distribution area of electromagnetic field, where the energy density of electromagnetic field is large, it means that the photon appears to be of great weight. So, the

every point of the electromagnetic field distribution region, all are a part of the photon, such as the points $\boldsymbol{r}_A$ and $\boldsymbol{r}_B$ in electromagnetic field distribution region, they can be represented as part of photon. The photon can be expressed as the superposition of the every point of the electromagnetic field distribution region, that is, the photon can appear at both point $\boldsymbol{r}_A$ and point $\boldsymbol{r}_B$. If there is $P_\gamma(\boldsymbol{r}_A) > P_\gamma(\boldsymbol{r}_B)$, the probability of photon at point $\boldsymbol{r}_A$ is larger than point $\boldsymbol{r}_B$. When a photon shows the electric field distribution at the area Ω, the photon behaves as a wave. When the area Ω of photon shrinks to approximately a point, for example, in the interference and diffraction experiments of photon, the bright spots on the screen, which manifests as the particle nature of photon.

3. The Gravitational Field of Particle

1) The non-relativistic gravitational theory

The gravitational potential for a continuous mass distribution is

$$\Phi(\boldsymbol{x}) = -\int \frac{G\rho(\boldsymbol{x}')}{|\boldsymbol{x}-\boldsymbol{x}'|} \mathrm{d}^3\boldsymbol{x}', \tag{49}$$

where $\rho(\boldsymbol{x}')$ is the mass density. The Equation (49) satisfies the Poisson equation

$$\nabla^2\Phi(\boldsymbol{x}) = 4\pi G\rho(\boldsymbol{x}), \tag{50}$$

the self gravitational energy is

$$\begin{aligned} w_g &= \frac{1}{2}\int \rho(\boldsymbol{x})\Phi(\boldsymbol{x})\mathrm{d}^3\boldsymbol{x} \\ &= -\frac{1}{2}\int G\frac{\rho(\boldsymbol{x})\rho(\boldsymbol{x}')}{|\boldsymbol{x}-\boldsymbol{x}'|}\mathrm{d}^3\boldsymbol{x}\mathrm{d}^3\boldsymbol{x}' \\ &= \int \frac{1}{8\pi G}\left(\nabla\Phi(\boldsymbol{x})\right)^2 \mathrm{d}^3\boldsymbol{x} + \int \rho(\boldsymbol{x})\Phi(\boldsymbol{x})\mathrm{d}^3\boldsymbol{x}, \end{aligned} \tag{51}$$

where

$$\rho_g = \frac{\left(\nabla\Phi(\boldsymbol{x})\right)^2}{8\pi G}, \tag{52}$$

is the energy density of gravitational field, and $\rho(\boldsymbol{x})\Phi(\boldsymbol{x})$ is the energy density of gravitational field interacts with matter.

2) The relativistic gravitational theory

In the presence of gravitational field, the dynamic problem of particle can be equivalently transformed into the geometric problem of Riemann space. That is, the motion profile of particle in the gravitational field is the geodesic line of Riemann space. Einstein not only geometrized the particle dynamics in the gravitational field, but also geometrized the gravitational field itself. That is, the metric field $g_{\mu\nu}$ of Riemann space represents the gravitational field. In this way, it is always controversial. The gravitational field, like electromagnetic field, is an objective material field, the geometrization of gravitational field is only an equivalent theory. The relationship between curved space-time metric $g_{\mu\nu}$, flat space-

time metric $\eta_{\mu\nu}$ and gravitational field $h_{\mu\nu}$ is as follows

$$g_{\mu\nu} = \eta_{\mu\nu} + kh_{\mu\nu}. \tag{53}$$

From Equation (53), we can find if there is the gravitational field $h_{\mu\nu}$ then there is the curved space-time metric $g_{\mu\nu}$, if there is no the gravitational field, the space-time is flat, and the metric is $\eta_{\mu\nu}$. Therefore, it is the gravitational field causes the space-time bending, and cannot be considered gravitational field as the curved space-time, the gravitational field and curved space-time are causal relation. It is only an equivalent theoretical method to study gravitational field with the curved space-time.

The electromagnetic field is from electromagnetic current

$$J^{\mu} = \left(c\rho, \boldsymbol{J}\right), \tag{54}$$

where ρ is the electric density, $\boldsymbol{J}$ is the electric current density, the electromagnetic field vector $A^{\mu} = \left(\varphi, \mathbf{A}\right)$ satisfy an equation

$$\Box A^{\mu} = -\mu_0 J^{\mu}, \tag{55}$$

and Lorentz condition

$$\partial_{\mu} A^{\mu} = 0. \tag{56}$$

The source of gravitational field is energy-momentum tensor $T^{\mu\nu}$, and the gravitational field tensor $h^{\mu\nu}$ equation is [16]

$$\Box\left(h^{\mu\nu} - \frac{1}{2}\eta^{\mu\nu}h\right) = -kT^{\mu\nu}, \tag{57}$$

and gauge condition is

$$\partial_{\mu}\left(h^{\mu\nu} - \frac{1}{2}\eta^{\mu\nu}h\right) = 0, \tag{58}$$

where k is a constant, $h = h^{\mu}_{\mu}$ is the trace of $h^{\mu\nu}$, and $\eta^{\mu\nu}$ is the metric of flat space-time.

Definition a new gravitational field

$$\phi^{\mu\nu} = h^{\mu\nu} - \frac{1}{2}\eta^{\mu\nu}h, \tag{59}$$

the Equations (57) and (58) can be written as

$$\Box\phi^{\mu\nu} = -kT^{\mu\nu}, \tag{60}$$

$$\partial_{\mu}\phi^{\mu\nu} = 0, \tag{61}$$

the energy-momentum tensor of field $\phi^{\mu\nu}$ is

$$t^{\mu\nu} = \frac{1}{4}\left[2\phi^{\alpha\beta,\mu}\phi^{,\nu}_{\alpha\beta} - \phi^{,\mu}\phi^{,\nu} - \eta^{\mu\nu}\left(\phi^{\alpha\beta,\sigma}\phi^{,\sigma}_{\alpha\beta} - \frac{1}{2}\phi_{,\sigma}\phi^{,\sigma}\right)\right], \tag{62}$$

where t^{00} is the energy density.

The Newton gravitational theory is the non-relativistic limit of relativistic gravitational theory, there are

$$\Phi = \frac{1}{2}kh_{00}, \tag{63}$$

$$\nabla^2 h_{00} = \frac{1}{2} k\rho, \tag{64}$$

with Equations (51) and (52), we can obtain the equation of the Newton gravitational field

$$\nabla^2 \Phi = 4\pi G\rho, \tag{65}$$

where $k = 4\sqrt{\pi G}$, and ρ is mass density. In the Newtonian approximation, the gravitational field energy density is

$$\rho_g = t^{00} = \frac{(\nabla\Phi)^2}{8\pi G}, \tag{66}$$

defining the strength of the gravitational field $\boldsymbol{E}_g$ as

$$\boldsymbol{E}_g = -\nabla\Phi, \tag{67}$$

the gravitational field energy density ρ_g becomes

$$\rho_g = \frac{\boldsymbol{E}_g^2}{8\pi G}, \tag{68}$$

the energy density of electromagnetic field is

$$\rho_{(EB)} = \varepsilon_0 \boldsymbol{E}^2. \tag{69}$$

From Equations (68) and (69), we find the gravitational field energy density is in direct proportion to the square of the gravitational field strength $\boldsymbol{E}_g$, and the electromagnetic field energy density is in direct proportion to the square of the electric field strength $\boldsymbol{E}$.

All material particles ($m_0 \neq 0$), such as electron, proton and neutron cannot be regarded as point particles, they have a tiny energy distribution area of electric field and gravitational field. For the electron and proton, because they have both charge and mass, they have both electric field distribution and gravitational field distribution. For the neutron, because it has only mass and has not charge, the neutron has only the gravitational field distribution.

We define a concept of partial neutron, which is described by the occupancy $P_g(\boldsymbol{r})$, it is

$$P_g(\boldsymbol{r}) = \frac{t^{00}}{\int_V t^{00} \mathrm{d}^3\boldsymbol{r}} = \frac{\boldsymbol{E}_g^2(\boldsymbol{r})}{\int_V \boldsymbol{E}_g^2(\boldsymbol{r}) \mathrm{d}^3\boldsymbol{r}}. \tag{70}$$

At space $\boldsymbol{r}$, the bigger the occupancy $P_g(\boldsymbol{r})$, the bigger the neutron component, *i.e.*, the bigger the probability of neutron in space $\boldsymbol{r}$. At the whole gravitational field distribution area V of the neutron, there is

$$\int_V P_g(\boldsymbol{r}) \mathrm{d}^3\boldsymbol{r} = 1. \tag{71}$$

where the volume $V \to \infty$, but the gravitational field of neutron can be divided into two areas, one area is the spherical area that the radius is about 50λ (when the slit width is about 100λ, the diffraction effect is not obvious), which is called interior zone, the gravitational field energy of neutron is largely concentrated in this area, the other one is the outer region. Where $\lambda = \frac{h}{p}$ is the de

Broglie wavelength. For the high energy neutron, its interior zone become small, it is particle-like. For the low energy neutron, its interior zone become large, it is wave-like.

4. The Quantum Wave Equation

In 1923, DE Broglie had extended the wave-particle duality of photon to material particles [2], like electrons, protons and so on. Later, he had perfected the theory of matter waves [3], and by analogy Fermat and Morperto principle, he believed the relation between the new wave theory and classical mechanics is similar to the relationship between wave optics and geometric optics, this analogy inspired Schrodinger when he founded wave mechanics. In the following, we should give the quantum wave equation of particle with the analogy method.

1) The time-independent wave equation of particle

The particle nature of photon is described by the Fermat principle, it is

$$\delta\int n\mathrm{d}s = 0, \tag{72}$$

the motion of material particles is described by Morperto principle, it is

$$\delta\int\sqrt{2m\left(E-V\right)}\,\mathrm{d}s = 0, \tag{73}$$

the time-independent photon wave equation is

$$\nabla^2\boldsymbol{E} + \frac{\omega^2 n^2}{c^2}\boldsymbol{E} = 0, \tag{74}$$

where $\boldsymbol{E}$ is electric field intensity of photon, ω is photon frequency, n is refractive index of medium and c is velocity of light.

Comparing Equations (72) and (73), we find

$$n \propto \sqrt{2m\left(E-V\right)}. \tag{75}$$

With Equations (74) and (75), the material particle wave equation can be written as

$$\nabla^2\boldsymbol{E}_g + A\cdot 2m\left(E-V\right)\boldsymbol{E}_g = 0, \tag{76}$$

the Equation (74) is about the equation of photon electric field, the analogy Equation (76) should be the field equation of material particles. For a neutral particle, the $\boldsymbol{E}_g$ is the gravitational field intensity of the neutral particle. For a charge particle, the field should be considered the electric field of the charge particle, except its gravitational field.

For the free particle, the potential energy $V = 0$, the Equation (76) has a plane wave solution, it is

$$\boldsymbol{E}_g\left(\boldsymbol{r}\right) = \boldsymbol{E}_{g0}\mathrm{e}^{i\left(\boldsymbol{k}\cdot\boldsymbol{r}-\omega t\right)}, \tag{77}$$

with Equations (76) and (77), there is there is

$$-k^2 + A\cdot 2mE = 0, \tag{78}$$

where $E = \dfrac{p^2}{2m}$, and the De Broglie's formula

$$k = \frac{p}{\hbar}, \tag{79}$$

with Equations (78) and (79), we get

$$A = \frac{1}{\hbar^2}, \tag{80}$$

substituting Equation (80) into (76), we obtain

$$\left[-\frac{\hbar^2}{2m}\nabla^2 + V(r)\right]\boldsymbol{E}_g(\boldsymbol{r}) = E\boldsymbol{E}_g(\boldsymbol{r}), \tag{81}$$

the scalar form of Equation (81) is

$$\left[-\frac{\hbar^2}{2m}\nabla^2 + V(r)\right]E_g(\boldsymbol{r}) = EE_g(\boldsymbol{r}). \tag{82}$$

The Equations (81) and (82) are the time-independent quantum gravitational field equations of particle. For the charge particle, such as electron and proton and so on, in addition to the gravitational field, there is electric field distribution $\boldsymbol{E}(\boldsymbol{r})$, which satisfies Equations (81) and (82), they are

$$\left[-\frac{\hbar^2}{2m}\nabla^2 + V(r)\right]\boldsymbol{E}(\boldsymbol{r}) = E\boldsymbol{E}(\boldsymbol{r}), \tag{83}$$

the scalar form of Equation (83) is

$$\left[-\frac{\hbar^2}{2m}\nabla^2 + V(r)\right]E(\boldsymbol{r}) = EE(\boldsymbol{r}). \tag{84}$$

We know the probability density $\rho_\gamma(\boldsymbol{r})\left(\left|\psi(\boldsymbol{r})\right|^2\right)$ of photon is equal to its electromagnetic fields energy density (Equation (47)), the probability density $\rho(\boldsymbol{r})$ of neutral particle in space $\boldsymbol{r}$ is proportional to the gravitational field energy density $\rho_g\left(t^{00}(\boldsymbol{r})\right)$. In Equation (66), the energy density ρ_g of gravitational field is in direct proportion to $\boldsymbol{E}_g^2$. We can define spatial probability amplitude distribution function $\psi(\boldsymbol{r})$ of particle, it satisfies

$$\rho(\boldsymbol{r}) = \left|\psi(\boldsymbol{r})\right|^2 \propto \rho_g = \frac{E_g^2(\boldsymbol{r})}{8\pi G}\mathrm{e}^{i\theta}, \tag{85}$$

then we have

$$\psi(\boldsymbol{r}) \propto \frac{E_g(\boldsymbol{r})}{\sqrt{8\pi G}}\mathrm{e}^{i\theta}, \tag{86}$$

where the θ is a phase factor, the $E_g(\boldsymbol{r})$ is the gravitational field intensity of particle. The Equation (82) becomes

$$\left[-\frac{\hbar^2}{2m}\nabla^2 + V(r)\right]\psi(\boldsymbol{r}) = E\psi(\boldsymbol{r}). \tag{87}$$

The position distribution function $\psi(\boldsymbol{r})$ is the wave function of quantum mechanics, the Equation (87) is the time-independent Schrodinger equation, which is from the gravitational field Equation (82).

For a electron, it has both the gravitational field distribution $E_g(\boldsymbol{r})$ and electric field distribution $\psi(\boldsymbol{r})$, because electron has very little mass, its gravitational field can be neglected, and its electric field is the primary. The electric field energy density of electron is

$$\rho(\boldsymbol{r}) = \varepsilon_0 E^2(\boldsymbol{r}), \tag{88}$$

similarly, we can define spatial probability amplitude distribution function $\psi(\boldsymbol{r})$ of electron, it satisfies

$$\rho(\boldsymbol{r}) = |\psi(\boldsymbol{r})|^2 \propto \rho(\boldsymbol{r}) = \varepsilon_0 E^2(\boldsymbol{r}), \tag{89}$$

there is

$$\psi(\boldsymbol{r}) \propto \sqrt{\varepsilon_0} E(\boldsymbol{r}), \tag{90}$$

with the Equation (90), the electric field Equation (84) of electron becomes the Schrodinger Equation (87).

2) The time-dependent field equation of particle

The time-dependent photon wave equation is

$$\nabla^2 \boldsymbol{E} - \frac{n^2}{c^2}\frac{\partial^2}{\partial t^2}\boldsymbol{E} = 0, \tag{91}$$

substituting Equation (75) into (91), we can obtain the time-dependent gravitational field equation of particle, it is

$$\nabla^2 \boldsymbol{E}_g - B \cdot 2m(E-V)\frac{\partial^2}{\partial t^2}\boldsymbol{E}_g = 0. \tag{92}$$

For the free particle, the potential energy $V = 0$, the Equation (88) has a plane wave solution, it is

$$\boldsymbol{E}_g = \boldsymbol{E}_{g0} \mathrm{e}^{i(\boldsymbol{p}\cdot\boldsymbol{r} - Et)/\hbar}, \tag{93}$$

with Equations (92) and (93), there is

$$B = \frac{1}{E^2}, \tag{94}$$

the Equation (92) becomes

$$\nabla^2 \boldsymbol{E}_g - \frac{1}{E^2} \cdot 2m(E-V)\frac{\partial^2}{\partial t^2}\boldsymbol{E}_g = 0. \tag{95}$$

By separation of variable

$$\boldsymbol{E}_g(\boldsymbol{r}, t) = \boldsymbol{E}_g(\boldsymbol{r}) f(t), \tag{96}$$

substituting Equation (96) into (95), there are

$$\nabla^2 \boldsymbol{E}_g(\boldsymbol{r}) - D \cdot 2m(E-V)\boldsymbol{E}_g(\boldsymbol{r}) = 0, \tag{97}$$

$$f''(t) - D \cdot E^2 f(t) = 0. \tag{98}$$

comparing Equation (81) with (97), we have

$$D = -\frac{1}{\hbar^2}, \tag{99}$$

$$f(t)=\mathrm{e}^{-\frac{i}{\hbar}Et}, \tag{100}$$

and

$$\boldsymbol{E}_g(\boldsymbol{r},t)=\boldsymbol{E}_g(\boldsymbol{r})\mathrm{e}^{-\frac{i}{\hbar}Et}, \tag{101}$$

taking the derivative of both sides of the Equation (101), we get

$$i\hbar\frac{\partial}{\partial t}\boldsymbol{E}_g(\boldsymbol{r},t)=\left[-\frac{\hbar^2}{2m}\nabla^2+V(r)\right]\boldsymbol{E}_g(\boldsymbol{r},t), \tag{102}$$

the scalar form of Equation (102) is

$$i\hbar\frac{\partial}{\partial t}E_g(\boldsymbol{r},t)=\left[-\frac{\hbar^2}{2m}\nabla^2+V(r)\right]E_g(\boldsymbol{r},t). \tag{103}$$

The Equations (102) and (103) are the time-dependent quantum gravitational field equations of a particle, and the $E_g(\boldsymbol{r},t)$ is the gravitational field intensity distributions of the particle.

By the Equation (86), there is

$$\psi(\boldsymbol{r},t)\propto E_g(\boldsymbol{r},t), \tag{104}$$

then the Equation (103) becomes

$$i\hbar\frac{\partial}{\partial t}\psi(\boldsymbol{r},t)=\left[-\frac{\hbar^2}{2m}\nabla^2+V(r)\right]\psi(\boldsymbol{r},t). \tag{105}$$

The Equation (105) is the time-dependent Schrodinger quantum wave equation, which is turned gravitational field equation into the Schrodinger equation.

For a charge particle, its electric field $\boldsymbol{E}(\boldsymbol{r})$ and gravitational field $\boldsymbol{E}_g(\boldsymbol{r})$ satisfy the same Equation (92). Repeating the same derivation as above, we can obtain the time-dependent quantum electric field equation of the charge particle, it is

$$i\hbar\frac{\partial}{\partial t}E(\boldsymbol{r},t)=\left[-\frac{\hbar^2}{2m}\nabla^2+V(r)\right]E(\boldsymbol{r},t). \tag{106}$$

With Equations (90) and (106), we can obtain the time-dependent Schrodinger quantum wave Equation (105), which is turned electric field Equation (106) into the Schrodinger Equation (105).

In the above, we can find the Schrodinger equation comes from the gravitational field equation or electric field equation of particle by the relation of Equations (90) and (104). The gravitational field intensity $\boldsymbol{E}_g(\boldsymbol{r},t)$ and electric field intensity $\boldsymbol{E}(\boldsymbol{r},t)$ are the hidden variable of quantum theory, they are the objective and measurable physical quantity. In quantum theory, why we introduce the probability? It is because microscopic particle is not point particle, it have the gravitational field or electric field distribution. In space $\boldsymbol{r}$, the energy density of the gravitational field or electric field determine the probability of particle in space $\boldsymbol{r}$. We study the quantum properties of hydrogen atom with the Schrodinger equation, we can give its energy level and wave function. For an electron,

it has both charge and mass, but the mass is very small, we can only consider the electric field of the electron, and neglect its gravitational field. The wave function of electron $\psi(\boldsymbol{r},t)$ is in direct proportion to its electric field distribution in the interior zone of electron (about 100λ). The so-called volatility of electron in hydrogen atom is from the electric field distribution of electron in hydrogen atom.

5. The Interference and Diffraction of Single Photon and Electron

In the interference and diffraction experiment, when a beam of light pass the single and double slit, it should form the interference and diffraction stripe immediately. Only one photon passes through the single or double slit at a time, only one highlight is displayed on the display. Making a long time observation, the interference and diffraction stripe can be obtained on the display. The previous experiment can be explained by the electromagnetic theory and Huygens-Fresnel principle, *i.e.*, the electromagnetic wave total amplitude on the display point p is obtained by infinitesimal of slit emit secondary waves superposition at this point, this theory explains the experimental results well. The previous experiment result is from the continuous electromagnetic wave superposition. Obviously, the latter experiment is from the interference and diffraction of a single photon itself. How can a single photon form its own interference? In order to solve this problem, we propose a single photon model. A single photon has volume V, and has the vibration electric field and magnetic field in the volume V. they are

$$E = E_0 \cos \omega t, \tag{107}$$

and

$$B = B_0 \cos \omega t. \tag{108}$$

The single photon model is reasonable, we know a beam of light is made of a lot of photons, and the beam of light corresponds to a plane electromagnetic wave, naturally, the single photon has the vibration electric field and magnetic field in its volume V. When the free photon moves to $\boldsymbol{r}$, its electric field and magnetic field intensity become

$$E = E_0 \cos \omega\left(t + \frac{r}{c}\right), \quad B = B_0 \cos \omega\left(t + \frac{r}{c}\right), \tag{109}$$

where $r = |\boldsymbol{r}|$. **Figure 1** is diffraction pattern of single photon passing through a single slit. The width of single slit is b. In the diffraction angle $\theta = 0$ direction, the total amplitude of electric field intensity on the single slit is E_0, then the amplitude of electric field intensity on narrow slit of width $\mathrm{d}x$ is $\frac{E_0 \mathrm{d}x}{b}$, and its vibration electric field intensity is

$$\mathrm{d}E = \frac{E_0 \mathrm{d}x}{b} \cos \omega t. \tag{110}$$

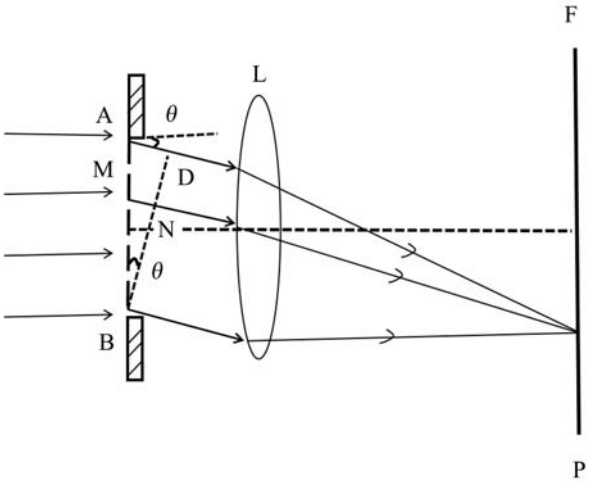

Figure 1. The single slit diffraction figure of single particle.

In the following, we shall give the single photon vibration electric field intensity, which passes through the single slit and travels in MN direction, and the diffraction angle $\theta \neq 0$. The electric field intensity vibration phase of the incident photon on the slit AB are all the same, when the photon spread to point p along the direction of θ angle, because of the interaction between photon and slit, the volume of photon should be deformed, the electric field intensity vibration phase of the deformed photon are different at every point of volume V_γ.

Let $BM = x$, then $MN = x\sin\theta$, the vibration electric field intensity of photon at point N is

$$\mathrm{d}E = \frac{E_0 \mathrm{d}x}{b}\cos\left(\omega t + kx\sin\theta\right), \tag{111}$$

the complex form of Equation (111) is

$$\mathrm{d}E = \frac{E_0 \mathrm{d}x}{b}\mathrm{e}^{i(\omega t + kx\sin\theta)}, \tag{112}$$

where wave vector $k = \dfrac{2\pi}{\lambda}$, when the photon pass through BD, the volume deformation of photon is over. The optical path Δ of the every point on the plane BD to the point p are all the same, then the vibration electric field intensity of photon from point M to point p is

$$\mathrm{d}E = \frac{E_0 \mathrm{d}x}{b}\cos\left(\omega t + k\left(x\sin\theta + \Delta\right)\right), \tag{113}$$

the complex form is

$$\mathrm{d}E = \frac{E_0 \mathrm{d}x}{b}\mathrm{e}^{ikx\sin\theta}\cdot\mathrm{e}^{ik\Delta}\cdot\mathrm{e}^{i\omega t}. \tag{114}$$

When the photon passes through the lens L and arrives at the point p on the screen F, which is situate in the focal plane of the lens L, the vibration electric field of photon should be superimposed, it is the integration of Equation (114) from $x = 0$ to $x = b$

$$E = \int \mathrm{d}E = \frac{E_0 \mathrm{d}x}{b} \mathrm{e}^{ik\Delta} \cdot \mathrm{e}^{i\omega t} \int_0^b \mathrm{e}^{ikx\sin\theta} \mathrm{d}x$$
$$= E_0 \frac{\sin\left(\frac{\pi b \sin\theta}{\lambda}\right)}{\frac{\pi b \sin\theta}{\lambda}} \cdot \mathrm{e}^{ik\Delta} \cdot \mathrm{e}^{i\left(\frac{\pi b \sin\theta}{\lambda} + \omega t\right)}, \tag{115}$$

the intensity of single photon at point p is in direct proportion to the norm of the total vibration electric field E, it is

$$I \propto \left| E_0 \frac{\sin\left(\frac{\pi b \sin\theta}{\lambda}\right)}{\frac{\pi b \sin\theta}{\lambda}} \right|^2. \tag{116}$$

We can find the diffraction intensity of single photon and a beam of light are the same, but the physics significance is different. For the beam of light, the Equation (116) gives out the diffraction intensity distribution of difference point on-screen at the same time. For the single photon, the Equation (116) can only gives the diffraction intensity at a certain point and at a certain time, over a long period of time, it can obtain the same diffraction intensity distribution as a beam of light. At point p, if the superposition electric field of photon is enhanced, the photon volume reduces, the electric field energy density of photon increases, it appears as a point-like particle, and show a bright spot at this point. From a quantum mechanical point of view, when a bright spot appears at point p, the probability of photon is more larger at this point, since the probability of photon is in direct proportion to its electric field energy density. So, we can see single localized clicks at point p. At point p, if the superposition electric field of photon decreases or disappears, it shall show a dark spot at this point, and the photon becomes dark photon (the photon with no electric or magnetic fields).

Figure 2 is the two-slit interference of single photon, the single photon with volume V_γ passes through two-slit at the same time. At every slit, the vibration electric field of photon should be superimposed, and then the electric field of two-slit should be superimposed again. Combining with the single slit diffraction, when the single photon passes through the two-slit, at point p on the screen F (situated in the focal plane of the lens L), the global vibration electric field is

$$E = \frac{E_0}{b} \mathrm{e}^{i\omega t} \left[\int_0^b \mathrm{e}^{i\frac{2\pi}{\lambda}x\sin\theta} \mathrm{d}x + \int_d^{d+b} \mathrm{e}^{i\frac{2\pi}{\lambda}x\sin\theta} \mathrm{d}x \right]$$
$$= E_0 \frac{\sin\left(\frac{\pi b \sin\theta}{\lambda}\right)}{\frac{\pi b \sin\theta}{\lambda}} \cdot \frac{\sin 2\left(\frac{\pi d \sin\theta}{\lambda}\right)}{\sin\left(\frac{\pi d \sin\theta}{\lambda}\right)} \cdot \mathrm{e}^{i\left(\frac{\pi(b+d)}{\lambda}\sin\theta + \omega t\right)}, \tag{117}$$

the two-slit interference intensity of single photon at point p is in direct proportion to the norm of the total vibration electric field E, it is

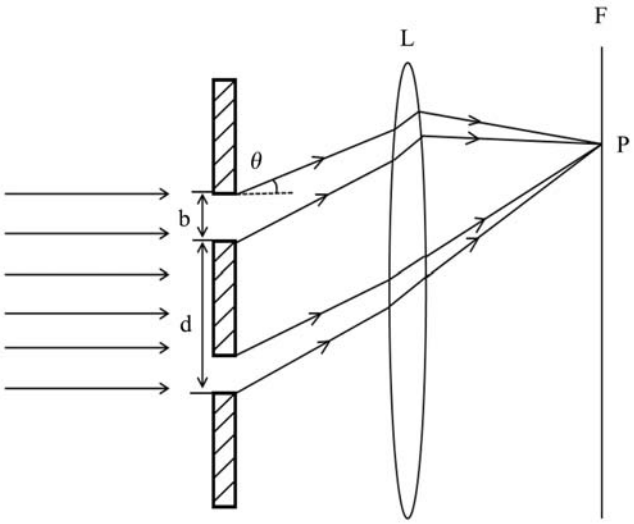

Figure 2. The two-slit interference figure of single particle.

$$I \propto \left| E_0 \frac{\sin\left(\frac{\pi b \sin\theta}{\lambda}\right)}{\frac{\pi b \sin\theta}{\lambda}} \cdot \frac{\sin 2\left(\frac{\pi d \sin\theta}{\lambda}\right)}{\sin\left(\frac{\pi d \sin\theta}{\lambda}\right)} \right|^2 . \tag{118}$$

We can find the interference intensity of two-slit for single photon and a beam of light are the same, but the physics significance is different. For the beam of light, the Equation (118) gives out the interference intensity distribution of difference point on screen at the same time. For the single photon, the Equation (118) can only gives the interference intensity at a certain point and at a certain time. On the screen *F*, Only one bright spot can be displayed at a time, we can see single localized clicks at point *p*. Over a long period of time, it can obtain the same interference fringe distribution as a beam of light.

For the material particles, like electrons, protons, neutrons, and so on, the single material particle can form the interference and diffraction over a long period of time. In order to solve this phenomena, we propose the material particles model, the single material particle has volume V, and has the vibration physical quantity of periodic alteration. For the charge particles, such as electron and proton, there are both the vibration gravitational field and electric field in the volume V, they are

$$\boldsymbol{G} = \boldsymbol{G}_0 \cos\omega t, \tag{119}$$

$$\boldsymbol{E} = \boldsymbol{E}_0 \cos\omega t. \tag{120}$$

For the neutral particle, such as neutron, there is only the vibration gravitational field. Because electron has very little mass, its gravitational field can be neglected, and the electric field is the primary. The proton has larger mass, its gravitational field cannot be neglected. It is similar to the interference and diffraction of single photon, when the single electron passes through the single slit or two-slit, the diffraction and interference intensity intensity are

$$I \propto \left| \boldsymbol{E}_0 \frac{\sin\left(\frac{\pi b \sin\theta}{\lambda}\right)}{\frac{\pi b \sin\theta}{\lambda}} \right|^2, \tag{121}$$

and

$$I \propto \left| \boldsymbol{E}_0 \frac{\sin\left(\frac{\pi b \sin\theta}{\lambda}\right)}{\frac{\pi b \sin\theta}{\lambda}} \cdot \frac{\sin 2\left(\frac{\pi d \sin\theta}{\lambda}\right)}{\sin\left(\frac{\pi d \sin\theta}{\lambda}\right)} \right|^2. \tag{122}$$

the Equations (121) and (122) can only give the diffraction and interference intensity of single electron at a certain point p and at a certain time. On the screen, Only one bright spot can be displayed at a time, we can see single localized clicks at point p. Over a long period of time, it can obtain the same diffraction and interference fringe distribution as a beam of electron.

For the single neutron passes through the single slit or two-slit, the diffraction and interference intensity intensity are

$$I \propto \left| \boldsymbol{G}_0 \frac{\sin\left(\frac{\pi b \sin\theta}{\lambda}\right)}{\frac{\pi b \sin\theta}{\lambda}} \right|^2, \tag{123}$$

and

$$I \propto \left| \boldsymbol{G}_0 \frac{\sin\left(\frac{\pi b \sin\theta}{\lambda}\right)}{\frac{\pi b \sin\theta}{\lambda}} \cdot \frac{\sin 2\left(\frac{\pi d \sin\theta}{\lambda}\right)}{\sin\left(\frac{\pi d \sin\theta}{\lambda}\right)} \right|^2. \tag{124}$$

For the single proton passes through the single slit or two-slit, the diffraction and interference intensity intensity are

$$I \propto \left| \boldsymbol{E}_0 \frac{\sin\left(\frac{\pi b \sin\theta}{\lambda}\right)}{\frac{\pi b \sin\theta}{\lambda}} \right|^2 + \left| \boldsymbol{G}_0 \frac{\sin\left(\frac{\pi b \sin\theta}{\lambda}\right)}{\frac{\pi b \sin\theta}{\lambda}} \right|^2, \tag{125}$$

and

$$I \propto \left| \boldsymbol{E}_0 \frac{\sin\left(\frac{\pi b \sin\theta}{\lambda}\right)}{\frac{\pi b \sin\theta}{\lambda}} \cdot \frac{\sin 2\left(\frac{\pi d \sin\theta}{\lambda}\right)}{\sin\left(\frac{\pi d \sin\theta}{\lambda}\right)} \right|^2 + \left| \boldsymbol{G}_0 \frac{\sin\left(\frac{\pi b \sin\theta}{\lambda}\right)}{\frac{\pi b \sin\theta}{\lambda}} \cdot \frac{\sin 2\left(\frac{\pi d \sin\theta}{\lambda}\right)}{\sin\left(\frac{\pi d \sin\theta}{\lambda}\right)} \right|^2. \tag{126}$$

where $\lambda = \frac{h}{p}$ is the de Broglie wavelength of material particle. With the Equations (121)-(126), we can obtain the diffraction and interference intensity distribution

of single slit and two-slit for the electron, proton, neutron, atomic molecule and so on. The diffraction of X ray, electron and neutron in crystal are from self field interference, which are the same as the slit diffraction. Through the above analysis and research, we obtain the following results: 1) For a free photon, it is not a point particle, it exists in a very small volume, and the photon has a vibration electric field in the very small volume the Equation (106). 2) When a photon passes through the slits, its own electric field are superimposed on each other, if the own vibration electric field superposition enhance, a bright spot shall appear on the screen, the bright spot manifested as the particle nature of photon. 3) The vibration electric fields of photon have the superposition, it manifested as the wave nature of photon. 4) For a free neutral material particle ($m_0 \neq 0$), such as neutron, it has a vibration gravitational field in the very small volume (the Equation (118)). 5) When a neutron passes through the slits, its own vibration gravitational field are superimposed on each other, if the own gravitational field superposition enhance, a bright spot shall appear on the screen, the bright spot manifested as the particle nature of neutron. 6) The vibration gravitational field of neutron have the superposition, it manifested as the wave nature of neutron. 7) For a free charge material particles, such as electron and proton, they have both vibration gravitational field and vibration electric field in the very small volume (the Equations (118) and (119)). 8) When a proton passes through the slits, its own gravitational gravitational field and electric field are superimposed on each other respectively, if the own gravitational field and electric field superposition enhance, a bright spot shall appear on the screen. The bright spot manifested as the particle nature of proton. 9) The vibration gravitational field and electric field of proton have the superposition, it manifested as the wave nature of proton. 10) For a free electron, because it has a very small mass, its vibration electric field is primary, and vibration gravitational field can be neglected. The electric field of free electron is the vibration electric field, its wave property or the particle property is determined by the external measurement condition. 11) For a non-free electron, such as the electron in hydrogen atom, it is described by the wave function $\boldsymbol{\psi}(\boldsymbol{r},t)$, the electron has only the volatility in hydrogen atom, and the electron volatility is from the electric field distribution of electron. 12) In quantum theory, we have introduced the probability concept, the reason is microscopic particle is not point particle, it have the gravitational field or electric field distribution, their energy density distribution of the gravitational field or electric field determines the probability of particle in space. 13) In hydrogen atom, the electric wave function $\boldsymbol{\psi}(\boldsymbol{r},t)$ is in direct proportion to its electric field distribution, *i.e.*, $E(\boldsymbol{r},t) \propto \psi(\boldsymbol{r},t)$, the probability of electron in space is in direct proportion to the occupancy, *i.e.*, $|\psi(\boldsymbol{r},t)|^2 \propto P(\boldsymbol{r}) \propto |\boldsymbol{E}(\boldsymbol{r},t)|^2$. 14) The electric field distribution of electron determines its probability distribution. Similarly, the gravitational field distribution of neutron determines the probability distribution of neutron in space. The material fields of gravitational field and electric field are the hidden fields in quantum theory, they satisfy the Equations (103) and (106), the hidden fields decide the wave function or probability dis-

tribution of particle in space. 15) For all microscopic particles, when they confined to very small areas, the internal vibration fields take dominant role, which manifested as the wave property. When the microscopic particles are in a larger area, their external field take dominant role, which manifested as the particle property, such as an electron moves in an electromagnetic field. 16) For all microscopic particles, they all come from the field distribution, the particle mass is from itself gravitational field distribution, and the particle charge is from itself electric field distribution, which can unify both the volatility and particle nature and field and particle. 17) For a macroscopic object, its gravitational field distribution is mainly concentrated on the areas of the object volume, which is called internal gravitational field areas, and the surrounding gravitational field is called external gravitational field areas. The total energy of internal gravitational field is far outweigh the external gravitational field, when the external gravitational field distribution are changed, it has a little influence on its motion state, but if we apply external force to a macroscopic object, the internal gravitational field distribution shall change, the motion state of the macroscopic object should be changed, and it follows the Newton's law.

6. Conclusion

In the paper, we have given the quantum equation of the gravitational field intensity $E_g(\boldsymbol{r},t)$ and electric field intensity $E(\boldsymbol{r},t)$ for the material particles, since the gravitational field intensity $E_g(\boldsymbol{r},t)$ and electric field intensity $E(\boldsymbol{r},t)$ is in direct proportion to the distribution function $\psi(\boldsymbol{r},t)$ of particle spatial position (wave function), these quantum equations are natural converted into the Schrodinger equation. In addition, we have proposed the new model about the photon and matter particles. For all particles, they are not point particles, but they have a very small volume. The photon has a vibration electric field in its very small volume. The neutral material particle, such as neutron, it has a vibration gravitational field in its very small volume. For the charge material particles, such as electron and proton, they have both vibration gravitational field and vibration electric field in their very small volume. With the model, we can explain the diffraction and interference of single slit and multiple-slit for the single photon and material particles, the volatility of all particles come from the superposition of their respective vibration field. After the vibration field of particle superposition, it shows up as a particle property. On this basis, we have obtained some new results, and realized the unification of both wave and particle and field and matter.

Fund

This work was supported by the Scientific and Technological Development Foundation of Jilin Province (No. 20190101031JC).

Conflicts of Interest

The authors declare no conflicts of interest regarding the publication of this paper.

References

[1] Planck, M. (1901) *Annalen der Physik*, **309**, 553-563. https://doi.org/10.1002/andp.19013090310

[2] Broglie, D.E. (1923) *Comptes Rendus*, **177**, 507.

[3] Broglie, D.E. (1925) *Annales De Physique*, **10**, 22-128. https://doi.org/10.1051/anphys/192510030022

[4] Schrodinger, E. (1926) *Annalen der Physik*, **79**, 361-376. https://doi.org/10.1002/andp.19263840404

[5] Schrodinger, E. (1926) *Annalen der Physik*, **79**, 489-527.

[6] Schrodinger, E. (1926) *Annalen der Physik*, **80**, 437-490.

[7] Einstein, A., Podolsky, B. and Rosen, N. (1935) *Physical Review*, **47**, 777. https://doi.org/10.1103/PhysRev.47.777

[8] Bohm, D.A. (1952) *Physical Review*, **85**, 166-193. https://doi.org/10.1103/PhysRev.85.166

[9] Bell, J. (1964) *Physics Physique Fizika*, **1**, 195-200. https://doi.org/10.1103/PhysicsPhysiqueFizika.1.195

[10] Bell, J. (1966) *Reviews of Modern Physics*, **38**, 447-452. https://doi.org/10.1103/RevModPhys.38.447

[11] Aspect, A., Grangier, P. and Roger, G. (1981) *Physical Review Letters*, **47**, 460-463. https://doi.org/10.1103/PhysRevLett.47.460

[12] Aspect, A., Grangier, P. and Roger, G. (1982) *Physical Review Letters*, **49**, 91-94. https://doi.org/10.1103/PhysRevLett.49.91

[13] Khrennikov, A. and Alodjants, A. (2019) *Entropy*, **21**, 157. https://doi.org/10.3390/e21020157

[14] Wu, X.-Y., Liu, X.-J. and Wu, Y.-H. (2010) *International Journal of Theoretical Physics*, **49**, 194-200. https://doi.org/10.1007/s10773-009-0192-x

[15] Wu, X.-Y., Zhang, X.-R., Liu, H., *et al*. (2019) *Physica E*, **114**, Article ID: 113563. https://doi.org/10.1016/j.physe.2019.113563

[16] Ohanian, H.C. and Ruffini, R. (1994) Gravitation and Space. W. W. Norton Company, New York.

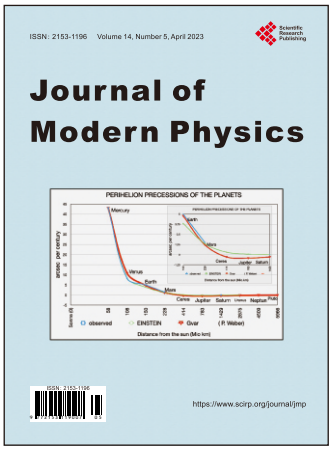

Call for Papers

Journal of Modern Physics

ISSN: 2153-1196 (Print) ISSN: 2153-120X (Online)
https://www.scirp.org/journal/jmp

Journal of Modern Physics **(JMP)** is an international journal dedicated to the latest advancement of modern physics. The goal of this journal is to provide a platform for scientists and academicians all over the world to promote, share, and discuss various new issues and developments in different areas of modern physics.

Subject Coverage

Journal of Modern Physics publishes original papers including but not limited to the following fields:

Biophysics and Medical Physics
Complex Systems Physics
Computational Physics
Condensed Matter Physics
Cosmology and Early Universe
Earth and Planetary Sciences
General Relativity
High Energy Astrophysics
High Energy/Accelerator Physics
Instrumentation and Measurement
Interdisciplinary Physics
Materials Sciences and Technology
Mathematical Physics
Mechanical Response of Solids and Structures
New Materials: Micro and Nano-Mechanics and Homogeneization
Non-Equilibrium Thermodynamics and Statistical Mechanics
Nuclear Science and Engineering
Optics
Physics of Nanostructures
Plasma Physics
Quantum Mechanical Developments
Quantum Theory
Relativistic Astrophysics
String Theory
Superconducting Physics
Theoretical High Energy Physics
Thermology

We are also interested in: 1) Short Reports—2-5 page papers where an author can either present an idea with theoretical background but has not yet completed the research needed for a complete paper or preliminary data; 2) Book Reviews—Comments and critiques.

Notes for Intending Authors

Submitted papers should not have been previously published nor be currently under consideration for publication elsewhere. Paper submission will be handled electronically through the website. All papers are refereed through a peer review process. For more details about the submissions, please access the website.

Website and E-Mail

https://www.scirp.org/journal/jmp **E-mail: jmp@scirp.org**

What is SCIRP?

Scientific Research Publishing (SCIRP) is one of the largest Open Access journal publishers. It is currently publishing more than 200 open access, online, peer-reviewed journals covering a wide range of academic disciplines. SCIRP serves the worldwide academic communities and contributes to the progress and application of science with its publication.

What is Open Access?

All original research papers published by SCIRP are made freely and permanently accessible online immediately upon publication. To be able to provide open access journals, SCIRP defrays operation costs from authors and subscription charges only for its printed version. Open access publishing allows an immediate, worldwide, barrier-free, open access to the full text of research papers, which is in the best interests of the scientific community.

- High visibility for maximum global exposure with open access publishing model
- Rigorous peer review of research papers
- Prompt faster publication with less cost
- Guaranteed targeted, multidisciplinary audience

Scientific Research Publishing

Website: https://www.scirp.org
Subscription: sub@scirp.org
Advertisement: service@scirp.org